Experimental and Theoretical Study of FM08 Electrical Fuses

Henning Leidecker

April 21, 1996

Abstract

An "FM08 cartridge instrument fuse" has an electrical current rating indelibly printed onto its case. However, the actual current that interrupts this fuse varies from roughly 80% of this value when the current is sustained for many hours in an environment of 125 °C, to more than 300% of this value when the current is sustained for less than a few milliseconds at 25 °C. Thus, the rating is only a guide to the interruption current, and is not identical with it. Since the design of an FM08 fuse is both simple and standardized, detailed modeling of the behavior is possible and allows accurate predictions of those current histories that will produce interruption and those that will not. Thus, a designer can better select an appropriate fuse for a given application. This model also generates derating schemes for the use of fuses in a vacuum and at off-design temperatures such as result when a fuse's mounting provides an out-of-specification thermal environment.

Further, in the case of opened fuses, this model allows estimation of the overcurrent that produced the interruption to be made from the degree of, and the character of, the "meltback" within the fuse or the amount of "flash" deposited onto the fuse's barrel.

Finally, mechanisms are discussed that change the interruption current while the fuse is used.

- Certain current histories can complete the annealing of an incompletely annealed fuse filament, removing any work hardening left by the drawing process that produced the wire and any work hardening produced during installation of the fuse filament, and increasing the interruption current by 2 to 3 percent for copper and nickel filaments and by about 20% for copper-silver alloy filaments.

- A current sustained at the rated value oxidizes the fuse filament when air is present inside the fuse (the normal case). Progressive oxidation lowers the interruption current; thus, a fuse is subject to latent damage.

- A current sustained at the rated value heats the fuse filament to the extent that creep under the shearing stresses installed during assembly can induce "creep rupture" and thus interruption. This mechanism can combine with oxidation when air is present: the temperature of the filament increases as oxidation advances, and so the creep rate increases strongly. Experience and modeling show that application of the rated current for as little as roughly 4 hours can produce interruption.

- A current pulse produces a thermal pulse, and thus a mechanical pulse: repetitions can produce mechanical fatigue and eventual interruption of the filament or latent damage that allows subsequent interruption at below-rated current.

- Escape of air from inside the fuse removes a filament-cooling mechanism: loss of air lowers the interruption current by about 5% for a fuse rated at 15 A and by about 45% for a fuse rated at 3/4 A; the reduction reaches a factor of 3 to 4 for fuses rated at 1/2 A and lower.

Contents

List of Tables

List of Figures

Chapter 1

Introduction

Experience has shown that malfunctions in electrical circuits can produce damaging current overload conditions, and that protection against such accidental current overloads is prudent. An electrical fuse provides such protection by melting open,[1] thus interrupting the circuit and permanently stopping all current flow through that circuit. Fuses are inexpensive and reliable *when used within their specifications*, and are widely used for overload protection. For example, the Hubble Space Telescope has more than 900 fuses; replacing these with circuit-breakers would add substantial cost and weight, and would substantially decrease reliability.

However, there are difficulties with the use of a fuse:

- The exact current-time conditions that cause a fuse to melt open are complicated enough to require a multiparameter model, but this model does not seem to be in the literature.[2] For steady-state currents, we can use the manufacture's rating for the fuse, together with an appropriate derating factor. For currents that jump from zero to a constant value, we can use published time-current curves. But real circuits involve more complicated pulses that are not covered by published curves. Also, reratings are required when the fuse is operated at off-design temperatures, and in a vacuum. In other words, many situations are encountered in practice *for which there are no specifications currently available*: this lowers reliability.

- Fuses fail! Fuses sometimes open when there was never a current overload condition, or do not open under the expected overload:

  - Processes driven by heat (e.g., creep, oxidation and alloy-segregation) steadily reduce the current-carrying capacity of the fuse until failure eventually occurs at

[1] "To fuse" means "to melt," and indicates the origin of the name of this device. The word "fuse" is also used for "detonating device," but this use comes from the spindle shape (in Italian, *fuso*) of the squibs used to ignite early cannons, and is unrelated.

[2] See Appendix 6.2.3 for a description of a simple SPICE-model of a fuse.

a subrated current. For example, a fuse rated at a current between 3/4 A and 4 A will carry a steady current of roughly 140% of the rated value for minutes; however, at 25 °C the rated current can produce sufficient oxidation to cause interruption of some fuses within 4 hours, as can 80% of the rated current at 125 °C.

- Mechanical fatigue, caused either by vibration or by thermal pulses driven resulting from the electrical transients at turn-on, reduces the strength of the fuse filament until failure occurs at a subrated current.
- Manufacturing variations sometimes result in a fuse for which the interruption current is distinctly larger than is implied by its rating. Such a fuse does not offer the expected protection: this is also a failure. A 20% increase of this sort was observed once in a hundred tests.
- While this style of fuse is called "hermetic," both the construction and the testing procedure allow leaks to be present that result in complete loss of the air that is normally present within them in as little as a month in a vacuum environment. The removal of air removes a filament cooling mechanism and consequently reduces the interruption current. The amount depends on the rating of the fuse. The reduction is about 5% for a fuse rated at 15 A and about 45% for a fuse rated at 3/4 A. The reduction is a factor of 3 to 4 for fuses rated at 1/2 A and less. However, while such leaks are allowed, they are rare: the majority of fuses retain their air for at least several years. Thus, there is uncertainty in the actual interruption current of a fuse after it has been exposed to a vacuum for more than a month.
- Certain current histories anneal filaments made of copper-silver alloy, removing the work-hardening that results from the wire drawing process and, thus, reducing the resistance. This increases the interruption current as much as 20% in extreme cases. Even a 20% increase would not usually be of consequence by itself, but could combine with other effects to become of consequence. Such annealing is at the root of certain discrepancies that have been noted in the measurements made at different times of the fuse's electrical resistance.

1.1 Purpose of this report

It is the purpose of this report to present an analysis of the behavior of FM08 fuses, and to demonstrate that it agrees with experiment. The behavior is complicated, and it seems appropriate to capture the results of this analysis in a sequence of models, beginning with a simple one that is accurate enough for some purposes, and proceeding to more complicated ones that can provide increased accuracy when this is needed.

The analysis allows computation of whether a given current-time condition will, or will not, open a fuse. And it allows us to inspect an opened fuse to determine the extent of the

overcurrent that caused the opening, or to determine if the opening was erroneous and not caused by an overcurrent condition.

1.2 The focus is on the temperature

A fuse is used in an electrical circuit to protect against certain electrical events, and is rated in terms of a characteristic electrical current. Hence, someone might imagine a fuse to be "purely" an electrical device, and that it could be treated using much the same concepts that have proven their worth in describing electrical devices.

However, all the behaviors of a fuse are driven by the temperature distribution along its filament, and this distribution is influenced by the thermal environment. For example, a fuse rated at 15 A will carry a current of 30 A (200% of rating) for at least one minute when its case and leads are clamped to 25 °C by forced cooling; however, this fuse can be interrupted by a current of 15 A (100% of rating) within one minute when held in air by the alligator clips at the ends of the current-supplying leads. By contrast, the value of an electrical resistor or an electrical capacitor changes by only a few percent at most (and usually much less) under the range of conditions found in typical circuits. Hence, the fuse is primarily a thermal device, and the analysis of fuse behavior must focus on the temperature of the filament of the fuse. Knowledge of the thermal resistance between the fuse and "thermal ground" can be important; indeed, knowledge of the thermal transmission line parameters of the environment may also be important in some cases.

1.3 The selection of a fuse

Certainly, the rating of a fuse chosen for a particular circuit must be large enough to avoid a "nuisance" interruption[3] — an interruption caused by a current-event that would be acceptable for continued circuit performance. But the rating should not be chosen to be arbitrarily large, or there is the possibility that a "smart short"[4] may occur, which could lead to reduced performance or failure.

The thermal environment of a fuse is often uncertain, and the actual currents that will flow through the fuse are typically either uncertain or different from the constant current used to establish ratings. Hence, the usual practice is to apply a safety factor — actually, a *factor of ignorance* — when choosing the fuse rating appropriate for a particular use. Typical derating factors are 50% for ratings from 15 A to 2 A, decreasing to 25% for a fuse rated at 1/8 A.

[3]The terms *nuisance interruption* and *nuisance failure* are terms of art in the fuse community, and unlikely to change. But "nuisance" is an inappropriate term for the event when it occurs in a spacecraft.

[4]A so-called *smart short* produces an overcurrent just small enough so that there is a greatly delayed interruption, or no interruption at all, even though the current is now greater than the circuit is designed for. The term suggests that the circuit anomaly is attempting to outwit the design criteria used to select the fuse's rating.

That is, if the fuse is to protect a system that will carry up to 3 A in normal circumstances, then a fuse rated at 6 A would be indicated; but since there there is no fuse rated at 6 A in the FM08 series, then a 7 A fuse would be chosen. The unfortunate consequence of this approach is that it avoids nuisance failures at the expense of increasing vulnerability to smart shorts.

But when the thermal environment is known, and the range of possible acceptable current-histories is known, then a much smaller safety factor is possible, and, hence, there can be a better balance between avoiding nuisance failures while protecting against smart shorts. One would capture the behavior of the FM08 fuse in a reliable mathematical model, query the model for the behavior to be expected for any particular current-history, and choose a rating that is more apt than would result from the use of a large factor of ignorance.

1.4 Order of presentation

Chapter 2 describes the style of fuse this report considers: this style is defined by MIL–F–23419/8F. It summarizes certain parts of MIL–F–23419/8F. It calls attention to MIL–F–23419/8F's implicit specification of the thermal resistance between the fuse and the thermal ground, and makes this specification explicit. It also notes that the specification of a fuse's "rating" given by MIL–F–23419/8F is not universal; rather, the specification in common use in Europe differs to such an extent that ratings are contradictory.

Chapter 3 augments the specifications of MIL–F–23419/8F with information supplied by the suppliers and obtained from direct testing.

Chapter 4 presents the mathematical model of the fuse and the environment: the complete model is complicated, so a sequence of models of increasing accuracy is given, along with guides for which level of accuracy is necessary in a given case. We find that the interruption of a fuse has a nonlinear dependence on the past current history: it does not depend on just the present value of the current through the fuse. This dependence is so complicated that it cannot be summarized by a single number. A computer model is presented that captures much of the required behavior. Standard analysis has been carried out on some particular current histories, and the following have been found to be of special interest:

- A pulse. When the duration of the pulse is shorter than the thermal relaxation time of the filament (roughly 0.1 sec), then the pulse shape is of no consequence for any currents that will be met in spacecraft practice; rather, it is the integrated value of the squared current, $\int i^2\,dt$, that matters. Many types of electrical circuits produce such transient pulses when they are switched on[5] and the peak currents have been found to exceed the rated value of the fuse, calling for special attention during design.

[5]It is noteworthy that many current-limited power supplies have been found to provide a turn-on pulse with a maximum current that exceeds the setting by 150% to 500% for a few milliseconds, since the regulation circuit requires this time to enforce the selected limit value.

- A chain of N transient pulses, each with the same value of $\int i^2\,dt$. It has been found that such a chain can interrupt a fuse even when every pulse in the chain would be nondamaging to a new fuse: a table of N vs. $\int i^2\,dt$ is included in this report. There is also the possibility that such a chain can produce latent damage to a fuse, so that it will interrupt later under a current that is well within normal design limits.

- A suddenly switched-on current, zero before $t = 0$, and constant after $t = 0$. This is the most important of the waveforms, as it best approximates most conditions of use. For example, all the standard "current-time" plots are made for this waveform.

- A suddenly stepped current, constant at I_1 before $t = 0$ and constant at I_2 after $t = 0$. This waveform is apt when a short suddenly develops in a circuit that has been carrying a current. The fuse is already hot when the current jumps to the higher value, and will therefore interrupt in a shorter time than predicted by the standard "current-time" plot, which is predicated on zero initial current, $I_1 = 0$. When the initial current is near the rated value, the interruption time roughly halves.

- A current-ramp: zero before $t = -T$, then linearly increasing to I_{max} at $t = 0$, and decreasing back to zero at $t = +T$ and remaining zero after that. This waveform is useful for probing the dependence of the fuse's electrical resistance vs. current and also some aspects of the thermal environment of the fuse. (See Appendix D: Hysteresis.)

- A biased sinusoidal current: $i(t) = i_{bias} + i_{probe}\sin(2\pi f t)$. The electrical and thermal behavior of a fuse is nonlinear, and this complicates both modeling and the analysis of measurements. By biasing the fuse with a current $i_{\rm bias}$ and then probing its response to a smaller current $i_{\rm probe}$ while varying the frequency f, the response is linearized and both modeling and analysis of measurements are considerably simplified. In particular, it becomes possible in principle to determine the amount of air contained within the barrel of the fuse and also some details of the thermal environment.

  Also, this waveform is sometimes encountered in practical applications. For example, ordinary AC current corresponds to zero-bias ($i_{bias} = 0$). If the frequency were low enough for the filament's temperature to oscillate, say, $f < 1$ Hz to 10 Hz, then this drive could produce the same sort of degradation as a chain of pulses.

Supporting material is given in the appendices.

Appendix A: The early history of the fuse provides an interesting context. Fuses were not invented because their need was thoughtfully anticipated or, indeed, even recognized in the face of disasters: accidental shorts had resulted in deaths and loss of property for decades before Edison invented the fuse. He digressed from his strenuous efforts to deliver a commercial lighting system to design shorting-protection after an accidental short circuit destroyed his electrical generator for the second time. His patent drawing has several points of similarity with the style of fuse considered in this report.

Appendix B: The material properties are presented in a context that allows an estimation of the reliability of their values.

Appendix C: The copper-silver alloy used for the filaments of fuses rated between 3/4 A and 4 A has special behavior that warrants its own discussion.

Appendix D: It has proved possible to use the hysteresis in the measured resistance of a fuse as the current is ramped to its rated value and back again as a measure of certain aspects of the thermal environment. This is discussed.

Appendix E: Oxidation converts electrically conducting metal in the filament into nonconducting oxide, and this concentrates the current into a narrower channel, raising the temperature of this channel. This leads to an increased oxidation rate. It also accelerates the creep rate (see Appendix F). A combination of oxidation and creep-rupture is responsible for interruption at currents near the rated current.

Appendix F: Creep rupture is the failure mechanism when the interruption time is longer than hundreds of seconds. The creep rate is increased by oxidation.

Appendix G: This appendix lists the symbols and defines some terms, and the Bibliography lists the literature used in this Report.

Chapter 2

Specifications for an FM08 fuse

This report discusses fuses described in Military Specification Sheet MIL–F–23419/8F: "Fuse, Cartridge, Instrument Type, Style FM08 (Subminiature - High Performance)," since these are the ones specified by the *Preferred Parts List*[1] in use at Goddard Space Flight Center. These fuses are typically used to interrupt the electrical supply to low power electrical, electronic, and communication equipment on direct current or alternating current (for frequencies up to 400 Hz) upon the occurrence of a short circuit. The two manufacturers certified as suppliers of FM08 fuses are Bussmann[2] and Littelfuse.[3] A representative FM08 fuse is shown in Figure 2.1.

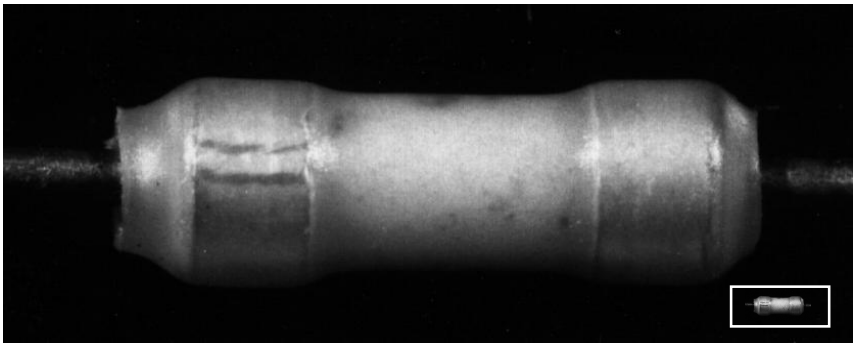

Figure 2.1: A typical example of an FM08 fuse magnified 13 times. The insert at the lower right shows the actual size.

There are a variety of other fuses constructed along the same lines, and much of the following analysis will apply to such other fuses too. In particular, the FM04-style and FM11-style fuses are similar. However, specific numerical values may be different for other fuses.

[1]This is a document authorized by Code 311. Electrical components selected from this document are preapproved by Code 311, as long as they are used within the stated guidelines; other parts require explicit approval.

[2]Cooper Industries, Inc., Bussmann Division; P. O. Box 14460; St. Louis, MO 63178–4460.

[3]Littelfuse, Inc.; 800 E. Northwest Highway; Des Plaines, IL 60016.

2.1 The current rating of a fuse

The *current rating* of a fuse is a concept of crucial importance. In this report, the definition is

> The *current rating* is the number in amperes that is marked on the case of the fuse.

Thus, the current rating does not depend on the temperature or the presence of air within the barrel of the fuse or the time characteristics of the current, among other things.

The current rating is related to the interruption current. The *overly simplified* relation is

> The fuse's filament melts and opens the circuit when, and only when, the current through the fuse exceeds the current rating of the fuse.

But this is too simple: the current that will interrupt a fuse has a much more complex relation to the fuse's rating. For example, laboratory testing shows that most FM08 fuses rated at 3 A will carry a current of 30 A for 1 millisecond without interrupting; however, most will interrupt at a current of 2.95 A that is sustained for several days, and at a still lower sustained current when the temperature of the fuse's case is elevated to 125 °C. And interruption under currents near the rated value is not usually produced by melting at all, but by creep rupture caused by shearing stress built into the filament during the assembly of the fuse. The accurate relation between the rated current and the interruption current requires specification of a number of details as described in Chapters 5 and 6 and in Appendices E and F. Standardization organizations have specified a series of procedures to determine certain of these relations.[4] MIL–F–23419/8F names three aspects of the relation between the interruption current of a fuse and the rating assigned to it:

1. **The rated value is limited on the high side:** MIL–F–23419D Supplement 1 states that "The current rating is the amount of current a fuse will carry indefinitely without interruption."[5, 6] This is clarified by the statement of the acceptance test for

[4]There are at least six standardization organizations currently active. The specifications of each can be distinct, and are in some cases contradictory. For example, the Underwriters Laboratory (UL) and the Canadian Standards and Testing (CSA) require a fuse to open within 1 hour when carrying 135% of its rated current, while the International Electrotechnical Commission (IEC) requires a fuse to carry 150% of its rated current for at least 1 hour. Hence, different definitions of terms are sanctioned by important organizations, and a user must be careful to use the appropriate choices.

[5]Paragraph 1.2.1.4 of the Supplement. Although this statement claims to be the definition of "rating," it is not: it only sets the high limit, and says nothing about the low limit. Hence, this statement uses wording that is inappropriate.

[6]The Supplement does not define its use of "indefinitely." I suppose the intended meaning is that the fuse will carry its rated current for an *unlimited* time, and I will interpret the word in this sense throughout this report. But whatever the intended meaning, Webster's *New Collegiate Dictionary* (9^{th} Edition) defines

current-carrying capacity: a fuse shall carry 110% of the rated current for not less than 1.5 hours.[7]

2. **The rated value is limited on the low side:** Throughout the temperature range −55 °C to +125 °C, the fuse will interrupt in

   - 0 to 5 seconds when driven at 200% of its rated value,
   - 0 to 0.1 second when driven at 300% of its rated value,
   - except that a 15-ampere fuse will have an interrupt time of 10 seconds maximum at 200% of its rated value, and an interrupt time of 0.3 seconds maximum at 300% of its rated value.

   After being interrupted by a current of no more than 300 A applied with a rise time of at least 3.25×10^6 amperes per second,[8] the fuse will present a minimum insulation resistance of 10 000 ohms at the maximum rated voltage (DC).

3. **The interruption current interacts with ambient temperature**, being rescaled as follows:

   - 110% at −55 °C
   - 100% at +25 °C
   - 80% at +125 °C,

   together with "The temperature of the case, body, or terminals shall, at no point, rise more than +70 °C above the ambient air temperature. The maximum temperature rise for 10 and 15 ampere fuses shall be +85 °C."[9, 10, 11]

2.2 The relation between interruption and temperature

The temperature of the fuse filament rises when the joule heat caused by the current passing through the filament generates heat at a faster rate than this heat is removed by conduction

"indefinite" as *not definite*, as
a: typically designating an unidentified or not immediately identifiable person or thing;
b: not precise: *VAGUE*;
c: having no exact limits.
Thus, *indefinite* is an inappropriate word.

[7] This is my paraphrase of Paragraph 4.8.4 of the Supplement. A recent revision of this document changes 110% to 100%.

[8] From "Short circuit interrupt" of the Specification, and Paragraph 4.8.8 of the Supplement.

[9] Page 2, "Current carrying capacity."

[10] "Room ambient temperature" is defined in the Supplement (section 4.8.6) as 20 to 25 °C.

[11] This definition cannot be applied when the fuse is operated in a vacuum, as is often the case for spacecraft use. But what matters is the temperature of the heat sink with which the fuse is in thermal contact, and not the presence of air. If the definition were reworded in terms of this heat sink, then it would apply to spacecraft use, as well as to more conventional uses.

into the case (i. e., the barrel and the caps) of the fuse. The filament melts open — and the fuse interrupts — if this temperature exceeds the melting temperature of the filament. Hence, the rate at which heat is conducted away from the fuse's filament critically affects the current at which interruption occurs; that is, the interruption current is affected by the case temperature, and this effect is essential: *it cannot be designed away and cannot be ignored.*

The most direct treatment of the effect of the temperature of the fuse's case on the fuse's interruption current is to exhibit the functional dependence as a graph or table or formula: various fuse manufacturers use this direct treatment. However, MIL–F–23419/8F uses an indirect treatment, involving two steps: (a) It supposes that the fuse is surrounded by some object that acts as a heat sink (that is, an object that can absorb, without changing its temperature, all the heat produced by the fuse), and then (b) it specifies this temperature (the "ambient temperature" of Rule #3) and also states that the thermal contact between the fuse and the environment at this temperature must be good enough to limit the temperature rise of the fuse's case to 70 °C (or 85 °C for 10 A and for 15 A ratings).

For example, while Rule #3 states that a fuse's interruption current is 80% of its rating at room ambient temperature when the environment is at +125 °C, the actual temperature of the fuse case could be anywhere in the range +125 °C to +195 °C (or +210 °C for 10 A and for 15 A ratings), depending on the effectiveness of the thermal contact between the fuse case and the environment. We shall see in Chapter 6 that this uncertainty introduces a substantial uncertainty in the interrupt current of fuses rated at 5 A through 15 A, so the consequence of this two-step approach is to introduce uncertainty in the interrupt current.

Since the effect of the thermal connection between the fuse and its environment is addressed as a limitation on the temperature rise, then this rule acts as a requirement on the way the fuse is mounted in its use. It is not a requirement on the construction of the fuse. It is implicitly a requirement that the fuse be mounted so that its thermal resistance to a heat sink at ambient temperature, $\mathcal{R}$, is not more than a certain value, $\mathcal{R}_{max}$, which depends upon the maximum current, I_{max}, that the fuse will carry in its assigned use: $\mathcal{R}_{max} = \Delta T/(I_{max}^2 R_{fuse})$, where ΔT is the maximum allowed temperature rise (70 °C for all ratings except 10 A and 15 A, and 85 °C for 10 A and for 15 A ratings) and R_{fuse} is the resistance of the fuse at the current I_{max} and the fuse's operating temperature. This implicit requirement is made explicit in Table 2.1, which lists the maximum value that the thermal resistance can have in order for a fuse not to suffer an excessive temperature rise when driven at its rated current.

The values of thermal resistance listed in Table 2.1 must be recalculated when the maximum current limits are changed. For example, in order to limit a fuse's temperature rise to 70 °C (or 85 °C for 10 A and for 15 A ratings) when it is being tested at 110% of its rating, the listed thermal resistances must by reduced by 40% (i. e., each value of $\mathcal{R}_{max}$ listed in Table 2.1 must be multiplied by 0.60).[12] On the other hand, fuses are usually chosen using a derating scheme: for example, a 3 A rating may be used in a circuit that will never carry more than 1.5 A during correct operation; then, that fuse's temperature rise can be limited

[12]Increasing the current by 10% increases i^2 by 21%, and the fuse's resistance also by about 20%; hence, the joule power increases by about 40%.

to less than 70 °C with a thermal resistance of about five times the value listed in Table 2.1.[13]

2.3 The effect of air, or of a vacuum, within the fuse

While MIL–F–23419/8F specifies some of the materials for the FM08 fuse, it says nothing about the gas filling the void region between the fuse filament and the barrel. This region is certainly filled with ordinary air during the assembly of this style of fuse. The loose-fitting end caps are slid into place, and a seal of uncertain permeability is effected during the soldering operation that attaches the fuse filament to the end caps. The heat shrink plastic tube further decreases the rate at which fluids (gases and liquids) can exchange between the inside and outside of the fuse. The integrity of this seal is tested by immersing the fuse into clear mineral oil at 125 °C for one minute: no bubbles should be detected.[14] That is, this test would see a leak rate no smaller than about 0.1 $mm^3 \cdot min^{-1} \cdot atm^{-1}$. However, when the fuse is placed in a vacuum, essentially all the air could leave the fuse cavity in a year with a leak rate several orders of magnitude lower, so this test is not sensitive enough to ensure that these fuses are sealed tightly enough for years of use under vacuum conditions. Without air within the cavity, an important heat conduction mechanism is lost, and the actual interruption current of the fuse changes. In practice, fuses installed into flight equipment are enclosed within conformal coatings and/or potting compounds, which would decrease the uncertain leak rate of the fuse by an unknown factor.

Air provides a thermally conductive path between the filament and the barrel of the fuse; this conduction is increasingly important as the rating decreases below 3 A, and becomes dominant for ratings of 1/2 A and below. For example, a fuse rated at 3 A by MIL–F–23419/8F will have its steady-state interruption current lowered by about 10% when its air is removed, while a fuse rated at 1/2 A by MIL–F–23419/8F will have its steady-state interruption current lowered by a factor of about 3 to 4 when its air is removed.

On the other hand, a hot filament oxidizes when air is present, thus, a fuse rated at 3 A that would never interrupt at 3.5 A when oxidation was precluded by evacuating the case, can interrupt after a few days at 3.0 A. Hence, the role of air in the case of a fuse is complicated: For spans of up to several minutes, air increases the steady-state interruption current. But for spans of hours to days, air decreases the steady-state interruption current.

The reliability of FM08 fuses would be increased, as will be shown in Appendix E, if (a) the fuse case were filled with an inert gas such as dry nitrogen, after out-gassing at an elevated temperature[15] and (b) the fuse case were sealed such that the fill gas would be retained for

[13] A more complete application of the principle of derating would require that the temperature rise be limited to distinctly less than 70 °C (or 85 °C for 10 A and for 15 A ratings).

[14] As per MIL–F–23419/8F, Quality assurance: (a) Seal. However, Reference [8] modifies this to "Insert in silicone oil at $125(+5, -0)$ °C one inch below the surface of the liquid: [there shall be] no continuous stream of bubbles."

[15] This was also the conclusion reached on the basis of both experiment and theory, reported in 1967 by Samuel J. Keene, Jr. of GSFC. See Reference [9]

at least 20 years.

2.4 The voltage rating of a fuse

Fuses also have a voltage rating, but this has a different meaning than the current rating. These fuses are physically small, and too large a voltage could evaporate the filament to produce a plasma and thus, an arc, leading to undesired flow of current for a much longer time than desired, or even an explosion. Or too large a voltage could vaporize the fuse filament, redepositing it as a uniform film of metal on the inside of the barrel, producing a low enough resistance to permit an undesired flow of current. Such arcs, or other breakdowns, will not happen when the fuse is used in circuits that cannot apply more than the rated voltage to the fuse. The specified maximum voltage for an FM08 fuse is 125 volts for current ratings from 1/8 A to 10 A, and is 32 volts for 15 A current rating; any smaller voltage is acceptable.

2.5 The cold resistance and the hot resistance

The primary variable controlling the current rating of a fuse constructed as shown in Figure 2.1 is the cold resistance of the fuse filament, R_{cold}, defined as its electrical resistance measured at 10% or less of the rated current, at a temperature between 20 °C and 25 °C.[16]

Since the cold resistance is as low as 3.6 mΩ, a conventional ohmmeter is not appropriate. Rather, it is necessary to use Kelvin's method of measuring resistance, also known as a "four wire arrangement."[17] Further, the resistance of the lead attached to each end of the fuse can be important: each lead is 1.50 inches long, and the total resistance of both leads is 4.0 mΩ (except for the 15 A rating, where the value is 2.5 mΩ), and so variability in the precise position of attachment of the Kelvin contacts can change the measured resistance by up to this amount. Hence, more attention to lead resistance is appropriate than is currently required by the directive: "Measurements shall be taken ... as close to the fuse element as practicable."[18]

MIL–F–23419/8F specifies minimum and maximum values for the cold resistance, as well as minimum and maximum values for the voltage drop across the fuse filament when it

[16]The current used to measure the fuse's resistance heats the filament and thus, increases its resistance; hence, this current must be limited so that this resistance increase is negligible. Modeling and experiment shows that (a) the resistance measured at 10% of the rated current is about 0.4% greater than the value extrapolated to zero current and (b) increasing the temperature from 20 °C to 25 °C increases the cold resistance by about 1.7%.

[17]The Specification calls explicit attention to this: Paragraph 4.8.3.

[18]Specification, Paragraph 4.8.3.

has been carrying the rated current for a minimum of 5 minutes.[19, 20] Table 2.1 is based on these specifications. Each voltage drop ΔV_{hot} has been converted to a hot resistance, $R_{hot} = I_{rating}\Delta V_{hot}$, in order to facilitate comparison with R_{cold}. And these minimum and maximum values have been replaced by the average values. Inspection shows that these minimum and maximum values are $\pm 10\%$ of R_{cold} and $\pm 15\%$ of R_{hot}.

Table 2.1: Fuse Parameters Per MIL–F–23419/8F

Rated Current	$R_{cold} \pm 10\%$ (mΩ)	$R_{hot} \pm 15\%$ (mΩ)	R_{hot}/R_{cold}	$\mathcal{R}$ (°C/W)
1/8	2 100	8 000	3.81	490
1/4	710	2 780	3.92	350
3/8	420	1 650	3.93	260
1/2	280	1 148	4.10	210
3/4	170	228	1.34	470
1	125	185	1.48	330
1.5	80.0	120	1.50	230
2	55.0	85	1.55	180
2.5	42.0	58.8	1.40	170
3	35.2	54.3	1.54	130
4	23.0	32.5	1.41	120
5	14.0	20.5	1.46	120
7	10.0	14.7	1.47	85
10	6.5	9.8	1.51	80
15	4.0	5.1	1.28	70

We shall see that the ratio of the hot to the cold resistance, R_{hot}/R_{cold}, of a mounted fuse provides important evidence of its reliability when used in that mounting: hence, we require values for it that have the tightest allowable tolerances, so we can obtain the sharpest discrimination possible. However, this ratio is not given explicitly by MIL–F–23419/8F; it must be computed from the separately specified cold resistance R_{cold} and hot voltage drop ΔV_{hot}. See Table 2.1 and also Figure 2.2. The tolerances computed for this ratio from the tolerances of the separate factors (25% if the worst case is assumed and 21% if the average case is assumed) are not the tolerances that are desired, since these reflect the *acceptance*-range for a fuse and not actually the range in values of R_{hot}/R_{cold} that would mark the limits for acceptable fuses. For example, MIL–F–23419/8F can accept a fuse with a cold resistance that 9% greater than the average value: this fuse would have (other things being equal) a hot resistance that is very nearly 9% greater than the average given by MIL–F–23419/8F.

[19] Table I of MIL–F–23419/8F.

[20] The choice of 5 minutes reflects experience with one type of fuse mounting which requires a soak of this length in order to reach thermal equilibrium. However, with proper attention to heat sinking, complete equilibrium can be obtained within 15 seconds: this would permit a useful increase in testing speeds and would decrease the accumulation of filament-oxidation.

Modeling and analysis shows that the proper tolerance of this ratio is ±5%.

2.6 Fuse filament material

It is clear that the material used for the fuse filament must affect the interruption current of the fuse; thus, it is noteworthy that this material is not explicitly mentioned by MIL–F–23419/8F for any fuse rating. However, the ratio of R_{hot}/R_{cold} imposes a firm constraint on possible materials. For example, inspection of this ratio (see Figure 2.2) shows a large discontinuity in behavior as the current rating increases from 1/2 A to 3/4 A: information obtained from the manufacturers, together with the modeling of Chapter 6, shows that this is caused by the change from nickel to a copper-silver alloy. Further modeling has not found any other metal for which the ratio has the values obtained for nickel, and so even though nickel is not explicitly mandated by MIL–F–23419/8F for fuses with ratings between 1/8 A and 1/2 A, few (if any) other materials could be used for this range of ratings of fuses of this style. There is no visible discontinuity between 4 A and 5 A as the fuse filament material is changed from copper-silver alloy to pure copper; modeling finds that few materials other than copper or copper-silver alloy give this observed ratio, and so the choice of this material is also implicitly constrained by MIL–F–23419/8F.

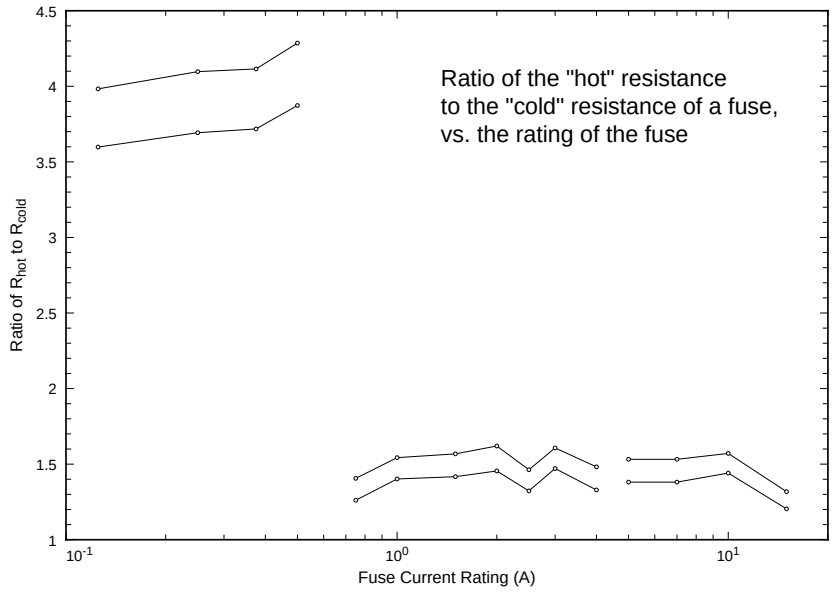

Figure 2.2: A plot of the ratio R_{hot}/R_{cold} versus the rating of the fuse. The discontinuity between ratings of 1/2 A and 3/4 A is the result of changing the filament material from nickel to copper-silver alloy. There is no visible discontinuity between 4 A and 5 A as the material changes to pure copper.

2.7 The time-current curve

A more complete specification of the interrupting behavior of a fuse is given by its *time-current* curve, which reports the time-to-interrupt when the current is suddenly changed from zero to a constant value, and the fuse is initially at ambient temperature, for a wide range of choices of this constant current. While MIL–F–23419/8F specifies certain conditions on the interrupt times at 100%, 110%, 200%, and 300% of the rated current, it does not specify a full time-current curve, including a measure of the reproducibility that can be expected in practice, even though the full curve (with an estimate of reproducibility) constitutes a minimum level of the specification of behavior necessary in professional practice. Such curves have been measured by users, of course, since these are absolutely necessary; one for a 3 A rated FM08 fuse is shown in Figure 2.3. The data are from Reference [8].

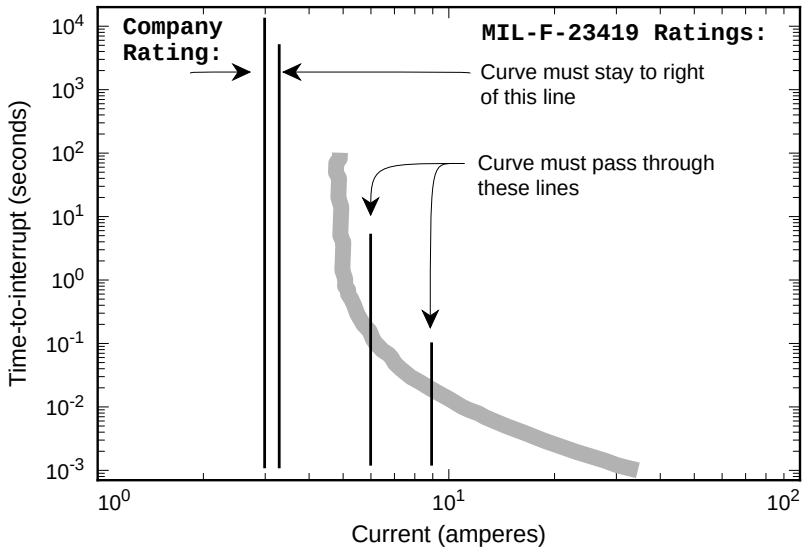

Figure 2.3: The time-current curves for a 3 A FM08 fuse. Also shown are the conditions imposed by MIL–F–23419/8F. Both Littelfuse and Bussmann specify that their FM08 fuses will carry their rated currents for a minimum of 4 hours; this line has also been indicated.

Measured time-current curves for the whole family of FM08 fuses are shown in Figure 2.4. Note that the curve for the 1/2 A fuse crosses over the curve for the 3/4 A fuse: this results from the change in filament material from nickel to copper-silver alloy.

In a real circuit, a fuse is exposed to a much richer variety of current-histories than those discussed in this Chapter, and the fuse's behavior for these to most of these cannot be predicted from either its rating or its standard time-current curve. For example, we often wish to know the time-to-interrupt when the fuse has been carrying a substantial fraction of its rated current, and the applied current then suddenly jumps to a larger value: since this fuse starts hot, its time-to-interrupt will be less than that given by the standard current-time curve. Another example: many circuits present a fuse with an initial inrush surge which may be several times larger than its rated current; hence, we would like to use an

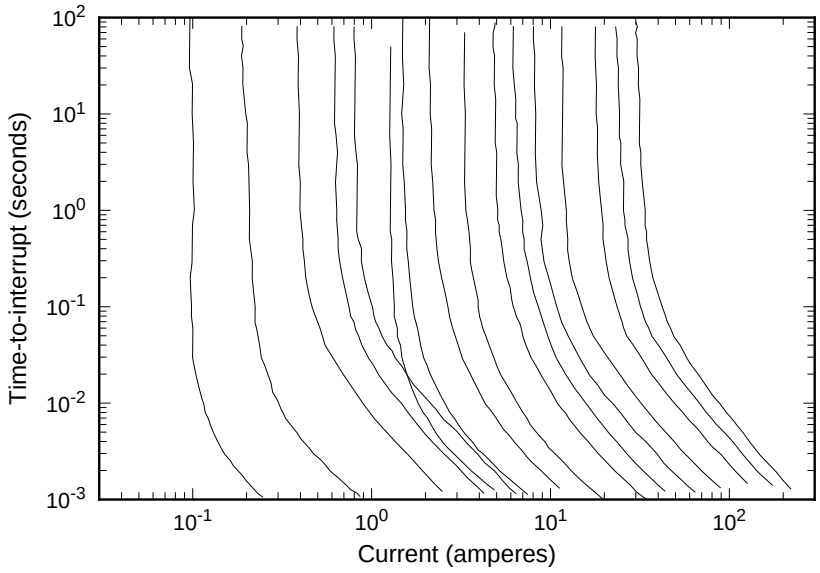

Figure 2.4: Time-current curves for FM08 fuses.

appropriate time-current curve to judge if the fuse will interrupt — but the surge-current is rarely of the form used to construct the standard time-current curve. A third example: the interruption behavior under sinusoidal AC current has a radically different feature — there is a substantial dip in the curve at about the period of the AC frequency, caused by the momentary cessation of the current. Because there are so many different current-histories met in practice, it is impractical to attempt to develop a complete set of answers in advance.

Chapter 3

Construction of an FM08 fuse

The materials used in the parts of the fuse and the method of assembly of these parts affect the behavior of the fuse. MIL–F–23419/8F specifies only some of the materials used in an FM08 fuse and none of the assembly steps. The other materials and assembly steps have been determined by direct inspection, supplemented by conversations with one of the makers (Littelfuse). The materials and the assembly steps have been subject to little or no variation in the past and so the following is likely to be accurate for all FM08 fuses. Still, only what is explicitly contained in MIL–F–23419/8F is required for FM08 fuses.

3.1 Parts and materials

Figure 3.1 is a cut-a-way diagram of an FM08 fuse and Table 3.1 lists the materials used for the parts of an FM08 fuse.

Table 3.1: Materials Used in FM08 Style Fuses

Item	Item Name	Material
1	outer sleeve	polyvinylidene fluoride, modified by radiation
2	barrel	ceramic (MIL–I–10, Grade L3B)
3	filament wire	nickel for ratings of 1/2 A and lower
	" "	copper-silver alloy (50%-50%) for 3/4 A to 4 A
	" "	pure copper with a silver coating for 5 A and greater
4	end cap	9010 brass alloy, gold plated
5	lead	soft copper, gold plated
6	solder	98% tin, 2% silver; melting point 232 °C

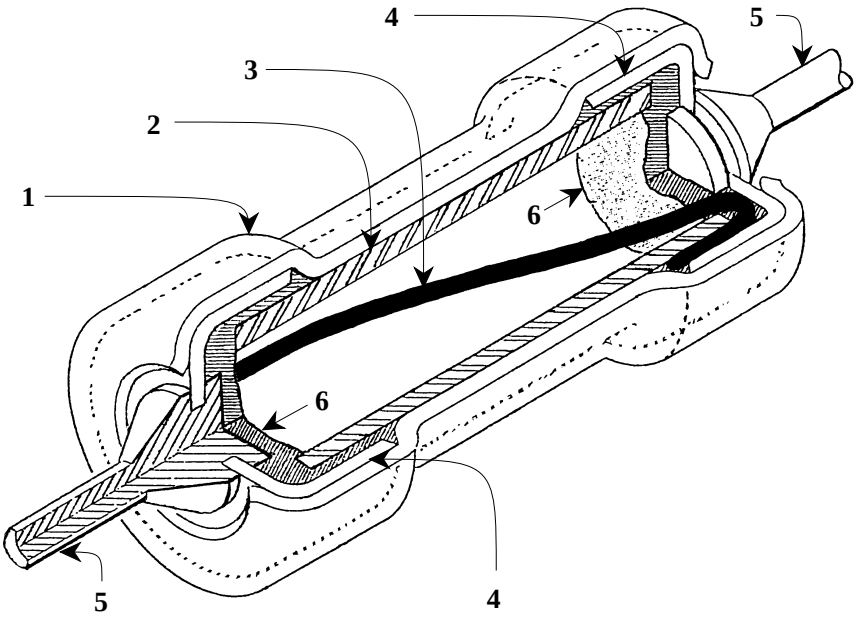

Figure 3.1: Schematic drawing of an FM08 fuse. The numbered items are described in Table 3.1.

3.2 Assembly procedure

Figure 3.2 illustrates one manner in which the parts of an FM08 fuse can be assembled.

1. A cap with attached lead is placed into a socket that clamps it into place, and will soon heat it; also shown is a solder ball that has been placed into the center of the cap.
2. The filament wire is threaded through the barrel, and bent around each end of the barrel; this assembly is about to be lowered and fitted into the cap.
3. The socket has been heated so that the solder ball melts into a flat disk filling the bottom of the cap and seals the filament into place, and also seals the cap and barrel. (This is not a dependably hermetic seal, especially when subject to tensions of a few pounds of force, or bending moments even as small as developed by bending the leads!)
4. The sealed unit has been removed from the socket and inverted. Also, a second cap with attached lead has been placed into the socket.
5. The socket has been heated so that this end is sealed, trapping air inside the barrel.
6. A shrink wrap tube is slid over the barrel and caps, and heated to (174 ± 3) °C to effect the shrinking. This tube increases the mechanical robustness of the fuse, improves the hermeticity, and protects the identifying marks printed onto the barrel just prior to this step.

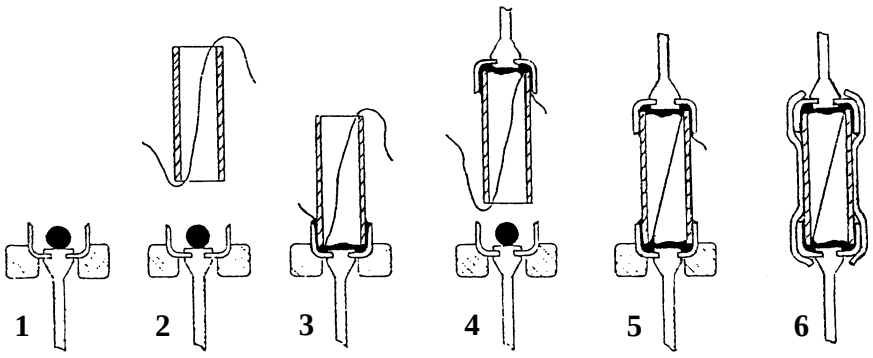

Figure 3.2: Cross sections of stages in the assembly of an FM08 fuse. The steps are described in the text.

3.3 Manufacturing variability

The physical size of the FM08 fuse does not depend on its rating: all ratings have identical packages, except for the gauge of the leads. Each lead is 38.1 ± 1.5 mm (1.50 ± 0.06 inches) long, and is annealed copper. FM08 requires the leads to be gold coated and FM04 does not; the gold coating is too thin to affect electrical and thermal conductivities. For all ratings except 15 A, the gauge of the wire leads is AWG #22; this has an electrical resistance per length of 0.53 mΩ/cm and a thermal resistance per length of 74 °C/(watt·cm) at 20 °C. For the fuse rated at 15 A, the gauge of the wire leads is AWG #20; this has an electrical resistance per length of 0.33 mΩ/cm and a thermal resistance per length of 46 °C/(watt·cm) at 20 °C.[1] Variations of these attributes have negligible effect on fuse behaviors.

MIL–F–23419/8F specifies the maximum length of the package to be 7.90 mm (0.311 inches), and its maximum diameter as 2.62 mm (0.103 inches). The size of the ceramic barrel is particularly important in setting the scale of the fuse, and measurement shows that there is variation (see Table 3.4), but analysis shows that it is too small to have a significant effect on fuse behavior.

[1] If a fuse rated between 3 A and 15 A (inclusive) is connected into a circuit using all of the lead-length that is provided, and no other heat-removal path is provided, then the thermal resistance of the leads exceeds the maximum allowed for operation at full rated current. In other words, leads as long as 38 mm are effectively part of the fuse for this range of ratings, and they affect its performance. Proper design calls for short fuse leads that are well-connected to large gauge circuit buses. One should also provide additional thermal paths for the larger ratings. Operation under reduced current (i. e., derated operation) relaxes these thermal concerns, but does not remove them.

3.3.1 Filament resistance

Table 3.2 lists the statistics in the cold resistance R_{cold} found during one set of measurements carried out by Mr. Peter O'Shea[2] in accordance with MIL–F–23419/8F for FM04 fuses. In this table, the average of the cold resistances of the fuses in each sample is $\bar{R}$, and $\hat{\sigma}_{data}$ is the estimated standard deviation of the population from which the sample is drawn. The estimated standard deviation of the average cold resistance is $\hat{\sigma}_{avg}$. The last column reports $z = (R_{\rm MIL} - \bar{R})/\hat{\sigma}_{avg}$, which measures the statistical significance of the difference between the cold resistances $R_{\rm MIL}$ and $\bar{R}$.

FM04 fuses are expected to show the same statistics as the FM08 fuses since they are made on the same assembly line to the same specifications as far as resistances are concerned.[3] MIL–F–23419/8F contains the provision that FM04 fuses can be qualified as FM08 style, provided that they meet four additional quality assurance requirements: seal testing, voltage drop, resistance, and visual and mechanical inspection. Mr. O'Shea carried out the required visual and mechanical inspection, and any failure of the seal tests that would be so dramatic as to affect measured resistances would produce a resistance "outlier." None were observed.

Table 3.2: Cold Resistance of FM04 Fuses

Rating (A)	Sample size	$\bar{R}$ (mΩ)	$\hat{\sigma}_{data}/\bar{R}$	$\hat{\sigma}_{avg}/\bar{R}$	$\frac{(R_{\rm MIL})-\bar{R}}{R_{\rm MIL}}$	z
1/8	16	2 070	3.7%	0.93%	1.43%	1.5
1/4	25	683	5.0%	0.99%	3.80%	3.8
3/8	75	415.7	2.6%	0.30%	1.02%	3.4
1/2	25	281.8	2.0%	0.39%	-0.64%	-1.6
3/4	25	172.0	3.7%	0.73%	-1.18%	1.6
1	25	126.2	2.2%	0.44%	-0.96%	2.2
1 1/2	25	75.80	2.5%	0.51%	5.25%	10.3
2	75	54.85	2.5%	0.29%	0.27%	-0.9
3	25	34.18	2.9%	0.58%	2.90%	5.0
4	25	21.99	2.6%	0.51%	4.39%	8.6
5	25	13.62	2.9%	0.57%	2.71%	4.8
7	75	9.33	2.2%	0.25%	6.70%	26.8
10	25	6.00	1.5%	0.29%	7.69%	26.5
15	25	3.49	4.3%	0.86%	12.75%	14.8

The average resistances are shown in Figure 3.3; also shown are the values specified by MIL–F–23419/8F. The values measured for these FM04 fuses are all within ±10% of the values specified by MIL–F–23419/8F, with the exception of the set of fuses rated at 15 A for which

[2]Mr. O'Shea made these measurements during 1992 while employed by Paramax at GSFC.
[3]Communication of Littelfuse to Mr. O'Shea.

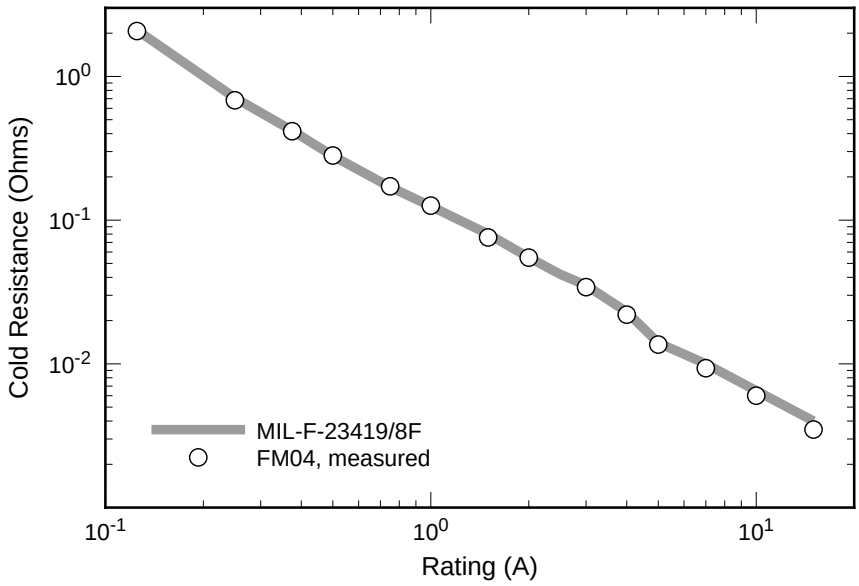

Figure 3.3: The average cold resistance of FM04 fuses versus the rating of the fuse. The specified values for MIL–F–23419/8F are displayed as a band whose width is $\pm 10\%$ of the value specified for each rating. The slight slope irregularities visible in the data and also in the measured values are real.

the measured resistance is 13% low. For ratings 1/8 A through 5 A, the relative differences, $(R_{\mathrm{MIL}} - \bar{R})/R_{\mathrm{MIL}}$, are scattered around 2% with a standard deviation of 2%: there is no clear pattern to the differences over this range; however, R_{MIL} grows steadily larger than $\bar{R}$ as the ratings increase to 7 A and beyond, and the difference exceeds 10% for the 15 A rating. This trend of increasing difference as the rating exceeds 7 A is statistically significant. It may result from a slightly different choice for the length of the leads included within the measurement: if the MIL–F–23419/8F apparatus captures 0.24 inch of lead (on each side of the fuse) more than the apparatus used to make the measurements reported here, then the difference vanishes entirely. In other words, the $\pm 10\%$ limits for R_{cold} mentioned in MIL–F–23419/8F cannot be defended for fuses rated at (or near) 15 A until the length of leads included in the measurement are explicitly stated to within about ± 0.1 inches.

Mr. O'Shea's measurements characterize the variability in cold resistance for fuses manufactured at the same time: all these fuses had the same date code. These measurements do not address characterization of variations related to different date codes. Such variations are of interest and so additional measurements are needed.

MIL–F–23419/8F specifies a range of $\pm 10\%$ for the cold resistance, R_{cold}. If a manufacturing process makes fuses that have a normal distribution of cold resistances with a mean that is at the center of the MIL–F–23419/8F range and a standard deviation of σ_R, then 68% of the run will be acceptable (at least with respect to R-values) when $\sigma_R/R_{cold} = 10\%$; 95.4% when $\sigma_R/R_{cold} = 5\%$; and 99.74% when $\sigma_R/R_{cold} = 3.3\%$. Thus, we can expect that there will be an economic pressure to design the manufacturing process so that the relative standard

deviation of R_{cold} is at least as low as 5% so the acceptance rate is at least as high as 95.4%, but that there is little pressure to obtain a relative standard deviation of R_{cold} much less than 3%, since this value already lowers rejections on this basis to less than 0.26% and other reasons for rejection then become dominant. Obtaining a relative standard deviation for R_{cold} of about 2.4% allows the mean value of R_{cold} to wander by a few percent from the middle of the MIL–F–23419/8F range, and still have an acceptance rate of 99+ %. These relative standard deviations are in good agreement with Mr. O'Shea's data, and this suggests a close conformity between the range for R_{cold} set by MIL–F–23419/8F and the process used to make these fuses.

For some of the ratings, the relative difference between the cold resistance specified by MIL–F–23419/8F and the average of the observed values, $(R_{\mathrm{MIL}} - \bar{R})/R_{\mathrm{MIL}}$, was especially large compared with the statistical uncertainty of this difference. The statistical significance of this difference is measured by $z = (R_{\mathrm{MIL}} - \bar{R})/\hat{\sigma}_{avg}$: "$|z| > 3$" is generally regarded as statistically significant, in the sense that values this large (or larger) are observed rarely (less than roughly 0.5% of the time for a normally distributed population). On this basis, the observed differences between R_{MIL} and $\bar{R}$ are not statistically significant for ratings 1/8, 1/2, 3/4, 1, and 2 A; and they are statistically significant for ratings 1/4, 3/8, 1 1/2, 3 A and higher. But only the difference for the 15 A rating is significant for MIL–F–23419/8F.

The measured cold resistance of the filament depends on its resistivity ρ, its length ℓ, and its cross-sectional area A (all measured at 20 °C to 25 °C) according to $R_{cold} = \rho\ell/A$. Therefore, so long as these factors vary independently, the relative variance of the cold resistance is the sum of the relative variances in ρ, in ℓ, and in A: $(\sigma_{R_{cold}}/\bar{R})^2 = (\sigma_\rho/\bar{\rho})^2 + (\sigma_\ell/\bar{\ell})^2 + (\sigma_A/\bar{A})^2$. We now discuss each of these factors, to better understand the origin of the observed variations in R_{cold}.

Resistivity

The resistivity of a 'commercially pure' copper is affected by the trace elements within it.[4] Nordheim's rule describes the effect on the resistivity of a metal M to which is added an element X: $\Delta\rho_{M,X} = x \cdot A_{X\,in\,M}$, where $A_{X\,in\,M}$ depends on the metal M and on the element X, but not on the concentration of X or x. (This is the linear form of the rule, and only applies when $x \ll 1$.) For example, $A_{S\,in\,Cu} = (10 \pm 1)$ $\mu\Omega$·cm/at-% for sulphur dissolved in copper. Hence, dissolving 0.01 weight-percent of sulphur into copper (so that $x_S = 0.02$ at-%) leaves the copper 'pure' at the level of trace element concentration given in many purchase specifications, but increases the resistivity by 0.2 $\mu\Omega$·cm, which is a relative increase of about 10%: this is a substantial increase. So we can expect some variation in the resistivity of various lots of "commercially pure" copper or copper-silver filament wire. The actual resistivity of the wire must be part of the purchase specification.

The filament wire is formed by drawing it through a die: this introduces a massive number of dislocations and, thus, increases the resistivity. For ratings of 4 A and higher, the wire is

[4]This effect is discussed in greater detail in Appendices B and C.

flattened after being drawn: this introduces more dislocations. And folding the ends of the filament around the barrel's wall (see Figure 3.2) adds still more dislocations. Subsequent heating can reduce, but not eliminate, the concentration of dislocations.[5] The net uncertainty of the resistivity caused by variations in the degree of subsequent annealing is limited to roughly 3% for pure copper and nickel, but reaches 20% for copper-silver alloy, and so the cold resistance — and hence the interruption current — could be uncertain by up to about this amount. All fuses produced in the same way presumably have the same extent of partial reannealing, and hence would be expected to show much less than 3% scatter for pure copper and nickel filaments, and much less than 20% scatter for copper-silver alloy filaments. And indeed, the scatter in the observed cold resistances ranged from 1.5% to 5.0%, with most values close to 2.4%. However, an advance in the extent of annealing is the probable explanation for the decreases (by up to 13%) of the cold resistance that Code 313, Paramax, and Unisys have each measured for copper-silver filament fuses, after repeatedly cycling these fuses at less than their rated currents.

Filament length

The length ℓ_{fil} of the filament varies with the length ℓ_{barrel} of the barrel, with the tightness with which the filament wire is wrapped around the end of the barrel, and with the amount of 'bow' in the filament. (And the effective electrical length also varies with the amount of solder that wicks up each end of the filament.)

The observed length of the barrel is $\ell_{fil} = 0.482$ cm and the variation is about 0.3%, and so this is not an important source of variation. The same is true for the tightness with which the filament wire is wrapped around the end of the barrel.

The barrel has a diameter of $d = 0.068$ cm with a variation of about one to two percent. If the filament is positioned diagonally across the inside of the barrel, which is the desirable positioning and is shown in Figure 3.1 or in part 6 of Figure 3.2, then its length is 1.0% longer than if it were positioned entirely along the same side of the barrel.[6] This increases to 1.3% when the wire is not stretched tightly along the diagonal, but is curved to the extent observed in numerous cases, with the mid-region of the filament near the axis of the barrel.[7] If the filament does not run diagonally, but rather is positioned so that both ends are on the same side of the barrel, with its middle bowed outwards to about the middle of the barrel, as has been observed in a few cases, then its length is also 1.3% longer than it would be without the bow. However, in a few percent of these cases, the filament bows almost to the far side of the barrel (this is an especially undesirable positioning since thermal expansion presses the filament against the inside of the barrel when current is applied, and this leads to different interruption characteristics), and so the increase in the filament's length approaches 5.3%

[5] This effect is discussed in greater detail in Appendices B and C.

[6] This is calculated from the pythagorean theorem $\ell_{fil} = \sqrt{\ell_{barrel}^2 + d^2}$.

[7] The arc length of a parabolic arch spanning a base b and achieving a height a over the midpoint of the base is $\sqrt{b^2 + 16a^2}/2 + [b^2/(8a)] \ln\{[4a + \sqrt{b^2 + 16a^2}]/b\}$, and we use $b = \ell_{barrel}$ and $a = d/2$.

of the barrel's length.[8] Hence, variations in the filament's shape can occasionally introduce a variation in its length, always on the side of increasing the filament's cold resistance. A pair of x-ray images at right angles to each other and to the fuse allows a nondestructive selection of fuses with correctly positioned filaments.

Occasionally, solder is observed to have wicked up one end of the filament for as much as 0.5 mm, which is about 10% of the filament's length: this solder blob provides an additional conductive path and hence lowers the resistance of the filament. Since the electrical resistivity of the 98%-tin 2%-silver solder is roughly 12 $\mu\Omega$·cm, which is roughly five times that of the copper-silver or copper filaments, then the reduction in the filament's resistance would never be as large as the length covered by the wicked solder: a maximum reduction in the filament's resistance of roughly 5% is plausible. The solder's resistivity is twice that of nickel's, and so the reduction could approach the full 10% for nickel filaments. Hence, solder wicking probably does account for some of the observed variation in R_{cold}. An x-ray image allows a nondestructive selection of correctly soldered filaments.

Shape of filament

The shape of the filament portrayed in Figures 3.1 and 3.2 is nearly straight line running diagonally from one end of the barrel to the other. In cylindrical coordinates with the z-axis concentric with the barrel's axis, and one cap at $z = -\ell_{barrel}/2$ and the other at $z = +\ell_{barrel}/2$, the portrayed filament has one end at $(r, \phi, z) = (b, 0°, -\ell_{barrel}/2)$ and the other at $(b, 180°, +\ell_{barrel}/2)$ where b is the inside radius of the barrel.

However, x-ray images indicate that there are substantial variations in this shape. Bending the filament wire around each end cap introduces some curvature such as shown in Figure F.2, while tension applied while completing the assembly can reduce the curvature: observations show that the curvature varies from zero to about double that shown in Figure F.2.

Further, the filament's ends are not always on opposite sides of the barrel (i. e., at 0° and 180°); rather, all values of $\phi_2 - \phi_1$ from 0° to 180° have been observed, where ϕ_1 and ϕ_2 are the locations of the ends of the filament. When the ends are on the same side of the barrel (i. e., when $|\phi_2 - \phi_1| < 45°$), then the filament's shape resembles an archer's bow, $\smile$, and is characterized by the position of the midpoint: in some cases, this midpoint nearly touches the opposite side of the barrel, presenting the possibility that this part of the filament will become pressed against the side of the barrel as a result of the thermal expansion that accompanies the passage of electrical current. As contact is made, further increases in temperature are clamped by the barrel, and so the filament becomes robust against interruption. (We have seen this happen once in the characterization of a hundred fuses.)

We have also observed several cases per hundred studied in which, after the first end of the filament was soldered into place, the second end was twisted: the middle of the filament was then deformed into a three-dimensional curve, and displayed twisting as well as curvature.

[8] This uses the same arc length formula, but with $b = d$ rather than $b = d/2$.

The length of the filament is a function of the shape, as well as the barrel's length, and so the cold resistance will be affected by these shape variations. However, these shapes also are associated with differing degrees of built-in stress. This stress is present along the length of the filament, and is maintained by the end-conditions. Since the ends never become hotter than roughly 125 °C during correct practice, then the stresses they impose are never annealed away but remain imposed, and so they drive creep. When air is present within the barrel and the current is near the rated value, then the temperature of the middle of the filament is substantially less than melting, but is large enough to increase the creep rate to the extent that creep rupture can happen in hours to days. Oxidation increases the mid-filament temperature and further accelerates the creep rate. Thus, the time to rupture becomes a sensitive function of the built-in stresses: the wide range in interruption times that is seen at near the rated current is at least partly caused by the variability in the shape of the filament. Nondestructive selection for shapes is straightforward using x-ray inspection at two angles.

Cross-section of filament

Before we consider the variations in the cross-sectional area A, we need to know its average value for each rating. Further, this average value is of interest in itself in several areas of the modeling of the behavior of the fuse. For example, the heat transported by the fill gas from the filament to the surrounding barrel is proportional to the surface area of the filament, which is related to its cross-sectional area A and the cross-section shape.

It is convenient to use, not A, but the radius a_{eff} of a wire of circular cross-section of the same area: $a_{\mathit{eff}} = (A/\pi)^{1/2}$. Littelfuse provided a table of effective radii (see Table 3.3 and Figure 3.4), but no measures of expected variations of these.

The filament has a circular cross-section for ratings up to and including 3 A; thus, the actual radius a is the same as the effective radius, $a_{\mathit{eff}} = a$. For ratings of 4 A and larger, the wire is flattened before insertion into the fuse, which makes it easier to bend the filament around the end of the barrel and also to fit the cap over the barrel and the wire's end. (See Figure 3.2.) Flattening nearly conserves the original cross-sectional area A, and therefore the effective radius a_{eff} of the flattened filament is nearly the same as that of the wire before flattening.

Peter O'Shea[9] extracted filaments from a fuse of each rating in the FM04 series and also from a fuse of each rating in the Picofuse series[10] supplied by Littelfuse, encapsulated it into epoxy, and prepared a polished cross-section. Mr. O'Shea obtained photographs using

[9]Mr. O'Shea did this work during 1992 while employed by Paramax at GSFC.

[10]Littelfuse names the series 265 Picofuse as the "commercial equivalent" of the FM08 fuse. However, Mr. O'Shea's observed that the filaments of the 265-Picofuses that were supplied to him were corrugated for certain ratings, and he measured current-time curves that are distinct from the current-time curves obtained for FM04 fuses and FM08 fuses. Also, Mr. O'Shea was told by Littelfuse that the 265-Picofuses are machine-assembled, while the FM04 and FM08 fuses were hand-assembled. I measured filament dimensions for these 265-Picofuses that were different from the FM08 fuses of the same ratings.

SEM of each cross-section, and reported the width and the thickness of the filaments. I used optical microscopy to measure to within 2% the same dimensions for the filaments of the six fuses rated from 3 A to 15 A, and found that the optical values were from 1% to 5% higher than the SEM measurements for 3, 4, 10, and 15 A ratings: these measurements are consistent, given the uncertainties in each method. But they were 9% higher for the 5 A rating, and 17% higher for the 7 A rating: these differences are certainly real, and the SEM measurements are in error.[11] I used the SEM photos to measure the shape of the filament for fuses rated from 1/8 A through 15 A, and optical microscopy for 3 A to 15 A; then I computed the area from these measurements of shapes and dimensions, and finally computed the effective radius from the area. See Table 3.3 and Figure 3.4. I estimate there are random uncertainties of about 2% in a_{eff}-Optical, and systematic uncertainties ranging between 2% and 20% in a_{eff}-SEM. These measurements were made on only one filament for each rating, and, thus, cannot be used to estimate the variability of a_{eff} over a population of fuses.

For measurements of the variability of A to be useful in understanding the variability in R_{cold} (which is roughly 3%), A must be measured with an accuracy of roughly 1%, and, thus, a_{eff} must be measured with an accuracy of roughly 0.5%. This cannot be done with routine SEM methods, or with optical microscopy for ratings of roughly 5 A and lower. It is at the edge of what can be achieved using optical microscopy for ratings of 7 A and higher. One method of measuring the variability of a_{eff} to the required sensitivity would be to illuminate the filament wire with a laser, and inspect the diffraction pattern produced on a screen or CCD array: visual inspection easily sees variations that translate into 0.3% changes in a_{eff}, while automated capture methods allow continuous inspection at the 0.03% level. This inspection could be carried out while running wire from one spool to another, or from a spool into the fuse assembly procedure.

I also computed effective radii from the values of cold resistance specified by MIL–F–23419/8F, R_{MIL}, values of the resistivity of the material used in the filament,[12] ρ, and the measured length of the filament ℓ_{fil}: $a_{\mathit{eff}} = \{\rho\ell_{\mathit{fil}}/[\pi(R_{\mathrm{MIL}} - R_{\mathit{leads}})]\}^{1/2}$, where R_{leads} is an estimate of the contribution of the leads (and the caps and the solder) to R_{MIL}: this is a small correction except for the 15 A rating. See Table 3.3 and Figure 3.4.

In the table are presented the effective radii a_{eff} of the filament of a fuse, in microns, from four sources. Littelfuse provided the values in the second column. The "optical" and "SEM" values were obtained using an optical microscope and a SEM, respectively, to determine the shape and dimensions of the filaments; then, a_{eff} was computed from the shape and these dimensions. The "R, ρ, ℓ" values were determined from the cold resistances as specified in MIL–F–23419/8F (with a small correction for lead and cap resistances), from the appropriate values of electrical resistivity ρ, and from the value of the filament's length ℓ measured for a number of fuses. The last column, a_{eff}-Average, is the average of the optical, SEM, and (R, ρ, ℓ) values; it agrees with the values provided by Littelfuse typically to within ±3%,

[11] A decade and more ago, magnifications reported by SEMs were rarely reliable to within ±10% unless special care was taken. Mr. O'Shea used a modern SEM whose magnification was supposed to be dependable to roughly 5%, but direct examination of the same specimens using calibrated optical microscopes (errors less than ±2%) shows that this SEM's errors were sometimes larger than expected.

[12] These values are discussed in the appendices.

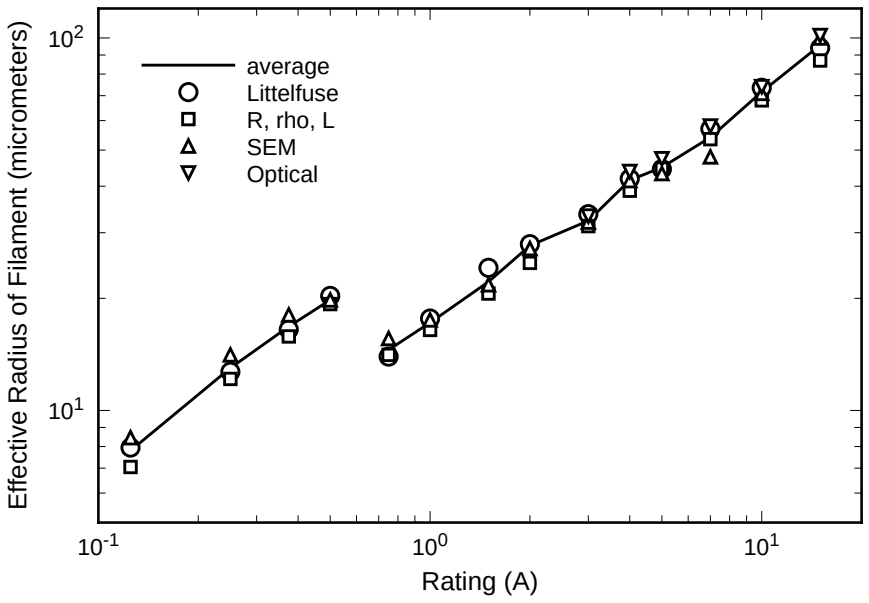

Figure 3.4: The effective radius a_{eff} of the filament of a fuse, for various ratings. The effect of the change from nickel to copper-silver is substantial.

with one excursion to 8% for the 1.5 A rating. The ratings at which the filament material changes are separated by lines. Note that filaments have a circular cross-section for ratings of 3 A and less, and a flattened cross-section for ratings of 4 A and greater.

Approximate values for the component standard deviations are 3% for R_{MIL}, 3% for ρ_{Cu} & ρ_{Ni} and 20% for ρ_{Cu-Ag}, and 3% for ℓ_{fil}. Hence the approximate standard deviation for a_{eff}-(R, ρ, ℓ) is 3% for those ratings having a pure metal filament (1/8 A through 1/2 A, and 5 A through 15 A) and 10% for those ratings having an alloy filament (3/4 A through 4 A).

The comparison between these different-sourced estimates of a_{eff} is sharpest for ratings 4 A through 10 A: the filament material is always copper (and so there is the least uncertainty in ρ) and the optical measurements should be reliable. The R-based value for 15 A is probably less reliable than for the other ratings since the effect of the leads and end caps on R is becoming large for the 15 A rating. We find that the resistance-based values of a_{eff} are (9 ± 3)% lower than the optically measured a_{eff} for ratings 4 A through 10 A; thus, there is a systematic difference that is larger than the uncertainty of 4% predicted from their individual uncertainties; the scatter around this value is about that expected from their individual uncertainties. This systematic difference is not statistically significant at the 95% level, but it is provocative. I have no explanation for it.

An average of the effective radii based on optical microscopy, SEM, and resistance methods is close to the values provided by Littelfuse: these agree typically to within ±3%, with one excursion to 8% for the 1.5 A rating. Hence, either the Littelfuse value or this average can be used for a_{eff}; the error should be less than 10%.

Table 3.3: Effective Radii of the Fuse Filaments

Rated (A)	a_{eff}-Littelfuse	a_{eff}-Optical	a_{eff}-SEM	a_{eff}-(R,ρ,ℓ)	a_{eff}-Average
	(μm)				
1/8	7.95		8.5	7.1	7.8
1/4	12.7		14.1	12.2	13.0
3/8	16.5		18.1	15.8	16.8
1/2	20.3		19.8	19.3	19.8
3/4	14.0		15.6	14.1	14.6
1	17.7		17.5	16.5	17.2
1.5	24.2		21.8	20.6	22.2
2	28.0		27.2	24.9	27.7
3	33.7	33.3	32.1	31.3	32.3
4	41.9	43.8	41.4	38.9	41.5
5	44.5	47.4	43.3	44.6	45.0
7	57.0	58.0	48.0	53.5	54.1
10	73.0	74.0	71.0	68.0	71.7
15	94.0	101.5	100.0	87.0	95.7

The variability of R_{cold}: summary

The standard deviation of R_{cold} is expected to be about 3.3% on the basis of the $\pm 10\%$ acceptance tolerance specified by MIL–F–23419/8F and the supposition that the manufacturing process is designed to produce a yield of at least 99%, but not 99.9+ %, on the basis of R_{cold} alone. And it was observed to range from 1.5% to 5.0%, with most values being close to 2.4%, in the measurements previously discussed in Chapter 3.3.1.

Since $R_{cold} = (\rho\ell)/(\pi a_{\mathit{eff}}^2)$, then $\sigma_R = [(\sigma_\rho/\bar{\rho})^2 + (\sigma_\ell/\bar{\ell})^2 + 4(\sigma_{a_{\mathit{eff}}}/\bar{a})^2]^{1/2}$, if variations in these quantities are independent of each other. The standard deviation of the resistivity is 3% for the copper and nickel filaments. It is as large as 20% for the copper-silver filaments. The standard deviation of the length of the filament is roughly 2%. And the standard deviation of the effective radius has not been determined, but is certainly a positive number. Combining these as if they were independent, we compute that the standard deviation of the cold resistance is at least 4% for fuses with copper and nickel filaments, and could be as large as 20% for fuses with copper-silver filaments. These are larger than observed, and this is evidence that variations in the component quantities are not independent. Perhaps the wire used for the filaments is accepted on the basis of its resistance per length, and not on the basis of separate resistivity and radius criteria: this would correlate variations in ρ and a_{eff}.

3.3.2 Parameters for the barrel, shrink wrap, and caps

The barrel is specified by MIL–F–23419/8F to be made of a ceramic as per MIL–I–10, Grade L3B. The range of thermal capacities and thermal conductivities of the various ceramics that are consistent with this specification are large enough to produce small but measurable differences in the constant-current behavior of FM08 fuses. In fact, Littelfuse uses AlSiMag665 L533C.[13] Fixing on the use of one particular ceramic, rather than using sometimes one and sometimes another, removes a possible source of variation.[14]

Barrels were extracted from ten FM08 fuses studied by Code 313 over the last four years; these were manufactured at different times over the last decade and a half. The lengths of all the barrels observed were within 0.4% of 0.482 cm: the lengths are tightly controlled. The inside diameter, the outside diameter, and the wall thickness of the barrels varied to a larger degree. Some typical examples of this variation are given in Table 3.4. Variations within a sample are small compared to variations between samples. But these variations are too small to affect the behavior of these fuses. The mass of several barrels were measured, and the density reported by Littelfuse for this ceramic, 2.8 g/cc, was confirmed.

Table 3.4: Dimensions Measured for Two Sets of Barrels

Sample Size	Inside Radius b, (mm)	Outside Radius (mm)	Wall Thickness (mm)	Length ℓ, (mm)
4	0.34 ± 0.02	0.67 ± 0.03	0.342 ± 0.002	4.83 ± 0.01
6	0.427 ± 0.002	0.713 ± 0.004	0.286 ± 0.002	4.81 ± 0.01

Measurements of the thickness of several specimens of shrink wrap give an average of 0.21 ± 0.01 mm. The mass of several specimens were measured, and the density computed: this density was consistent with that reported by several tables for this material, 1.77 g/cc.

The mass of one cap was determined by weighing and by computation from the observed dimensions: 19.9 mg.

The mass of each fuse in a sample of four fuses, each without leads, was determined by direct weighing, and by summation of its parts: (69.2 ± 3.1) mg. The agreement between the direct weighing and the summation of the parts supports the computation of the total heat capacity of the fuse by summation of the heat capacity of each of its parts: (38 mJoule/°C) $\pm 10\%$. This value is of interest in computing the time for the fuse to approach thermal equilibrium.

[13] Document supplied by Littelfuse.

[14] 265-Picofuses use a glass tube, with a thermal conductivity that is roughly an order of magnitude lower in thermal conductivity than AlSiMag665 L533C. These allow the steady-state mid-barrel temperature to be significantly higher than if AlSiMag665 L533C were used.

Chapter 4

Thermal model of fuse: Principles

An electric current flowing through the fuse works against the electrical resistance of the fuse's leads and its filament to produces joule heat. By design, most of this heat is produced within the filament, and the filament is relatively thermally isolated, and so the largest increase in temperature happens there. As the filament's temperature increases, it loses heat by conduction along its length into the end caps of the fuse, by conduction through the air into the barrel, and by radiation into the barrel. The temperatures of these parts increase, which affects their rates of heat exchanges with each other and with the environment. If the current becomes large enough, then the filament's temperature can be raised to the melting point of the filament material: the filament will open and interrupt the flow of current.

But other processes also can be important. A steady current that is too low to melt the filament can still heat it enough to oxidize its conductive metal into nonconductive oxide: this leads to increased heating and therefore an increased rate of oxidation, and eventual interruption at a current too low to melt the unoxidized filament.[1] Also, the assembly of the filament leaves it in a stressed condition, and so mechanical creep must be considered for temperatures above about half the melting temperature (measured on a absolute scale); this creep can result in an interruption even when the temperature is always below the melting temperature.[2] Also, repeated pulses, no one of which would lead to the interruption of a new filament, can accumulate sufficient thermal fatigue to produce interruption.[3]

Hence, the computation of the current that will produce an interruption requires attention to the rates of heat production and loss, to fatigue, creep, oxidation, and melting, and perhaps to other processes as well. In general, the competition among these rates and processes makes for a complicated problem. However, there are several situations that allow a great simplification:

- When the current I is applied as a large enough pulse, then the time to raise the

[1] See Appendix E.
[2] See Appendix F.
[3] See the discussion at the end of Chapter 5.

filament's temperature to its melting point is so short that heat losses, creep, and oxidation can be ignored. Fatigue can also be ignored when only a single pulse is applied to a new filament. Hence the problem simplifies to the thermal behavior of the filament alone. This is considered in Chapter 5. The result is that interruption happens in a time τ such that

$$\int_0^\tau I^2\,dt \approx \text{constant}\,,$$

where the value of the constant depends only on the rating of the fuse. This relation between the current-history $I(t)$ and the interruption time τ controls the short-time behavior of the time-current plots presented in Figures 2.3 and 2.4.

- When the current is increased slowly enough so that thermal equilibrium always applies (i. e., heat losses are important, while transient effects are negligible), then dynamical effects can be ignored. The problem is still complicated, but further simplifications are possible. Suppose the current is large enough to produce interruption before the filament has time to oxidize:

  - Fuses with low ratings generate little heat, and so it is a good approximation that their environment remains isothermal during their operation: their casing (barrel and end caps) can be regarded as remaining at the ambient temperature, and a model of the thermal environment is not needed. The discussion of Chapter 6.3 (i. e., Chapter 6, Section 3) shows that this approximation is useful for ratings up to roughly 4 A.
  - Fuses with large ratings have thick filaments and so thermal conduction through the filament into the end caps dominates thermal conduction through the air in the barrel: air conduction can be ignored to a good approximation. The discussion of Chapter 6.3 shows that this approximation is useful for ratings down to roughly 1 A.

  Hence, the simplest possible model of a fuse considers only the filament in a vacuum, with each end clamped at the ambient temperature; and this model offers an approximation to the behavior of fuses over a narrow range of ratings, 1 A to 4 A. This model is developed in Chapter 6. The effects of the fuse's heating of the immediate environment can be treated as a perturbation of the simplest model, and this extends its usefulness up to ratings of 15 A: see Chapter 6.3. And the effects of air conduction on the filaments temperature can also be treated as a perturbation, extending the usefulness to ratings down to 1/8 A: see Chapter 6.2.

  Oxidation and creep-to-rupture can also be treated as appropriate perturbations on the simplest model. These processes are discussed in the Appendices.

We will begin with the equations that describe the production of heat within the filament, and its flow into its sinks, with the accompanying changes of temperature. Then we will construct the various approximations as per the list just given, and compare results with

experiment. We find that the behavior of real fuses under certain common current histories can be successfully modeled with simple combinations of these ideas.

Direct inspection of the temperature distribution along the fuse filament would be desirable: It is the life-controlling quantity, and so it is of interest in its own right, and it would allow direct comparisons to be made with the models. However, there is no nondestructive way to measure this distribution directly. For example, the fuses of interest have fuse filaments that are too small to permit the nonintrusive attachment of thermocouples or other thermal gauges, and the barrels of most fuses are opaque in the thermal infrared and this prevents IR imaging.[4]

Fortunately, the structure of FM08 fuses is simple enough that a theoretical model is reliable. Further, as shown in Chapters 5 and 6, and in Appendix D, the electrical resistance computed from this model agrees with measurements, giving us increased confidence in the model.

4.1 The behavior of thermal currents

The equations that control the temperature distribution are based on (a) energy conservation, (b) Fourier's law of heat flow, (c) Joule's law of electrical heating, (d) Ohm's law of electrical flow, and (e) Stefan-Boltzmann's law of radiation. See for example Reference [6].

Conservation of energy is expressed as

$$\partial_t u + \nabla \cdot \mathbf{J}_h = \mathcal{P}\,, \tag{4.1}$$

where the energy density is $u = \lim_{V\to 0} U/V$ (where U is the energy in the volume V of the material), $\mathbf{J}_h$ is the heat current density, and $\mathcal{P}$ is the power source density.

The Thermal capacity of a piece of material relates its change in temperature to the amount of heat absorbed during this change, when there are no phase transitions or chemical reactions happening:

$$C = \frac{d(\text{heat})}{dT} = \frac{dU}{dT} + \frac{d(\text{work})}{dT}\,. \tag{4.2}$$

The conventional measurements of heat capacity hold constant the pressure exerted by the environment, and the result is called the isobaric heat capacity C_p; other values are obtained for other processes of heat absorption, and conventional thermostatics organizes the interrelations among a number of these. For the materials of interest in the study of FM08 fuses, and for the processes of interest, it is the isobaric heat C_p (and its value per volume, the

[4]Ms. D. Kolos (Code 313) was successful in removing enough of the side of a fuse to expose its filament without damaging the filament. When current was passed through this fuse, its electrical resistance showed a dependence on current that was typical for fuses of this rating, for short times. Thus, it is possible to directly measure the temperature distribution along the filament of an FM08 style fuse using a microscope operating in the far IR. Code 313 has since obtained this equipment, and so perhaps this direct inspection can be made in the future.

isobaric specific heat $c = C_p/V$) that is needed, and

$$\partial_t u = c \cdot \partial_t T \,. \tag{4.3}$$

However, when the filament is melting, then $\partial_t u = L \cdot \partial_t v_{liq}$ where v_{liq} is the volume fraction of liquid and L is the latent heat of melting.

FOURIER'S LAW applies to the materials used in fuses: The heat current density $\mathbf{J}_h$ is proportional to the temperature gradient ∇T:

$$\mathbf{J}_h = -k_T \nabla T \,, \tag{4.4}$$

where k_T is the thermal conductivity. The thermal conductivity k_T is a material property of the substance at that location: it depends on the state-specifiers for that substance, such as the temperature T and mass-density ρ. The thermal resistivity, which is the inverse of k_T, is sometimes more convenient to use.

These relations provide a rule for the dynamics of the temperature distribution within a material when there are no phase transitions or chemical reactions:[5]

$$c \cdot \partial_t T - (\nabla k_T) \cdot (\nabla T) - k_T \cdot (\nabla^2 T) = \mathcal{P} \,, \tag{4.5}$$

where the material parameters c and k_T are appropriate for the particular material.

Within each of the materials used in the construction of fuses, the thermal conductivity develops a spatial variation caused by temperature changes: $\nabla k_T = (dk_T/dT) \cdot \nabla T$. Thus, the ratio of the two terms involving k_T is

$$\frac{\nabla k_T \cdot \nabla T}{k_T \cdot \nabla^2 T} = \frac{1}{k_T}\frac{dk_T}{dT} \cdot \frac{(\nabla T)^2}{\nabla^2 T} = \frac{d\ln(k_T)}{dT} \cdot \frac{(\nabla T)^2}{\nabla^2 T} \,; \tag{4.6}$$

inspection of $d\ln(k_T)/dT$ and of $[(\nabla T)^2/\nabla^2 T]$ throughout the fuse shows that the ratio is negligibly small, except for air inside the barrel for which both terms must be considered. When the spatial variations of k_T are neglected, then T satisfies a driven diffusion equation:

$$\partial_t T = \mathcal{D} \cdot \nabla^2 T + \mathcal{P}/c \,; \tag{4.7}$$

this explains the name of the thermal diffusivity $\mathcal{D} = (k_T/c)$: this parameter measures the dynamics with which a temperature event diffuses from one location to another.

The solution of Equation 4.5 or 4.7 requires conditions on T and $\hat{\mathbf{n}} \cdot \nabla T = \partial_n T$ over the boundary of each material. Along a boundary surface where one material (X) joins another

[5] Air within the fuse cavity is free to move, and gravity (or other impressed accelerations) acting on the differential density that results from the differential temperature distribution of this air can drive air into motion: this motion is called *convection*. However, both my theoretical estimates, and direct experimental tests by Mr. Van Sant and Mr. Munoz (Code 313), show that the convective effects are negligible compared with conductive effects for accelerations of one g or less. This depends on the small size of the fuse. Convective effects would be important if the fuse barrel's inner diameter were more than an order of magnitude larger, or if the impressed acceleration is increased by three orders of magnitude, or if a combination of these changes were made.

(Y), the temperature is continuous: $T_X = T_Y$, and the normal component of the heat current is continuous:

$$\hat{\mathbf{n}} \cdot (\mathbf{J}_h)_X = \hat{\mathbf{n}} \cdot (\mathbf{J}_h)_Y \,, \tag{4.8}$$

where $\hat{\mathbf{n}}$ is a unit vector normal to the boundary surface. The latter boundary condition on $\mathbf{J}_h$ can be expressed entirely in terms of $\nabla T(\mathbf{r})$:

$$\mathbf{n} \cdot [(k_T)_X (\nabla T)_X] = \mathbf{n} \cdot [(k_T)_Y (\nabla T)_Y] \,, \tag{4.9}$$

or

$$(k_T)_X (\partial_n T)_X = (k_T)_Y (\partial_n T)_Y \,. \tag{4.10}$$

Ohm's law applies with useful accuracy to the conductors used in the construction of the fuse: The electrical current density $\mathbf{J}$ is proportional to the electrical field intensity $\mathbf{E} = -\nabla V$:

$$\mathbf{J} = \sigma \mathbf{E} = -\sigma \nabla V, \tag{4.11}$$

where V is the electrical potential and σ is the electrical conductivity, which depends on the material and its state. The electrical resistivity ρ is sometimes more convenient than σ; these are related by $\rho\sigma = 1$ at each point.

Joule's law of electrical heating specifies the heat power density caused by an electrical current $\mathbf{J}$ working against an electrical field $\mathbf{E} = -\nabla V$, where V is the electrical potential, as

$$\mathcal{P}_J = \mathbf{J} \cdot \mathbf{E} = \rho \cdot J^2 = \sigma \cdot (\nabla V)^2 \,; \tag{4.12}$$

the first form is always valid, while the second and third are valid when Ohm's law applies.

The Stefan-Boltzmann law for the intensity of radiation $\mathcal{I}_{SB}$ emitted by a surface of (hemispherical) emissivity ϵ and temperature T is

$$\mathcal{I}_{SB} = \epsilon \sigma_{SB} T^4 \,, \tag{4.13}$$

where σ_{SB} is the Stefan-Boltzmann's constant. At the surface between an opaque material and a transparent one, the opaque surface S_1 radiates with a heat source surface density of strength $-\epsilon_1 \sigma_{SB} T_1^4$, where ϵ_1 is the emissivity of surface 1. And this surface absorbs with a heat source surface density of strength $\alpha_1 \mathcal{I}_1$, where α_1 is the (hemispherical) absorptivity of the surface and $\mathcal{I}_1$ is the radiant intensity incident onto it. The radiant intensity is caused by radiation from another surface S_2:

$$\mathcal{I}_1 = \int_{S_2} \frac{\epsilon_2 \sigma_{SB} T_2^4}{r^2} \, \hat{\mathbf{r}} \cdot d\mathbf{s} \,, \tag{4.14}$$

where r is the radius vector from the emitting surface element to the absorbing surface element, $\hat{\mathbf{r}} = \mathbf{r}/r$ is the unit vector in that direction, and $d\mathbf{s}$ is the element of surface area emitting the radiation. Hence, the energy source surface density at an interface S_1 is

$$\text{energy source surface density} = -\epsilon_1 \sigma_{SB} T_1^4 + \alpha_1 \int_{S_2} \frac{\epsilon_2 \sigma_{SB} T_2^4}{r^2} \, \hat{\mathbf{r}} \cdot d\mathbf{s} \,. \tag{4.15}$$

4.2 The general model of the fuse

Applying these ideas to the heating of a fuse filament, we take $\mathcal{P} = \mathcal{P}_J +$ surface sources, where $\mathcal{P}_J$ is the Joule heat and the second term measures the effects of the loss of heat from the surface of the filament by air conduction and by radiation. We then work from the fuse filament outward, applying the differential equation for the temperature distribution within each material and the boundary relations at each interface, until enough of the thermal environment is included.

4.2.1 Application to the fuse filament

Within the fuse filament, the equation for the temperature distribution is

$$c \cdot (\partial_t T) - k_T \cdot (\partial_z^2 T) = \mathcal{P}_J - \frac{2}{a}\left[J_r^{air}(a) + J_r^{rad}(a)\right] , \tag{4.16}$$

where $\mathcal{P}_J$ is the Joule heat source density, $J_r^{air}(a)$ is the heat current drained out of the filament by air conduction, and $J_r^{rad}(a)$ is the heat current drained out of the filament by radiation; each term is a function of the time t and the position z along the filament. The laplacian of the temperature, $\nabla^2 T = (1/r)[\partial_r(r\partial_r T)] + (1/r^2)(\partial_\theta^2 T) + (\partial_z^2 T)$, is dominated by the z-term only: variations of the temperature with azimuthal angle θ or with the radial distance from the center of the filament r are negligible. The boundary conditions are that $T = T_{caps}$ at each end of the filament, $z = \pm\ell/2$, where ℓ is the length of the filament.

The Joule heat source density is $\mathcal{P}_J = \rho\mathbf{J}^2 = \rho \cdot (I/A)^2$ where I is the current through the filament, whose cross-sectional area is A.

The heat current drained out of the filament by air conduction is computed from the temperature distribution throughout the air within the barrel:

$$\mathbf{J}_h^{air} = -k_T^{air} \cdot \nabla T^{air} , \tag{4.17}$$

where this distribution satisfies

$$c^{air} \cdot (\partial_t T^{air}) - (1/r)[\partial_r(r k_T^{air} \partial_r T^{air})] = +\frac{2J_r(a)}{a} - \frac{2J_r(b)}{b} . \tag{4.18}$$

In this case, it is the variation of T^{air} with the radial distance from the axis of the filament r that dominates the spatial variations; both $\partial_z T^{air}$ and $\partial_\theta T^{air}$ are negligible. The variation of k_T^{air} with position is not negligible and must be addressed. There are boundary conditions at $r = a$ (the radius of the filament) and at $r = b$ (the inside radius of the barrel): the temperature is continuous at each location. This equation assumes that there is no convection of air, which is a good approximation for FM08 fuses operated under accelerations of no more than some tens of g's: the viscosity of air, the small radius of the barrel, and the relatively low operating temperatures of the fuse all limit air convection to negligible levels. The time-dependence of T^{air} may be important, depending on the current history.

The heat current drained out of the filament by radiation is approximated by

$$J_r^{rad}(a) = \epsilon_{SB}\sigma_{SB} \cdot (T^4 - T_{barrel}^4)\,, \tag{4.19}$$

where the complicated integrals over the various view factors have been greatly simplified, and T_{barrel} is the temperature of the inside of the barrel. Radiation effects for the filaments of FM08 fuses are, in fact, very small compared with the conduction of heat along the filament into the end caps; thus, crude approximations in the radiation term do not degrade the model. This loss is established in the time for light to travel across the fuse's barrel (roughly 10^{-11} seconds), so we can ignore dynamical effects associated with radiation. But there may be an indirect time-dependence: for example, in certain cases in which a fuse is operated at a constant current in an environment of constant temperature, its resistance is still found to drop slightly with time. One possible cause is the formation over some interval of time of a black oxide on the surface of the filament which increases the emissivity ϵ from that of unoxidized metal, roughly 0.1, to roughly 0.9 and hence lowers the filament's temperature (and its electrical resistance) slightly.

The size of radiation's effect on resistance is shown in Figure 6.6 for emissivities of 10% (this curve is indistinguishable from the curve for 0%: no radiation) and of 90%. The effect is less than 0.5% for fuses rated at 3 A that contain air, so long as the current is less than the rated current. When the fuse is evacuated, then the middle of its filament reaches a higher temperature at the rated current: the effect of radiation is therefore larger[6] and reaches 3% to 4% at the rated current. The effect of radiation is larger for fuses with nickel filaments than for copper-silver or for copper filaments, and must be included.

The filaments of fuses rated at 4 A and higher are flattened; however, these models are for filaments with circular cross-sections only. General experiences with thermal flows indicates that the effects of flattening on the heat loss will increase the heat loss by less than 25% for the extent of flattening encountered in fuse filaments. Further, the entire impact of air conduction and radiation on the resistance is less than 10% for ratings of 4 A and larger. Hence, errors made in the computation of these effects by using a circular cross-section instead of a flattened one are expected to affect the resistance by less than 3%, and will not be considered further.

The radial heat losses from the filament caused by air conduction and caused by radiation appear explicitly in Equation 4.16. However, the longitudinal heat losses from the filament into the end caps are implicit only: the end caps at $z = \pm\,\ell/2$ receive the heat current $A \cdot J_z = k_T \cdot [\partial_z T]_{z=\pm\ell/2}$, which tends to increase their temperature. Each end cap leaks heat into the environment, and this tends to limit the extent of its temperature rise. Knowledge of the temperature of each end cap is necessary for the solution of Equation 4.16. Similarly, the temperature of the inside of the barrel is necessary for the solutions of Equations 4.18

[6]These rules apply to incandescent lamps as well as fuses. The filament material in a lamp is tungsten operating at temperatures on the order of 2 200 K to 2 700 K in a nonoxidizing environment. Then radiation carries away roughly 20% to 40% of the entire I^2R power deposited into the lamp. Roughly 2% to 5% of the total radiation is in the visible, and the rest is in the IR region of the spectrum. A more exacting treatment of the radiation is necessary for accuracy for lamps.

and 4.19, and this temperature is determined by the balance of heat delivered into it by air conduction and by radiation, and heat lost from it into the environment. Hence, a model for the way in which the fuse and its environment exchange heat is necessary in order to proceed, even approximately.

4.2.2 Application to the fuse casing

There are no sources of heat within the barrel or the shrink wrap tubing. Current flowing through the end caps produces a heat source within them, but it is negligible. The current flowing through the leads produces a heat source density within the leads, but it is no more than 1.3% of the heat source density within the filament for any rating, and so it will also be ignored. Hence, the temperatures of these parts is determined as a result of the balance of the heat currents flowing through them: we can ignore any heat generated within them.

The simplest model for the behavior of these parts is to suppose that the end caps, the barrel, and the shrink wrap — which constitute the casing of the fuse — are all at the same temperature, which we will identify with the temperature of the end caps: T_{cap}.

Analysis of the heat delivered into the barrel by the hot filament shows that the barrel will become hot at its middle, but that the temperature rise is less than roughly 30 °C when the filament is nearly melting, so long as the barrel is made of a material at least as thermally conductive as AlSiMag 665; however, it will be several times that large when glass is used as is permitted by MIL–F–23419/8F. A temperature rise at the middle of the barrel of no more than roughly 30 °C has no significant effect on fuse performance, but a rise of more than 100 °C could.

4.2.3 Application to the environment and fuse

We must divide the environment into at least two parts: a local environment that forms a shell around the fuse casing (this local part contains the leads and any additional thermally conductive paths), and the rest of the environment. The simplest model for the behavior of the local environment is that it has negligible thermal capacity and a thermal resistance $\mathcal{R}$. And the simplest model for the behavior of the rest of the environment is that it is isothermal at T_{env} and has sufficient thermal capacity that it remains isothermal even while the fuse delivers heat into it.

Then the temperature of the casing is

$$T_{cap} = T_{env} + \mathcal{R} I \Delta V, \tag{4.20}$$

where ΔV is the electrical potential across the fuse, and $I\Delta V$ is the joule power deposited within the fuse.

This model has proven useful for fuses connected by only their leads to massive heat sinks: see

Figure F.1 for an example of the effect of different thermal resistance on the mid-filament temperature of FM08 fuses. Indeed, the observed values of $\mathcal{R}$, which have ranged from 30 °C/watt to 100 °C/watt, agree to within 10% to those computed using the values of thermal resistance per length of the leads named in Chapter 3.3. Further, the observed dynamics of heating are in substantial agreement with those computed using $\mathcal{R}$ and the heat capacity of the fuse casing. However, this is only true for leads whose lengths are between roughly 0.3 cm and 2 cm: shorter leads conduct heat from the casing so rapidly that case-dynamics must be treated, while longer leads have nonnegligible thermal capacity and must be modeled as thermal transmission lines rather than as thermal resistors.

This model is too crude to accurately describe fuses that are potted into cans, such as the Fuse Plugs used in some spacecraft. Some heat flows rapidly along the leads which are highly thermally conductive but small in cross-section, while some heat also flows slowly through the potting material which is far less thermally conductive but large in cross-section: this sort of environment requires modeling as a collection of thermal transmission lines. While such modeling is required for detailed discussion of such cases, it is not of direct interest to the principles governing the behavior of fuses and so it will not be treated in this report.

Chapter 5

Response to a current pulse

When the current is delivered as a pulse so brief that there is insufficient time for the heat generated within the filament to flow into the caps, or into the air (if any) surrounding the filament, then thermal coupling to these parts can be ignored and a particularly simple treatment is possible: this is the best place to begin modeling the behavior of fuses. This interval of time is sometimes called the *adiabatic regime* since no heat enters or leaves the filament.

The time for a thermal pulse to diffuse from the middle of the filament to the end is roughly $(\ell/2)^2/\mathcal{D} \sim 60$ msec for copper-silver and for copper filaments (since the length of the filament is $\ell \sim 0.5$ cm and the thermal diffusivity of copper and of the copper-silver alloy is $\mathcal{D} \sim 1$ cm^2/sec), so we expect the following analysis to apply to pulses shorter than roughly 60 msec for ratings between 3/4 A and 15 A. Indeed, inspection of the time-current curves for this range of ratings (see Figure 2.4) finds that there is a transition from a time-independent interruption current for times longer than a few seconds, to an interruption current proportional to time$^{-1/2}$ for times shorter than a few milliseconds, and that the middle of the transition is near 60 msec. Thus, the adiabatic regime extends from zero up to tens of milliseconds for this range of ratings.

Since the thermal diffusivity for nickel is roughly a fifth that of copper, then these times increase by roughly a factor of five for fuses rated at 1/2 A and lower: the middle of the transition region between the adiabatic and steady-state regimes is near 300 msec for the 1/2 A rating: the different thermal properties are responsible for the cross over in the current-time curves of the 1/2 A and 3/4 A rated fuses.

As the rating decreases from 1/2 A, the radius of the filament also decreases, and the heat conducted through the filament to the caps becomes small compared with the heat conducted through the air into the barrel. The time for a thermal pulse to move through air from the filament to the barrel is roughly $(d/2)^2/\mathcal{D}_{air} \sim 3$ msec (since the barrel diameter is $d \sim 0.07$ cm and $\mathcal{D}_{air} \sim 0.4$ cm^2/sec), and inspection of the current-time curves (see Figure 2.4) finds that the transition between adiabatic and steady-state regimes moves steadily towards shorter times as the rating decreases, reaching roughly 10 msec for a rating of 1/8 A. This

time asymptotes to about 3 msec for fuses constructed according to the same design, but with smaller ratings.

The heat conducted through the air (if present) to the barrel has an increasingly noticeable effect as the rating of the nickel filament fuses decreases. And the melting point of nickel is high enough that radiation is also important. Hence, an accurate treatment of nickel filament fuses requires attention to these effects, although a semi-quantitative treatment can be obtained when these effects are ignored. And these effects are small for the copper-silver and the copper filaments: we can ignore these effects and still obtain useful accuracy for these cases. Hence, in the treatment of this chapter, both radiation and thermal conduction through the air (if present) are ignored.

When the filament begins to separate, there is a voltage across the gap: the electric field strength jumps to a large value (since the gap starts small) and so there is a spark as electrons are forced to move across the gap.[1] This spark develops into an arc when enough filament material is turned into plasma (ionized vapor) to fill the gap and make it conducting. And the arc endures so long as the joule heat acting on the reservoir of plasma-forming material continues to maintain a sufficient plasma density throughout the increasing gap that the gap stays conducting. As a matter of experience, the spark does not develop into an arc in the kinds of circuits for which the FM08 fuse is intended: this is the intent of the voltage rating specified for this style of fuse. And so the arc process will not be discussed further in this Report.[2]

We begin with the premelting dynamics, and then consider melting dynamics before filament separation can happen, and finally we develop the dynamics of separation under three distinct stresses: gravity (and other applied accelerations), stresses built in during assembly, and surface tension, concluding that built in stresses are the effective cause of interruption. This model is then compared with the behavior observed for FM08 fuses and generally good agreement is found for the adiabatic regime.

5.1 Premelting and melting dynamics

When radiation and air conduction are both ignored, the dynamical equation for the temperature distribution along the filament is

$$c \cdot \left(\frac{dT}{dt} \right) = \rho \cdot \left(\frac{I}{A} \right)^2 , \tag{5.1}$$

[1] The actual voltage that appears across the gap depends on the circuit, including the fuse itself. If the circuit is purely resistive, then the voltage across the gap is the supply voltage minus the drop caused by the current through the load and line resistances. Since the fuse's resistance quickly dominates the other resistances, then essentially the full supply voltage appears across the gap. However, most fused circuits have an appreciable inductance L and so there is an inductively induced voltage jump, $-L \cdot (dI/dt)$: since the rapidly increasing fuse resistance produces a rapidly decreasing current I, then this voltage jump can be many times the supply voltage.

[2] Reference [4] discusses the arc process.

with $T = T_{cap}$ at each end of the filament, up until the material begins to melt. When melting begins, then the state of the filament at z is no longer given just by its temperature $T(z)$; rather, the fraction x_{liq} of liquid at z must also be included, together with its dynamical equation. If the melting section can be treated as being in thermal equilibrium, then the temperature is constant throughout that section, while the mole fraction of the liquid x_{liq} increases:

$$\Lambda \cdot \left(\frac{dx_{liq}}{dt} \right) = (\rho_s + \Delta\rho \cdot x_{liq}) \cdot \left(\frac{I}{A} \right)^2 , \tag{5.2}$$

where Λ is the latent heat of melting per volume, ρ_s is the resistivity of the solid phase at the melting temperature, ρ_{liq} is the resistivity of the liquid phase, and $\Delta\rho = \rho_{liq} - \rho_s$: all these values are measured at the melting point, T_{melt}. (The expression for the resistivity is an approximate one.)

Numerical integration can be carried out for realistic behaviors of $c(T)$ and $\rho(T)$ while the filament is completely solid or completely liquid, and for realistic values of $\rho(T, x_{liq})$ while the filament is melting. However, for copper-silver and for copper filaments, it is a good approximation that c is constant and that ρ is proportional to the absolute temperature T almost to the melting point, and these approximations allow an analytic treatment. The equation becomes

$$\left(\frac{dT}{dt} \right) = \left[\frac{\rho_0}{c\,T_0} \cdot \left(\frac{I}{A} \right)^2 \right] \cdot T \,, \tag{5.3}$$

with the solution

$$T(t) = T_{cap} \cdot \exp\left(\frac{\rho_0}{c\,T_0 A^2} \int_0^t I^2 \, dt \right) , \tag{5.4}$$

where $\rho = \rho_0 \cdot T/T_0$ where T_0 is a reference temperature (always 300 K = 27 °C in this report). Note that T_{cap} and T_0 do not depend on the fuse, while c and ρ_0 are the same for all fuses using a particular material for its filaments. Further, c and ρ_0 are approximately the same for copper and copper-silver alloy. Thus, the dominant variable over the range of ratings from 3/4 A to 15 A is $A^2 = \pi^2 a_{eff}^4$.

This treatment remains valid until the temperature reaches the melting temperature of the fuse material. The filament does not break at the instant that the melting point is reached: first, some fraction of the filament must be (at least partly) melted, and then this (at least partly) molten section must separate. Hence, after melting begins, then some parts along the filament will be solid material that is being heated (no change in phase, but rather an increase in temperature), some will be material that is being melted (no change in temperature, but rather an isothermal conversion from solid phase to liquid phase), and some will be molten material that is being heated further. The time for the middle to completely convert from a solid at T_{melt} to a liquid at T_{melt} is obtained from Equation 5.2:

$$\tau_{liq} = \left(\frac{\Lambda A^2}{\Delta\rho I^2} \right) \cdot \ln\left(\frac{\rho_{liq}}{\rho_s} \right) . \tag{5.5}$$

The resistance of the fuse's filament is, until melting starts,

$$R(t) = R_0 \cdot \frac{T_{cap}}{T_0} \cdot \exp\left(\frac{\rho_0}{c\,T_0 A^2} \int_0^t I^2 \, dt \right) , \tag{5.6}$$

where $R_0 = \rho_0 \ell / A$ is the cold resistance of the fuse. After melting starts, computation requires knowledge of how much of the filament has liquified: this will not be quantitatively addressed in this report. The resistance continues to increase during melting since the resistivity of the liquid is substantially larger than that of the solid. Indeed, since this increase in resistance increases the rate at which joule heat is produced, then there will be a substantial rate of increase in resistance once melting starts.

When the current is constant at I_0, then the time-dependence of T and R is purely exponential, $\exp(t/\tau)$, with a characteristic time $\tau = (c\,T_0 A^2)/(\rho_0\, I_0^2)$. The time to raise the temperature of the filament from its initial value T_{cap} to the melting temperature T_{melt} is

$$t_{[T_{cap} \to T_{melt}]} = \left(\frac{c\,T_0 A^2}{\rho_0 I_0^2} \right) \cdot \ln(\frac{T_{melt}}{T_{cap}}) = \tau \cdot \ln(\frac{T_{melt}}{T_{cap}}) \tag{5.7}$$

and the time to liquify the middle of the filament is

$$t_{liquify} = \left(\frac{\Lambda A^2}{\Delta\rho\, I_0^2} \right) \cdot \ln(\frac{\rho_{liq}}{\rho_s})\,. \tag{5.8}$$

Hence, the ratio of these times is

$$\begin{aligned} \frac{t_{liquify}}{t_{[T_{cap} \to T_{melt}]}} &= \left(\frac{\Lambda}{c\,T_0} \frac{\rho_0}{\Delta\rho} \right) \cdot \frac{\ln(\rho_{liq}/\rho_s)}{\ln(T_{melt}/T_{cap})} \\ &= \left(\frac{\Lambda}{c\,T_0} \right) \cdot \frac{\ln(\rho_{liq}/\rho_s)}{(\rho_{liq}/\rho_s) - 1} \cdot \frac{1}{(T_{melt}/T_0) \cdot \ln(T_{melt}/T_{cap})}. \end{aligned} \tag{5.9}$$

This shows that the relative length of the premelting and melting times does not depend on the current, or on the radius or length of the filament, for this model.

We next discuss the dynamics with which the liquified section separates, forming a gap that interrupts the flow of current.

5.2 Dynamics of filament separation

Interruption does not happen at the instant that any part of the filament liquifies; rather, the liquified section will move under stresses until a discontinuity develops and this takes a short (not a zero) time. And the current continues to heat the filament during this time. If the liquified section gets hot enough, then an appreciable fraction of the filament may evaporate and then recondense onto the inside of the barrel where it is visible as a metal "flash."[3]

[3]This flash can be seen in x-rays of the un-opened fuse barrel, as well as in optical and SEM images of the opened fuse barrel. The distribution of the thickness of the flash along the length of the barrel can serve as a measure of the interruption current when this current is more than roughly an order of magnitude greater than the rated current of the fuse, and can be useful in failure analyses.

The stresses that act to break the liquified section of filament include the action of gravity or other applied accelerations (i. e., the liquid section can fall out of place, or be shaken out of place), the release of the assembly stress stored in each solid filament-stub, and the action of surface tension (i. e., the liquid section can reform into a string of beads).

5.2.1 Motion caused by gravity or other accelerations

Gravity, or an impressed acceleration, acts on the mass of the filament to produce a force that can move the liquified section away from the solid stubs that are still attached to the end caps. When a constant effective acceleration g_{eff} is impressed on an object that starts at rest, then it's displacement after a time t is $g_{eff}t^2/2$, and so the time for the liquified section to move far enough to interrupt the current (about an effective diameter, a_{eff}) is

$$t_g \approx 2\sqrt{\frac{a_{eff}}{g_{eff}}} \ . \tag{5.10}$$

This is about 5 msec in a one-g field for a fuse rated at 10 A. This time scales roughly as (rating)$^{1/4}$; for example, it decreases to about 3 msec for a fuse rated at 1 A.

This time will decrease under applied acceleration (such as when there is shock or vibration), but will increase to very long durations under zero-g (zero-g_{eff}) conditions.

5.2.2 Motion caused by stresses built in during assembly

During assembly, each end of the filament is folded around the end of the barrel (see Figure 3.2), and this builds stress into each end; this built-in stress produces a bending moment at each end. Each end is heated briefly to melt the solder there, but then never gets hotter than roughly 125 °C in correct practice; hence, the built-in stresses are never entirely annealed away. When a filament is broken at its middle, the assembly stress installed at each end of the filament snaps each stub sideways for some distance: see Figure 5.1 for a typical example: note that the direction of the motion of each stub is consistent with the way each end of the filament is folded around the barrel. This is discussed further in Appendix F.

The time for the solid stubs of the filament to spring apart sideways under the action of the stresses that remain from those built in during assembly is

$$t_{built-in\ stress} = \frac{T_{canti}}{2\pi} \cdot \arccos(1 - \frac{2a_{eff}}{b}) \approx \frac{T_{canti}}{\pi}\sqrt{\frac{a_{eff}}{b}}\,, \tag{5.11}$$

where T_{canti} is the fundamental period of transverse vibration of one stub. This assumes that electrical continuity is broken when the left and right stubs move sideways (one stub moves up and the other moves down) by their effective diameter, i. e., when one stub has moved a distance a_{eff}. It also records the observation that numerous interrupted fuses have the free tips of the left and right stubs separated by roughly the inner radius b of the barrel:

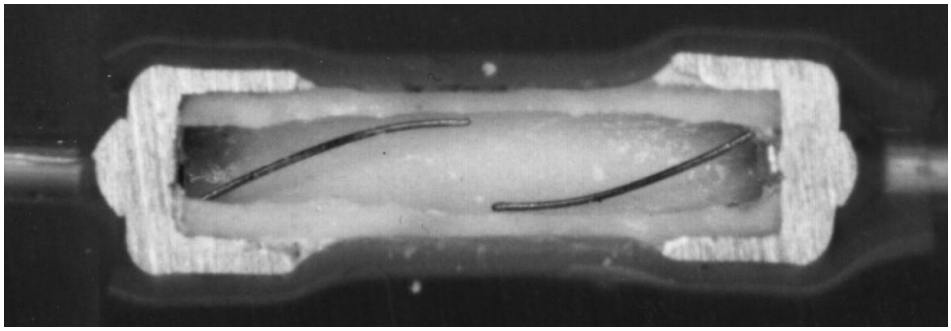

Figure 5.1: Cross section of an FM08 fuse rated at 3 A that has been interrupted. The tip of the left stub has moved upwards to press against the inside of the top of the barrel, while the tip of the right stub has moved downwards: this demonstrates the presence of bending moments at the root of each stub. The cross-sectioning and photography were done by UNISYS.

the actual distance of separation of the two tips of the stubs is a measure of their built in stress following assembly.

The fundamental period for transverse vibration of a cantilever (a bar rigidly fixed at one end and free to move at the other end) is

$$T_{canti} = \frac{2\pi L^2}{\kappa_1}\sqrt{\frac{\rho_m A}{Y I_{geo}}}\,, \tag{5.12}$$

where $\kappa_1 \approx 3.516$ is the eigenvalue associated with the lowest vibrational mode, L is the length of the bar, ρ_m is the mass-density of the bar and Y is its Young's modulus, A is the cross sectional area, and I_{geo} is the geometrical moment of inertia. For a bar of rectangular cross section, with a height h_{bar} and width w_{bar}, $I_{geo} = w_{bar}h_{bar}^3/12$. For a bar with a circular cross section, with a diameter d_{bar}, $I_{geo} = \pi d_{bar}^4/64$.

Hence for a filament with a circular cross section (radius a),

$$t_{built-in\ stress} \approx (0.28)\cdot\frac{\ell^2}{\sqrt{ab}}\cdot\sqrt{\frac{\rho_m}{Y}}\,, \tag{5.13}$$

and for a flattened filament (height h_{fil} and width w_{fil}),

$$t_{built-in\ stress} \approx (0.49)\cdot\frac{\ell^2}{\sqrt{h_{fil}b}}\cdot\sqrt{\frac{\rho_m}{Y}}\,. \tag{5.14}$$

Note that the width of the flattened filament does not appear. In each case, b is the inner radius of the barrel, and the length of the stub is $\ell/2$, where ℓ is the length of the uninterrupted filament.

For a fuse rated at 10 A, the time is $t_{built-in\ stress} \approx 15$ μsec $\pm$ 30%. For fuses with other ratings (so long as the filament is made of copper-silver alloy or of copper), this time scales roughly as rating$^{-1/4}$; for example, it increases to roughly 25 μsec for a fuse rated at 1 A.

The two dominant sources of uncertainty are the actual amount of built in stress that is present in a given fuse; and, for ratings of 4 A and larger, the actual thickness of the flattened filament, which observation shows is not as well controlled as the effective radius. But the effect of these uncertainties on the interruption time is reduced by the operation of the square root. For example, the time for built in stress to interrupt the filament, $t_{built-in\,stress}$, would increase by a factor of roughly three if the built in stress were reduced by a factor of ten, which would correspond to observing the left and right stubs of an interrupted filament to be off-set by about a filament radius instead of about half a barrel radius.

5.2.3 Motion caused by surface tension

The time for the liquified column to form into beads under the action of surface tension is

$$t_{bead} = (15 \text{ to } 32) \cdot \sqrt{\rho_m a^3/\mathcal{T}}\,, \tag{5.15}$$

where ρ_m is the mass-density and $\mathcal{T}$ is the surface tension of the liquified filament and a is its radius. For a fuse rated at 10 A, $t_{bead} \approx 0.4$ msec to 1.4 msec. So long as the filament is copper-silver or copper, this time scales roughly as $(\text{rating})^{3/4}$; for example, it decreases to the range 50 μsec to 160 μsec for a fuse rated at 1 A.

Plateau (1873) experimented with columns of liquid of length L and average radius a, with each end attached to a rigid boundary of radius a; Lord Rayleigh (1877) provided an analysis of these observations. Plateau caused the radius a to undulate along the length of the column at an initial time: $a(z) = a + a_\lambda \sin(2\pi z/\lambda)$; and he found that the size a_λ of the undulation changed with time. The motion was oscillatory when the wavelength λ was shorter than the circumference $2\pi a$ of the column, and so the column endured. But when the wavelength was longer than the circumference, then the initial undulations grew in amplitude until the column broke up into beads. Rayleigh showed that the growth was exponential so long as $a_\lambda \ll a$, with a time constant

$$\tau(\lambda) = \mathcal{F}(\frac{2\pi a}{\lambda}) \cdot \sqrt{\rho_m a^3/\mathcal{T}}\,, \tag{5.16}$$

where $\mathcal{F}(\eta)^2 = I_0(\eta)/[(1-\eta^2)I_0(\eta)]$, and $I_\nu(\eta)$ is the Bessel function of index ν and imaginary argument. This function diverges to infinity as $\eta \to 1$: the time for growth becomes infinite as the wavelength decreases to the circumference. And it has a minimum of about 2.913 at $\lambda/(2\pi a) \approx 1.435$: undulations of this wavelength grow most rapidly.

The driver for this motion is surface tension, and the determiner for the motion that surface tension will drive is the ratio of the length of the column to its initial circumference. When this ratio is less than unity, then small undulations increase the area of the liquid column, and surface tension resists this so that oscillation results: these motions are stable. When this ratio is greater than unity, then small undulations decrease the area, and surface tension promotes this, so that the size of the undulation increases: this motion is unstable.

Hence, the molten part of the filament is stable against beading under surface tension so long as its length is less than its circumference. Hence there can be no large melt balls for

currents that increase slowly enough that built in stresses have time to snap the filament apart before more than a length $2\pi a$ has melted; rather, each stub will end with a melt ball only large enough to collect the material in a column whose length is about πa or less, i. e., a ball of radius $1.33 \cdot a$ or less. This is the situation shown in Figure 5.1 for example.

When the current is large enough so that a column whose length is many times the circumference is melted before the filament interrupts, then the column can collapse into a string of beads which then solidify. The dynamics are computed as follows. Fourier-resolve the variations in the radius of the filament just before it melts, to obtain the amplitude of each wavelength initially present: a_λ. The amplitude of each wave grows with its own time constant as per Equation 5.16; wavelengths near $\lambda_{fastest} = 1.435 \cdot 2\pi a = 9.016 \cdot a$ grow fastest, with a time constant of $\tau_{min} = 2.913 \cdot (\rho_m a^3/\mathcal{T})^{1/2}$. The first wave whose amplitude reaches roughly a will reform the filament into a string of beads, each of volume $\pi a^2 \lambda$; this takes a time on the order of $\tau(\lambda) \cdot \ln(a/a_\lambda)$.

We do not know the exact initial variation of the radius of the filament as a function of the position along its length, and so we cannot carry out the Fourier analysis to obtain exact initial sizes of the a_λ, and so we cannot compute exact values of the desired time for the filament to reform into beads. Still, this time is so insensitive to the size of the initial variations that we can make some useful estimates of the time even without exact knowledge of these initial radius-variations. The filament wire is manufactured to have nearly constant radius, so the initial values of each a_λ are small, probably smaller than roughly a percent of a, but certainly larger than a few atomic diameters, say 10 Å. Further, variations in radius are likely to be random, so that the values of the a_λ are likely to be about the same for a few orders of magnitude around $\lambda_{fastest}$, so we will focus on the growth of undulations of this wavelength. Consider a fuse rated at 10 A, for which $a_{\mathit{eff}} \approx 74$ μm.[4] Using 1% of a, i. e., 0.74 μm, gives[5] $\ln(a/a_\lambda) = \ln(100) = 4.6$, while using 10 Å gives $\ln(a/a_\lambda) = 11.2$, which is only a factor of 2.4 larger. Hence, the time for initially present values of $a_{\lambda_{fastest}}$ to grow large enough to break up the filament into beads is probably between 5 and 11 times τ_{min}, which gives Equation 5.15. This range for the estimate of the surface tension driven breakup time is small enough to permit useful comparisons with the interruption times caused by other mechanisms, and also with data. So we are able to make a useful estimate of this time even though we have only a vague knowledge of the size of the initial undulations.

Next, note that the characteristic time for the growth of an undulation λ has the following Taylor's expansion around the minimum value:

$$\tau(\lambda) = \tau_{min} \cdot [1 + 0.9171 \cdot (\frac{\lambda}{2\pi a} - 1.435)^2 + \mathcal{O}((\frac{\lambda}{2\pi a} - 1.435)^3)] \tag{5.17}$$

so that the size of these undulations after the time t, relative to the size of the undulations

[4] In view of the approximate character of the estimates of this paragraph, the effect of flattening of filament wires used for ratings of 4 A and larger is ignored.

[5] Using other choices, such as 3% or 0.3%, does not change this estimate much; thus, the exact choice does not matter.

that grow most rapidly, is

$$\frac{a_\lambda(t)}{a_{\lambda_{fastest}}(t)} \approx \frac{a_\lambda(0)}{a_{\lambda_{fastest}}(0)} \exp[-0.9171 \cdot \left(\frac{\lambda}{2\pi a} - 1.435\right)^2 \cdot \left(\frac{t}{\tau_{min}}\right)] \,. \tag{5.18}$$

Thus, the exponential growth factor has a gaussian shape which is peaked at the wavelength of fastest growth, and the sharpness of this peak increases with time. The smoother the wire is initially (i. e., the smaller the size of the initial undulations), the longer it takes for the undulations to grow to about the radius of the wire, and the more certain it will be that those undulations will have a wavelength close to $\lambda_{fastest} = 1.435 \cdot 2\pi a = 9.016 \cdot a$.

Thus, we obtain a fairly definite result, even though the initial shape of the filament wire is only indefinitely known.

Figure 5.2 shows a wire that was heated by a current pulse adjusted to melt it just long enough for undulations to develop, but not long enough for the undulations to break the wire into separate beads. The initial diameter of the wire was $2 \cdot a = 0.33$ mm so that $\lambda_{fastest} = 1.425 \cdot \pi \cdot 0.33\,\text{mm} = 1.48$ mm, while the observed wavelength of the major undulation is $\lambda_{obs} = 1.47$ mm: the agreement is satisfactory.

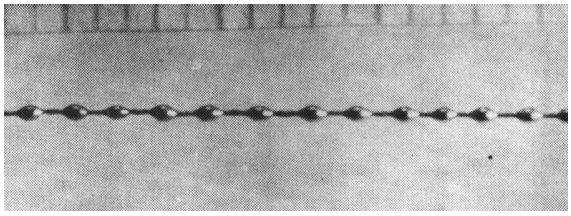

Figure 5.2: Undulations along a silver wire, initially 0.33 mm in diameter, after it was heated to melting for a short time. A millimeter scale is shown at the top of the image. The undulations are the result of the "beading" that was induced by surface tension. This figure is from [10].

Figure 5.3 is an x-ray image of an FM08 fuse rated at 1 A that experienced a constant current of 10 A: this was large enough to melt the filament along most of its length, and small enough so that there was ample time for beads to form and then interrupt the current. There are nine beads visible along a line at the bottom of the inside of the barrel, and one visible near the top of the midpoint of the barrel: perhaps several more have moved as the fuse was handled after interruption happened (just as the top bead has moved), and are now hidden within one of the caps. The distance between the left-most and the right-most of the visible beads is 1.93 mm, where the known length of the barrel ($\ell = 4.82$ mm) is used to establish the scale factor of the image. Hence, the spacing of the beads along the filament as interruption happened was 0.21 mm if all the beads are visible, and is as low as 0.16 mm if as many as three beads that formed along this line have become hidden. The initial radius of the filament of a fuse rated at 1 A is about 17.5 μm so that $\lambda_{fastest} = 0.16$ mm. Given the reduced precision of this example, the agreement is satisfactory.

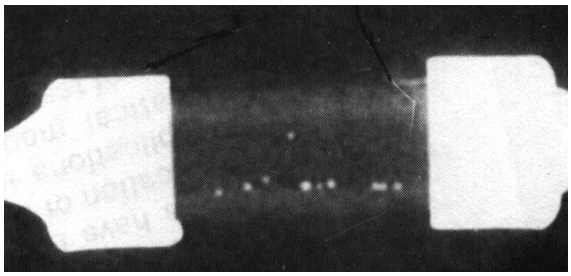

Figure 5.3: Beads of metal visible in x-ray of a 1 A Littelfuse driven at 10 A. This figure is from [10].

5.3 Probable cause of interruption under pulsed currents

We conclude on the basis of this analysis that the action of gravity and other accelerations (unless these are much larger than one-g) can be ignored: these fuses are not interrupted by having the molten section of the filament fall out of position. Rather, these fuses are interrupted by the stored stresses snapping the remaining stubs sideways until electrical contact is broken, and this happens less than 0.1 msec after a short section of the middle of the filament liquifies.

When the current pulse is large enough, then a substantial section of the middle of the filament liquifies before the current is interrupted, and this column can reform into beads: the length of the remaining stubs is a measure of the current that produced the interruption. For very high currents, there can be substantial evaporation before interruption, and a metal flash will deposit on the inside of the barrel: the amount of this flash is a measure of the current that produced interruption.

Time-current curves are not typically extended to times much shorter than 1 msec. Partly this is because such extension requires particularly large currents, and also attention to particularly short time intervals: previous needs did not seem to warrant gathering interruption data for times shorter than about 1 msec. However, several projects are expressing interest in the behavior for shorter times. When attempts are made to study behaviors at times shorter than about 1 msec, then the latent times of the interruption mechanisms discussed previously are encountered, and these introduce both a new functional dependence and a new sort of manufacturing-induced variability into the study. This task needs attention.

5.4 Comparison with observations

Figure 5.4 illustrates the electrical resistance versus time when a constant 100 A current was passed through a fuse rated at 10 A. Also shown is an exponential adjusted to fit the data over the range 0 to 2.1 msec: this fit gives an initial resistance of 6.9612 mΩ which

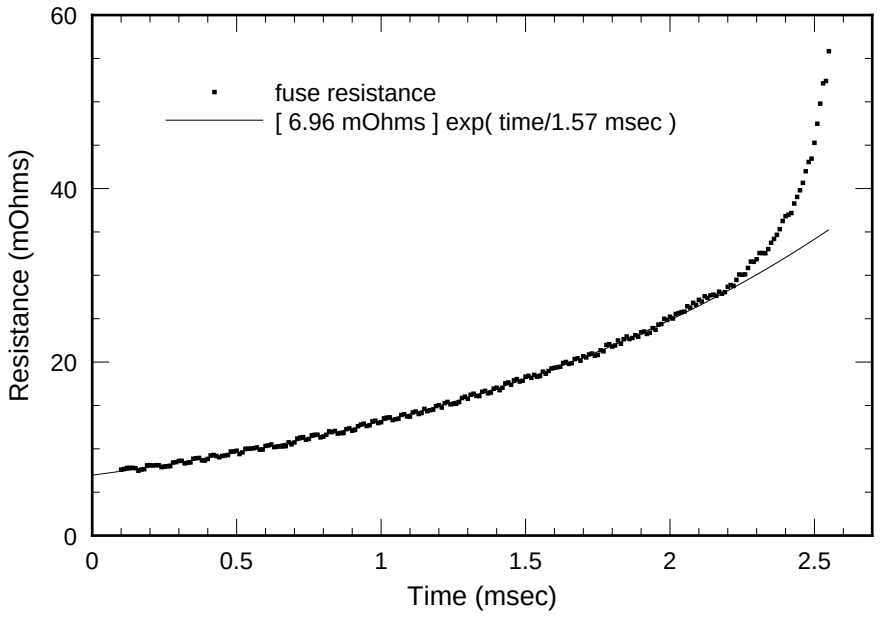

Figure 5.4: The increase in resistance of a fuse rated at 10 A subjected to a constant current of 100 A. These data were obtained by Mr. P. O'Shea of Paramax.

is therefore the observed cold resistance R_{cold}. For a fuse rated at 10 A, MIL–F–23419/8F specifies the range $5.9 < R_{cold} = 7.0$ mΩ, which includes the observed value. The observed interruption time was 2.55 msec, while the Littelfuse chart gives an interruption time of 2.3 msec for a fuse rated at 10 A driven at 100 A. Hence, both the observed cold resistance and the observed interruption time are in satisfactory agreement with the values expected for this fuse.

Noting that copper melts at 1357 K, and using the approximation $R(T) = R_0 \cdot T/T_0$, we find that the fitted exponential gives the time at which the melting temperature is reached to be 1.57 msec $\cdot$ ln(1357 K/300 K) = 2.37 msec: inspection of Figure 5.4 shows that the measured resistance begins to show a super-exponential increase at about (2.1 to 2.4) msec, and so we conclude that this does indeed closely mark the moment at which melting begins. Further, the residuals of the fitted curve are randomly distributed with a range of ± 0.2 mΩ, which is also the experimental uncertainty; hence, the observed increase in the resistance is accurately exponential up to the melting point, as the model states.

Using $c = 3.43$ J/(K cc), $\rho_0 = 1.74 \times 10^{-6}$ Ω·cm, and $a_{\mathit{eff}} = 71.7$ μm, the computed value of the characteristic time of increase is $(cT_0A^2)/(\rho_0 I^2) = 1.54$ msec, which is 2.0% lower than the observed time 1.5716 msec. Since the computed time depends on the fourth power of the effective radius, which is uncertain to several percent, then the agreement is satisfactory. The computed value of the time to reach the melting temperature is (1.54 msec)$\cdot$ ln(1357 K/300 K) = 2.32 msec, which is in satisfactory agreement with the observed time at which the resistance data shows that melting has begun.

Taking $t \approx$ (2.1 to 2.4) msec as the time at which the middle of the filament begins to

melt, and observing that the filament interrupts at $t = 2.55$ msec, then the observed time for for interruption to happen after melting has begun is about (0.15 to 0.45) msec. Using $\Lambda = 1\,834$ J/cc and $\rho_{liq}/\rho_s = 2.1$ at the melting temperature, the computed value of the time to completely melt the middle of the filament is 0.41 msec. Recalling that the computed value of the time for the melted filament of an FM08 fuse rated 10 A to snap apart is about 0.02 msec, then the total time for the melting and interruption is about 0.43 msec, which is within the observed range. Indeed, we can use this value to more sharply estimate the moment that melting began: 2.55 - 0.43 = 2.12 msec.

5.5 The stress index $\int I^2\,dt$

Suppose the current is constant at I_0. The total time to interrupt the fuse is the time to bring the middle of the filament from its initially cold temperature (T_{cap}) to a liquified condition, plus the time for the liquified middle to separate:

$$t_{cold\to liquify} = (1 + \frac{t_{liquify}}{t_{T_{cap}\to T_{melt}}}) \cdot \tau \cdot \ln(\frac{T_{melt}}{T_{amb}}) + t_{built-in\ stress}, \tag{5.19}$$

where $\tau = (c\,T_0 A^2)/(\rho_0 I_0^2)$ and the ratio of the melting time to the premelting time is independent of the current. This ratio is about 0.18 for copper-silver filaments and copper filaments, and about 0.19 for nickel filaments. The time $t_{built-in\ stress}$ is a tenth of a millisecond or less, and does not depend on the current.

When knowledge of interruptions at times as short as a few microseconds is interest, then all terms must be retained. However, when the interruption times are a millisecond or longer, then the last term is negligible, and the $I_0^2 \cdot t_0$ product (where t_0 is the interruption time) is

$$I_0^2 \cdot t_0 = \frac{c\,T_0 A^2}{\rho_0} \cdot (1 + \frac{t_{liquify}}{t_{T_{cap}\to T_{melt}}}) \cdot \ln(\frac{T_{melt}}{T_{amb}})\,. \tag{5.20}$$

When the current is not constant, then the left hand side is $\int I^2\,dt$ to a good approximation: this is the general measure of the electrical stress (in the general sense of "influence") that the pulse exerts on the filament, and it will be called the stress index of the pulse.

Figure 5.5 plots the value of $I_0^2 t_0$ versus t_0 for interruptions at a time t_0 under a constant current I_0 for several ratings in order to illustrate the way in which this stress index becomes constant as $t_0 < 50$ msec (i. e., as the time becomes short enough so that all the joule-heat remains within the filament). Table 5.1 lists for various fuse ratings the values of this stress index that produce interruption.

5.5.1 Practical computation of the stress index $\int I^2\,dt$

The stress index $\int I^2\,dt$ is easy to compute when the current is constant at I_0 throughout the entire interval of duration t_0, which is possible to arrange in laboratory testing: the stress

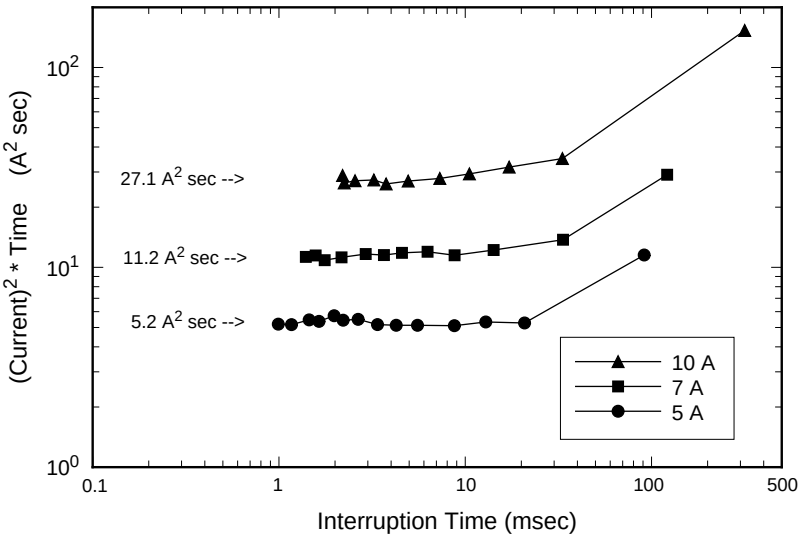

Figure 5.5: Values of the stress index that produce melting, as measured for three ratings by Mr. O'Shea of Paramax. Note that these values become constant as the interruption times shorten through the decade 100 msec to 10 msec, so that joule heat generated within the filament is retained until the middle is completely melted.

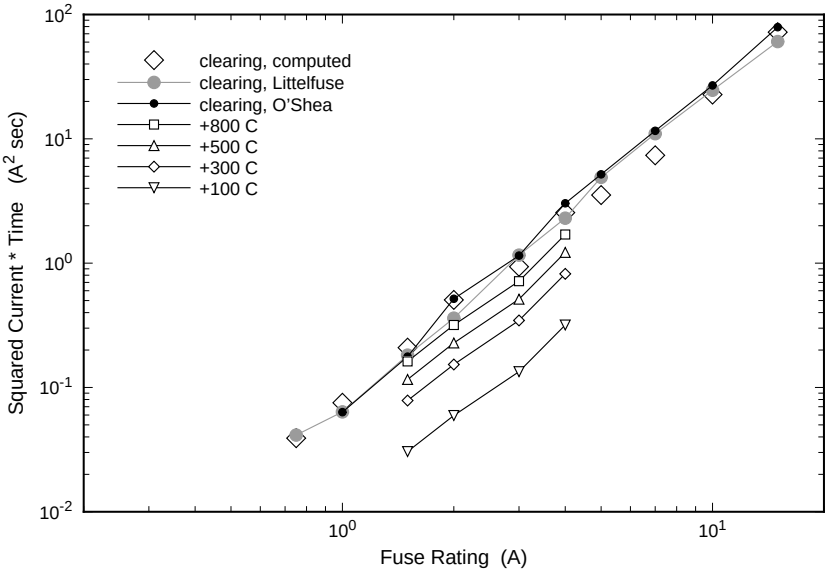

Figure 5.6: Values of the stress index that produce melting, as reported by Littelfuse (who claim an uncertainty of $\pm 25\%$) and as measured by Mr. P. O'Shea of Paramax (whose data are scattered by $\pm 10\%$); the agreement is satisfactory. Also shown are the computed values; the agreement is acceptable. Also shown are values that produce temperature rises of various amounts: Williams and Battel ([10]) have shown that a fuse may fail after a certain number of such pulses have been applied to a fuse (see text).

Table 5.1: Values of the Stress Index that Produce Interruption by Melting

Rated Current	Littelfuse (A^2·sec)	O'Shea (A^2·sec)	Computed (A^2·sec)
1/16	7.76×10^{-5}		10.3×10^{-5}
1/8	7.93×10^{-4}		13.3×10^{-4}
1/4	7.84×10^{-3}		10.2×10^{-3}
3/8	0.0212		0.0285
1/2	0.0462		0.0550
3/4	0.0414		0.0391
1	0.0636	0.0633	0.0753
1.5	0.182	0.178	0.209
2	0.361	0.520	0.506
2.5	0.700		
3	1.16	1.15	0.936
4	2.30	3.03	2.55
5	4.90	5.18	3.53
7	11.0	11.2	7.37
10	24.6	27.1	22.7
15	60.6	79.1	72.1

index is then $I_0^2 t_0$. However, in all practical cases, the current is not constant and so the integral must be carried out using such instruments as scope traces or digitizing ammeters to capture $I(t)$ over the interruption interval, followed by numerical integration of $[I(t)]^2$. It has seemed to some workers that a satisfactory estimate of the value of the stress index can be gotten by judicious fitting of rectangles and triangles to such records of I, and then using the classic values for the areas under these shapes. However, our experience has been that different workers obtain results this way that have differed by factors of 50% to 300%: the source of this variation is that $\int I^2\,dt$ is required, rather than $\int I\,dt$, so a plot of I verses t can be misleading. When the value of the stress index found by graphical estimation is more that a factor of three on one side or the other of a critical value, then one can safely make a decision based on such uncertain estimates of the stress index. However, knowledge of the value of the stress index to within better than roughly 50% requires careful digitization of the current over the interruption interval, followed by numerical computation of $\int I^2\,dt$. In practical cases using ordinary scope traces, this gives stress index values that are reliable to within 10%, and the total time spent is much less than has sometimes been spent trying to resolve disagreements among the values obtained by workers who have tried to save time by using approximate graphical methods.

5.5.2 Mechanical deformation caused by temperature increases

An adiabatic current pulse heats the filament to a temperature T that is substantially uniform along most of its length, and this would cause an increase $\delta\ell = \alpha \cdot (T - T_0) \cdot \ell$ in its length ℓ if it were unconstrained, where α is the coefficient of linear expansion. However, the ends are fixed and so the effect will be to transfer all this strain into the sections that actually deform under the stress: the details depend strongly on the particular initial shape of the filament. (This is discussed in Appendix F 1.5 for steady state currents.)

Inspection of many fuses shows that there is considerable manufacturing variability in the shape of the filament when it is cold. Some filaments are nearly straight, running diagonally across the inside of the barrel: these resemble the fuse shown in step six of Figure 3.2. Some resemble an archer's bow, with both ends anchored on the same side of the barrel and the middle arching outwards towards the opposite side of the barrel. And some have the compound curve shown in Figure F.2. Each of these initial shapes will deform in a different manner under thermal expansion, and will cause a different strain along the filament.

The force that produces buckling in an initially straight long beam was studied by Leonhard Euler; his work founded the theory of elastic stability. Suppose the beam has a uniform Young's modulus Y and geometrical moment of inertia I_{geo}. Suppose the beam is originally straight and has each end clamped so that end rotation is impossible. Slide one end of the beam towards the other (without rotation) to apply a compressive force parallel with the beam: the arc-length of the beam is $\mathcal{L}$ and its ends are separated by the distance ℓ. Then the beam remains straight so long as the applied force is less than the critical value

$$F_{crit} = \frac{4\pi^2 Y I_{geo}}{\ell^2}\,. \tag{5.21}$$

When the force equals or exceeds this critical value, then the beam bends into the compound bow

$$\eta(z) = \eta_M \cdot [1 - \cos(2\pi z/\ell)]\ , \tag{5.22}$$

where the position along the beam is z which runs from the end at $z = 0$ to the other end at $z = \ell$, $\eta(z)$ is the sideways displacement at z from the original straight line, and the maximum displacement η_M,

$$\eta_M = \frac{1}{\sqrt{\pi}} \cdot \sqrt{(\frac{\mathcal{L}}{\ell} - 1)}\ \cdot \left[1 + \frac{3}{8}(\frac{\mathcal{L}}{\ell} - 1) + \mathcal{O}((\frac{\mathcal{L}}{\ell} - 1)^2)\right]\ , \tag{5.23}$$

is a measure of the amount of buckling.

Thus, we compute a critical temperature rise above which an initially straight filament will buckle:

$$\Delta T_{crit} = \frac{4\pi^2}{\alpha\ell^2}\frac{I_{geo}}{A} \tag{5.24}$$

$$= \frac{1}{\alpha}\left(\frac{\pi a}{\ell}\right)^2 \quad \text{circular cross section} \tag{5.25}$$

$$= \frac{1}{3\alpha}\left(\frac{\pi h}{\ell}\right)^2 \quad \text{rectangular cross section}\,, \tag{5.26}$$

where a is the radius of the filament when it is circular and h is the thickness of the filament when it is rectangular, and ℓ is its length. This critical rise in temperature ranges from 2 °C for a fuse rated at 1/8 A to about 30 °C for a fuse rated at 15 A. This demonstrates that an initially straight begins to bend for even small rises in temperature.

Consider a fuse rated at 10 A, and heated to near melting. If the filament were to remain straight, then thermal expansion would exert a force of about 7.3 pounds on the end caps: this has the potential to push the end caps off the barrel since the cap-barrel seal is only specified to withstand 5 pounds. But $F_{crit} \sim 0.086$ pounds, which is two orders of magnitude smaller: the filament will actually bend rather than remain straight, and this is important for the correct operation of the fuse. Also, we find $\eta_M = \ell \cdot (\alpha\Delta T/\pi)^{1/2}$. For a copper filament adiabatically heated to nearly its melting point, this sideways displacement is about 0.33 mm and would be visible under examination by a microfocus x-ray.[6] The compound bend produces a strain of $y \cdot \eta''(z)$ at the location z along the filament and at the distance y from the neutral plane of the filament. This becomes $22.3 \cdot (y/\ell) \cdot (\alpha\Delta T)^{1/2}$ at the middle of the filament, which amounts to 2.5% on the outsides of the filament of a fuse rated at 4 A heated to nearly its melting point.

When the initial shape is already bent, then there is no buckling at a critical force (i. e., a critical ΔT); rather, the extent of the bend increases with ΔT at a rate that depends on the initial shape.

Young's modulus decreases with increasing temperature, and strongly so as the melting point is approached. Thus, the filament will develop a sharp bend at its midsection, where it gets hottest: most of the strain will be concentrated there. See Figure 5.7 for an example. If the concentration factor is 10, as suggested by this figure, then the estimate of the strain rises to 20%, which is large enough to quickly produce fatigue when repeated a number of times.

5.5.3 Interruption by repeated pulses

Fuses have been observed to interrupt under a succession of pulses, none of which are strong enough to interrupt a new fuse. The filament of a fuse interrupted this way is typically broken at its midpoint, with no melt balls visible on the stubs, and show oxide crusts and other evidence of heating but not melting. Williams and Battel ([11] and [12]) found that the number of pulses that result in this sort of failure can be characterized by the temperature rise produced by a single pulse: see Table 5.2.

[6] This computed sideways displacement is about the inner radius of the barrel ($b = 0.32$ mm). If a heating filament moves enough for its middle to contact the side of the barrel, then the additional cooling provided by this contact will sharply limit further heating: such a fuse could have a cold resistance within normal limits, but would have a significantly reduced hot resistance, and a significantly increased interruption current. At least one such FM08 fuse has been observed during test by Code 313. Hence, it is prudent to observe the MIL–F–23419/8F requirement that the hot resistance, as well as the cold resistance, be within certain limits.

This temperature rise can be related to the stress index, and values are given in [12]; these generally agree with those computed by Equation 5.4. These stress index values are plotted in Figure 5.6, and a clear pattern emerges: A fuse is not interrupted by even many thousands of pulses whose stress index is low enough; but, interruption after fewer and fewer pulses is possible as the stress index is increased, until interruption within one pulse is probable.

Williams and Battel attribute the mechanism of this sort of failure to the formation of a copper oxide crust around the filament and the formation of a copper-poor, silver-rich layer just under this crust. This would suggest that fuses with nickel filaments (used for ratings of 1/2 A and less) and fuses with copper filaments (used for ratings of 5 A and more) would not fail under repeated sub-melting pulses, to show a midpoint break with no melt-balls. However, the proposal advanced in this report is that these failures are caused by metal fatigue under cyclically applied stresses, and will happen for all FM08 fuses and not just those with copper-silver alloy filaments. Indeed, a similar failure has been observed in a fuse with a nickel element. It seems worthwhile to carry out an experimental extension of the testing program begun by Williams and Battel to fuses with ratings of 1/2 A and smaller, and of 5 A and larger.

This mechanism leads to a kind of latent damage that progressively builds up within a filament. There are no accepted methods that measure the extent of such damage. The damaged section of the filament would have an electrical resistivity that would be perhaps 3% to 10% higher than normal, but, since the damage is sharply localized to the center of the filament (say, to the central 10% of its length), then the total resistance of the filament would be roughly 0.3% to 1% higher than the original value: this is too small to reliably measure. A developing kink at the middle of the filament would become evident under examination with a microfocus x-ray of modern capabilities, provided no other parts obscured the image. Scanning along the filament with a micro-hardness tester might show an effect in the neighborhood of the break, as might examination of a polished and etched section. However, post-interruption examination of the ends of the broken filament almost always shows at least a slight degree of melting caused by the discharge of energy stored in the inductances of virtually all electrical circuits: this energy must be dumped somewhere when the current is interrupted and at least some of it gets dumped into the tips of the stubs as they separate, producing some post-interruption melting. (If the fuse is used in a circuit that attempts to put constant current through the fuse, which is what an inductor does, then the last tenths of milliseconds of the interruption can see large voltages applied across the fuse, launching arcing that obliterates records of previous current-levels.)

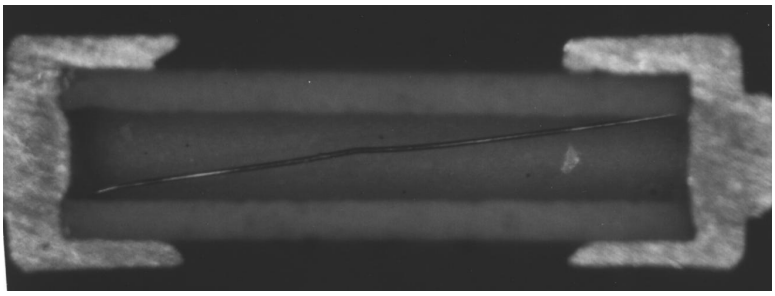

Figure 5.7: This FM08 fuse rated at 1.5 A was cross-sectioned to show its filament. Note the kink, and the darkening caused by "black" CuO. Optical interference bands are visible near each end: these happen when the film of "red" Cu_2O is in the range 100 Å to 1000 Å.

Table 5.2: The William-Battel Relation

Temperature Rise	Impact on the Fuse
100 °C	maximum life condition
300 °C	extended life condition ($>$ 20 000 cycles)
500 °C	shortened life condition ($>$ 1 000 cycles)
800 °C	potential single-pulse damage condition

Chapter 6

Steady-state response of an FM08 fuse

When the current is held constant for a long enough time, then the heat that is generated within the filament saturates each part of the fuse and its environment: all parts come to a steady-state temperature, and a nondynamical treatment is possible. The filament, the end caps, the barrel, and the shrink wrap come into mutual thermal equilibrium within a few seconds: note the time-current chart (Figure 2.4) shows that steady-state behavior is largely achieved after one to three seconds.

The time for the fuse to thermally saturate its environment depends on details of the environment and are not part of the fuse specifications; hence, this time cannot be reported in general. In particular, there is no such thing as a "typical" environment. But one case is worth mentioning since it is tacitly part of MIL–F–23419/8F: the particular fuse holder specified by MIL–F–23419/8F has poor thermal heat sinking to the fuse leads; further, the fuse holder has little thermal capacity, and so steadily warms under the joule heating delivered by fuses of even modest ratings; finally, the fuse holder is mounted on a base with sluggish thermal dynamics: hence, the immediate environment of the fuse does not come to thermal equilibrium for several minutes, and this is reflected back into the fuse which cannot develop steady-state behavior until its environment does. This effect is visible in the time-current chart (Figure 2.4) as a steady decrease in the interruption current as the time increases from one to one hundred seconds, especially for fuses of larger ratings: this is entirely a result of testing in a thermal environment with sluggish thermal dynamics.

If the fuse were connected through a low thermal resistance to a thermal environment clamped (perhaps using forced air or water) to a constant temperature (to within a degree or two), then it would closely approach steady-state within three to ten seconds, and achieve it with high accuracy within twenty seconds, rather than after the five minutes that MIL–F–23419/8F presently requires: this would allow a substantial increase in rates of fuse testing, and a substantial reduction in the exposure of a fuse to full rated currents.

We shall begin modeling the steady-state behavior of an FM08 fuse by supposing that the temperature of its casing is clamped to a constant temperature, T_{cap}; later, we will allow this temperature to change as heating develops. We have found that a particularly simple model obtains when there is no air within the barrel of the fuse, which is indeed a case that is of direct interest for applications to spacecraft; later, we will include air, and find that its effects are small for fuses rated at 3 A and larger, but are large for lower ratings and enormous for ratings of 1/2 A and smaller.

When the rated current is maintained for longer than roughly an hour, then the filament develops substantial oxidation near its middle: this is the subject of an appendix and is ignored in this chapter. When a copper-silver filament oxidizes, it develops a copper-depleted silver-rich shell under the outer oxide layer: this limits the rate of further oxidation and is therefore a protection mechanism; this will be discussed in the appendices on oxidation and on the behavior of copper-silver alloy.

6.1 Simplest steady-state model

We now introduce the simplest behavior for the steady-state response of the FM08 fuse:

- Suppose the barrel, end caps, and shrink wrap (i. e., the fuse's casing) are all thermally clamped to the same temperature T_{cap} despite the flow of heat from the filament into the casing. This is a good approximation when the filament is much thinner than the leads, i. e., when the rating is low.

- Suppose that the case temperature T_{cap} is thermally clamped to a constant temperature as the current is varied, which is the same thing as assuming that the product of the thermal resistance $\mathcal{R}$ and the heating power generated in the fuse $I\Delta V$ is vanishingly small, and that the environment has a large heat capacity. This is a good approximation when the rating is low (i. e., $I\Delta V$ is small), when the leads are well heat sunk (i. e., $\mathcal{R}$ is small), and when the environment is isothermal. (See for example Figure F.1: this illustrates the effect of thermal resistance on the midfilament temperature when the rated current flows through fuses of each rating.)

- Suppose the loss of heat from the filament into the barrel (through air conduction and IR radiation) is ignored in comparison with the loss of heat along the filament into the end caps, so that $J_r(a) = 0$. This is increasingly more accurate the thicker the filament (i. e., as the rating is higher) when air is present within the barrel, and is also accurate for all ratings when the barrel is evacuated. Radiative losses are never more than a few percent for copper-silver and for copper filaments; they are important for nickel filaments, however.

- Suppose the actual temperature dependences of the specific heat per volume c and the electrical resistivity ρ are replaced by the approximate ones: c = constant and

$\rho = \rho_0 \cdot T/T_0$ where T_0 is a reference temperature (always 300 K = 27 °C in this report). Further, replace the actual thermal conductivity k_T with the resistivity ρ and the quantal value of the Lorenz number $\mathcal{L}$, using the Wiedemann-Franz rule $\mathcal{L} = \rho k_T/T$, so that $k_T = \mathcal{L}T_0/\rho_0$. Inspection of data (see Appendix B and especially Figure B.7) shows that these are good approximations for copper-silver and for copper filaments, but are poor for nickel filaments. The conduction electrons of copper and copper-silver behave as nearly free (the Fermi surface is nearly spherical), and the same electrons contribute to both electrical and to thermal conductivity. Nickel is ferromagnetic with a Curie temperature of 631 K, and the spin-orientation of its conduction electrons with its core electrons interferes with the electrical mobility of the conduction electrons: the conduction electrons contribute differently to electrical and to thermal conductivity. And so the temperature dependence of ρ and k_T changes abruptly at the Curie temperature.

Then the equation for the temperature distribution along the filament is

$$c \cdot (\partial_t T) - (\mathcal{L}T_0/\rho_0) \cdot (\partial_z^2 T) = \rho_0 \cdot \frac{T}{T_0} \cdot \left(\frac{I}{A}\right)^2 , \tag{6.1}$$

with $T = T_{cap}$ at each end of the filament. And the steady-state solution is

$$T(z) = T_{cap} \cdot \frac{\cos(\kappa z)}{\cos(\kappa \ell/2)} , \tag{6.2}$$

where z is the distance along the filament (whose ends are at $z = \pm\ell/2$), and $\kappa\ell = (R_0 I)/(\sqrt{\mathcal{L}}\, T_0)$ is a dimensionless measure of the effectiveness of the current to heat the filament against the effectiveness of the conductivity to keep it uniformly at T_{cap}. It is often convenient to regard $\kappa\ell$ as the electrical current, scaled so that it is dimensionless: $\kappa\ell = I/I_{scale}$ where $I_{scale} = \sqrt{\mathcal{L}}\, T_0/R_0$, since various events such as melting happen at the same value of $\kappa\ell = I/I_{scale}$ for all fuse ratings. The scaling current I_{scale} depends on the cold resistance directly, which is fixed by MIL–F–23419/8F for each rating; on $\sqrt{\mathcal{L}}$, which depends weakly on the choice of filament material; and on T_0, which is fixed at 300 K.

The resistance of the fuse is

$$R(I, T_{cap}) = R_0 \cdot \frac{T_{cap}}{T_0} \cdot \mathrm{tanc}(\frac{\kappa\ell}{2}) , \tag{6.3}$$

where $\mathrm{tanc}(\chi) = \tan(\chi)/\chi$. Figure 6.1 illustrates the good agreement between this equation and some observations for a fuse that was placed in a vacuum.

The data plotted in Figure 6.1 were obtained by chosing a maximum current I_{max}, and computing twenty values of current: $I_n = n \cdot I_{max}/20$; then the current was ramped upwards ($n = 1, 2, \ldots, 20$) to the maximum, with each intermediate current I_n held for twenty seconds, and then downward through the same currents ($n = 20, 19, \ldots, 1$). Several trials showed that twenty seconds was sufficient for the fuse's filament and casing to approach thermal steady-state; ten seconds was not quite enough, and thirty seconds was unnecessarily long. Each lead was about 0.9 cm, and terminated in a large block of copper for heat sinking.

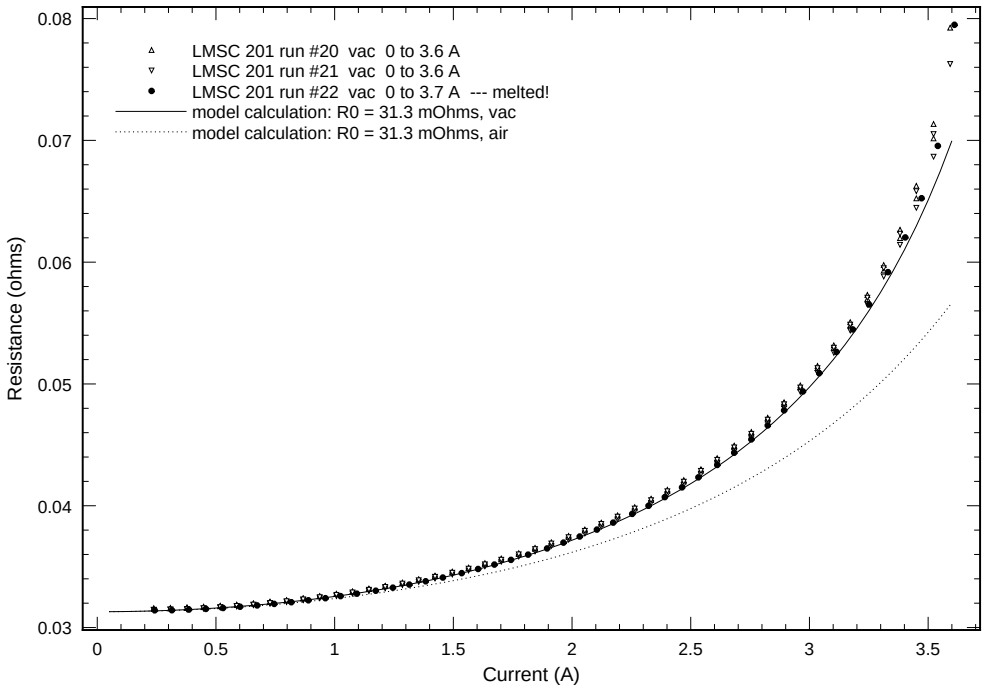

Figure 6.1: Three cycles of measurements of the resistance of an FM08 fuse rated at 3 A, called LMSC 201, versus current. Also shown are the results given by the vacuum model and by the model that supposes that the filament is bathed in air.

On the first trial (not shown here), the fuse was kept in a vacuum (pressure less than a microtorr) for a day, and then its resistance versus current up to a maximum of 3 A was measured: the result matched that for a filament bathed in air (developed in a later section). On the second trial, the shrink wrap was removed and the fuse again placed in a vacuum for a day: again, the results up to a maximum of 3 A matched that for a filament bathed in air. For the third trial, a hole was drilled through the barrel and the fuse again placed in a vacuum: the result now matched that of a filament operating in a vacuum.[1] Later trials were made with larger choices of maximum current. Figure 6.1 shows runs #20, 21, and 22 to illustrate the consistency of the results: there is no observable change in cold resistance, while the changes in hot resistance are on the order those resulting from the changes in T_{cap} allowed by operation in the vacuum chamber used here. In particular, there is no evidence of the oxidation that profoundly degrades a fuse rated at 3 A operated at above 3.6 A, when its filament is bathed in air. Note that this fit was made by adjusting only the cold resistance R_0 to the observations — no other fitting parameters were used. The observations are distinctly above the vacuum model curve at the higher currents: we will show later in this chapter that this is accounted for when the actual thermal resistance of the fuse is included.

[1] We expected the first exposure to a vacuum to remove the air within the fuse barrel: clearly, it did not. While these fuses are not sealed in such a way as to guarantee that their charge of air will be long retained in a vacuum, we know that the air does not always escape within a day.

Also shown in Figure 6.1 is the resistance versus current for a model (developed later in this chapter) that includes air within the barrel: the air provides an additional thermal conduction path, so that the filament is cooler at a given current, and so the resistance is lower. The effect of air conduction is large compared with the uncertainty of the data: the vacuum model gives a good fit to these observations, while the air model gives a poor one: it is clear that this method can establish the presence or absence of air within the barrel of a fuse rated at 3 A.

The temperature and the resistance both diverge to infinity as $\kappa\ell \to (\kappa\ell)_\infty = \pi$, that is, as the current approaches $I_\infty = \pi\sqrt{\mathcal{L}}T_0/R_0 = \pi I_{scale}$. This cannot happen in a real fuse since the filament will melt when the temperature at the middle of the filament reaches T_{melt}, and this happens when the current reaches

$$\begin{aligned} (\kappa\ell)_{melt,vac} &= 2\arccos(\frac{T_{cap}}{T_{melt}}) \quad \text{(dimensionless current)} \\ I_{melt,vac} &= \frac{2\sqrt{\mathcal{L}}\,T_0}{R_0}\arccos(\frac{T_{cap}}{T_{melt}}) \quad \text{(dimensional current).} \end{aligned} \tag{6.4}$$

This gives a convenient rule for the relation between the melting current and the cold resistance of the fuse, when the filament is in a vacuum:

$$I_{melt,vac} \cdot R_0 = 2\sqrt{\mathcal{L}}\,T_0 \arccos(\frac{T_{cap}}{T_{melt}}); \tag{6.5}$$

this product is almost constant at 0.12 to 0.13 volts as the range varies from 1/8 A to 15 A, that is, by a factor of 120. The product $I_{rating} \cdot R_0$ is not as constant: it varies over a range of roughly two around 0.1 volts.

Equation 6.5 shows that it is the cold resistance R_0 that most directly controls the melting current $I_{melt,vac}$, and observation shows that R_0 exerts a strong control over $I_{melt,air}$. The choice of material for the fuse filament affects $I_{melt,vac}$ only through the resulting values of $\mathcal{L}$ and T_{melt}, and indirectly affects other behaviors by requiring a new effective radius a_{eff} in order to retain the desired value of $R_0 = \rho_0\ell/A$ (where the filament's length ℓ is fixed and the cross-sectional area $A = \pi a_{eff}^2$). For most metals, the Lorenz number is close to the value $\mathcal{L}_q$ given by the Sommerfeld model. And so long as the melting temperature $T_{melt,vac}$ is several times T_0, then the arccos-term is close to its maximum value, $\arccos(0) = \pi/2 \approx 1.571$. For example, this term is 82% of the maximum value when the filament is copper-silver alloy, 86% when it is copper, and 89% when the filament is nickel. (The situation would be different if low melting point metals were used: then the arccos term would depend strongly on the particular value of T_{melt}.)

The expansion of the resistance at low currents is

$$R(I, T_{cap}) = R_0 \cdot \frac{T_{cap}}{T_0} \cdot [1 + \frac{(\kappa\ell)^2}{12} + \frac{(\kappa\ell)^4}{120} + \mathcal{O}(\kappa\ell)^6], \tag{6.6}$$

so the cold resistance is approached rapidly as the current is reduced, as is also evident in Figure 6.1. Using this to compute the relative change in resistance caused by the heating

produced by a current that is 10% of the rated current, we find

$$\frac{R_{10\%}}{R_0} \approx \frac{T_{cap}}{T_0} \cdot [1.002]\,; \tag{6.7}$$

thus, the rule for the measurement of R_0 given by MIL–F–23419/8F is satisfactory.

The ratio of the hot resistance to the cold resistance is

$$\frac{R_{hot}}{R_{cold}}\Big|_{T_{cap}} = \frac{R(I, T_{cap})}{R(I, T_{cap})} = \text{tanc}((\kappa\ell/2)_{rating}) \tag{6.8}$$

and the values will be discussed later in this chapter, after the effects of air conduction and heat sinking are considered.

6.1.1 Steady-state stress index I

Since the total resistance of a fuse is a small fraction of the total resistance of the circuit within which it is used,[2] until the fuse interrupts, then this increase in fuse resistance produces a small decrease in the current flowing: for practical purposes, the current can be taken as constant while the fuse responds. Further, this response is simple when expressed in terms of the current through the fuse, while it is complicated when expressed in terms of the voltage across the fuse. Hence, fuses are normally considered to be current-driven, and not voltage-driven. We will consider the current I to be the steady-state stress index, and the interruption current I_{inter} to be the critical value of this stress index: interruption under steady-state conditions happens when $I \geq I_{inter}$.

The filament will break apart, and interrupt the flow of current when its middle melts: breakup of a melted filament will happen within fractions of a millisecond, and is negligible in the context of steady-state behavior. Hence, the current I_{melt} that increases the midpoint temperature to T_{melt} is enough to interrupt the fuse: we can estimate the critical value I_{inter} as I_{melt}.

However, it may not be necessary to actually melt the middle: creep of the hot middle may lead to rupture while it is still solid: see Appendix F. The middle of the filament is under stress as a result of the bends made at both its ends during assembly, as well as thermal expansion that develops as it heats; thus, the middle will creep at some rate that depends on its temperature and the particular value of the midpoint stress. The creep rate increases to very large values as T_{melt} is approached, and so the filament will actually break by creep rupture at a current that is less than that required for melting: $I_{inter} < I_{melt}$, and so the estimate $I_{inter} \overset{\text{estimate}}{=} I_{melt}$ gives an upper bound and not an equality. The longer this mechanism is able to act, the larger is the creep-induced depression of I_{inter}; hence, creep was ignored in the discussion of interruption under current-pulses lasting a fraction of a second, but creep is suggested as significant when currents slightly below I_{melt} are applied

[2]The cold resistance of the lowest rated FM08 fuse is 2.1 Ω, and might not be negligible in some circuits.

for many seconds. Creep rupture may contribute to the steady decrease in I_{inter} frequently visible in current-time charts for times longer than hundreds of seconds. The signature of creep rupture will be a break in the middle of the filament, and an absence of melting at the separated tips of the filament stubs; there will be no missing segment of filament.[3]

6.1.2 Comparison with the pulse stress index

There is an analogy between this steady-state situation and the one considered in the presentation of the pulse stress index in the previous chapter. There, a value of the pulse stress index $I_0^2 \cdot t_0$ that achieved or exceeded a critical value would interrupt the fuse promptly, but the fuse could also be interrupted eventually by a succession of pulses, each of which had a pulse stress index that was somewhat below the critical value, as the work of Williams and Battel showed. There the mechanism is cyclic fatigue, while here it could be creep rupture.

We will focus on interruptions happening in between 10 seconds and 100 seconds, and will suppose that the creep-induced depression of the interruption current is negligible over this regime, so that the critical value of the steady-state stress index is essentially the melting current: $I_{inter} \stackrel{\text{estimate}}{=} I_{melt}$. This critical value depends on whether the filament is bathed in air or not; that is, on whether $I_{melt,air}$ or $I_{melt,vac}$ applies, and we now examine the extent to which these differ.

The interruption current when the filament is bathed in air can be read from a conventional current-time curve for the fuse; we will use the interruption current at a time of 10 seconds. The results from the curve published by Littelfuse for the commercial equivalent of the FM08, and the curves independently measured by Lockheed Missiles & Space Company ([8]), are in substantial agreement: the average of these interruption currents is displayed in Figure 6.2 as a band whose width is representative of the range shown in the Lockheed data.

Any particular fuse may differ from the average behavior: this is called "manufacturing variability." The range that can be expected for these differences is not published by the manufacturers or specified by MIL–F–23419/8F; however, experience suggests that the standard deviation is roughly 8%, and the range is roughly 25% (5% and 15% respectively for fuses rated at 10 A and 15 A), as shown in Figure 6.2.

Since the melting current is mainly controlled by the cold resistance, which has a standard deviation of about 3% and a range of 10%, then the variability in the observed interruption currents is about a factor of three greater than expected. That is, two-thirds of the variation is not accounted for.[4] Since the steady-state interruption current is a critical fuse parameter, this unexplained variation presents an important concern.

[3]Unless circuit inductance delivers some of its stored energy, $\frac{1}{2}LI^2$, into the tips of the filament just as they separate and interrupt the current: this will happen if the circuit couples some of the voltage developed across the inductance, $-L(dI/dt)$, into the fuse.

[4]Since the creep rupture time depends exponentially on the driving stress, and this stress has a variability of roughly a factor of two to five (judged from observations of the off-set of separated filaments), then there would be some variability to the creep rupture depression of I_{inter}. This seems to be worth exploring.

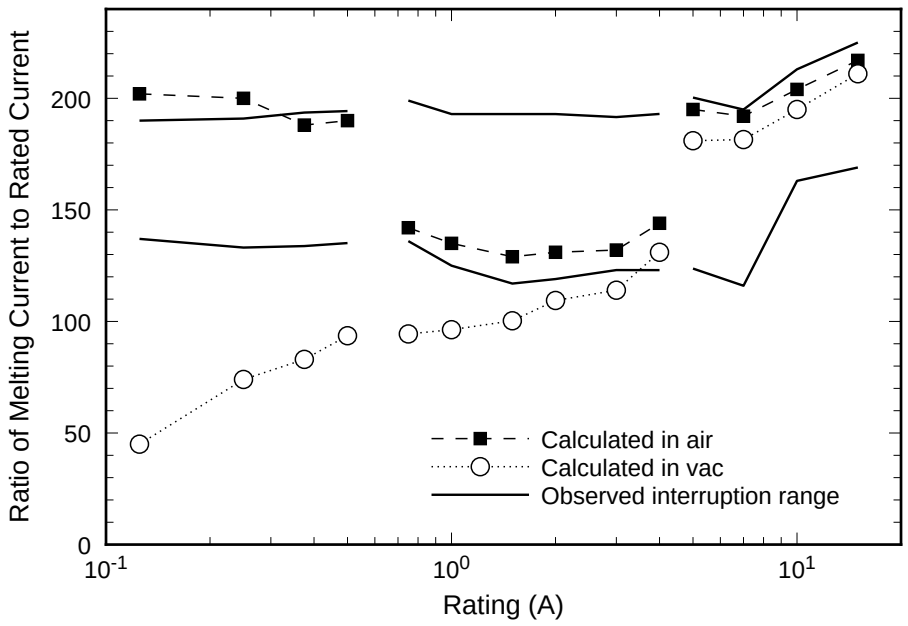

Figure 6.2: Various characteristic currents for FM08 fuses, as ratios to the rated current. The curves are broken as the filament material changes from nickel to copper-silver, and again to copper.

By way of comparison, Littelfuse attaches a range of ±25% to their critical values of the pulse stress index, $(I_0^2 t_0)_{critical}$. The critical value of the pulse stress index is proportional to the second power of the filament's effective cross-sectional area, which mainly controls the variations of the cold resistance; thus, the observed variation in the cold resistance (10%) implies a range in critical value of 20%; thus, four-fifths of the variation of this index are immediately explained, and the remaining part can be assigned to variations in the resistivity and to measurement uncertainties.

Since any fuse of the style considered in this report must carry its rated current for at least four hours (manufacturer's specification), then the manufacturer assigns a rating I_{rating} that is distinctly lower than the average melting current $I_{melt,air}$: this allows for manufacturing variations and also for interruption mechanisms other than melting (e. g., oxidation and creep rupture). Indeed, inspection of Figure 6.2 shows that the average ratio of the melting current to the rated current is close to 160% for all fuses, except for those rated at 10 A and 15 A for which the ratio is about 190%. This ratio has been set by experience, which has taught that setting the ratio this high provides appropriate margin against nuisance failures caused by manufacturing variability, other interruption mechanisms, and to sometimes marginal thermal heat sinking. Even more protection against these concerns could be obtained by setting the ratio even higher; however, the higher this ratio is set, the less there is protection against "soft shorts" or "smart shorts" that draw slightly more than the rated current: the present values for the ratio represent a compromise between these competing concerns.

If a particular fuse is characterized by measuring its properties and is then used in a thermal

environment of known behavior, then its melting current becomes known to about 10%, rather than the usual 25% range:[5] one is protected against inadvertently having that fuse's actual value of I_{inter} be too low or too high, caused by manufacturing variability or inadequate heat sinking.

Inspection of Figure 6.2 shows that:

- When the fuse barrel contains air, then the computed interruption current agrees reasonably well with the range of observed interruption currents.
  - The computed interruption currents are at the high side of the observed range for fuses rated between 1/8 A and 1/2 A. Strictly speaking, the computed values are above the observed range for fuses rated at 1/8 A and at 1/4 A; however, the discrepancy is not significant of a real difference when the uncertainties of the model predictions (about 30% for this range) and the uncertainties of the upper limit of the observed range (about 10%) are acknowledged.

    These fuses use nickel filaments and the assumptions of the modeling are not as accurate for nickel as they are for copper-silver and for copper. If the actual values of electrical resistivity and thermal conductivity of nickel were used, the computed values of interruption current would be lowered.
  - The computed interruption currents are within the observed range for fuses rated between 3/4 A and 4 A. No adjustable parameters are used to obtain this agreement: it is *a priori* and supports the general accuracy of the model for this range of ratings. The model has captured the curvature of the observed data as well as the general location, except that the agreement for 4 A is slightly degraded in comparison with the other ratings (but see the next item).

    The "observed values" are taken from the literature provided by the manufacturers and by Reference [8]. However, testing by Code 313 of fuses rated at 3 A has supported the lower side of this range of "observed values."
  - The computed interruption currents are within the observed range for fuses rated at 5 A and above. And the slope of the observed data (and even the "kink" at 7 A) is captured by the model.

    However, the computed values are near the upper limit of the observed range. This is probably caused by the assumption made in this application of the model that the fuse's case is thermally clamped to 27 °C: this assumption is easy to satisfy for fuses rated at up to 3 A since conventional electrical assembly procedures (e. g., conventional sizes of bus wires and conformal coatings) are able to effectively remove the relatively small joule heat produced by these fuses. However, the joule heat produced by fuses rated at 4 A and above is relatively large: either one adopts nonconventional procedures aimed at aggressively removing joule heat, or one accepts that the fuse's case will rise markedly above 27 °C. It is implicit in Figure 6.2 that the "observed interruption current" for this range of ratings is

[5] We have seen FM08 fuses outside that range: measurement of at least the cold and the hot resistance is prudent for all high reliability applications.

based on data obtained from fuses that are not agressively heat sunk: instead of connecting the fuse to a thermal ground anchored to 27 °C through a thermal resistance of less than a few degrees per watt, rather, a thermal resistance of 50 to 100 °C/watt is used. This is a perfectly reasonable reflection of practice, but deserves to be made more explicit.

In other words, fuses with large ratings interrupt at a current that depends somewhat on the value of the thermal resistance used to connect them to thermal ground. This effect is relatively large for ratings of 15 A down to 5 A, and is visible for 4 A. (This probably explains the slight anomaly noted in the previous item for the fuse rated at 4 A.) Figure 6.2 details the meaning of "relatively large" and "visible."

- When the fuse barrel is evacuated, then the computed interruption current decreases by an amount that depends strongly on the rating.
  - Every FM08 fuse rated at 1.5 A and below will melt within 10 seconds at its rated current (or less) when the barrel is evacuated: loss of air for this range of fuses is catastrophic.
  - Every FM08 fuse rated from 1.5 A to 4 A has lost the factor of 1.6 protection. The ratio of interruption current to rated current now ranges from 0.9 to 1.3: this is too low a ratio to protect against manufacturing variations and inadequate heat sinking.
  - The vacuum interruption current for each of the highest ratings, 5 A to 15 A, decreases by a few percent only, and is well within the range observed for air. That is, the vacuum-induced decrease is small compared with the normal variation. The reason is that the filament's cross-sectional area is so large for this range of ratings, and heat transport along the filament into the caps is so large, that the presence of air is unimportant for thermal transport. (However, the oxidation promoted by air results in long-term degradation.)

There is a problem apparent in Figure 6.2 for ratings 10 A and 15 A. Recall that MIL–F–23419/8F requires an FM08 fuse to interrupt in 0 to 5 seconds under a 200% overload, but a substantial fraction of the fuses that were used to obtain the data shown in Figure 6.2 failed this condition: they carried a 200% overload for at least 10 seconds. Both the vacuum model and the air model agree with this observation. We shall return to this later in this chapter when we consider heat sinking quantitatively, and show that the fuses rated at 10 A and at 15 A are in compliance with MIL–F–23419/8F when operated with appreciable values of thermal resistance: but this deserves to be made more explicit than present specification documents and manufacturer's literature make it.

The difference between the current that melts a filament in a vacuum and the current that interrupts it in air is implicit in Figure 6.2; this difference is made explicit in Figure 6.3. This can be used to rerate a fuse that is known to be evacuated. For example, a fuse whose air-rating is 1/8 A would be assigned a vacuum-rating of 30% of 1/8 A, or 1/25 A; and a fuse whose air-rating is 1 A would be assigned a vacuum-rating of 65% of 1 A, or 0.65 A. However,

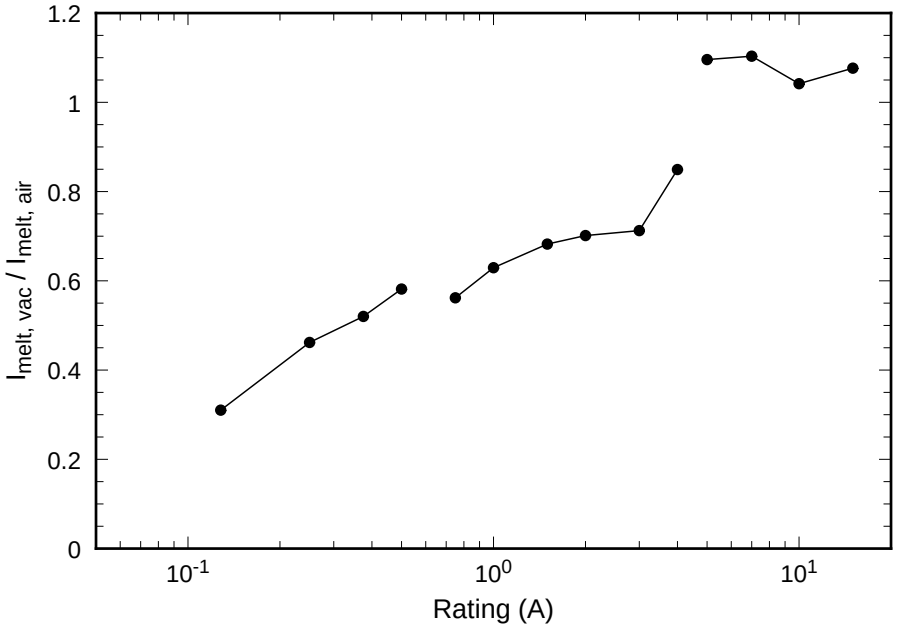

Figure 6.3: The ratio of the melting current for a filament in a vacuum to the interruption current for a filament in air.

the seal on FM08 fuses is undependably hermetic for use in vacuum for more than a few weeks: these fuses may lose their air under vacuum exposure after as little as a few weeks, but many have been observed to retain their air after several years of vacuum exposure. Hence, a fuse rerated from 1 A to 0.65 A may still in fact interrupt at the average value for air operation, 1.6 A, which is 2.5 times the rerated value; thus, the window of opportunity for noninterruption under a "soft short" has been increased from a factor of 1.6 to a factor of 2.5, which decreases the level of protection provided by the fuse. The problem is in the seal: the seal should be designed so that it will either leak all the air in every case, or will leak none of the air in every case.

6.2 Estimate of the effect of air conduction and IR radiation

In this section, we set up the equation for the steady-state distribution of the filament's temperature when air conduction and IR radiation are considered. This equation can be solved numerically, and gives accurate values for the melting current, I_{air}. However, analytic solutions are not just difficult: they are impossible, in the sense introduced by Liouville. Analytic solution becomes possible when the temperature dependence of the air's conductivity is ignored, and the radiative term is linearized: this is acceptable when the effects of these losses are small, since even big errors in a small correction give small errors in the desired result. This approximation is useful for ratings down to 3/4 A, and serves at least as a guide

for smaller ratings. The effect of air is huge for the nickel filaments: an accurate treatment requires a computer model.

6.2.1 Thermal transport through air

A moving volume element of a fluid carries heat from one location to another: the heat is *convected* by the gas. This mechanism can strongly dominate the rate of *conduction* of heat through the fluid. So we must determine if convection happens in the fill gas of the fuse. The driver for convection is the difference in density between the hot and cold parts of the gas, and the acceleration caused by gravity (perhaps augmented by centrifugal acceleration or other applied accelerations). This drive must overwhelm the viscosity of the gas, which acts to limit its motion. So convection is controlled by the dimensionless Rayleigh number (see for example [21]):

$$Ry = \left(\frac{g\beta\Delta T S^3}{\mathcal{D}\nu_k} \right) , \tag{6.9}$$

where

g is the acceleration of gravity (plus any other acceleration that acts);

β is the volumetric thermal expansion of the fluid ($= 1/T$ for an ideal gas);

ΔT is the temperature difference across the length scale distance, S;

$\mathcal{D}$ is the thermal diffusivity of the fluid; and

ν_k is the kinematic viscosity of the fluid.

Many experiments show that heat flow driven by convection begins to become important relative to that driven by conduction when $Ry > 10^3$. We find the the Rayleigh number for the air in a fuse ranges from 0.05 when the filament is elevated by 100 °C from the barrel, to 0.5 when the elevation is 1000 °C; thus, we expect convection to be negligible for these fuses. However, the Rayleigh number would increase to 10^3 if the barrel radius were to increase by a factor of about 10. The acceleration would have to increase by a factor of about 10^3.

Measurements carried out by Mr. Van Sant and Mr. Munoz on a fuse rated at 3 A operated with its barrel horizontal show that the midbarrel temperature is about 20 °C higher than the temperature of the caps when driven at the rated temperature and when the leads are well heat-sunk. This temperature rise is caused by heat transported from the middle of the filament. If convection provided part of this total heat transport, then the midbarrel temperature elevation would change as one moved around the barrel from top to bottom since the convective air plume transports heat upwards to the top of the barrel, after which the cooled air moves around the side to the bottom of the barrel. However, any temperature difference was smaller than the 0.1 °C uncertainty of this experiment. This experiment shows that convective effects are smaller than about 0.1 parts in 20, or 0.5%.

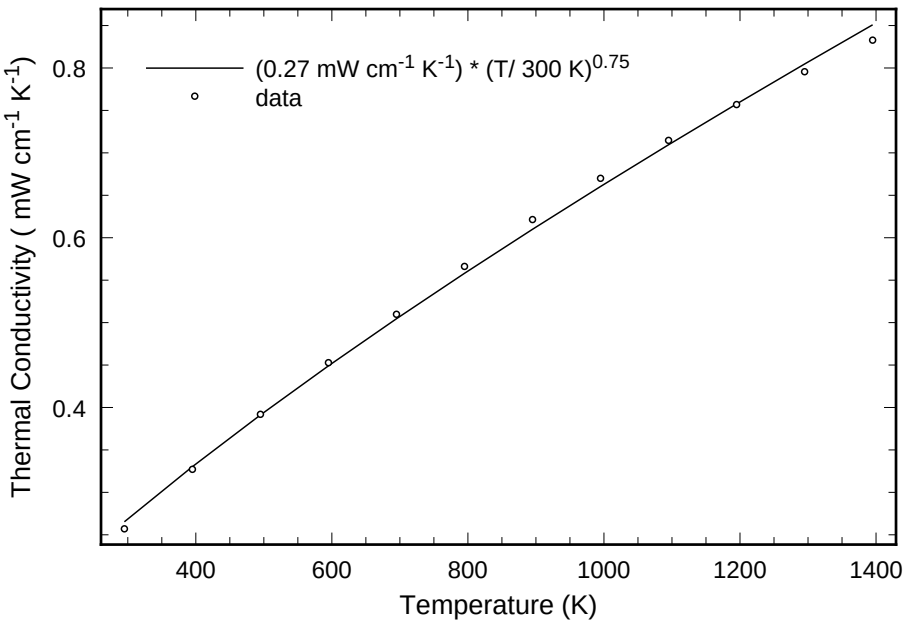

Figure 6.4: Thermal conductivity of air versus temperature

Also, heat transported through the fill gas reduces the electrical resistance of a 3 A rated fuse by about 8% relative to its value when there is no fill gas: see Figure 6.1 which shows that a 3 A rated fuse driven at 3 A has a resistance of about 45 mΩ when the barrel is filled with air, and 49 mΩ when the barrel is evacuated. If convection provided part of the total heat transport that causes this resistance reduction, then the amount of reduction would change as the fuse is rotated from a horizontal barrel condition to a vertical barrel condition since the air plume cools differently when it rises vertically across the filament than when it rise along the filament. But further measurements carried out by Mr. Van Sant and Mr. Munoz show that any change was smaller than the 0.05 mΩ uncertainty of the experiment. This shows that convective effects are smaller than about 0.05 parts in 4, or 1%.

Thus, convection will be ignored: thermal transport is through essentially stagnant air; hence, the heat current is driven by only the thermal gradient: $\mathbf{J}_h = -k_T^{air} \nabla T$ where k_T^{air} is the thermal conductivity of air: see Figure 6.4.

The constant value $k_T^{air} \approx 4.4 \times 10^{-4}$ watt$\cdot$cm$^{-1}\cdot$K^{-1} is useful for crude estimates of the effect of air conduction over the range from $T_0 = 300$ K to T_{melt}. For more accurate estimates, a power law is much better. The power law shown in Figure 6.4 is accurate to within two percent over the range from 300 K to 922 K (= 1200 °F, the upper limit of the table) using the values $T_0 = 300$ K, $k_T^{air,0} = 2.7 \times 10^{-4}$ watt$\cdot$cm$^{-1}\cdot$K^{-1}, and $\delta = 0.75$. The estimate given by Equation 6.17 can be used to systematically compute the best temperature-independent value, given the temperature range in interest.

There are no heat sources within the cavity between the fuse filament and the inside radius of the barrel, and so, for steady state conditions, using cylindrical coordinates:

$$0 = \nabla \cdot \mathbf{J}_h^{air} = \frac{1}{r}\frac{\partial(rJ_r^{air})}{\partial r} + \frac{1}{r}\frac{\partial J_\theta^{air}}{\partial \theta} + \frac{\partial J_z^{air}}{\partial z} \tag{6.10}$$

$$\approx \frac{1}{r}\frac{\partial(rJ_r^{air})}{\partial r}, \tag{6.11}$$

since the approximate θ-symmetry implies that the θ variations approximately vanish, and since z variations are much smaller than r variations. This implies that rJ_r^{air} is a constant from the outside radius of the filament $r = a$ to the inside radius of the barrel $r = b$. And so

$$-k_T^{air}(T)\left(\frac{dT}{dr}\right) = J_r^{air}(r) = \left(\frac{a}{r}\right)J_r^{air}(a+). \tag{6.12}$$

Using the power law model for $k_T^{air}(T)$ transforms this to

$$-k_T^{air,0}\left(\frac{T}{T_0}\right)^{\delta}\left(\frac{dT}{dr}\right) = \left(\frac{a}{r}\right)J_r^{air}(a+), \tag{6.13}$$

which can be integrated and solved for $J_r^{air}(a+)$ to obtain

$$J_r^{air}(a+,z) = \left(\frac{1}{1+\delta}\right)\left[\frac{T_0\,k_T^{air,0}}{a\ln(b/a)}\right]\left[\left(\frac{T(a,z)}{T(b,z)}\right)^{1+\delta} - 1\right], \tag{6.14}$$

where the z-dependences of the heat current density $J_r^{air}(a+,z)$ and of the temperatures of the filament $T(a,z)$ and the inside of the barrel $T(b,z)$ are noted. This result is not exact since it ignores small variations with θ and z.

This model assumes that the filament is mounted at the axis of the barrel, that is, the filament is concentric with the barrel. But examination of the filaments in real fuses shows that they usually touch the inside of the barrel at each end, and are concentric only when they are near the middle; indeed, some filaments have their midsection substantially eccentric and not concentric. Hence it may seem that this thermal conduction model is not apt for most fuses. However, air conduction is only important where the filament is hot, which only happens near its middle; thus, the location of the relatively cold ends is of no consequence and we may safely ignore that the ends are not concentric. Also, analysis shows that the concentric geometry gives the same result as an eccentric one, up to a substantial amount of eccentricity: the brief explanation is that the decrease in the heat flux on the side of the filament that moves away from the barrel is compensated by the heat flux increase on the other side.

A more detailed explanation is given by Vargaftik[6] who reports the ratio of the heat flux per length delivered from a cylinder of radius a displaced by the distance e from the central axis of an enclosing cylinder of radius b, to the value when the central cylinder is concentric

[6] "Dependence of the Coefficient of Gases and Vapors on Pressure," J. Tech. Phys. **7**, 1199–216 (1937). As referenced in [21], Volume 3.

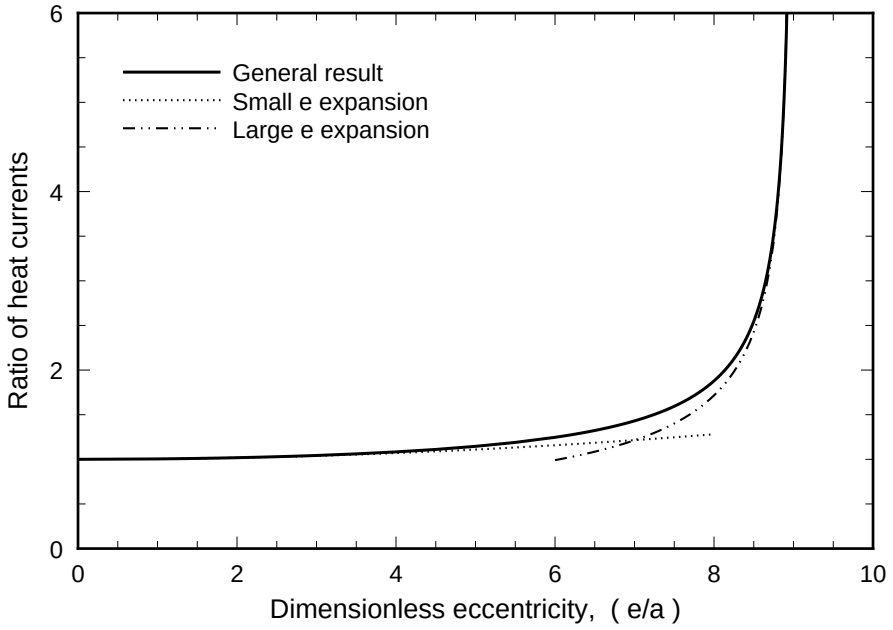

Figure 6.5: The ratio of the heat current with increasing eccentricity e/a to the heat current with $e/a = 0$ for a hot cylinder of radius a inside an enclosing cold cylinder of radius b, when $b/a = 10$. Also shown are the small e and large e expansions given in the text.

($e = 0$). The analytic expression of this ratio is complicated in general, but simplifies both when e is small, and when e is so large that the inner cylinder is nearly touching the enclosing one:

$$\text{ratio} = 1 + \frac{e^2}{(b^2 - a^2)\ln(b/a)}\,, \quad e \sim 0 \tag{6.15}$$

$$= \frac{\ln(b/a)}{\sqrt{2(1/a - 1/b)}} \cdot \frac{1}{\sqrt{b - a - e}}\,, \quad e \sim b - a\,. \tag{6.16}$$

Numerical values are shown in Figure 6.5 for the case appropriate for a fuse rated at 3 A: $b/a = 10$. The heat flux remains at nearly its concentric value as the filament is displaced by almost half the barrel's inner radius: the increase is less than 10% for $e/a < 4.3$ which is $e < 43\%$ of b. Hence a small eccentricity has a negligible effect: the concentric thermal conduction model continues to be usefully accurate even for displacements of roughly half of the barrel radius b (for $b/a \sim 10$).

However, large translations do have an effect: note that the heat flux shown in Figure 6.5 diverges to infinity as the filament approaches the inner wall of the barrel. Some filaments are mounted — not diagonally as shown in Figure 3.1 — but with both ends on the same side of the barrel (i. e., both ends have the same value of θ, rather than these θ-values being different by π radians). These filaments are shaped like an archer's bow with the midsection approaching the far side of the barrel. Under thermal expansion, the midsection of certain of these fuses can approach the far side and the heat flux becomes very large as this happens. The model just discussed is then not apt. (There is the possibility that the midsection can

touch the side of the barrel as the current is increases: then, the thermal path that is created can effectively clamp further increases in temperature, and the fuse can carry substantially more current that the FM08 design allows.)

This model also assumes that the filament has a circular cross-section. But filaments are flattened for ratings of 4 A and larger: it may seem that the model is not apt for these ratings. However, deformation of the inner boundary from a circle to an ellipse, under constant enclosed area, is a second order effect for the flow of heat; hence, small flattenings do not change the θ-integrated heat flux. The actual flattening of the filaments of 4 A and higher rated fuses is large enough so that a change by a factor as large as two or three might result; however, the total importance of air losses for these rating is small (less than 8% at 4 A, decreasing to 2% for 15 A, computed on the basis of a circular cross-section) and so an accurate consideration of the effect of flattening seems unrewarding at this time.

A cruder approximation results by ignoring the temperature dependence of k_T^{air}, and choosing $\delta = 0$ to obtain $\langle k_T^{air} \rangle$, and using this during the double integration over z: the advantage is that the double integration can now be carried out analytically. Since $k_T^{air}(T)$ increases by a factor of roughly three as the temperature increases from T_0 to T_{melt}, it may appear that this approximation is subject to an uncertainty of about this size, but analysis shows that it is distinctly less: the larger the value of k_T^{air}, the smaller the temperature gradient at $r = a$, and so the product $k_T^{air} \nabla T|_a$ shows a distinctly smaller variation than does k_T^{air}.

There are various ways of constructing an average. We chose an average such that it gives the correct value of the heat flux at the middle of the filament; that is, we match the value of J_r at $r = a$ and $z = 0$:

$$\langle k_T^{air} \rangle = \left(\frac{1}{1+\delta} \right) \cdot \left[\frac{(T_{mid}/T_{cap})^{1+\delta} - 1}{(T_{mid}/T_{cap}) - 1} \right] \cdot \left(\frac{T_{cap}}{T_0} \right)^{\delta} \cdot k_T^{air,0} \,. \tag{6.17}$$

This overestimates the heat loss everywhere else along the filament, but, since the heat loss is small everywhere else, then this error will not much affect the desired results. For quick estimates, we use a value for T_{mid} that is anywhere between T_{cap} and T_{melt}. For more careful estimates, we use the quick result as the first step in an iterative sequence: experience shows that this sequence rapidly converges to a consistent result.

Another kind of objection to the treatment of air conduction given here is that it supposes that the gas in contact with a surface has the same temperature as the surface. But it is well-known that there is a temperature jump at this surface.[7] The effect of this is to give the thermal conductivity an apparent pressure dependence which increases as the filament radius decreases. But direct computations for the range of parameters encountered in FM08 style fuses shows that this effect is less than a few percent for all ratings, for air at atmospheric pressure. This effect could become significant in a study of the thermal conductivity of a fill gas at reduced pressure.

[7] See almost any text on gases, such as pp. 483 of Kennard, *Kinetic Theory of Gases*, McGraw-Hill (1938).

Finally, the suggestion was made[8] that the thermal conductivity of the fill gas used in current practice (the air that is present in the fuse assembly room: close to a standard atmosphere at about 50% relative humidity) would be so different from dry nitrogen that a distinct fuse performance would result. But standard tables ([21] for example) show that the difference between the thermal conductivity k_T^{gas} of air at 20% to 80% relative humidity and dry nitrogen is less than ten percent from room temperature to 1000 °C. So the effect on thermal transport of switching the fill gas from air to dry nitrogen should be negligible.

6.2.2 IR radiation

The estimate is $J_r^{rad}(a+,z) = (\epsilon\sigma_{SB}) \cdot [T(a,z)^4 - T(b,z)^4]$, where ϵ is the emissivity of the fuse filament and $\sigma_{SB} = 5.6696 \times 10^{-12}$ watt$\cdot$cm$^{-1}\cdot$K^{-4} is the Stefan-Boltzmann constant. When the filament's temperature $T(a,z)$ is only a little greater than the barrel's temperature $T(b,z)$, then $J_r^{rad}(a+,z) \approx (4\epsilon\sigma_{SB}) \cdot T(b,z)^3 \cdot [T(a,z) - T(b,z)]$, which is of the same form as for air conduction when $\delta = 0$; then, the ratio is $J_r^{rad}(a+,z)/J_r^{air}(a+,z) \approx 4\epsilon\sigma_{SB}T(b,z)^3 a \ln(b/a)/k_T^{air,0} \approx 10^{-3}$ using $\epsilon \approx 0.1$, and so IR radiation is completely negligible for temperatures up to roughly 600 K. When the filament develops a layer of black CuO after operation at high temperature, the emissivity rises to about 0.9, and the effect of IR radiation increases to roughly 1% of air conduction: this is just visible as a change in resistance during certain measurements when care is taken to maintain constant current and constant case temperature.

Computer modeling shows that IR radiation becomes increasingly important as the temperature is increased to near the melting point, where it affects the melting current by 1% to 5% percent.[9] Hence, we will treat IR radiation as a small perturbation on the other loss mechanisms.

6.2.3 Steady state behavior when air is present: approximate treatment

The equation for the steady-state temperature distribution is, using the results for air conduction and IR radiation:

$$-(\mathcal{L}T_0/\rho_0) \cdot \left(\frac{d^2T}{dz^2}\right) = \rho_0 \cdot \frac{T}{T_0} \cdot \left(\frac{I}{A}\right)^2 - \left(\frac{2}{1+\delta}\right)\left(\frac{T_0\, k_T^{air,0}}{a^2 \ln(b/a)}\right)\left[\left(\frac{T}{T(b,z)}\right)^{1+\delta} - 1\right] - \left(\frac{2\epsilon\sigma_{SB}}{a}\right) \cdot [T^4 - T(b,z)^4]\,. \tag{6.18}$$

There are no analytic solutions of this equation. However, computer solutions are straightforward, and allow useful checks on the approximations introduced next.

[8] Private communication from Mr. Art Siegal, reporting on a meeting with a fuse manufacturer.

[9] Incandescent lamps use filaments of tungsten operated in the range 2 000 K to 2 400 K. IR radiation then removes as much as one third to one half of the power.

This equation can be solved in analytic form when: (a) the temperature dependence of the thermal conductivity of air is neglected: use $\delta = 0$; (b) the IR radiation term is neglected, or linearized and combined with the air conduction term; and (c) the barrel temperature is held constant: $T(b, z) = T_{cap}$. Then the equation becomes

$$\frac{d^2T}{dz^2} = -\kappa^2 \cdot T + \chi^2 \cdot (T - T_{cap}) \ , \tag{6.19}$$

where the boundary conditions are $T(\pm\ell/2) = T_{cap}$ and

$\kappa\ell$ $= (IR_0)/(\sqrt{\mathcal{L}}\,T_0)$ is the dimensionless measure of the effect of the joule power to heat, relative to the effectiveness of the filament's thermal conductivity to cool, and I is the current;

ℓ is the length of the fuse filament;

R_0 is the electrical resistance of the filament at the temperature T_0;

$\mathcal{L}$ $= k_T\,\rho/T$ is the Lorenz number, whose quantal value is 2.443×10^{-8} volt^2/K^2;

k_T is the thermal conductivity of the fuse filament;

ρ is the electrical resistivity of the filament, modeled as $\rho(T) = (T/T_0) \cdot \rho_0$;

T_0 is a reference temperature on the absolute scale (we use 300 K);

$\chi\ell$ $= [\frac{T_0}{T_{cap}} \frac{\langle k_T^{air} \rangle}{k_T} \frac{2\ell^2}{a^2 \ln(b/a)}]^{1/2}$ is a dimensionless measure of the heat current extracted from the fuse filament by thermal conduction through air, relative to that conducted through the filament's cross-section;

$\langle k_T^{air} \rangle$ is the thermal conductivity of air at some temperature between T_{cap} and T_{melt}, chosen to balance errors (see Equation 6.17);

a is the radius of the fuse filament; and

b is the inside radius of the fuse barrel.

Note that the dimensionless measures $\kappa\ell$ and $\chi\ell$ are independent of temperature and position, to a good approximation.

The temperature distribution is:

$$T = T_{cap} \cdot \left\{ \chi^2 - \kappa^2 \cdot \left[\frac{\cosh(\sqrt{\chi^2 - \kappa^2}\, z)}{\cosh(\sqrt{\chi^2 - \kappa^2}\, \ell/2)} \right] \right\} / (\chi^2 - \kappa^2) \quad \text{for } \kappa < \chi, \tag{6.20}$$

$$= T_{cap} \cdot \left\{ 1 + \frac{1}{2} \left(\frac{\kappa\ell}{2} \right)^2 \left[1 - \left(\frac{2z}{\ell} \right)^2 \right] \right\} \quad \text{for } \kappa = \chi, \tag{6.21}$$

$$= T_{cap} \cdot \left\{ \kappa^2 \cdot \left[\frac{\cos(\sqrt{\kappa^2 - \chi^2}\, z)}{\cos(\sqrt{\kappa^2 - \chi^2}\, \ell/2)} \right] - \chi^2 \right\} / (\kappa^2 - \chi^2) \quad \text{for } \kappa > \chi. \tag{6.22}$$

And the electrical resistance of the fuse is obtained from $R = \int_{-\ell/2}^{+\ell/2} [\rho(T(z))/A]\, dz$, with the result:

$$R = R_0 \cdot \frac{T_{cap}}{T_0} \cdot \left[\chi^2 - \kappa^2 \,\mathrm{tanhc}(\sqrt{\chi^2 - \kappa^2}\,\ell/2)\right] / (\chi^2 - \kappa^2) \text{ for } \kappa < \chi, \tag{6.23}$$

$$= R_0 \cdot \frac{T_{cap}}{T_0} \cdot \left[1 + \frac{1}{3}\left(\frac{\kappa\ell}{2}\right)^2\right] \text{ for } \kappa = \chi, \tag{6.24}$$

$$= R_0 \cdot \frac{T_{cap}}{T_0} \cdot \left[\kappa^2 \,\mathrm{tanc}(\sqrt{\kappa^2 - \chi^2}\,\ell/2) - \chi^2\right] / (\kappa^2 - \chi^2) \text{ for } \kappa > \chi, \tag{6.25}$$

where $\mathrm{tanhc}(\xi) \stackrel{def}{=} \tanh(\xi)/\xi$ and $\mathrm{tanc}(\xi) \stackrel{def}{=} \tan(\xi)/\xi$.

These results are listed in a form suitable for immediate calculation using standard tables or programs; these usually require "real" (not "imaginary") arguments. However, the $\kappa < \chi$ results are actually the same as the $\kappa > \chi$ results on the complex plane, as the identities $\cos(\sqrt{-1}\,\xi) = \cosh(\xi)$ and $\cosh(\sqrt{-1}\,\zeta) = \cos(\zeta)$ remind us: only one of these results is needed when programming on the complex plane. And the temperature distribution and the resistance for the special case $\kappa = \chi$ can be obtained either by direct solution of the differential equation under this equality, or as the limit of either the $\kappa > \chi$ or the $\kappa < \chi$ case: that the special case is the limit of either of the other two demonstrates it is also not really distinct.

Figure 6.6 illustrates the good agreement between this equation and some observations for a fuse containing air: only the cold resistance R_{cold} was used as a fitting parameter. Also shown for comparison are the results of the vacuum model. The effects of IR radiation on each result are shown for two values of emissivity, corresponding to an unoxidized filament ($\epsilon \approx 0.1$) and one with a film of CuO ($\epsilon \approx 0.9$); these IR effects were computed using a computer model described on page 81 and following. The difference between $\epsilon = 0.1$ and $\epsilon = 0$ (i. e., no radiative losses) is too small to display on this plot.

The values of $\kappa\ell$ and $\chi\ell$ are computed from the definitions given on page 76, using the average cold resistance specified by MIL–F–23419/8F, the quantal value of the Lorenz number $\mathcal{L}$, $T_0 = 300$ K, and $\langle k_T^{air} \rangle$ specified as in Equation 6.17. Values are given in Table 6.1. These values are not corrected for IR radiation losses.

For ratings of 3/4 A and larger, the model-results should be within 10% to 20% of the observed results since that is the accuracy with which the model describes the material data and the physical processes. And Figure 6.2 shows agreement on this order.

However, the results for ratings 1/2 A and below are not expected to be as accurate as for ratings of 3/4 A and larger for two reasons: (a) the resistivity and thermal conductivity of nickel are approximated poorly by the simple rules used here, and (b) air conductivity plays a major role while the simplified treatment used here only works when the role is modest. Hence, agreement to within only roughly 50% is expected. However, Figure 6.2 shows that somewhat better agreement is actually obtained: apparently some errors compensate.

The temperature of the middle of the filament at the rated current is only a fraction of the

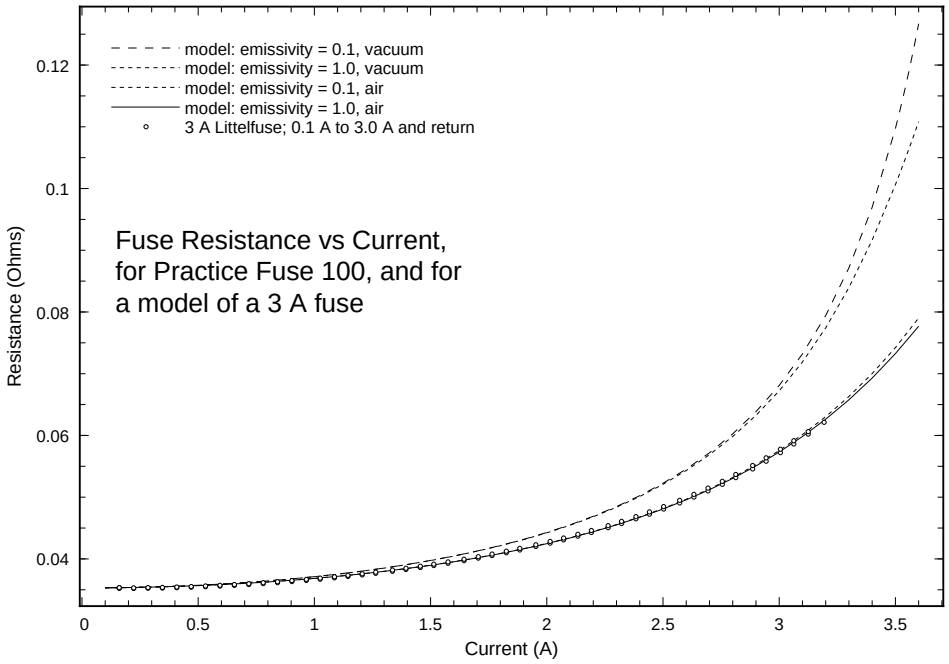

Figure 6.6: Measurements of the resistance of an FM08 fuse rated at 3 A, called Practice Fuse 100, versus current. Also shown are the results given by the vacuum model and by the model that supposes that the filament is bathed in air. The effects of IR radiation are shown for two values of emissivity.

melting temperature, so IR radiation affects the rated-current results only slightly, on the order of roughly a few tenths of one percent. However, the melting points are several times higher and radiation effects increase as T^4: IR radiation affects melting point results by as much as 5% for the 3/4 A rating. These IR-corrected results are shown in Figure 6.2. Inspection shows that the results are in fair agreement with the observed interruption currents for all ratings. The agreement for ratings of 1/2 A and below results from a cancellation of large errors: fuses in this range of ratings require attention to the complicated temperature dependence of the material parameters, which in turn requires a computer model, and not this analytic one.

Further inspection of Table 6.1 indicates that $\chi\ell$ is greater than $\kappa\ell$ at the rated current for all the fuses rated at 3/4 A and below: hence, the top of the three possible forms for the temperature and resistance equations must be used. This leads to a relatively "flat-topped" temperature distribution, and to a slow increase in resistance with current. Air conduction removes heat everywhere along the fuse filament, and so its temperature is more nearly uniform versus z.

In order to measure the resistance of the fuse, it is necessary to pass a current through it: this current heats the filament and increases its resistance. MIL–F–23419/8F specifies that the cold resistance be measured using a current that is 10% or less of the rated current: it is of interest to check the extent to which $R(I_{rating}/10)$ exceeds $R(0)$. The values of $\kappa\ell$ at the

rated current range from 5.6 for a fuse rated at 1/8 A, to 1.3 for a fuse rated at 15 A, while the corresponding values of $\chi\ell$ range from 9.7 to 0.7. The results of Equations 6.23 through 6.25 show that $R(I_{rating})/R(0)$ is never more than 1.0039, so the cold resistance is defined to within 0.39% by this current-limiting rule. This same change is produced by increasing T_{cap} by 1.2 °C. MIL–F–23419/8F allows a 5 °C range in the temperature, and this corresponds to a range of 1.7% in the resistance; hence, the current-limiting rule is more than adequate.

If the fuses are evacuated, however, then $R(I_{rating})/R(0)$ is as large as 1.2%: we conclude (a) the rule is still an adequate one and (b) air conduction is important even at low currents. The following double Taylor's expansion shows the effect of air conduction at low currents more directly:

$$\frac{R}{R_0} = 1 + \left[1 - \frac{(\chi\ell)^2}{10} + \mathcal{O}(\chi\ell)^4\right] \frac{(\kappa\ell)^2}{12} + \left[1 - \frac{102(\chi\ell)^2}{509} + \mathcal{O}(\chi\ell)^4\right] \frac{(\kappa\ell)^4}{120} + \mathcal{O}(\kappa\ell)^6 \,. \quad (6.26)$$

Setting $\chi\ell = 0$ returns the vacuum result, as it should. Increasing $\chi\ell$ decreases each term in R, and decreases R. That is, as air is introduced into an evacuated fuse, under constant current, the filament will cool and the resistance will decrease. (While this series illustrates that the effects of air conduction are visible even at low current, the values of $\chi\ell$ are so large for most FM08 ratings that series-convergence requires many terms; it is better to use Equations 6.23 through 6.25 for practical computations.)

For a large current, the fuse filament temperature diverges to infinity at $\kappa_{\infty,0}\ell = \pi$ when $\chi = 0$ (the vacuum case), and at $\kappa_\infty\ell = [\pi^2 - (\chi\ell)^2]^{1/2}$ for $\chi < \kappa$. The ratio of these currents gives an indication of the manner in which air conduction and fuse filament dimensions affects the filament's heating:

$$\frac{i_{\infty,air}}{i_{\infty,vac}} = \frac{\kappa_\infty\ell}{\kappa_{\infty,0}\ell} = \sqrt{1 + \frac{2}{\pi^2}\frac{T_0}{T_{cap}}\frac{\langle k_T^{air}\rangle}{k_T}\frac{\ell^2}{a^2\ln(b/a)}} \,. \quad (6.27)$$

Heat is conducted through the fuse filament in proportion to its thermal conductivity k_T and its cross-sectional area $A = \pi a^2$ and the gradient dT/dz which is proportional to ℓ^{-1}, while heat is conducted through the surrounding air in proportion to its thermal conductivity $\langle k_T^{air}\rangle$ and the surface area $2\pi a\ell$ and the thermal gradient which is proportional to $\ln(b/a)$: hence, the ratio has the factors shown in the expression of the previous paragraph.

Integration of the steady-state equation by quadratures

Equation 6.19 cannot be solved in the form $T = T(z)$ by analytic methods for either $\delta \neq 0$ or $\epsilon \neq 0$ (or both). However, it can be solved in the form $z = z(T)$ by expressing it as an integral, so long as the terms in Equation 6.19 (or a generalization of it) depends only on T (i. e., so long as the coefficients do not depend on z). This integral (see Equation 6.33) also eludes analytic methods for nonvanishing δ and ϵ; however, it already has the correct boundary conditions embedded within it, and this facilitates numerical work.

Only a sketch of this method is given here. Write the equation in the form

$$\frac{d^2T}{dz^2} = \mathcal{F}(T)\,. \tag{6.28}$$

Then multiply both sides by dT/dz, and recognize certain identities to obtain

$$\frac{d}{dz}\left[\frac{1}{2}\left(\frac{dT}{dz}\right)^2\right] = \frac{d^2T}{dz^2}\frac{dT}{dz} = \mathcal{F}(T)\frac{dT}{dz} = \frac{d}{dz}\int^T \mathcal{F}(T')\,dT'. \tag{6.29}$$

Integrate on z to obtain

$$\frac{1}{2}\left(\frac{dT}{dz}\right)^2 - \frac{1}{2}\left(\frac{dT}{dz}\right)^2_{mid} = \int_{T_{mid}}^{T} \mathcal{F}(T')\,dT', \tag{6.30}$$

where $\{\ \}_{mid}$ means "middle of the fuse filament, $z = 0$." Recall that T is a maximum at the middle of the fuse filament, so $(dT/dz)_{mid} = 0$, and solve for dT/dz to obtain

$$\frac{dT}{dz} = \pm\sqrt{2\int_{T_{mid}}^{T} \mathcal{F}(T')\,dT'}, \tag{6.31}$$

where the top sign applies for $z < 0$ and the bottom sign applies for $z > 0$. This is rearranged as follows:

$$dz = \pm\frac{dT}{\sqrt{2\int_{T_{mid}}^{T} \mathcal{F}(T')\,dT'}}, \tag{6.32}$$

and integrated again to give the position corresponding to a given temperature (i. e., the inverse of the temperature distribution):

$$z = \mp\int_{T_{mid}}^{T} \frac{dT''}{\sqrt{2\int_{T_{mid}}^{T''} \mathcal{F}(T')\,dT'}}\,. \tag{6.33}$$

This result, which gives $z(T)$ in terms of a doubly iterated definite integral, applies so long as the right hand side of Equation 6.19 (or a generalization of it) depends only on the temperature T, and not also on explicit position z. When the integrals can be solved completely in terms of the known elementary (in the sense of Liouville) functions, then $z(T)$ is said to be reduced to quadratures. However, since the integrals are definite, numerical methods are always directly applicable.

This result for $z(T)$ can sometimes be analytically inverted into the standard form $T(z)$, and can always be numerically inverted. However, this is not necessary for the computation of the dependence of the resistance on the current, $R(i)$, since integration by parts allows direct use of $z(T)$:

$$\begin{aligned} R &= \int_{-\ell/2}^{+\ell/2} [\rho(T(z))/A]\,dz \\ &= \frac{R_0}{\ell T_0}\int_{-\ell/2}^{+\ell/2} T(z)\,dz \end{aligned} \tag{6.34}$$

$$
\begin{aligned}
&= \frac{R_0}{\ell T_0}\left\{[zT(z)]_{-\ell/2}^{+\ell/2} - 2\int_{T_{mid}}^{T_0} z(T)dT\right\} \\
&= R_0\left\{1 + \frac{2}{\ell T_0}\int_{T_0}^{T_{mid}} z(T)dT\right\}.
\end{aligned}
$$

For Equation 6.19, the inner integral is straightforward:

$$
\int_{T_{mid}}^{T} \mathcal{F}(T)\,dT = \tag{6.35}
$$
$$
\kappa^2\left[\frac{T_{mid}^2 - T^2}{2}\right] - \chi^2\left[\frac{T_{mid}^{2+\delta} - T^{2+\delta}}{(2+\delta)T_0^{\delta}} - T_0(T_{mid} - T)\right] - \psi^2\left[\frac{T_{mid}^5 - T^5}{5T_0^3} - T_0(T_{mid} - T)\right].
$$

The second integral can only be carried out analytically for certain values of δ, not including values of δ near 0.8. Many standard numerical packages fail to handle the divergence at the ends of the filament, which is especially important for large air conduction (i. e., small filaments): special packages or special attention is necessary. The physical source of the divergence is that the temperature distribution is flat-topped.

This method is fast and precise, and can easily be extended to use temperature dependent material properties. However, oxidation proceeds fastest where the filament is hottest, so that the thermal emissivity ϵ becomes a function of location along the filament: then this method is no longer applicable, except as a starting point.

Integration of the steady-state equation by shooting methods

Equation 6.19 can also be solved using conventional numerical integration methods such as a Runge-Kutta stepping integrator. However, these "marching methods" all start at one end point, say $z = -\ell/2$, and require knowledge of both $T(z)$ and dT/dz there: but we do not know dT/dz there until we have already solved for the full distribution. Hence, a guess is made for the value of dT/dz at $z = -\ell/2$ and the distribution for this guess is generated, and used to compute the value it gives for dT/dz at $z = +\ell/2$: except by a numerical fluke of vanishing probability, this will be wrong. The error is then used to correct the guess for dT/dz at $z = -\ell/2$, and the process is repeated until the error is tolerable. Hence, this is called the "shooting method" since it resembles aiming a gun by firing it, and using the error between the target and the observed hit to correct the aim of the next shot, until the target is hit (closely enough).

This method works for the steady-state equation even when the correct experimental behaviors of the material parameters are used. Since the temperature distribution is symmetric, it is only necessary to integrate to the middle of the filament and require that $dT/dz = 0$ there, rather than to integrate to the end of the filament. It is necessary to use a robust method for correcting the guesses: for example, a Newton-Cotes method is too easy to drive into instability, especially as the air conduction term becomes large. The analytic solution given in Equations 6.20 through 6.22 has proven valuable as a starting point in iterative

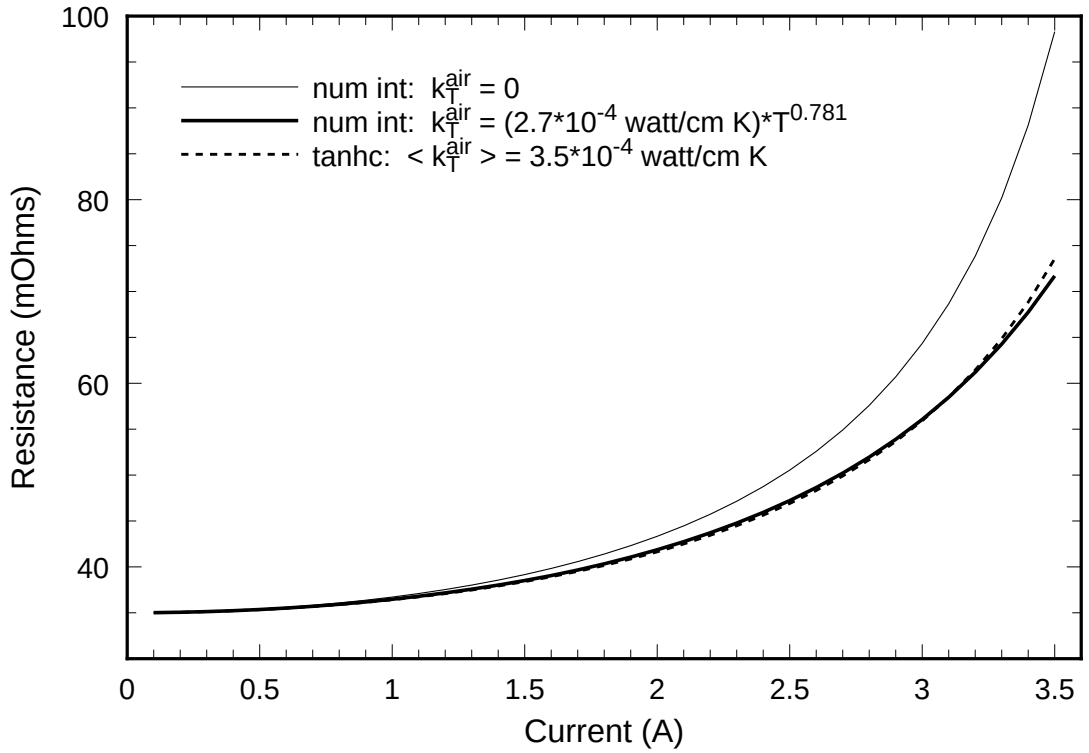

Figure 6.7: The resistance of a model fuse rated at 3 A, computed using a numerical integration of an accurate but analytically intractable equation, and computed using the analytical solution to an approximation of the accurate equation: these results are labeled "num int" and "tanhc" respectively. The solutions for the vacuum case are too close to be distinguished, so only the numerical solution is shown. The solutions "num int" and "tanhc" when the filament is bathed in air agree to within a few percent up to 3.5 A. The effect of radiation is not shown in this plot ($\epsilon = 0$).

root-finding procedures. Running on a desktop computer, several solutions per second can be obtained when coding in `C` and about one solution every five seconds when coding in *Mathmatica*, when adjusted to give a relative precision of $\pm 0.02\%$.

Using the numerical integration of the full equation for the distribution of the temperature along the filament, Equation 6.19, we can now address the accuracy of the approximations that allowed derivation of the analytic expressions given in Equations 6.23 through 6.25. These are illustrated in Figure 6.7 for parameters appropriate for a fuse rated at 3 A. The analytically challenging terms of Equation 6.19 vanish when the fuse barrel is evacuated, and IR radiation is ignored: the analytic solution is exact then, and serves as a check on the precision of the numerical method. Direct numerical solutions show that the effect of IR radiation is less than a few percent at the rated current for this model fuse; it does begin to depress the resistance by as much as 5% at the melting current.

The analytic curve is labeled by "tanhc." A constant value of $\langle k_T^{air} \rangle = 3.5 \times 10^{-4}$ watt/(cm$\cdot$ K) was used. This is too large at low currents, and indeed, "tanhc" is depressed there. And it

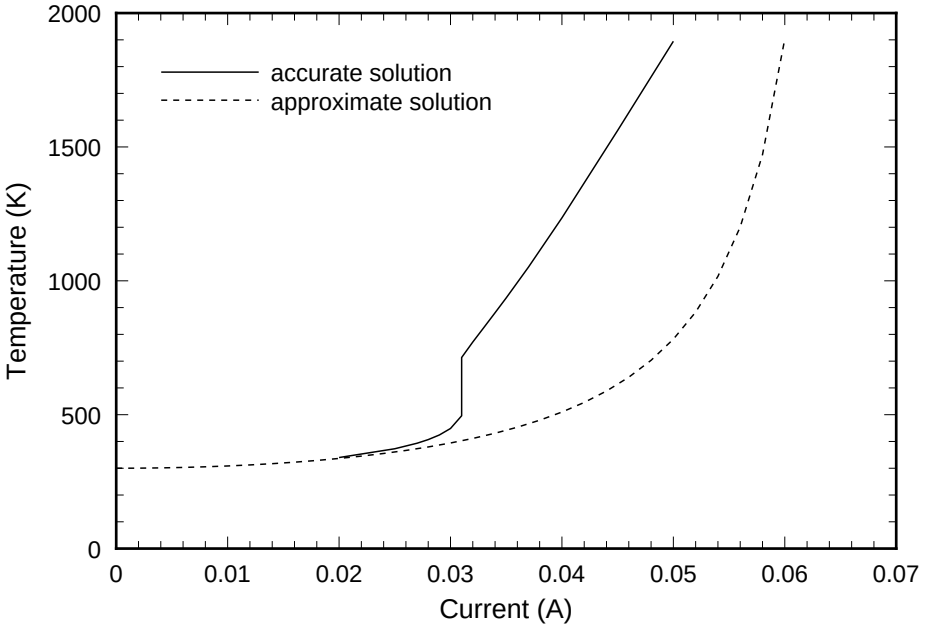

Figure 6.8: The midfilament temperature versus current of an FM08 style fuse rated at 1/8 A: the fuse case is evaluated, radiation is ignored ($\epsilon = 0.00$), and the case temperature is $T_0 = 27$ °C. The "accurate" solution uses accurate descriptions for $\rho(T)$ and $k_T(T)$ for nickel, and the "approximate" solution uses $\rho(T) = \rho(T_0) \cdot T/T_0$ and $k_T(T) = k_T(T_0)$.

is too small at large currents: "tanhc" exceeds the numerical results then. Somewhat better results are obtained using the rule given in Equation 6.17, but the improvement is small and adds to the complexity of the calculations.

The numerical approach is able to use accurate temperature dependences for the material properties of the filament, including the volume specific heat $c(T)$, the thermal conductivity $k_T(T)$, and the electrical resistivity $\rho(T)$. These greatly increase computational complexity, while affecting results for the copper-silver and the copper filaments by less than 10% up to the rated current. However, the behavior of the nickel filaments is poorly described by the model just presented, nor is any simple model possible for nickel: an accurate treatment of nickel requires a numerical approach throughout.

Application to nickel: Figure 6.8 shows the midfilament temperature versus current for an FM08 style fuse rated at 1/8 A (this fuse has a nickel filament) with a vacuum within the barrel; radiation is ignored. Inspection shows that the dependence of the midfilament temperature on current is described poorly when the filament is made of nickel and the simple approximations $\rho(T) = \rho(T_0) \cdot T/T_0$ and $k_T(T) = k_T(T_0)$ are used instead of the accurate behaviors of $\rho(T)$ and $k_T(T)$. There is a dramatic jump in the midfilament temperature at $I = 32$ mA that is completely missed by the approximate treatment: this jump may have experimental consequences. Suppose this fuse is selected for use in a circuit that sustains a nearly steady current of 30 mA. (Note that 1/8 A = 125 mA, and that 25% of this is

31.3 mA; thus, a common de-rating scheme would choose this fuse for use in a circuit that would sustain about 30 mA.) Should this circuit subject this fuse to currents ranging from 30 mA to 32 mA, then the midfilament temperature would range from 500 K to 800 K! This is a dramatic change in temperature for a modest change in current. There would be substantial stress changes with each modest current change, and so there would be the possibility of fatigue failure. It is a curious coincidence that this critical current is so close to the one that is selected as a result of applying the typical rule, "Rerate to 25% of the rated current for use in a vacuum."

However, the difference between the accurate and the approximate curves decreases near the melting current: the difference is even smaller when radiation is included. Hence, the approximate treatment remains useful for the melting current of the nickel filaments, although it completely misses the jump around the Curie temperature.

The temperature is not directly observable; however, the resistance is observable and is compared with experimental data in Figure 6.9. Four FM08 style fuses rated at 1/8 A were placed into a vacuum chamber (about 10^{-6} torr) after the case of each was punctured. These fuses were held at 85 °C. The model was numerically integrated with $T_{cap} = 85$ °C, and with three values of emissivity: $\epsilon = 0.00$, 0.25, and 0.50. The first returns to the case that radiation is ignored, while experimental data (Reference [21]) show that $0.25 < \epsilon < 0.50$. There are no adjustable constants in the model: the agreement is good. Radiation is obviously important.

Integration of the steady-state equation by other methods

A classic method for integration of equations of the form of Equation 6.19 is relaxation. The method is slow when only a vague initial guess for the solution is available. However, the analytic solution for $T(z)$ is an excellent guess and modern versions (see for example [13]) refine a good initial guess very rapidly.

The method of finite elements dates back several centuries, so it too is classic; however, the complexities of its use have delayed its wide acceptance until digital computers became widely available. Probably the best treatment of the fuse's behavior would emerge from a finite element based treatment of the filament and the full body of air within the barrel and the full barrel and caps: this is now a completely feasible treatment, and is certainly worth carrying out.

A very different approach is the use of SPICE.

A SPICE model of a fuse

Computer-aided analysis of electrical circuits first became popular in the mid1960s with the introduction of ECAP (Electric Circuit Analysis Program) by IBM. Various other simulation programs followed this, including ASPEC, CANCER, CIRCUS, NET, SPECTRE, TAP, and

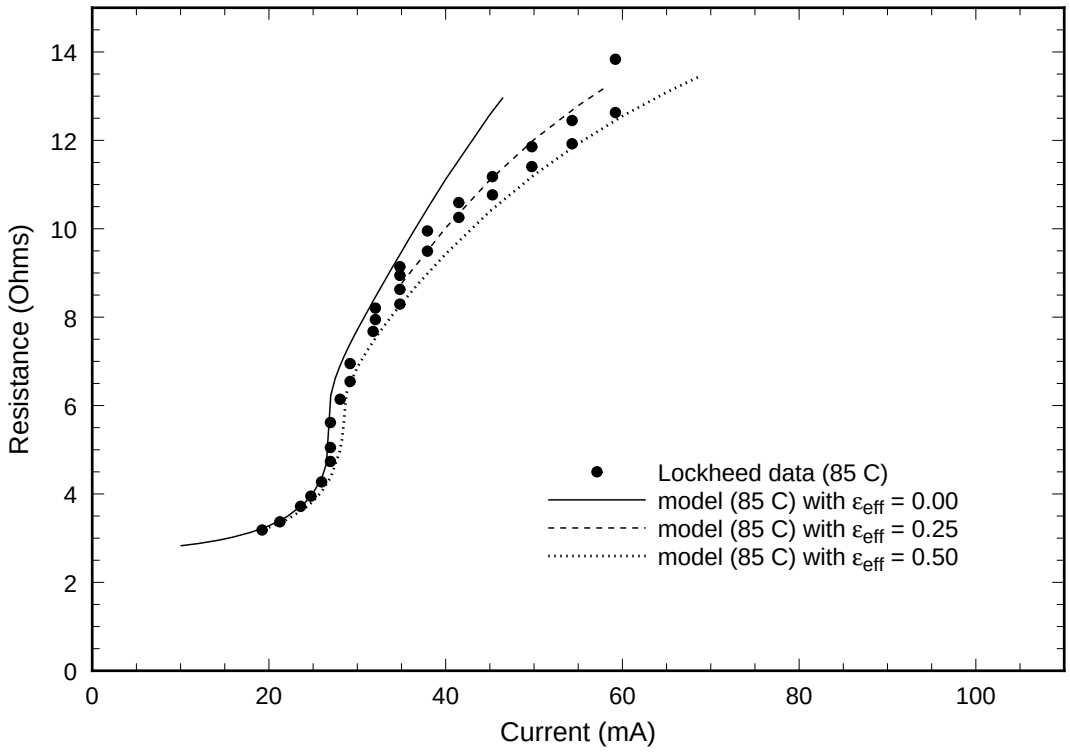

Figure 6.9: The resistance of a model fuse rated at 1/8 A, computed using a numerical integration of the accurate steady-state equations and using the accurate material properties of nickel: a vacuum is assumed. The experimental values for four different evacuated fuses are shown as dots.

TRAC. The CAD group at the University of California, Berkeley, offered the first release of SPICE (Simulation Program with Integrated Circuit Emphasis) in 1972, and have periodically released improved versions (SPICE-2 and SPICE-3). SPICE is well-documented by many publications of the Electronics Research Laboratory of the University of California, Berkeley, and by a growing library of articles and books describing its uses. It is widely regarded as the "industrial strength" standard among analog circuit simulators. Versions are available for a number of different computers, and various preprocessing and postprocessing utilities have been created that greatly increase its usability.

SPICE is the sole property of the Regents of the University of California, who provide for the distribution of the code. Versions that run on desk-top computers have been marketed by several companies, who have added detailed manuals and auxiliary programs (such as schematic translators), and who provide support. One SPICE-vendor is Intusoft[10] who markets Berkeley-SPICE-3 (modified by them to match the abilities of MS-DOS PCs and Macintoshes), and numerous auxiliary programs to support circuit design and analysis. Intusoft publishes the *Intusoft Newsletter* four times a year; this includes SPICE-circuits for new electronic components and parameter data for SPICE-modeling new circuit elements.

The April 1991 issue of the *Intusoft Newsletter* included an article "Modeling a Fuse," written by Mr. Charles Hymowitz of Intusoft. This details a SPICE-model of a fuse, with parameters appropriate for (Bel 8AG/8AP)-type fuses. The model with these parameters, and also parameters appropriate for other fuses (including slow-blow and Littelfuses), are offered on disk.

The basic technical problem is that SPICE does not have any direct accounting of the temperature of each circuit element, or for the processes that would change this temperature. (It can accept temperature coefficients for some of its parameters, such as resistance, and then run a simulation for any specified temperature. But this temperature is a constant throughout the simulation, and applies simultaneously to all components of the circuit. This blindness to a circuit's temperature distribution is a significant weakness in SPICE, and should be fixed.) So Mr. Hymowitz ingeniously used the analogy between temperature flows and electrical current flows, and introduced an auxiliary electrical circuit corresponding to the fuse. A voltage-sensitive switch (e. g., a silicon controlled rectifier) is used to simulate the melting of the fuse. Inspection of the behavior of this circuit shows that it gives interrupt-times in fair agreement with experiment when the over-current exceeds 135%. However, the structure of the model is distinctly wrong for FM08 style fuses: Hymowitz's model uses the IR radiation term as the only source of cooling and ignores thermal conduction. However, it should not prove difficult to revise the model into accordance with the correct physics.

Knowledge of the conditions under which a fuse will interrupt can be vital! Hence, a fuse model that could be incorporated into SPICE electrical models would be a notable improvement in the comprehensiveness of the electrical model. Mr. Hymowitz's model seems to be the only fuse SPICE-model extant, but does not have the required level of accuracy. Still, it addresses a significant need and is an excellent beginning, and could probably be improved

[10]P.O.BOX 710; San Pedro, CA 90733-0710; Tel. No. (310) 833-0710

to operate within about the intrinsic variability of the fuse itself, ±25%.

6.3 Estimate of the effect of imperfect heat sinking

Both experiments and modeling show that the behavior of a fuse is affected by the thermal behavior of the environment. For example, when a fuse rated at 15 A is subject to forced cooling so that its casing temperature is clamped to within a few degrees of 25 °C, then it will carry about 30 A for at least several minutes. However, if a similar fuse were mounted so that the tips of its leads (each 1.50 inches long) were attached to a heat sink at 25 °C, and no other cooling paths were provided, then it would interrupt at about 15 A within a few minutes. Thus, the environment must be included in the modeling of fuses, and this is especially important for large ratings.

It would be attractive if there were a "standard environment" that could be modeled; however, there is not: practice varies greatly.

The simplest nontrivial model of the effect of the environment on the fuse uses a two-layer model: the outer layer is isothermal at T_{amb}, and the inner layer, in contact with the fuse's casing, is a thermal resistance $\mathcal{R}$ with no thermal capacity. We have found this to be an accurate model for certain situations, including a mounting using leads of length 0.3 to 1 cm clamped to isothermal conductors.

However, we have found situations, including the fuse plugs used in the Hubble Space Telescope, for which the fuse's environment has an important "dynamics": there are several layers that heat at separate rates, and are also coupled to each other, so the inner environment must be modeled as a complex of leaky and coupled thermal transmission lines. These more complicated environments require their own study, separate from that of fuses.

In this section, we will consider only the simplest model. The joule power deposited into the fuse is $I\Delta V = I^2\,R(I, T_{cap})$, and so the temperature of the case is

$$\begin{aligned} T_{cap} &= T_{amb} + \mathcal{R}\,I^2\,R(I, T_{cap}) \\ &= T_{amb} + [\mathcal{R}\,I^2\,R_0\,T_{cap}/T_0]\,\mathcal{Q}(\kappa\ell, \chi\ell)\,, \end{aligned} \tag{6.36}$$

where $\mathcal{Q}(\kappa\ell, \chi\ell)$ is the dimensionless function given in Equations 6.23 through 6.25:

$$\mathcal{Q} = \left[\chi^2 - \kappa^2\,\mathrm{tanhc}(\sqrt{\chi^2 - \kappa^2}\,\ell/2)\right]/(\chi^2 - \kappa^2) \text{ for } \kappa < \chi, \tag{6.37}$$

$$= \left[1 + \frac{1}{3}\left(\frac{\kappa\ell}{2}\right)^2\right] \text{ for } \kappa = \chi, \tag{6.38}$$

$$= \left[\kappa^2\,\mathrm{tanc}(\sqrt{\kappa^2 - \chi^2}\,\ell/2) - \chi^2\right]/(\kappa^2 - \chi^2) \text{ for } \kappa > \chi, \tag{6.39}$$

where $\text{tanhc}(\xi) \stackrel{def}{=} \tanh(\xi)/\xi$ and $\text{tanc}(\xi) \stackrel{def}{=} \tan(\xi)/\xi$. Hence,

$$T_{cap} = \frac{T_{amb}}{1 - \Theta \cdot [(\kappa\ell/2)^2 \, \mathcal{Q}(\kappa\ell, \chi\ell)]} \,, \tag{6.40}$$

where $\Theta = 4\mathcal{L}\mathcal{R}T_0/R_0$ is a dimensionless measure of the importance of joule-heating of the case relative to cooling by heat sinking. Since χ implicitly depends on T_{cap} through $\langle k_T^{air} \rangle$, this expression is not yet in a form in which T_{cap} can be directly computed. Further, this equation is transcendental: it cannot be solved for T_{cap} in a finite number of algebraic steps. Still, iteration converges rapidly, and so the expression is useful. Indeed, case heating is most important for fuses of the largest ratings and air conduction is not very important for them. Hence, $\mathcal{Q}(\kappa\ell, \chi\ell) = \text{tanc}(\kappa\ell/2)$, and the equation becomes explicit for T_{cap}.

The resistance of the fuse's filament is

$$\begin{aligned} R &= R_0 \cdot \frac{T_{cap}}{T_0} \cdot \mathcal{Q}(\kappa\ell, \chi\ell) \\ &= R_0 \cdot \frac{T_{amb}}{T_0} \cdot \frac{\mathcal{Q}(\kappa\ell, \chi\ell)}{1 - \Theta \cdot [(\kappa\ell/2)^2 \, \mathcal{Q}(\kappa\ell, \chi\ell)]} \,. \end{aligned} \tag{6.41}$$

This is used to compute the ratio of the hot resistance to the cold resistance shown in Figure 6.10. The value of thermal resistance $\mathcal{R}$ used for each rating is that which makes T_{cap} exceed T_{amb} by 70 °C (or 85 °C for 10 A and 15 A ratings); also, $T_{amb} = 298$ K (= 25 °C) was used.

For the largest ratings, 5 A through 15 A, the difference between the case of perfect heat sinking and imperfect heat sinking is substantial: inspection of Figure 6.10 indicates that the limits specified by MIL–F–23419/8F are chosen for the imperfect heat sinking that is found in many practical applications. Operating fuses with these ratings under conditions of excellent heat sinking will bring them outside the limits specified by MIL–F–23419/8F. The leads of the fuse rated at 15 A are AWG #20 while all other ratings use AWG #22; thus, the highest rated fuse has somewhat better heat sinking than the others and this is reflected in Figure 6.10, where the MIL–F–23419/8F limits turn sharply downward towards the values for perfect heat sinking.

The presence or absence of air surrounding the filament is unimportant for the largest ratings, and so the vacuum case has been omitted from Figure 6.10. For ratings between 3/4 A and 4 A, the presence of air is important, and grows rapidly as the rating decreases: both cases are plotted to demonstrate this. However, normal wiring practices usually provide a low enough thermal resistivity to prevent large elevations of case temperatures in this range, and so the effect of increasing the thermal resistance is not shown for this range.

The analytic models developed in this Chapter give a poor description for the ratio of hot to cold resistance of the nickel filament fuses (a ratio of about 1.8), and so they are not displayed in Figure 6.10.

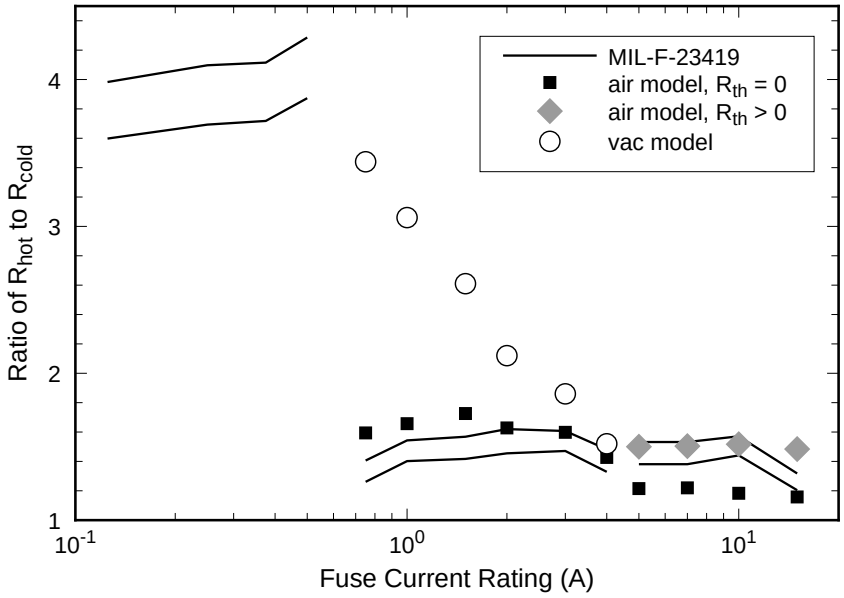

Figure 6.10: The ratio of the hot resistance to the cold resistance for each rating. The solid lines are the upper and lower limits specified by MIL–F–23419/8F. The open circles are computed for a filament surrounded by a vacuum. The black-filled squares are computed for air when the fuse is connected to its environment by a thermal resistance $R_{\rm th}$ of zero. The gray-filled diamonds are computed for air for the thermal resistance that gives the maximum allowed rise in case temperature.

The effect of $\mathcal{R}$ on the rating is found by solving

$$T_{melt} = \frac{T_{amb}}{1 - \Theta \cdot [(\kappa\ell/2)^2 \, \mathcal{Q}(\kappa\ell, \chi\ell)]} \cdot \frac{(\chi\ell)^2 - (\kappa\ell)^2 / \cosh(\sqrt{(\chi\ell)^2 - (\kappa\ell)^2}\,/2)}{(\chi\ell)^2 - (\kappa\ell)^2} \tag{6.42}$$

for $\kappa\ell$, given the fuse's parameters. For example, for a fuse rated at 15 A, using the value of $\mathcal{R}$ that produces a 85 °C rise at the rated current (namely, 63 °C/watt), we compute that the melting current is 22.6 A, which is 151% of the rated current. When this fuse is perfectly heat sunk ($\mathcal{R} = 0$), the melting current is computed to be 32.6 A, which is 217% of the rated current.

Table 6.1: Values of Fuse Parameters

Rating (A)	$(\kappa\ell)_{I_{rating}}$	$(\chi\ell)_{I_{rating}}$	$(T_{mid})_{I_{rating}}$ (K)	$(\kappa\ell)_{I_{melt,air}}$	$(\chi\ell)_{I_{melt,air}}$	$I_{melt,air}/I_{rating}$
1/8	5.59	8.57	505	11.28	12.20	2.02
1/4	3.78	5.50	497	7.56	7.87	2.00
3/8	3.35	4.48	517	6.31	6.34	1.88
1/2	2.98	3.88	501	5.67	5.54	1.90
3/4	2.78	2.79	567	3.73	3.31	1.37
1	2.66	2.46	597	3.48	2.88	1.31
1.5	2.56	2.02	630	3.20	2.34	1.25
2	2.34	1.66	586	3.02	1.95	1.29
3	2.25	1.46	572	2.93	1.73	1.30
4	1.96	1.16	494	2.81	1.42	1.44
5	1.49	0.91	397	2.91	1.27	1.95
7	1.49	0.80	400	2.86	1.11	1.92
10	1.37	0.65	384	2.81	0.91	2.04
15	1.28	0.53	371	2.77	0.76	2.17

Chapter 7

Acknowledgments

Ms. Diane Kolos and Ms. Patricia Friedberg (both of Code 313; GSFC) prepared fuses for photography, and made optical photographs. Ms. Rebecca J. Derro (Code 313; GSFC) made SEM and EDAX studies. Ms. Jeannette Benavides (Code 313; GSFC) made AUGER studies. Mr. J. Timothy Van Sant and Mr. Bruno Munoz (Code 313; GSFC) made highly accurate measurements of fuse behaviors under a wide range of types of currents. Mr. Peter O'Shea (Paramax; GSFC — since moved to Analog Devices, Inc.) contributed discussions, and a complete set of data on the cold resistances, the filament diameters, and the resistances up to interruption under overload currents for most ratings. Mr. Denis McCloskey (Lockheed Technical Office at GSFC) provided HST Fuse Plugs as well as other specimens. Mr. Scott Hull and Mr. John Slonaker (Unisys at GSFC) shared their testing data. Mr. Fred Reschke shared HST bus data and many discussions. Mr. Robert Sticka (GSFC) supported much of this work through its connection with flight assurance for the HST Repair Mission. Dr. Steven J. Battel and Ms. Esther Williams (Lockheed Missiles & Space Co.) provided extensive discussions and copies of their work, including raw data. Mr. Jon Bayuss (Electronics & Metrology Section; Failure Analysis & Materials Evaluation Branch; Kennedy Space Center) kindly sent me some reports, and discussed them with me in detail. Mr. Robert Capdevielle (Littelfuse, Inc.) provided literature published by Littelfuse, and also a number of specialized data not published as part of the general catalogues. Mr. Art Siegal and Mr. Nat Kronstadt (both of NKA) shared their experience with the design and use of MIL–F–23419/8F, and also provided data on the behavior of fuses.

Mr. Richard Marriott (Branch Head, Code 313) provided a detailed review of the first draft of this report that improved both its technical content and its presentation.

Appendix A

Several Historical Remarks

Thomas A. Edison designed the electrical fuse during 1879 and filed for a patent on it on 25 March 1880, which was granted 4 May 1880.[1] [2] The design — see Figure A.1 — is similar to the cartridge instrument fuses that are the focus of this report (compare with Figure 2.1): the current leads are substantially larger than the fuse filament, which is arranged to be slightly slack, and there is a tubular case of a nonconducting material which provides mechanical support and also captures any hot material produced during an interruption.

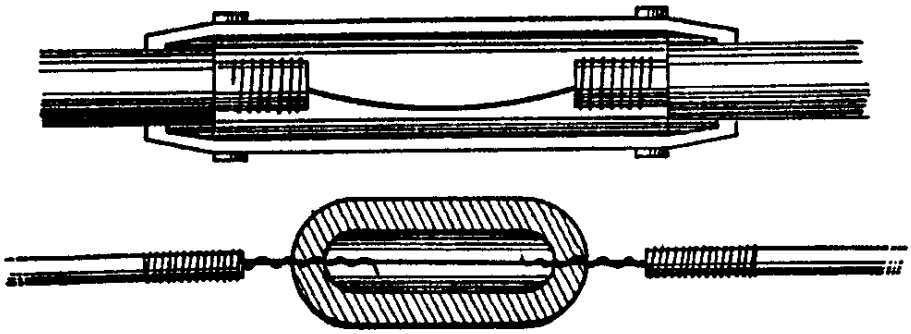

Figure A.1: Patent drawing of Edison's 1880 fuses.

Edison had been taught by experience that such a device was needed: short circuits had destroyed several electrical generators during the development of his electrical lighting system. And not all the short circuits were accidental: when he exhibited his electrical lighting system at Menlo Park (New Jersey) on New Year's Eve, 31 December 1879, a "maliciously disposed person was caught trying to short-circuit the wires by placing across them a small

[1] A. M. Clark obtained British patent #2094 on 24 May 1877 for a "safety device," which we would call a fuse. But this patent was not pursued by him, and was overlooked for years in subsequent patent examinations. There is no doubt that Edison's work was independent, and that it was Edison's developments that gives us the device in use today.

[2] Reference [4] has a detailed discussion of some aspects of the early history of the fuse.

piece of copper."[3]

The great Paris Exposition of 1881 showcased a number of electrical lighting systems. For example, arc lighting had been introduced in 1850, and was commonplace by 1878, and there were numerous attempts to introduce incandescent lighting since 1820. Edison's system operated successfully throughout the Exposition; the competitor systems started five fires. The point was immediately grasped by all, and, while Edison's lighting system was adopted by many groups, Edison's fuses were adopted by essentially everyone.

These devices were originally called safety switches, safety catches, safety cutouts, safety conductor, or safety plugs. Only when competing methods for dealing with over-currents were being introduced, were these devices distinguished by noting that they depended upon fusible wire, that is, wire which would melt upon application of an over-current. Later, this got shortened to "fuse." The first use of the term seems to be in 1883.

It became clear that convenience in installing and replacing incandescent lamps and fuses was essential, and it flashed on Edison, as he was unscrewing the metal cap on a kerosene can, that [it] "would make a bang-up socket for the lamp" and for the fuse. With this, these household items achieved much of their form as we know them today.

When a fuse opens, and interrupts current in a circuit containing a large inductance, a large voltage appears across the fuse. This can strike an arc inside it, converting material into a conducting plasma and allowing current to flow. Much of the energy stored in the inductor can be converted into heating this plasma. When this happens in power-circuits, the fuse can explode with great violence. In 1882, Edison sent a cablegram to his distributors in England: "Vapors of a conductor are also a conductor. Punch a hole in every one of the safety plugs."[4] This begins the separation of fuses into low voltage and high voltage designs: fuses used in circuits in which large voltages can develop must be designed to accommodate the potentially explosive events that can result, and this considerably complicates their design. Already in 1891, American Telephone and Telegraph (AT&T) patented a design in which the fuse wire was jacketed in a loose and porous cover of asbestos, to control the arc and make its effects less severe. Many materials have since been tried (including sand and oil) for this purpose.

As a result of its design, a fuse can interrupt once only. It is sometimes convenient to be able to reset the interrupting device immediately, or even have the device reset itself. This class of devices are called "circuit-breakers" and "self-resetting circuit breakers." Many types have been designed, and some of these patented as well, and a few have been marketed; but all are more complex than a fuse and are indeed less reliable. The situation was described in 1888 by a French observer, H. Fontaine, in words that have remained apt to this day: "Cutouts are generally made of a wire of lead or of fusible alloy which is intercalated in a circuit and which melts when the current exceeds a given intensity. Cutouts exist which dispense with the replacement of lead wires, but which are much less simple, and consequently more costly and more subject to getting out of order."

[3]Reference [3] attributes this quote to the New York *Herald* of 2 January 1880.

[4]His remark is pithy but incomplete: a metal's vapor is not conducting unless it is ionized.

Groups with interest in damage-avoidance began to list specifications for the use of fuses soon after they were available. For example, in 1889 the Boston Fire Underwriters' Union required that safety cutouts be used, and specified a number of aspects of their use, including the following: the fuse must melt at a lower carrying capacity in amperes than that of the smallest conductor they protected; the fuse must melt immediately at any excess of its marked rating; the fuse must be provided, if fusing at more than ten amperes, with contact surfaces of harder metal having perfect electrical connection with the fuse contacts; the leakage of electricity through the fuse must be impossible; and that plugs or other devices for enclosing the fusible filament should be noncombustible and moisture-proof, and so constructed as not to maintain an arc across the terminals when fusing occurred. Many of the same ideas appear in MIL–F–23419/8F.

In summary, it was recognized within the first several years of the introduction of mass distributed electrical power that over-current protection is necessary, and that the construction of a cartridge fuse is so simple, relative to circuit breakers, that it is correspondingly much more reliable, and less expensive.

Looking to the future, we can foresee "smart circuit breakers" designed around dedicated computers that sample current continuously, and continuously compare the current with stored profiles of what is acceptable and what is not, and interrupt (when necessary for protection) to the degree necessary, and then restore full current if appropriate. We can expect that these would also log features of the current and make these available for analysis, so that circuit degradations and anomalies can be better diagnosed. But these smart circuit breakers will never be as reliable and as inexpensive as a fuse, and so might never be as good a choice for the kinds of circuits whose protection-needs are compatible with what fuses can do.

Appendix B

Material properties

Any model of an FM08 style fuse requires mechanical, electrical, and thermal properties of the fuse filament, the fuse caps, and the two fuse leads. Also required are the thermal properties of the air (if any) filling the barrel of the fuse, the fuse barrel, and the shrink wrap tubing surrounding the fuse. The thermal properties of the environment also play a role; we include the thermal properties of a representative potting material as an example of a case that has occurred in practice.

The standard operating range of an FM08 fuse is −55 °C to +125 °C (218 K to 398 K), and so the properties of the materials are needed over at least this range. But the properties of the air (if any) in the barrel, and of the fuse filament, are needed up to the filament's melting point T_{melt} just to estimate steady state behaviors, and to many times T_{melt} in order to estimate behavior under great overcurrents.

B.1 Properties of fuse filament materials

Fuse filaments are made of pure nickel for ratings of 1/8 A to 1/2 A; of copper-silver alloy (50%/50% by weight) for ratings of 3/4 A to 4 A; and of silver clad copper (99.9% pure) for ratings of 5 A through 15 A.

The material property controlling the rate of power generated in the fuse filament is the electrical resistivity. The material property controlling the rate of heating is the heat capacity per volume, while the rate of cooling is controlled by the thermal conductivity. Mechanical fatigue develops as a result of thermal expansion. All of these material properties are affected by the intensity of lattice vibrations, whose quantal description is in terms of phonons, and so the physical models that have been designed to describe the material properties will consider these photons.

The goal here is to establish, not only estimates of the values of these properties, but also estimates of the reliability of these estimates. Good models have been developed for some of

the properties of interest, and these models allow estimates of reliability: hence, the available models are presented here along with measured values.

Some general properties are listed in Tables B.1 and B.2. The values of the properties named in Table B.1 apply at $T_0 = 300$ K and a pressure of one atmosphere. The mass density is ρ_m, the molecular weight is $\mathcal{A}_\mathcal{M}$, the molar volume is $\nu_\mathcal{M}$, Young's modulus is Y, and Poisson's ratio is σ_P. Values for the copper-silver alloy (50%/50% by weight) are also shown, when available.

The values of the properties named in Table B.2 apply at a pressure of one atmosphere. The melting temperature is T_{melt}, the Debye temperature measured from heat capacity data is $\Theta_D(C_p)$ and measured from electrical resistivity data is $\Theta_D(\rho)$, and the ferromagnetic Curie temperature is T_{Curie}. Values for the copper-silver alloy (50%/50% by weight) are also shown, when available.

Table B.1: Some Properties of Fuse Filament Materials

Material	ρ_m (gm/cc)	$\mathcal{A}_\mathcal{M}$ (gm/mole)	$\nu_\mathcal{M}$ (cc/mole)	Y (pascals)	σ_P
Nickel	8.90	58.69	6.59	21×10^{10}	0.32
Copper	8.96	63.55	7.09	11×10^{10}	0.35
Silver	10.50	107.87	10.27	8×10^{10}	0.38
Cu–Ag	9.67	79.99	8.27	—	—

B.1.1 Heat capacities

We require values of heat capacity in order to follow heating time-dynamics. Also the analysis of the dependence of heat capacity on temperature provides an introduction to the notion of lattice vibrations and phonons, which affect all the thermal properties.

Table B.2: Characteristic Temperatures of Some Fuse Filament Materials

Material	T_{melt} (K)	$\Theta_D(C_p)$ (K)	$\Theta_D(\rho)$ (K)	T_{Curie} (K)
Nickel	1726	375 – 450	390	633
Copper	1357	315 – 340	333	none
Silver	1235	212 – 226	223	none
Cu–Ag	1052	—	—	none

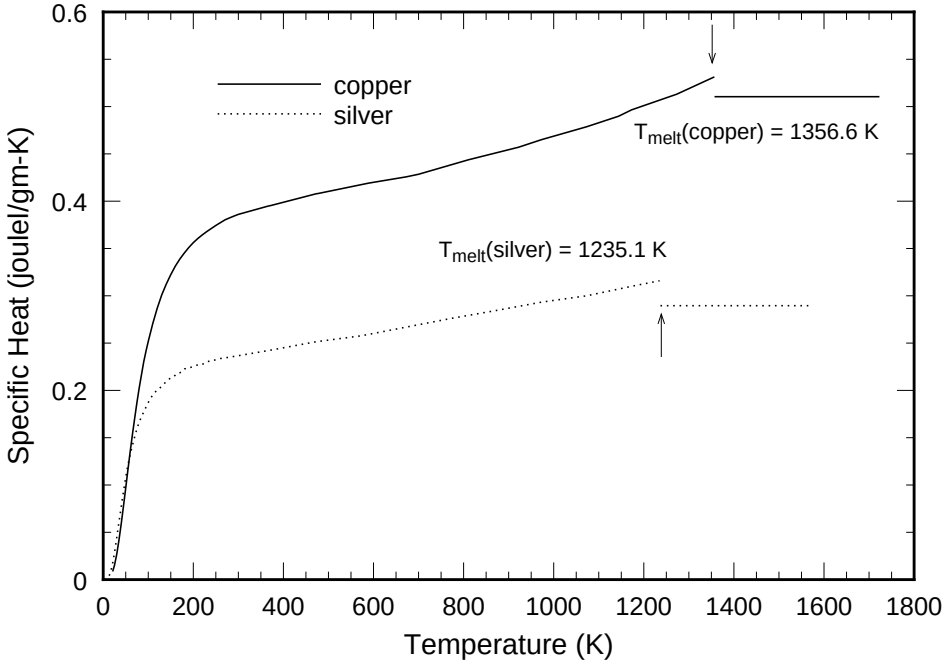

Figure B.1: Isobaric heat capacity of copper and silver, in units of joule·mole^{-1}·K^{-1}.

Heat capacity of copper and silver

Figure B.1 shows the isobaric heat capacities of copper and silver throughout their solid regions and the beginning of their liquid regions.[1] This behavior is described to within a few percent by Debye's model of a lattice of atoms, the standard thermostatic transformation from constant-volume to constant-pressure heat capacity, and the standard model of the heat capacity of the conduction electrons.

It is conventional to report the isobaric heat capacity for a specified mass of material. Heat capacities per volume and per mole are computed from these using the mass density ρ_m and the molecular weight $\mathcal{A}_\mathcal{M}$; the molar volume $\nu_\mathcal{M} = \mathcal{A}_\mathcal{M}/\rho_m$ is also useful. These are listed in Table B.1.

Debye's Model of the Heat Capacity of a Solid The behavior of the lattice of atoms of a material affects all its properties. Debye's model gives the simplest description that has practical accuracy, and so it is presented here in connection with the heat capacity of copper and silver. Also, the concepts will be used repeatedly in the discussions of other properties.

At low enough temperatures, the thermal excitations of the atoms of a lattice can be usefully modeled as harmonic vibrations; other motions, such as an atom jumping to another location, have a negligible effect on the heat capacity.

[1]These data are from the *Thermophysical Properties of Matter*, Volume 4. Y. S. Touloukian, Series Editor. IFI/Plenum (1970). [21]

Each possible vibrational mode is described by a wavevector $\mathbf{k}$ and a frequency $f = f(\mathbf{k})$, and the detailed thermal behavior of any given lattice is controlled by the frequency dependence of the number-density of these vibrational modes, $\nu(f) = \int_{f=f(\mathbf{k})} d\mathbf{k}$.

The excitation of each mode is described by quantal mechanics: the average number of phonons in mode $\mathbf{k}$ is proportional to $[\exp(hf(\mathbf{k})/k_BT) - 1]^{-1}$, where h is Planck's constant and k_B is Boltzmann's constant. Hence, as the temperature is reduced below $hf(\mathbf{k})/k_B$, the number of phonons in mode $\mathbf{k}$ drops sharply to negligible values: the excitation of that mode is quantally "frozen out" at low temperatures.

Determination of the number-density $\nu(f)$ for a given lattice is a complicated problem, both from the point of view of experiment and theory. Debye made an important contribution by observing that this number-density can be approximated by use of the result for a continuum, together with a cut-off frequency f_{max}, adjusted so that the correct total number of modes is obtained. The resulting heat capacity for a mole of material is

$$C_v = (3\mathbf{R})\, \mathcal{D}(\Theta_D/T)\,, \tag{B.1}$$

where $\mathbf{R} = N_A k_B$ is the gas constant and N_A is Avogadro's number, the Debye temperature is $\Theta_D \stackrel{def}{=} (hf_{max})/k_B$, and the Debye function is

$$\mathcal{D}(x) = \frac{3}{x^3} \int_0^x \frac{s^4 \exp(s)}{[\exp(s) - 1]^2}\, ds\,. \tag{B.2}$$

The integral cannot be written as a finite number of algebraic combinations of elementary functions; rather, numerical integration is used. It has been tabled in many places including the Landolt-Börnstein tables. Limiting values are useful,

$$\begin{aligned} \mathcal{D}(x \gg 1) &\rightarrow \frac{4\pi^4}{5} \left(\frac{T}{\Theta_D}\right)^3 \\ \mathcal{D}(x \ll 1) &\rightarrow 1, \end{aligned} \tag{B.3}$$

and give the results

$$\begin{aligned} C_v(T \ll \Theta_D) &\rightarrow \frac{12\pi^4 \mathbf{R}}{5} \left(\frac{T}{\Theta_D}\right)^3 \\ C_v(T \gg \Theta_D) &\rightarrow 3\mathbf{R} \quad \text{(Dulong-Petit value).} \end{aligned} \tag{B.4}$$

Debye's approximation gives the correct low and high temperature limits for the lattice heat capacities and also gives a useful interpolation for intermediate temperatures, especially when Θ_D is regarded as a parameter to be adjusted to give the best fit. Because the number-density $\nu(f)$ for any real material is far more complicated than Debye's model, the precise value of Θ_D determined by fitting data depends on details of the fitting process rather than being independent of it; variations of some 5% to 10% are typical, as shown in Table B.2.

Debye's model gives the heat capacity at constant volume, since the lattice is supposed to occupy constant volume during temperature changes. For example, the vibrational density of states is constant versus temperature changes. The Debye heat capacity for copper (using $\Theta_D = 315$ K) is shown in Figure B.2.

Thermal Expansion Effects on Heat Capacity Most experiments measure the heat capacity at constant pressure, C_p, while the model just described computes the heat capacity at constant volume, C_v: these are distinct in principle. Standard thermostatics derives the expression $C_p = C_v + 9T\nu_{\mathcal{M}}\alpha^2/\mathcal{K}$ where T is the absolute temperature, $\nu_{\mathcal{M}}$ is the volume per mole, α is the linear thermal expansion, and $\mathcal{K}$ is the compressibility. Over the temperature range of interest, the main temperature dependence of this difference is caused by thermal expansion. The thermal expansion of silver, copper, and nickel are shown in Figure B.4, and the C_v to C_p correction for copper is shown as part of Figure B.2.

Electronic Heat Capacity A significant result of modern solid state theory is an understanding of the contribution of the electrons in a metal to its total heat capacity. The classical and quantal results are

$$\begin{aligned} C_{el,c} &= Z\left[\frac{3\mathbf{R}}{2}\right] \\ C_{el,q} &= z\left[\frac{\pi^2\mathbf{R}}{2}\right]\left(\frac{T}{T_F}\right), \end{aligned} \tag{B.5}$$

where Z is the atomic number of the element (which is the number of electrons per atom), z is the number of conduction electrons per atom, and $T_F = (\hbar^2/2m)(3\pi^2 N)^{3/2}/k_B$ is the Fermi temperature of the metal (where $\hbar = h/2\pi$ and h is Planck's constant, m is the mass of the electron, and N is the number of electrons per volume); this result applies from $T = 0$ up to $T \approx T_F/10$, which is roughly 6 to 8 thousand degrees Kelvin for these metals.

The classical results are 43.5 $\mathbf{R}$ per mole of copper and 70.5 $\mathbf{R}$ per mole of silver, which are far larger than the total heat capacities of these materials, and so are hoplessly wrong. Quantal theory gives values in good agreement with experiment:[2]

$$\begin{aligned} C_{v,copper} &= [(0.87 \text{ to } 0.91) \times 10^{-4}\ \mathbf{R}\cdot\ \mathrm{K}^{-1}]\cdot T \\ C_{v,silver} &= [(0.78 \text{ to } 0.81) \times 10^{-4}\ \mathbf{R}\cdot\ \mathrm{K}^{-1}]\cdot T. \end{aligned} \tag{B.6}$$

Analysis of the Heat Capacity of Copper The heat capacity for copper is replotted in Figure B.2 in units of the gas constant $\mathbf{R}$. Clearly visible is the way that the lattice vibrations are "frozen out" for temperatures below Θ_D, and the way that they produce the Dulong-Petit value for temperatures above Θ_D: the Debye model goes beyond merely illustrating these effects, to producing usefully accurate values. The $C_p - C_v$ difference caused by thermal expansion ($9T\nu_{\mathcal{M}}\alpha^2/\mathcal{K}$) is larger than the electronic heat capacity for copper. The sum of the component effects is in excellent agreement with the observed values for copper from vanishing temperatures to the melting point of copper. Consequently, we understand the heat capacity of solid copper to within an accuracy of several percent, both experimentally and theoretically. The analysis for solid silver is similar, and it too is understood.

[2]From [22], page 259.

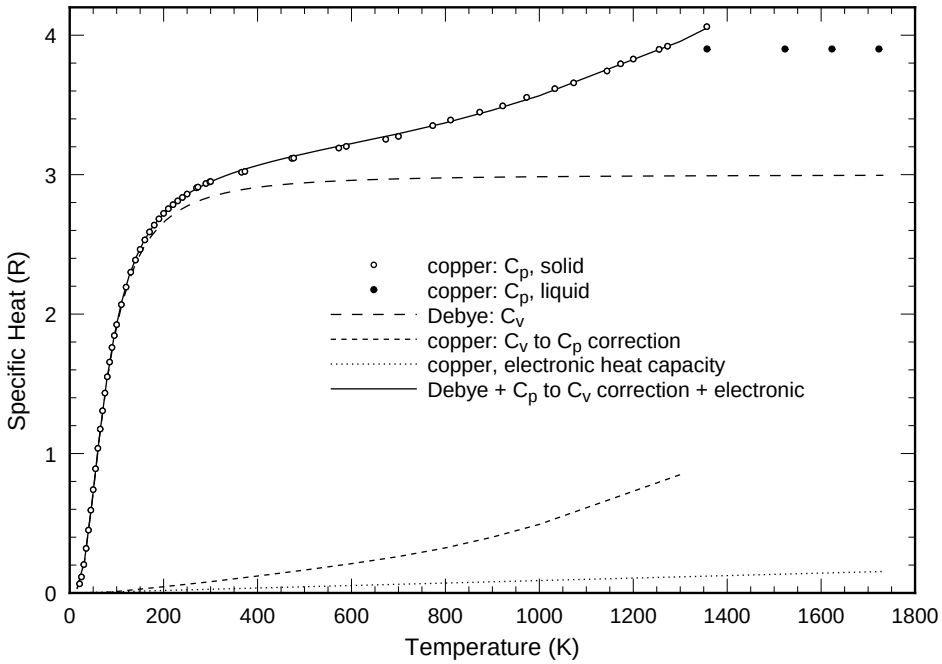

Figure B.2: Heat capacity of copper in units of the gas constant $\mathbf{R}$.

The thermal excitations of the atoms in the liquid phase of a material cannot be usefully described as harmonic vibrations: profoundingly nonharmonic vibrations as well as nonvibrational motions (e.g., jumps to other locations) are also important. That is, some vibrational modes are lost, to be replaced by modes that resemble translations. And, since a vibrational mode contributes $3k_B$ to the heat capacity while a translational mode contributes $3k_b/2$, we have a qualitative understanding of the lower heat capacity of this liquid.

Heat capacity of copper-silver alloy

The heat capacities of silver and copper are similar and there are no solid state reactions driven by temperature. Hence, an atomic fraction weighted average gives a good approximation to the heat capacity of an alloy of these materials.

Heat capacity of nickel

Figure B.3 shows the heat capacities of nickel. Nickel is a ferromagnetic material with a ferromagnetic Curie temperature of 633 K. Below this temperature, some of the conduction electrons are spin-aligned; as the temperature is increased, this alignment is reduced, which requires energy that augments the heat capacity. The alignment changes particularly rapidly as the Curie temperature is approached and so the heat capacity shows a sharp peak. There is still some alignment above this temperature and so the heat capacity is still augmented

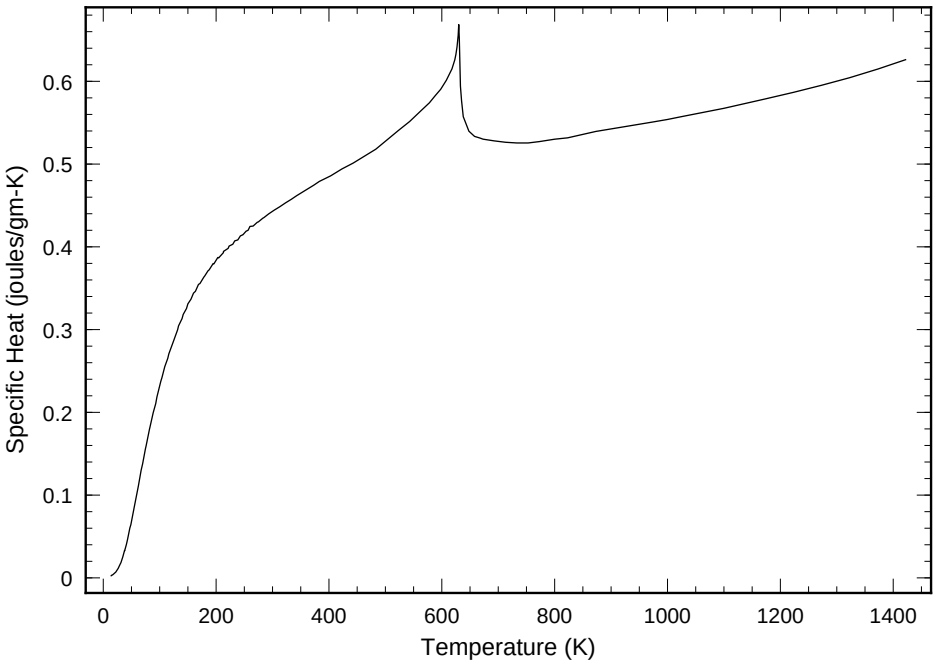

Figure B.3: Heat capacity of nickel.

above the Curie temperature; this alignment vanishes as the temperature is further increased and so the heat capacity augmentation vanishes.

B.1.2 Thermal expansion

The thermal expansion of silver, copper, and nickel are shown in Figure B.4.[3] These values are needed both to estimate stresses developed during current pulses and to estimate the difference between the heat capacities.

B.1.3 Electrical resistivity

We require the electrical resistance in order to compute Joule heating. The electrical resistivity of some pure metals is described with good accuracy by the standard model of noninteracting charged fermions moving nearly freely within a periodic lattice of atoms executing nearly harmonic vibrations.[4] Resistance is a consequence of the scattering of conduction fermions from the thermal phonons moving throughout the lattice. As long as the temperature is above Θ_D, the density of phonons is proportional to the temperature, so the

[3]These data are [21], Volume 12.

[4]See for example [22], Chapter 12. Each fermion is a "quasi-particle," i. e., a collective motion of many electrons. Individual electrons interact strongly with each other and with the atoms, but their collective motions act like nearly independent fermions.

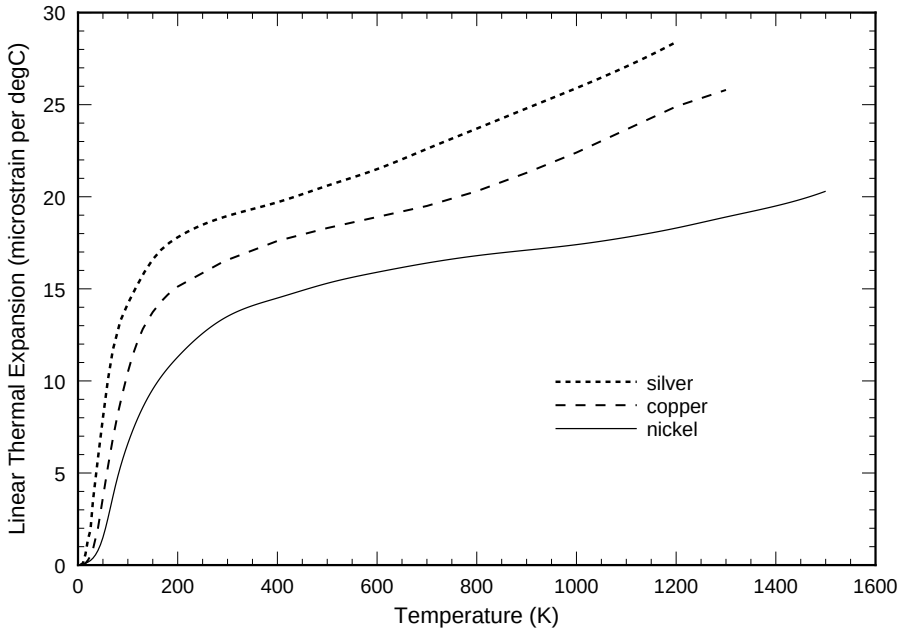

Figure B.4: Plot of the linear thermal expansion α of copper, nickel, and silver. The volume thermal expansion β is three times greater: $beta = 3\alpha$.

vibrationally-induced scattering, and hence the electrical resistivity, is also proportional to the temperature. However, as the temperature is lowered below Θ_D, phonons are frozen out and the resistivity decreases faster than the temperature.

A formula derived by Bloch was found by Grüneisen to describe the observed temperature dependence of the electrical resistivity of some pure metals with good accuracy:

$$\rho(T) = \left(\frac{K}{\mathcal{A}_{\mathcal{M}}\Theta_D}\right) \cdot \left(\frac{T}{\Theta_D}\right) \cdot \mathcal{G}(\frac{\Theta_D}{T}) \,, \tag{B.7}$$

where K is a constant characteristic of the pure metal, $\mathcal{A}_{\mathcal{M}}$ is the molecular weight of the metal, Θ_D is the Debye temperature, and

$$\mathcal{G}(x) = \frac{1}{x^4} \int_0^x \frac{s^5}{(e^s - 1)(1 - e^{-s})} \, ds \tag{B.8}$$

is the Grüneisen function. A value of the Debye temperature can be obtained by fitting this model to data. The value depends on the details of the fitting procedure; variations of some 5% to 10% are found. While the effect of a phonon on the specific heat depends only on the energy of the phonon, its effectiveness for electron scattering depends also on its mode-shape, and so there are systematic differences between the Debye temperature determined from heat capacity data and from resistivity data.

The effect of impurities and lattice defects (such as introduced by cold working, as when a wire is drawn through a die to reduce its diameter) is described for some metals by Matthiessen's rule: $\rho(T, x) = \rho(T) + x\rho_0$ where $\rho(T)$ is the resistivity of the pure metal, x

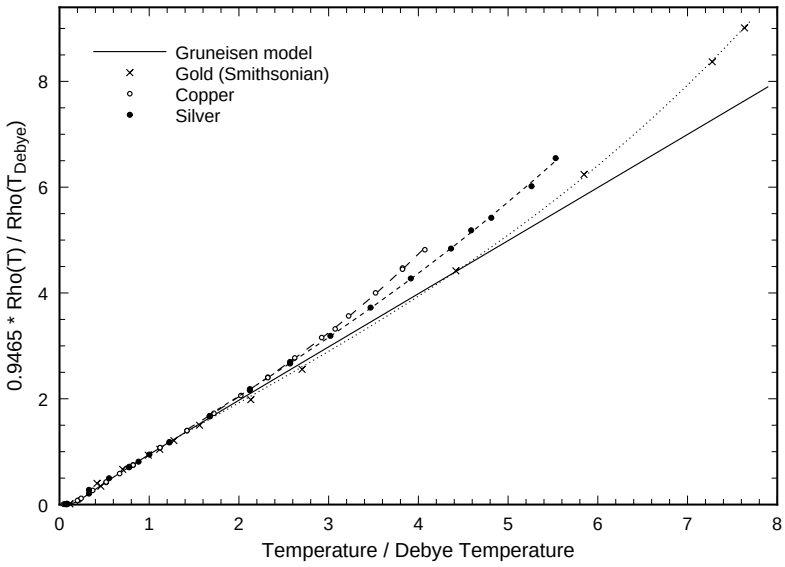

Figure B.5: Scaled resistivities of the noble metals versus scaled temperatures compared with two models: $\rho \propto T$ and $\rho \propto (T/\Theta_D)\,\mathcal{G}(\Theta_D/T)$.

is the mole fraction of the impurity (or lattice defect), and ρ_0 is a temperature-independent resistivity coefficient that depends on the kind of impurity (or the kind of lattice defect). This is discussed in the following Appendix devoted to the copper-silver alloy.

Resistivity of silver and copper

Figure B.5 illustrates (i) that the resistivities[5] of silver and copper are reduced to nearly a single curve for temperatures below roughly twice Θ_D when plotted as $\rho/\rho(\Theta_D)$ vs. T/Θ_D; (ii) that this single curve is closely described by the Bloch-Grüneisen model: $\rho \propto T^5$ when $T \ll \Theta_D$ and $\rho \propto T$ for $T \gtrsim \Theta_D$; and finally (iii) that these metal's resistivities ascend distinctly above the $\rho \propto T$ curve for when the temperature is several times Θ_D.

The super-linear behavior of the resistivity has been semi-empirically described with good accuracy as an effect of thermal expansion: $\rho \approx (1 + 2\alpha\gamma_G T) \cdot T$, where α is the thermal expansion and $\gamma_G \stackrel{def}{=} d(\ln f_{max})/d(\ln V)$ is the Grüneisen constant, f_{max} is the highest vibrational frequency of the lattice, and V is the volume of the material.

The resistivity of an annealed copper wire is increased when it is drawn out under tension, which induces defects. The increase at $T_0 = 300$ K is roughly proportionally to the relative reduction in cross-sectional area up to 20% reduction in area, where the resistivity increase is 1.3%; the resistivity increase at 90% reduction in area is 2.5%. This resistance can be reduced within a few tenths of a percent of the original value upon reannealing since this reduces the concentration of lattice defects; more exact recovery requires the copper to be

[5]Data are from [5].

returned to the exact condition as it began, and ordinary annealing does not do this. We may conclude that the resistivity of annealed copper filaments is known to within better than one percent.

B.1.4 Thermal conductivity

Heat is transported by phonons in all materials, and also by the conduction electrons in metals. The total thermal conductivity is the sum provided by each carrier: $k_T = \sum_j C_j v_j \lambda_j / 3$, where C_j is the contribution of the carrier j to the heat capacity, v_j is the (group) velocity of the carrier, and λ_j is a suitably defined mean free path. The mechanisms controlling the mean free path λ are complicated: while theory can predict trends, it cannot compute reliable values and so these must be obtained from experiment. Experimental values for the common metals are now known to within several percent over a wide range of temperatures and this is adequate for the purposes of this report.

But thermal conductivity values for many nonmetallic solids of interest to the behavior of fuses are sometimes scattered by a factor of two, and occasionally by much more, when obtained from different sources. For example, measurements of the thermal conductivity of some candidate potting materials have scattered by a factor of three: should analysis show that the thermal resistivity to thermal ground might be driven into an unsafe range if the thermal conductivity of the potting material is changed by a factor of two or three, then it would be prudent to locate additional measurements of this property.

At least part of the variation in values can be caused by variability of the material. For example, as discussed in Appendix B.3.1, the range of materials allowed for the fuse's barrel have a range of thermal conductivity from more than 50 $\mathrm{mW{\cdot}cm^{-1} \cdot K^{-1}}$ (high density alumina) to 7 $\mathrm{mW{\cdot}cm^{-1} \cdot K^{-1}}$ (glass).

Thermal conductivity of copper, silver, and nickel

See Figure B.6: these values are expected to be reliable to within 3% for copper and to within 5% for silver and nickel.

The Lorenz number

G. Wiedemann and R. Franz observed (1853) that the product $\rho\, k_T$ is almost independent of the metal they studied. L. Lorenz showed (1881) that $\rho\, k_T / T$ was independent of temperature and almost independent of the metals studied: this quantity is now called the Lorenz number, $\mathcal{L} = \rho\, k_T / T$. This is strong evidence that the same mechanism that controls the electrical conductivity also controls the thermal conductivity. Lorentz and also Drude used the classical theory of metals to compute a value $\mathcal{L}_c = 3(k_\mathbf{B}/e)^2$ where $k_\mathbf{B}$ is Boltzmann's constant and

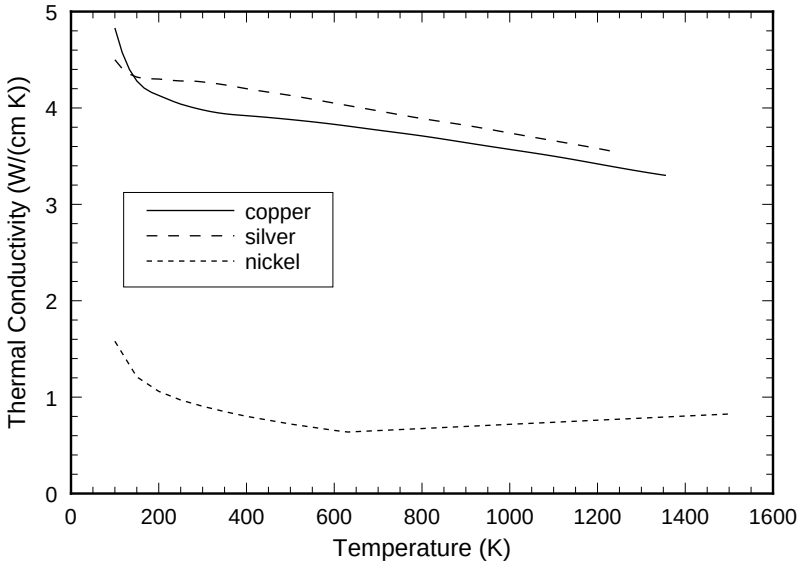

Figure B.6: Thermal conductivity of copper, silver, and nickel.

e is the charge on an electron. Sommerfeld used the quantal theory to compute a slightly larger value: $\mathcal{L}_q = (\pi^2/3)(k_{\mathbf{B}}/e)^2 = 2.443 \times 10^{-8}$ (V/K)^2.

The electronic contribution to the thermal conductivity dominates that of the phonons above the Debye temperature for those metals that have a high electronic conductivity, such as copper and silver: the observed value of the Lorenz number is typically very close to $\mathcal{L}_q$. As the temperature is lowered below Θ_D, and the electronic contribution becomes small, the phonon contribution becomes more visible and the observed value of the Lorenz number decreases. At very low temperatures (say, $T < \Theta_D/50$) the phonon contribution vanishes as T^3 while the electron contribution vanish as T; hence, the electronic contribution again dominates: the observed value of the Lorenz number approaches very close to $\mathcal{L}_q$. See Figure B.7 for values for copper, silver, and nickel. Inspection shows that measured values of the Lorenz number for copper and for silver closely approach $\mathcal{L}_q$ over the range of temperatures of interest to fuse applications; the decrease in the measured Lorenz number as the temperature is lowered below about 300 K is also apparent. The measured value of the Lorenz number of nickel is close to $\mathcal{L}_q$ at 300 K, but increases to 122% of it as the temperature increases to the ferromagnetic Curie temperature, and beyond.

Alloys of metals in which the electronic contributions dominate those of phonons reduces both the electrical and the thermal conductivities in about the same proportion, and so does not much affect the value of the Lorenz number. In particular, the Lorenz number of copper-silver alloy is within a few percent of $\mathcal{L}_q$.

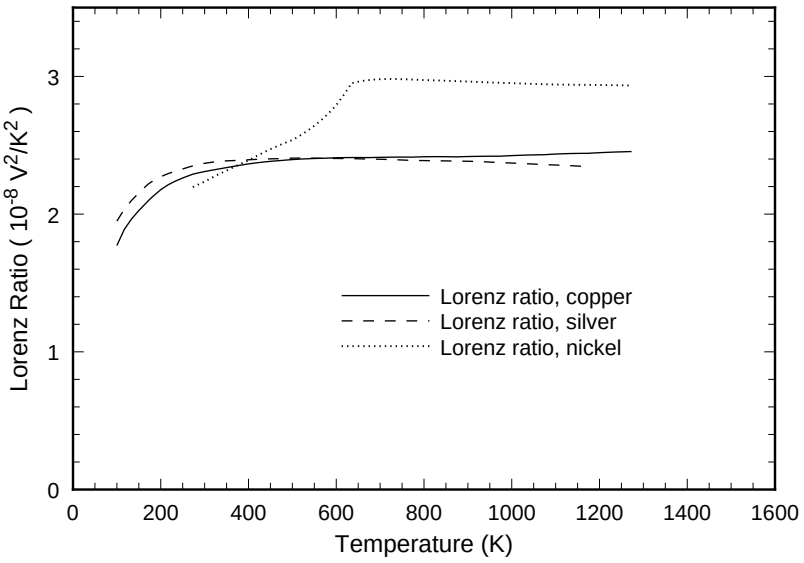

Figure B.7: The Lorenz number $\mathcal{L}$ for copper, silver, and nickel.

The $\mathcal{H}$-ratio: $\rho/(k_T\ T)$

The quantity $\rho/(k_T\ T)$ appears naturally in the differential equation controlling the temperature distribution along the fuse filament, and so it is of interest to examine its values directly. We name it for convenience: $\mathcal{H} = \rho/(k_T\ T)$. By introducing the definition of the Lorenz number of a metal and the approximation that the measured values of the Lorenz number are close to $\mathcal{L}_q$, and also introducing the approximation that $\rho(T) = \rho_0 \cdot (T/T_0)$ where T_0 is a reference temperature, then $\mathcal{H} = (\rho_0/T_0)^2/\mathcal{L}_q$: it is approximately temperature-independent. This approximation has been used in the simple versions of the fuse models developed in this Report. As a direct check on the quality of this approximation, Figures B.8 and B.9 show the temperature dependences of this ratio for copper, silver, and nickel. Inspection shows that the variation $\mathcal{H}$ is small for copper and for silver; indeed, the effective value of $\sqrt{\mathcal{H}}$ (note that it is the square root that directly relates to measured quantities) averaged over the length of the filament increases by less than 15% from room temperature to the melting temperature. However, $\mathcal{H}$ for nickel shows considerable temperature variation: direct numerical treatment is preferable for this material.

Empirical fitting functions

For numerical solutions of the differential equation controlling the temperature distribution along the filament, it is necessary to have numerical representations of the material properties. The following empirical functions are at least as accurate as the data used to generate them, for the temperature range from 200 K to the melting temperature of each material. These functions have been chosen to be as simple as is consistent with accuracy over this limited temperature range, rather than to conform with any theoretically expected functional

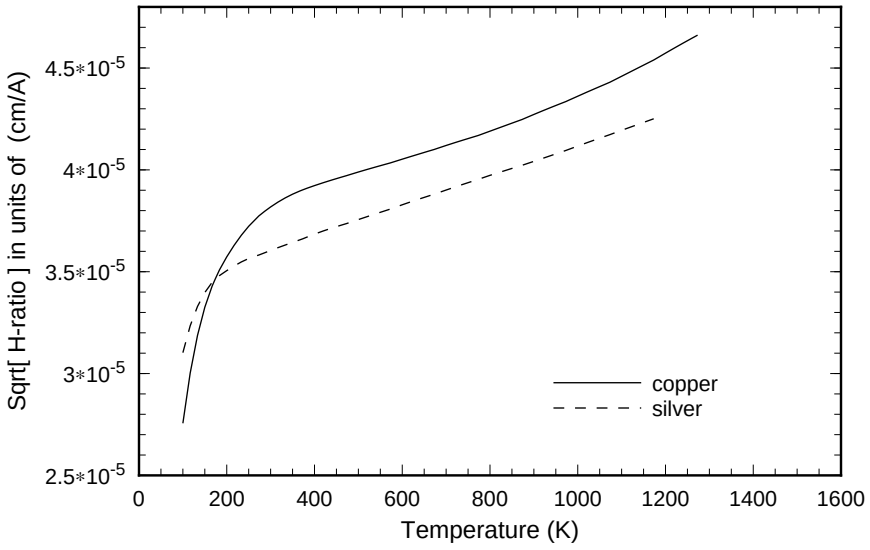

Figure B.8: The square root of the $\mathcal{H}$-ratio for copper and for silver.

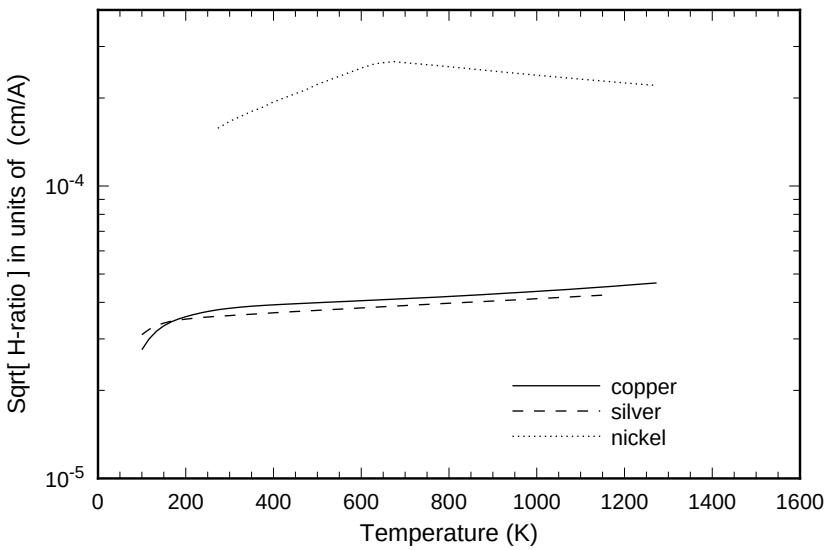

Figure B.9: The square root of the $\mathcal{H}$-ratio for nickel; copper and silver are also shown for comparison.

forms (such as a Debye function for the heat capacity) and therefore should not be used to extrapolate outside this range.

The heat capacities are, in units of joules/(gm· K), when T is in degrees Kelvin,

$$C_{p,Cu} = 0.313 + (3.01 \times 10^{-4}) \cdot T - (2.75 \times 10^{-7}) \cdot T^2 + (1.28 \times 10^{-10}) \cdot T^3 \quad \text{(B.9)}$$

$$C_{p,Ag} = 0.210 + (8.49 \times 10^{-5}) \cdot T \quad \text{(B.10)}$$

$$C_{p,Ni} = \begin{cases} 0.556 + (6.51 \times 10^{-4}) \cdot T - (6.44 \times 10^{-7}) \cdot T^2 \\ \qquad -0.044 \cdot |631\,\text{K} - T|^{0.30} & \text{for } T < 631\,\text{K} \\ 0.309 + (6.84 \times 10^{-4}) \cdot T - (1.62 \times 10^{-7}) \cdot T^2 \\ \qquad -0.063 \cdot |T - 631\,\text{K}|^{0.25} & \text{for } T > 631\,\text{K}. \end{cases} \quad \text{(B.11)}$$

The linear thermal expansions are, in units of $10^{-6}/\,\text{K}$, when T is in degrees Kelvin,

$$\alpha_{Cu} = 14.32 + (6.3 \times 10^{-3}) \cdot T + (1.94 \times 10^{-6}) \cdot T^2 \quad \text{(B.12)}$$

$$\alpha_{Ag} = 16.52 + (7.0 \times 10^{-3}) \cdot T + (2.37 \times 10^{-6}) \cdot T^2 \quad \text{(B.13)}$$

$$\alpha_{Ni} = 7.85 + (2.44 \times 10^{-2}) \cdot T - (2.31 \times 10^{-5}) \cdot T^2 + (8.34 \times 10^{-9}) \cdot T^3\,. \quad \text{(B.14)}$$

The thermal conductivities are, in units of watt/(cm· K), where T is in degrees Kelvin,

$$k_{T,Cu} = 4.097 \cdot (1 + 1.66e^{-T/46.0})[1 - (8.42 \times 10^{-5}) \cdot T - (4.41 \times 10^{-8}) \cdot T^2] \quad \text{(B.15)}$$

$$k_{T,Ag} = 4.426 \cdot (1 + 500\ e^{-T/10.3})[1 - (1.21 \times 10^{-4}) \cdot T - (3.33 \times 10^{-8}) \cdot T^2] \quad \text{(B.16)}$$

$$k_{T,Ni} = \begin{cases} 1.109 \cdot (1 + 2.809e^{-T/59.6})[1 - (6.733 \times 10^{-4}) \cdot T] & \text{for } T < 631\ \text{K} \\ 0.502 \cdot [1 + (4.29 \times 10^{-4}) \cdot T] & \text{for } T > 631\ \text{K}. \end{cases} \quad \text{(B.17)}$$

The electrical resistivities are, in units of $\mu\Omega$·cm, where T is in degrees Kelvin,

$$\rho_{Cu} = -0.355 + 0.0073 \cdot T - (1.60 \times 10^{-6}) \cdot T^2 + (1.41 \times 10^{-9}) \cdot T^3 \quad \text{(B.18)}$$

$$\rho_{Ag} = -0.156 + 0.0060 \cdot T + (2.25 \times 10^{-7}) \cdot T^2 + (3.08 \times 10^{-10}) \cdot T^3 \quad \text{(B.19)}$$

$$\rho_{Ni} = \begin{cases} 7.064 - 0.0298 \cdot T + (1.026 \times 10^{-4}) \cdot T^2 & \text{for } T < 631\ \text{K} \\ 3.273 + 0.047 \cdot T - (9.59 \times 10^{-6}) \cdot T^2 & \text{for } T > 631\ \text{K}. \end{cases} \quad \text{(B.20)}$$

B.2 Thermal properties of air

The barrel of an FM08 style fuse is filled with air during assembly. As long as this air is retained, it presents a thermal reservoir (related to its heat capacity) and a thermally conductive path between the filament and the walls of the barrel.

The heat capacity of air over the temperature range of interest is understood[6] well enough from a theoretical point of view that values are computed with a reliability about that of

[6]For a discussion and for data, see Volume 6, [21].

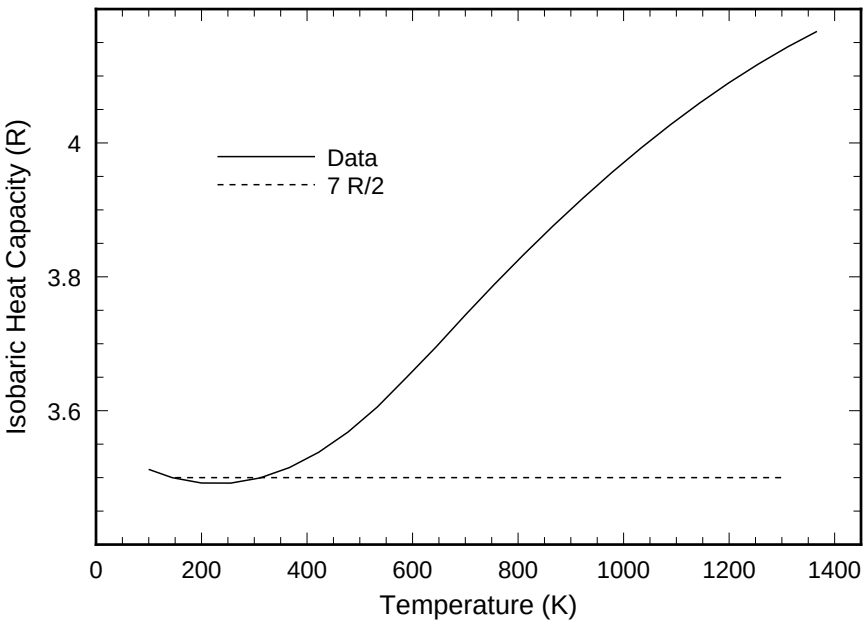

Figure B.10: Isobaric molar heat capacity of air extrapolated to vanishing pressures. These values also apply for pressures up to several atmospheres.

good experiments: $\pm 0.5\%$. The isobaric molar heat capacity C_p is near $7\mathbf{R}/2$, the classical value for a polyatomic molecule, when the temperature is near room temperature and the pressure does not exceed a few atmospheres; it increases steadily with temperature and with pressure. Pressure effects can be neglected for this study, and the temperature effect is shown in Figure B.10. The isochoric molar heat capacity is $C_v = C_p - \mathbf{R}$ to a good approximation over the ranges of interest for this study. Converting to heat capacity per mass requires the molecular weight of air, 28.964 gm/mole for $T \leq 1800$ K;[7] converting to heat capacity per volume requires the density of air, 0.001 177 gm/cc for $T = 300$ K and at one standard atmosphere of pressure.[8] The density at other conditions can be computed from the ideal gas law with satisfactory accuracy for the purposes of this study.

The thermal conductivity of a gas depends on its temperature; however, it does not depend on pressure so long as the pressure is high enough so that the mean free distance between collisions of the gas molecules is small compared with the distances between the walls of the enclosure, and low enough so that the frequency of collisions of three or more molecules is negligible. For FM08 style fuse cases (scale-lengths in the range 0.05 cm to 0.5 cm), the thermal conductivity of air is independent of pressure for pressures above about 10^{-5} atmospheres and below about 10 atmospheres. An elementary theory of the thermal conductivity of a gas finds that the temperature dependence is $T^{0.5}$; however, a more complete theory shows a more rapid increase with temperature, and also shows that a detailed treatment for diatomic molecules is too complex for practical work at this time: accurate values of thermal conductivity are presently best obtained from experiment. Inspection of experimental values

[7]Pages F–12 to F–15 of [15].
[8]Pages F–11 of [15].

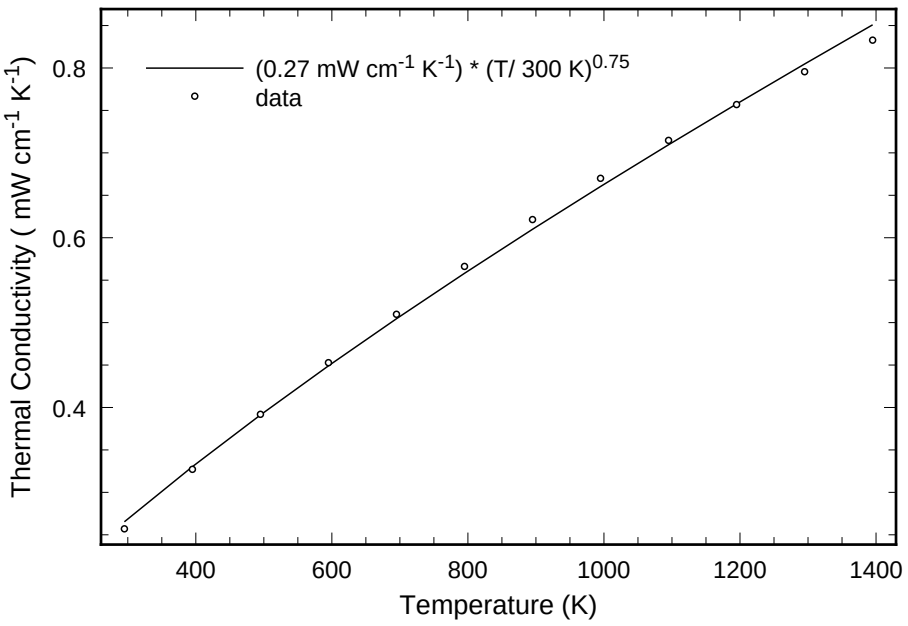

Figure B.11: Thermal conductivity of air at a pressure of one atmosphere.

shows that they are fit to within about 2% over the temperature range of interest by a power law: $k_T^{air}(T) = k_T^{air,0}(T/T_0)^\delta$ with δ nearer 0.75 than 0.5: see Figure B.11.

The thermal diffusivity of a gas is $\mathcal{D} = k_T/(c_v\rho_m) = (\mathbf{R}k_T T)/(c_v\nu_{\mathcal{M}}p)$, and is seen to be inversely proportional to the density or to the pressure. The temperature dependence for air is shown in Figure B.12 for a density of 0.001 177 gm/cc (corresponding to $T_0 = 300$ K and one standard atmosphere of pressure): values are comparable with those of metals. Values for other densities can be scaled using the ideal gas law with sufficient accuracy for the purposes of this study.

Suppose a fuse is slowly leaking its air. The air remaining in the barrel will continue to provide the same degree of thermal cooling to the filament so long as the pressure remains above roughly 10^{-5} atmospheres since k_T^{air} remains unchanged until then. However, the air responds to transient effects with increasing swiftness as the pressure drops since $\mathcal{D} \propto 1/p$.

B.3 Properties of other materials

The behavior of the fuse is somewhat affected by the thermal properties of its barrel, its end caps, its lead wires, the shrink wrap tubing, and the potting (if any). These materials are not greatly heated by the fuse filament, even when the filament is driven to its melting temperature; hence, we need their properties only over the range −55 °C to +125 °C. Further, since their effect is limited, we do not require high accuracy, which is fortunate as high accuracy is not available for most of these materials. Selected values of suitable

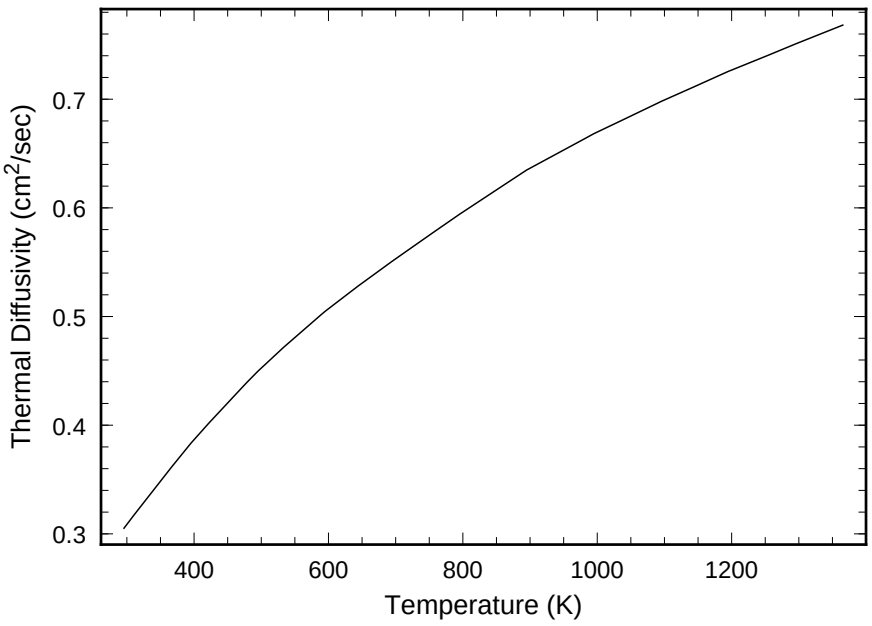

Figure B.12: Thermal diffusivity of air at a density corresponding to $T_0 = 300$ K and one standard atmosphere.

accuracy are shown in Table B.3.

B.3.1 Fuse barrel

According to MIL–F–23419/8F, the fuse barrel can be either a glass or a ceramic (MIL–I–10: Grade L311 or higher grade). One practical choice[9] is a form of steatite ($MgO{\cdot}SiO_2$) available commercially from American Lava Corporation as AlSiMag 665, rated as Grade L533. Some property values supplied by the manufacturer are listed in Table B.3. The claimed density, 2.7 gm/cc, agrees with that measured for some fuse barrels: (2.66 ± 0.05) gm/cc.[10]

However, alumina (Al_2O_3) as well as some glasses are allowed by MIL–F–23419/8F. The properties of alumina change dramatically as it is made denser. For the measured density, (2.66 ± 0.05) gm/cc, the room temperature thermal conductivity is about 17 $mW{\cdot}cm^{-1}{\cdot}K^{-1}$, which is about a third of AlSiMag 665. (The room temperature thermal conductivity of denser alumina ranges up to 3000 $mW{\cdot}cm^{-1}{\cdot}K^{-1}$.) And the room temperature thermal conductivity of suitable glasses ranges between 7 and 10 $mW{\cdot}cm^{-1}{\cdot}K^{-1}$, which is a tenth to a fifth of that of AlSiMag 665. There would slight but observable differences between fuses constructed with these barrel materials.

[9]Private communication from Mr. Capdevielle, Application Engineer for Littelfuse.

[10]I made these measurements on ten fuses selected to span a range of ratings and manufacturing dates between about 1980 and 1988. The masses were determined using a microbalance (precision of $\pm 10\mu$g), and the dimension were determined by using a traveling microscope (precision of $\pm 1\mu$m).

B.3.2 Shrink wrap tubing

The plastic shrink tubing is polyvinylidene fluoride (AMS 3632, $(C\ H_2–C\ F_2)_n$), conditioned as shrink wrap tubing by exposure to radiation.[11] The density is 1.76 ± 0.02 gm·cm^{-3}, the heat capacity is 1.38 joule· K^{-1}·gm^{-1}, and the thermal conductivity is 2.5 mW·cm^{-1}·K^{-1} at 25 °C and 1.9 mW·cm^{-1}·K^{-1} at 163 °C. Hence the thermal diffusivity is computed to be 10×10^{-4} cm^2·sec^{-1} at 25 °C and 8×10^{-4} cm^2·sec^{-1} at 163 °C. After the end caps are fixed to the fuse barrel, a length of shrink tubing is slid over them, and a temperature of (174 ± 3) °C (= 447 ± 3 K = 345 ± 5 °F) is applied for ten minutes to shrink the tubing tightly onto the caps and barrel. The LM&SC drawing asserts that this assembly should not subsequently be heated as high as (or higher than) 171 °C (= 444 K = 340 °F), for any interval longer than ten seconds, or "fuse reliability will be degraded" and fuse failure could result. The heat deflection temperature at 66 psi loading is 132 °C (= 405 K = 270 °F), and at 264 psi is 88 °C (= 361 K = 190 °F); the melting temperature is 155 °C to 170 °C (= 428 K to 443 K = 311 °F to 338 °F). Its continuous service temperature is 129 °C (= 402 K = 265 °F).

B.3.3 Fuse caps

The end caps are 9010 brass alloy, MIL-C-2176B, gold plated. The density is 8.6 gm/cc, the heat capacity is 0.39 J/(gm °C), and the thermal conductivity is 1.1 W/(cm °C). Hence, the thermal diffusivity is computed to be 0.33 cm^2/sec. The electrical resistivity is 5.8 $\mu\Omega$·cm.

B.3.4 Fuse leads

The leads are soft copper (QQ–W–343), gold plated. Their diameter is 0.64 ± 0.05 mm for fuses rated from 1/8 A to 10 A (inclusive) and 0.82 ± 0.05 mm for fuses rated at 15 A; these are, respectively, American Wire Gauges #22 and #20, with resistances of 0.530 mΩ/cm and 0.333 mΩ/cm at 20 °C.[12] Their thermal resistances per length are 80 °C/(watt·cm) and 49 °C/(watt·cm), respectively.

If the fuse were wired into a circuit using 1.0 cm of lead at each end of the fuse, then the leads would present an electrical resistance of 1.1 mΩ and 0.7 mΩ, respectively; and a thermal resistance of 160 °C/watt and 100 °C/watt, respectively.

[11] Pennsalt Chemical Corporation's trade name is *Kynar*; other trade names include *Foraflon* and *Solef*.
[12] Data are from the Wire Table, Standard Annealed Copper, page F–160 of [15].

Table B.3: Some Properties of Fuse Case Materials

Part	Material	ρ_m gm/cc	C_p J/(gm °C)	k_T W/(cm °C)	$\mathcal{D}$ cm^2/sec	α μ-strain/°C
barrel	steatite	2.7	0.25	0.057	0.084	6.9
barrel	alumina	2.6	0.50	0.017	0.012	6.8
caps	brass	8.6	0.39	1.1	0.33	17.4
leads	copper	8.96	0.40	3.9	1.1	16.5
wrap	PVDF	1.76	1.38	0.0022	0.0009	—
potting	RTV-566	1.51	1.46	0.0031	0.0014	200 to 300

Note: The mass density is ρ_m, the heat capacity at constant pressure is C_p, the thermal conductivity is k_T, the thermal diffusivity is $\mathcal{D}$, and the linear thermal expansion is α.

B.3.5 Solder

The solder attaching the fuse filament to the caps is (98% tin, 2% silver). It becomes plastic at 221 °C and melts at 232 °C. This allows eutectic lead-tin solder, which melts sharply at 181 °C (there is no plastic range), to be used to attach the fuse. Care must still be used: for example, the soldering iron should have a scrupulously clean tip so that contaminants (such as dissolved copper) will not change the solder properties, nor interfere with thermal contact; the tip should be adjusted to some 210 °C to 220 °C, and should be massive enough so that contact with the work will not quench the tip below about 200 °C; and heat sinks should be attached to the fuse lead between the soldering point and the fuse cap.

Appendix C

The Copper-Silver alloy system

The electrical resistivity of the copper-silver (Cu-Ag) filaments used by Littelfuse can be computed from the specified cold resistance of fuses rated from 3/4 A to 4 A (Table 2.1) and the diameters of each filament as reported by Littelfuse (Table 3.3). These range from about 1.9 $\mu\Omega$·cm to about 2.7 $\mu\Omega$·cm at 25 °C. This 30% variation is more than an order of magnitude larger than the variation of resistivity for copper filaments and for nickel filaments. It is the purpose of this Appendix to consider the factors that affect Cu-Ag resistivity so that these relatively large variations can be understood.

Manufacturing controls are good enough to deliver fuses with Cu-Ag filaments that are within the specified range for the cold and hot resistances, at least in the "as delivered" condition. However, studies by Code 313 show that repeatedly cycling a fuse with a Cu-Ag filament between zero current and its rated current using a triangular shaped profile (such as displayed in Figure D.1; note that the rated current is passing through the fuse for only small fraction of the total time) steadily lowers its cold resistance: a decrease in cold resistance of more than 10% after twenty cycles has been observed, shifting the cold resistance to below the specified low limit of cold resistance.

This reduction can happen when the current is applied in other ways as well. Several similar reductions were observed by Unisys during preparation of the fuse plugs for the 1994 Hubble Space Telescope Servicing Mission.[1] Changes in cold resistance between stages in constructing assemblies containing fuses are monitored as an index to possible fuse degradation, and a typical rejection-threshold is ±3% in the cold resistance of any fuse in the assembly. Such changes are sometimes observed for fuses using Cu-Ag filaments. On the other hand, such shifts are less common in the cold resistances of fuses with nickel and with copper filaments.

Thus, the relatively large variations of the resistivity of Cu-Ag alloy can have consequences for the performance of these fuses and for their acceptance for use in spacecraft, and an analysis of how such changes can happen is in order.

[1] Private communication from Mr. Scott Hull (then of Unisys).

The electrical resistivity of an alloy often has the form $\rho_{alloy} = \rho(T) + \Delta\rho$ where $\rho(T)$ has the same temperature behavior as for a pure metal, and $\Delta\rho$ is independent of temperature and depends on the kinds of materials being alloyed, their concentrations, and details of microstructures in the alloy. In many cases, the added resistivity $\Delta\rho$ is so much greater than the temperature-dependent term that the total resistivity ρ is nearly temperature-independent. This is the principle behind the alloy Constantan[2] so-named since its resistivity is nearly constant versus temperature. The total resistivity of a complete series of copper-nickel (Cu-Ni) alloys is presented in Figure C.1. Inspection shows that the added resistivity $\Delta\rho$ for Cu-Ni at near 50 at-% copper is more than an order of magnitude greater than the resistivity of either of the pure materials at room temperature. Thus, the temperature dependence of the resistivity of a filament made of this alloy would be better modeled as a constant than modeled as proportional to T as has been done in the body of this report.

However, the added resistivity $\Delta\rho$ for Cu-Ag alloys is relatively small for two reasons: (a) Each kind of atom is similar enough to the other with respect to the scattering of conduction electrons that the dissolution of a small amount of one metal into the other increases the resistivity only slightly. (b) Each kind of atom is distinct enough from the other with respect to factors that affect lattice stability that only a small amount of one metal will dissolve into the other. We now discuss each of these reasons in more detail, to obtain a model of the resistivity of Cu-Ag alloys.

C.1 Alloys: a sketch of solubility and resistivity

Consider a single crystal of a metal and replace one of its atoms with a foreign atom: this produces a local strain field around the foreign atom as the crystal structure (atomic cores and their locations, plus conduction electrons and their wavefunctions) shifts to accommodate it, and it also produces an increase in resistivity as conduction electrons are scattered by these local changes in structure. The increase in resistivity will be proportional to the number of foreign atoms so long as their concentration is small enough so that their scatterings are independent, and so that they do not produce a discontinuous change in the original crystal's structure. Perturbations of the original structure increase with foreign atom concentration, and, if the foreign atoms differ too much from the ones they are replacing, the structure may become unstable relative to other structures as the concentration is increased past a critical value: there will be a discontinuous change at this critical value. However, there are examples for which the original structure changes continuously throughout: then the lattice type is retained throughout, and the lattice spacing changes continuously with concentration.

For example, copper forms a face centered cubic crystal with lattice constant 3.61 Å.[3] Ob-

[2]The term is used for a range of concentrations. A typical version of Constantan is 58 at-% Cu, 42 at-% Ni. This alloy is ferromagnetic for copper concentrations up to about 62 at-%, and this somewhat affects the temperature dependence of the resistivity.

[3]The lattice constants of this Appendix are from Table 4 of *Introduction to Solid State Physics* by C. Kittel (John Wiley; third edition, 1966), and apply at 25 °C.

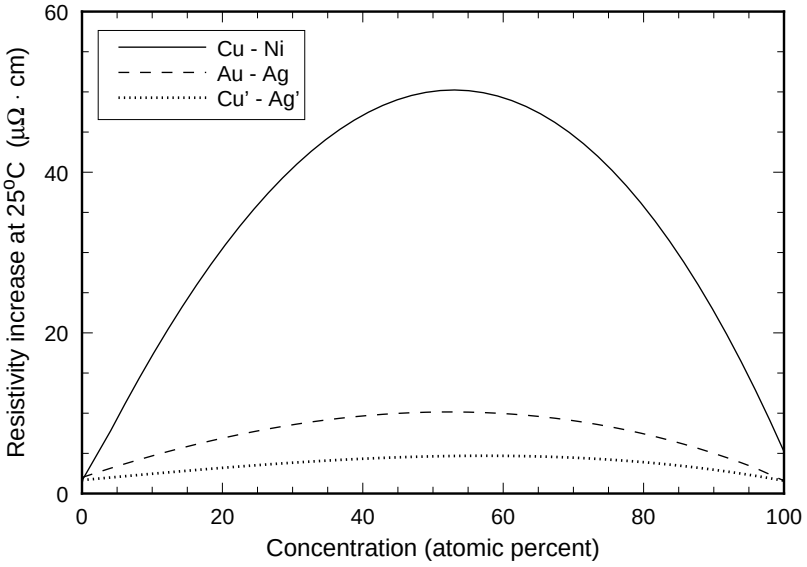

Figure C.1: Electrical resistivity of three alloy systems. The curve for Cu-Ni is based on data from Figure 6-7 of *Elements of Physical Metallurgy* by A. G. Guy (Addison-Wesley, 1959). The curve for Au-Ag is based on data from Figure 103 of *The Theory of the Properties of Metals and Alloys* by N. F. Mott and H. Jones (Dover, 1958). The curve for Cu'-Ag' is based on the values of ρ_{Cu}, ρ_{Ag}, $(d\rho/dx)_{Cu\,in\,Ag}$ and $(d\rho/dx)_{Ag\,in\,Cu}$ discussed in this appendix. A simple model for $\rho_{Cu-Ag}(x)$ allows computation for any x between 0% and 100%, but single crystals are stable only for x near 0% and 100%; thus, the curve is labeled Cu'-Ag' to indicate that most of its middle cannot be measured experimentally.

servation shows that this lattice type is retained as nickel is added up to a concentration of 100%, and that the lattice constant decreases continuously until it reaches the lattice constant of nickel, 3.29 Å, a decrease of 9.3%. The resistivity of Cu-Ni alloy is shown in Figure C.1: it is a smoothly changing function of nickel concentration with a maximum near 50 at-%. The maximum resistivity is more than thirty times greater than that of pure copper at room temperature. So copper and nickel atoms are similar from the point of view of fitting into each other's structure, but dissimilar from the point of view of scattering of conduction electrons.

As another example, silver forms a face centered cubic crystal with lattice constant 4.08 Å. Observation shows that this lattice type is retained as gold is added up to a concentration of 100%, and that the lattice constant decreases continuously until it reaches the lattice constant of gold, 4.04 Å, a decrease of 0.2%. The resistivity of silver-gold (Ag-Au) alloy is shown in Figure C.1: it is a smoothly changing function of gold concentration with a maximum near 50 at-%. The maximum resistivity is about a factor of five greater than that of pure silver at room temperature. So silver and gold atoms are similar from the point of view of fitting into each other's structure, and somewhat similar from the point of view of scattering of conduction electrons.

The difference in the lattice constants of copper and silver is 12%, and observation shows

that addition of silver to copper perturbs the copper structure sufficiently that a copper-like structure is stable only up to a silver concentration of a few percent (the precise value depends on temperature and is discussed below). The reciprocal is also true: addition of copper to silver perturbs the silver structure sufficiently that a silver-like structure is stable only up to a concentration of a few percent. If copper formed a complete sequence of solid solutions, which it does not, then its resistivity in this sequence would resemble the curve labeled Cu'-Ag' in Figure C.1, where the primes denote that this curve describes a fictitious situation.[4] The maximum resistivity is about three times greater than that of pure copper at room temperature. So copper and silver atoms are dissimilar from the point of view of fitting into each other's crystal structure, and fairly similar from the point of view of scattering of conduction electrons. A silver atom placed into a copper crystal presents a conduction electron scattering cross-section that is 1% to 3% of its geometrical cross-section (based on the lattice parameter), and vice versa.

We will now consider the observed phase diagram of the Cu-Ag alloy system to determine accurate ranges of concentrations for which thermodynamic equilibrium prevails. Also, we consider diffusion rates to estimate some limits to the applicability of equilibrium. Then we will apply the various experimentally based rules for estimating the change in resistivity upon the addition of foreign elements. Finally, we will discuss measurements of the resistivity of various Cu-Ag alloys including fuse filaments, and show that the main features of the observed data are within the scope of these ideas.

C.2 The phase diagram of the Cu-Ag system

The phase diagram of the Cu-Ag system is shown in Figure C.2. It summarizes the kinds of phases that are present when the system is in thermodynamic equilibrium at one atmosphere of pressure and at a specified temperature. It also specifies the concentration of Cu and Ag in each phase and the amount of each phase. These concentrations are also shown in Table C.1. Certain nonequilibrium effects will be discussed below.

A phase diagram is a compact summary of many experiments. This compactness can conceal some behaviors from people who are not expert in reading them. In the interest of making certain behaviors explicit, I will now relate Figure C.2 to the cooling of Cu-Ag alloys from the melt.

Consider the system at the eutectic concentration: $x_{Cu} = 39.9$ at-%, $x_{Ag} = 60.1$ at-%. This system is liquid above the eutectic temperature, $T_{eut} = 1052$ K, and solid below it. As this system is cooled to just below T_{eut} slowly enough that the system is always in thermodynamic phase equilibrium, it solidifies into a so-called "eutectic structure" with a

[4]The copper-like structure with any amount of silver in it is well-defined in the context of solid state computations: it is just not stable relative to another discontinuously distinct structure, and so cannot be prepared experimentally. However, it can be used to compute the resistivity increase and that is what I have done here. The actual resistivity of a sequence of Cu-Ag alloys is presented in several plots displayed below: see for example Figure C.5.)

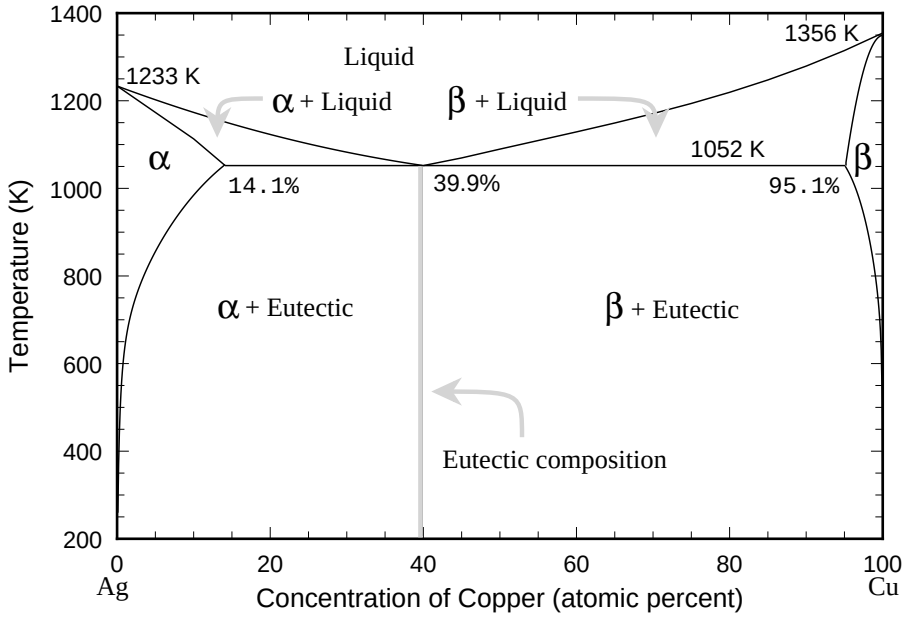

Figure C.2: Phase diagram of the Cu-Ag system. This plot is redrawn from values given on pages 18 to 20 of *Constitution of Binary alloys* by Max Hanson and Kurt Anderko (McGraw-Hill, 1958).

characteristic appearance: the copper-rich β phase solidifies as isolated grains within a solid matrix of continuously connected silver-rich α phase. The grains of β phase are needle-shaped and tend to be parallel throughout an extended region. The concentration of copper in the α phase matrix is 14.1 at-%, while the concentration of silver in the β phase grains is 4.9 at-%.

Consider a system with a copper concentration between 14.1 at-% and the eutectic value. The system will be liquid above the melting point of pure silver, $T_{melt}^{Ag} = 1233$ K. Between T_{melt}^{Ag} and T_{eut}, solid α phase forms in the liquid. The α phase has the copper concentration specified by the curve joining the phase diagram points $(0\%, 1233\ \text{K})$ and $(14.1\%, 1052\ \text{K})$ shown in Figure C.2. The α phase typically forms as dendrites which grow when the temperature is constant. (Commercial practice is to cool quickly and there is limited growth before the melt solidifies.) The formation of the silver-rich grains of α phase preferentially removes silver from the liquid; thus, the liquid approaches the eutectic composition, reaching this composition when the temperature reaches T_{eut}. When the system is then cooled to just below T_{eut}, it will therefore be composed of grains of α phase surrounded by the characteristic eutectic structure. The size of the α grains will be the larger, the slower the system has been cooled to T_{eut}. In usual practice, these grains are substantially larger than the α phase regions in the eutectic structure, and are called "primary α phase grains." Figure C.3 shows an example.

Consider a system with a copper concentration x_{Cu} between 0% and 14.1 at-%. As the system is cooled below T_{melt}^{Ag}, solid grains of α phase form in the liquid. When the system is cooled

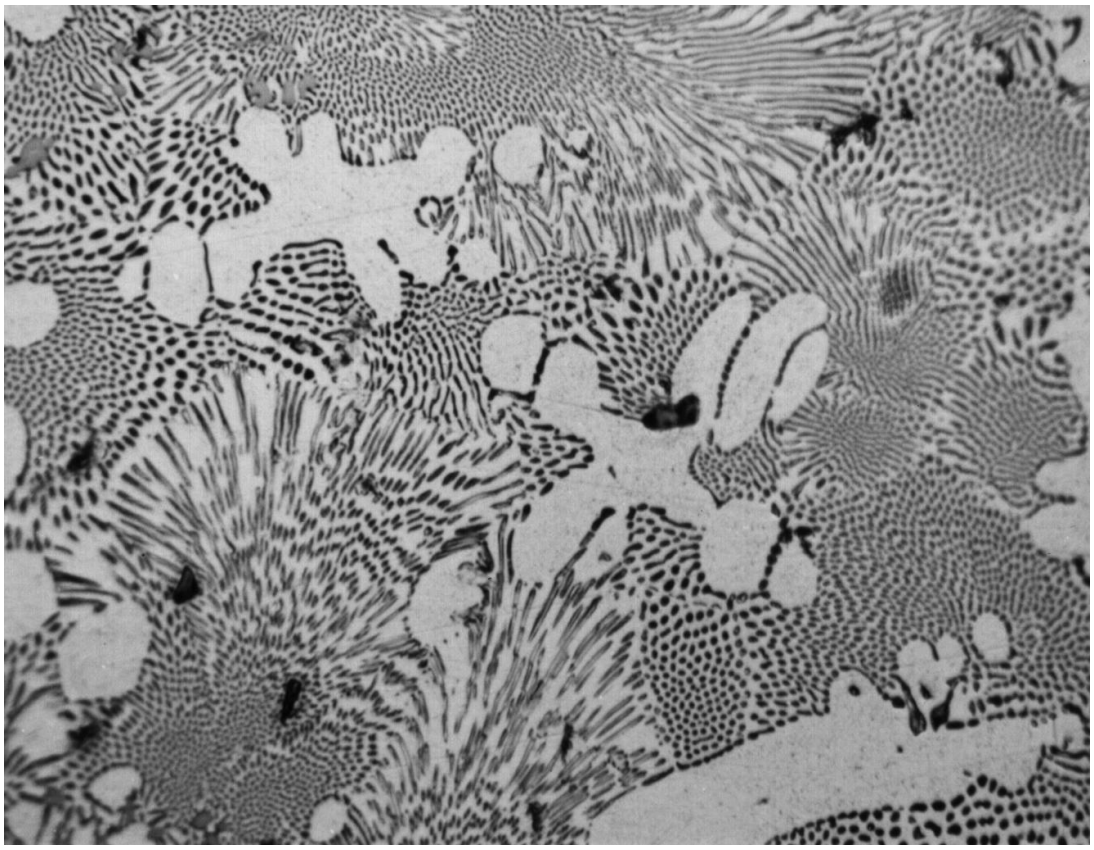

Figure C.3: Optical image (500 power) of Cu-Ag alloy; $x_{Cu} \sim 36$ at-%. The silver-rich α phase is light gray, and the copper-rich β phase is dark gray. The primary α phase grains are dendrites: their cross-section scale is of order 15 μm, and their length scale is of order 70 μm. In the eutectic structure, the β phase is in the form of unconnected needles immersed within the continuous α phase; the scale of the cross section of the needles is of order 1 μm. Some grains of eutectic structure show the needles predominantly lengthwise, while other grains show the needles predominantly in cross section; the scale of these grains is of order 100 μm. Photograph by Ms. Jellison.

to the temperature $T(x_{Cu})$ along the curve joining the phase diagram points $(0\%, 1233\ \text{K})$ and $(14.1\%, 1052\ \text{K})$, all the liquid is consumed by the solid α phase: the system solidifies as it is cooled to just below this temperature. It will consist entirely of primary α phase grains; there is no eutectic structure.

Systems with a copper concentration x_{Cu} between the eutectic value and 100% have behaviors complimentary to those just discussed. When the concentration of copper is increased above the eutectic value, then grains of β phase form in the liquid as the temperature is lowered into the interval T_{melt}^{Cu} to T_{eut}. The size of these grains increases with time. When the copper concentration is less than 95.1 at-%, the system will solidify at T_{eut}, and will be composed of both the grains of β phase and the eutectic structure. In usual practice, the copper-rich β grains are substantially larger than the β phase regions in the eutectic structure, and are called the "primary β phase grains." Each primary β phase grain is surrounded by the eutectic structure so long as there is enough eutectic structure to do this. The amount of the eutectic structure present in the solid at just below T_{eut} decreases to zero as the copper concentration increases to 95.1 at-%. The solid consists only of contiguous grains of primary β phase grains for still larger copper concentrations.

When the solid is cooled below T_{eut} under conditions of thermodynamic phase equilibrium, the concentration of the minority element in each phase decreases rapidly toward zero. There are two processes enabling this: either the minority atoms diffuse out of that phase and into the other phase (diffusion process), or the minority atoms cluster together to form a precipitated grain of the other phase within that phase (precipitation process). The diffusion process is faster than the precipitation process just below the eutectic temperature, and so slow cooling from T_{eut} initially results in the increase in the size of the grains of α phase and β phase. However, as the temperature is lowered, the diffusion process slows more than the precipitation process does, and so these relative speeds are eventually reversed: then precipitation dominates. The rate of the diffusion process also scales as the square of the distance over which diffusion must operate; hence, there can be precipitation within the primary grains even when there is only diffusion within the eutectic structure.

If the rate of cooling is too fast for these processes to maintain the concentrations of thermodynamic phase equilibrium, then each phase becomes supersaturated. Since the equilibrating rates decrease rapidly with decreasing temperature, it is inevitable that supersaturation will happen in practice.

C.2.1 Diffusion rates

The rate at which minority atoms in a given phase diffuse into the other phase is controlled by the diffusion path (e. g., diffusion through an ideal crystal, diffusion along a dislocation, diffusion along a crystal grain boundary) and the diffusion parameter for that kind of path. Reliable values of the diffusion parameters for the complete equilibration process are not available. However, values reported in [23] for the bulk diffusion of copper in silver, and for

silver in copper, are at least illustrative of the principles: the diffusion parameters are

$$D_{Cu\ in\ Ag} = 5.9 \times 10^{-5} \exp[-(12\,490\ \text{K})/T]\ \text{cm}^2/\text{sec} \quad \text{(C.1)}$$

for 2 at-% copper in silver from 650 °C to 895 °C; and

$$D_{Ag\ in\ Cu} = 6.8 \times 10^{-6} \exp[-(11\,330\ \text{K})/T]\ \text{cm}^2/\text{sec} \quad \text{(C.2)}$$

for 2.4 to 3.5 at-% silver in copper from 400 °C to 970 °C.

These are close to each other: for example, the ratio $D_{Ag\ in\ Cu}/D_{Cu\ in\ Ag}$ varies from 0.43 at 600 °C to 0.31 at 900 °C.

A numerical example: Consider the specimen pictured in Figure C.3. The radius of the β phase needles in the eutectic structure is on the order of 0.5 μm and the radius of the primary α phase dendrites is on the order of 10 μm. The diffusion mediated equilibration times for diffusion through a distance d is one the order of $d^2/(4D)$. Thus, diffusion-mediated equilibration times for the β phase needles in the eutectic structure are on the order of seconds at 779 °C and of tens of seconds at 600 °C. Using Equations C.1 and C.2 to extrapolate to lower temperatures, computed times are on the order of minutes at 500 °C, tens of minutes at 400 °C, tens of hours at 300 °C, months at 200 °C, and a century at 100 °C. And the times for the primary α grains are two to three orders of magnitude longer at the same temperature, if the diffusion paths are the same. Thus, when cooling at a steady rate from the melt, the α and β phases in the eutectic constituent remain in thermodynamic phase equilibrium down to appreciably lower temperatures than the primary α grains do.

C.2.2 Wire

The preparation of a wire involves mechanical working as the casting is beaten into a bar and then drawn through a succession of dies of decreasing diameter. This distorts and elongates the structures that formed when the original melt cooled, creating dislocations and defects: the result is an increase in electronic scattering, which gives an increase in the electrical resistance and a decrease in the thermal conductivity. There is almost no change in the Lorenz number however, since the increase in electronic scattering affects both electrical and thermal transport about equally. This happens for both pure metals and for alloys; however, the density of defects is greater for an alloy.

The concentration of defects can be reduced by then holding the wire at an elevated temperature for some time: the rate of reduction depends on the type of defect as well as the temperature. The defects introduced into a pure metal when it is formed into a wire are different than those introduced into an alloy, and so the rate and extent of recovery are different too.

C.2.3 Melting of the fuse filament

The Cu-Ag system is entirely liquid above $T_{melt}^{Ag} = 1356$ K. The liquid state continues down to about 1141 K for a system of 50 wt-% copper – 50 wt-% silver (i. e., 62.9 at-% copper – 37.1 at-% silver). Between this temperature and the eutectic temperature $T_{eut} = 1052$ K, there are copper-rich primary grains of β phase within the liquid. Below T_{eut}, the system is a solid.

The solid material supports shear forces while showing some rate of creep; the creep rate is negligibly small near room temperature, but increases to significant values as the temperature is increased to $T_{eut} = 1052$ K. Practically speaking, filaments made of this alloy are strong for temperatures well below 1052 K, but their resistance to mechanical shock and vibration decreases sharply as the temperature is increased to 1052 K, and vanishes at and above 1052 K. Even in an environment free of shock and vibration, the filament will melt open under the forces of gravity (if present), surface tension, and assembly stresses when some length of it is raised to 1052 K or above. Melting open will require some time: the part of the filament that has become liquid must deform from its initially cylindrical shape into an interrupted shape, pushed against its viscosity and its inertia by the applied forces. Since a liquid that is filled with a suspension of solid grains has a viscosity that is substantially larger than the unfilled liquid, then the deformation time is substantially larger when a length of filament is just above 1052 K (and hence contains many solid grains) than when it is hotter (and contains fewer grains): hence the dynamics of formation of beads will be more sluggish than for pure copper or pure nickel, and the interruption time for fuses using Cu-Ag filaments will be longer than those using pure copper or nickel.

C.3 Electrical resistivity of Cu-Ag alloy

Dissolve a small amount x of an element X in a metal M. The effect on the resistivity is described by these empirical rules:

Matthiessen's rule: $\rho_{M,X}(T, x) = \rho_M(T) + \Delta\rho_{M,X}$, where $\rho_M(T)$ is the resistivity of the pure metal, and the influence coefficient $\Delta\rho_{M,X}$ depends on M and X, but not on the temperature.

Nordheim's rule: $\Delta\rho_{M,X} = x \cdot A_{X\,in\,M}$, where $A_{X\,in\,M}$ depends on the metal M and on the element X, but not on the concentration x of X. (This is the linear form of the rule, and only applies when $x \ll 1$.)

Linde's rule: $A_{X\,in\,M} = a_M^L + b_M^L \cdot (\Delta Z)^2$, where ΔZ is the valence difference between the metal M and the element X, and a_M^L, b_M^L are constants for a given row L of the periodic table, but change as this row changes and as the metal M changes.

Mott's rule: $A_{X\,in\,M} = A_{M\,in\,X}$, when both M and X have the same atomic volume, valence, and crystal structure.

Experiment shows that the rules of Matthiessen, Nordheim, and Linde are accurate for silver dissolved into copper and for copper dissolved into silver. Linde's rule correctly predicts that each material will only slightly increase the resistivity of the other (since $\Delta Z = 0$).The several values reported in the literature show some scatter; I have examined the data[5] and have found $A_{Cu\ in\ Ag} = (0.08 \pm 0.02)\ \mu\Omega$·cm/at-% and $A_{Ag\ in\ Cu} = (0.16 \pm 0.03)\ \mu\Omega$·cm/at-%.

We have already seen the resistivity for the Cu-Ni and for the Ag-Au systems: these pairs of materials resemble each other. As an example of the resistivity increase when a nonmetal is dissolved into copper, consider the result for sulphur. The rules suggest a large change in resistance, and measurement shows that $A_{Cu\ in\ Ag}$ and $A_{Ag\ in\ Cu}$ are some two orders of magnitude smaller than that for sulphur dissolved in copper: $A_{S\ in\ Cu} = (10 \pm 1)\ \mu\Omega$·cm/at-%. A specimen of copper or silver will have its resistivity increased by 1% by dissolving 0.2% sulphur into it. This illustrates that a uniform specification of purity such as "the maximum concentration of an impurity must be less than 1%" is not so appropriate for resistivity as a specification that specifically targets those elements that particularly affect resistivity.

Since copper and silver crystallize in the face centered cubic structure, and since their valence is each unity (so than $\Delta Z = 0$), then two of the three conditions of Mott's rule are met. Mott used some early experimental data and reported each coefficient to be 0.07 $\mu\Omega$·cm/at-%, and claimed this pair of metals as an example of Mott's rule. However, the atomic volumes are not equal: $v_{Ag}/v_{Cu} = 1.45$; hence, this condition for the application of Mott's rule is not met. And later experiments show that the coefficients are only approximately the same.

Suppose a sequence of Cu-Ag alloys are prepared with copper concentrations ranging from $x_{Cu} = 0$ at-% to 100 at-%, and that each is held at a fixed temperature T_{fix} long enough so that phase equilibrium is attained, and is then quenched so quickly to 20 °C that the compositions of its grains can be computed from the temperature T_{fix} and Table C.1. The resistivity of the α and β phases are then computed from the rules just discussed.

The resistivity of the mixture of phases depends in principle on the geometry with which they are arranged. For example, if grains of α phase and grains of β phase were to each grow until they reached the diameter of the filament, then the effective resistivity would be

$$\rho = v_\alpha \cdot \rho_\alpha + v_\beta \cdot \rho_\beta \qquad \text{series combination,} \tag{C.3}$$

where v is the volume fraction of each phase. On the other hand, if all the β phase material were to form needles surrounded within an α phase matrix, then the effective resistivity would be

$$\rho = 1/(v_\alpha/\rho_\alpha + v_\beta/\rho_\beta) \qquad \text{parallel combination.} \tag{C.4}$$

For an alloy of aluminum and silicon, for example, whose phase diagram is topologically similar with that of copper and silver, but whose α and β phase resistivities are markedly different, these expressions give markedly different results and so it becomes necessary to study the actual geometry of the arrangement of these phases.

[5]The sources are pages 224 and 228 of [24], and pages 156 and following of [25].

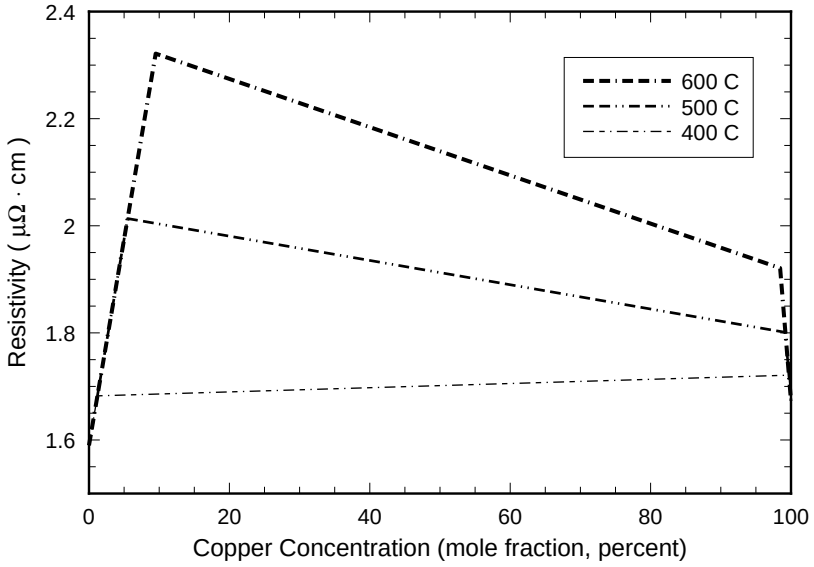

Figure C.4: Electrical resistivity of the Cu-Ag system computed using the concentrations given in the phase diagram and $\rho = \bar{\rho} + (v_\beta - v_\alpha) \cdot (\Delta\rho/2)$. See the text for comments.

But the resistivity of the α and β phases of the Cu-Ag system are nearly the same, and so both the series and the parallel combinations give the same result to first order:

$$\rho = \bar{\rho} + (v_\beta - v_\alpha) \cdot (\Delta\rho/2) \ , \tag{C.5}$$

where $\bar{\rho} = (\rho_\beta + \rho_\alpha)/2$ is the average resistivity and $\Delta\rho = \rho_\beta - \rho_\alpha$. This expression is accurate to first order for the actual geometry, and so we do not need to use this geometry but only the concentrations. The resulting resistivity at 20 °C is shown in Figure C.4 for three choices of T_{fix}: 600 °C, 500 °C, and 400 °C. This computed resistivity increases linearly with increasing copper concentration (since $\rho = x \cdot A_{Cu\ in\ Ag}$) so long as the copper concentration is less than its saturation value at T_{fix}, since only the α phase is then present. The eutectic phase, with its α phase and β phase forms when the copper concentration exceeds this saturation value. When the copper concentration is large enough so that the β phase can dissolve all the silver present, then the resistivity decreases linearly with increasing copper concentration. Thus, there are sharp corners as the eutectic structure first forms (roughly at $x_{Cu} \sim 10$ at-% depending on T_{fix}), and again as the eutectic structure no longer forms (roughly at $x_{Cu} \sim 95$ at-% depending on T_{fix}). However, this is true only when thermodynamic phase equilibrium holds. In actual practice, nonequilibrium effects will round these corners: this effect is seen in the following plots of experimental data. The comparisons with experimental data are carried out in Figures C.5, C.6, and C.7; three figures are used since there is too much data to display in a single figure.

Figure C.5 shows the measured resistivity of alloys of copper and silver prepared in various ways: the sources are listed in the figure's caption. All three measured curves show an initial increase of resistivity with increasing copper content that agrees with the computed curve; #3 also shows agreement with the final decrease in resistivity as the material approaches pure copper.

Curve #1 is based on data for wires held at 725 °C and then quenched to 20 °C. The resistivity increases linearly with copper content up to $x_{Cu} \sim 8$ at-%, corresponding to equilibration at about 580 °C, and then approaches values just below the intermediate concentration curve computed for 600 °C. Apparently the rate of quenching was slow enough so that the concentrations remained in equilibrium down to a temperature in the neighborhood of 580 °C; this is consistent with the earlier estimate that equilibration times are on the order of minutes at 600 °C, but increase to the order of hours at 400 °C.

Curve #2 is based on data for "commercial wire, annealed." The increase of resistivity with increasing copper content is similar to that of #1 up to $x \sim 5$ at-% corresponding to equilibration at about 500 °C, and then approaches the intermediate-concentration curve computed for 500 °C. Apparently the concentrations reflect equilibration at about 500 °C, which is associated with time scales intermediate between minutes and hours, in line with the times available during commercial production.

Curve #3 is based on data for "annealed wire" reported in [25]. It shows resistivity increasing linearly with increasing copper content up to $x_{Cu} \sim 2$ at-%, corresponding to equilibration at about 450 °C. The resistivity then approaches a horizontal line intermediate between those computed for 400 °C and 500 °C for concentrations up to $x \sim 40$ at-%. For still higher copper content, the data approaches the line computed for 500 °C; this suggests that equilibration within a given time requires a higher temperature as the copper content increases past 50%. Indeed, $D_{Ag\ in\ Cu}(500\ °C) \approx D_{Cu\ in\ Ag}(470\ °C)$ according to the diffusion parameters just quoted. And the temperature dependence of $D_{Cu\ in\ Ag}$ indicates that the wires of #3 were cooled at half the rate of those of #2. Finally, the resistivity decreases linearly with decreasing silver content for x_{Cu} >97 at-%.

Figure C.6 shows the measured resistivity of several more alloys of copper and silver prepared in various ways. Curve #3 is repeated from the previous figure; it shows the resistivity of a family of specimens of increasing copper content "after annealing"; Curve #4 is the resistivity of that same family "before heat treatment." Curve #4 suggests equilibration at about 550 °C for low copper content and equilibration at roughly 700 °C for high copper concentration; these compare with 450 °C and 500 °C, respectively, for Curve #3: annealing has reduced the apparent equilibration temperatures by about 100 °C and 200 °C, respectively. But another explanation is possible: the higher resistivities of Curve #4 may represent the cold working that the material experiences as it is fashioned into wire, and the reduction in resistance upon annealing may measure the reduction in the density of dislocations and other defects. Supporting this interpretation is the roughly constant reduction of about 0.4 $\mu\Omega$·cm (for copper concentrations between 10 at-% and 95 at-%), which is about 20% of the annealed resistivity.

Curve #5 is the resistivity of a family of specimens "quenched and then annealed for 2.5 hours at 280 °C"; #6 is "quenched and then annealed for 17 hours at 280 °C." Clearly there are changes proceeding on a time scale of hours to days, which is consistent with the earlier computed estimates of hours at 300 °C, and weeks at 200 °C. Comparison with the curve computed for equilibrium at 400 °C (which is only a little above the curves for lower temperatures) suggests that even the specimens annealed at 280 °C for 17 hours are not yet

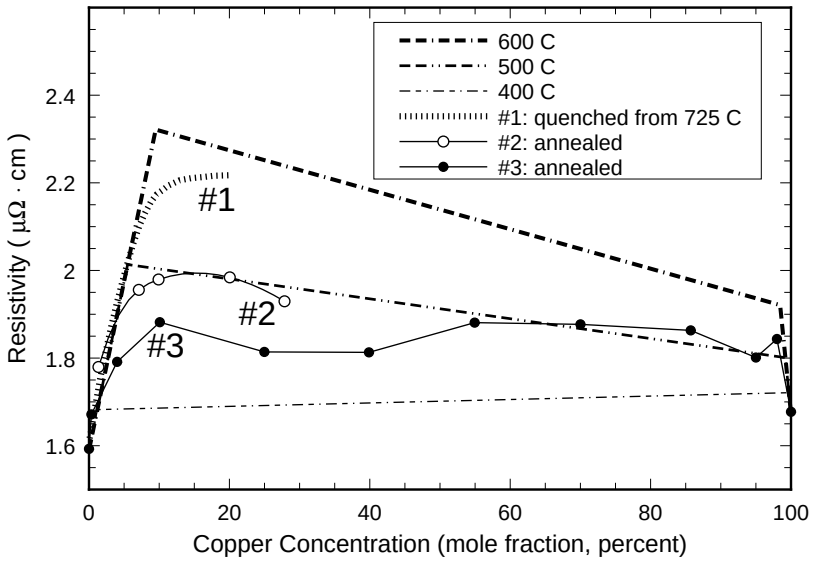

Figure C.5: Curves #1 and #2 are from Figure 3 of the chapter "Properties of Silver & Silver Alloys" in the *Metals Handbook*, Volume 2, Ninth Edition (1979); the abscissa has been transformed from weight fraction to mole fraction. Curve #1 is for a specimen "quenched from 725 °C," and curve #2 is for a specimen of "commercial wire, annealed." Curve #3 is from data reported in the *International Critical Tables* for "annealed wire." The computed curves of the previous figure are repeated for comparison.

in equilibrium for copper contents above about 5%.

Figure C.7 displays the resistivity named by Littelfuse as part of their procurement specification for Cu-Ag filaments: $\rho(20\ ^\circ\mathrm{C}) = 2.57\ \mu\Omega\cdot\mathrm{cm}$. Also shown is a value, 2.05 $\mu\Omega\cdot$cm, for a fuse rated at 3 A that had been operated at its rated current for an hour: the temperature of the middle of its filament is roughly 300 °C to 400 °C, while its ends are at 25 °C, according to the model developed in this report: there is some small degree of annealing during this time.

The computed curve for equilibrium at 700 °C is to be compared with the resistivity measured for specimens "quenched from 725 °C" (curve #2). Agreement is satisfactory for copper concentrations below about 5 at-%, but the measured resistivity falls below the computed curve for larger copper concentrations: probably, the specimens partially equilibrate to temperatures lower than 725 °C, and actually have a smaller amount of copper in the silver-rich grains than assumed in the model. The observed resistivity of $\rho \approx 2.2\ \mu\Omega\cdot$cm suggests the α phase has a copper concentration of 6%, which corresponds to a temperature of slightly above 600 °C; estimated equilibration times are on the order of minutes at this temperature, so this explanation is possible.

Curves #3 and #4 show that annealing at 280 °C takes place on a time-scale of tens of hours, in rough agreement with the estimations just given. Curve #1 illustrates what can be expected of "commercial wire, annealed." The silver-rich grains contain about 4% copper and

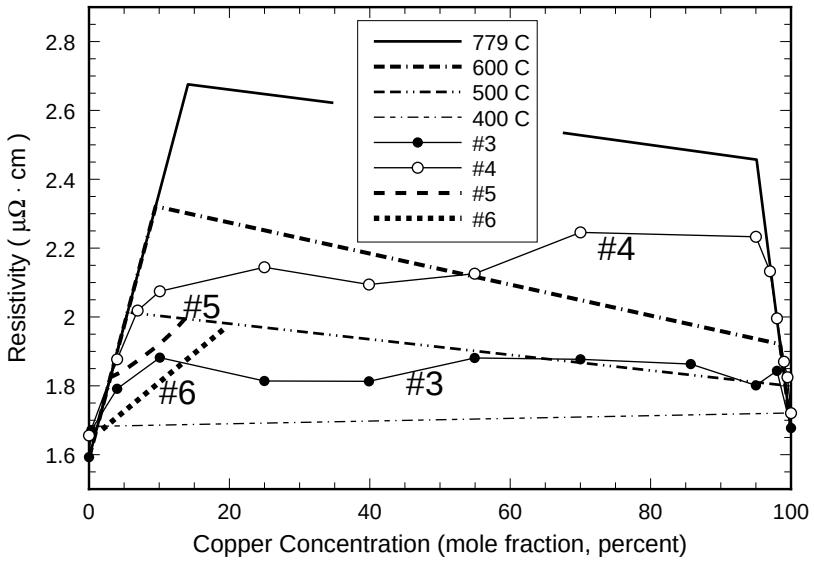

Figure C.6: Curves #3 and #4 are data from the *International Critical Tables*. Curve #3 is for a specimen of "annealed wire," and #4 is for a specimen of wire "before heat treatment." Curves #5 and #6 are from Figure 3 of the chapter "Properties of Silver & Silver Alloys" in the *Metals Handbook*, Volume 2, Ninth Edition (1979); the abscissa has been transformed from weight fraction to mole fraction. Curve #5 is for wire that has been "quenched and then annealed for 2.5 hours at 280 °C," and curve #6 is for wire "quenched and then annealed for 17 hours at 280 °C." Computed curves are included for comparison.

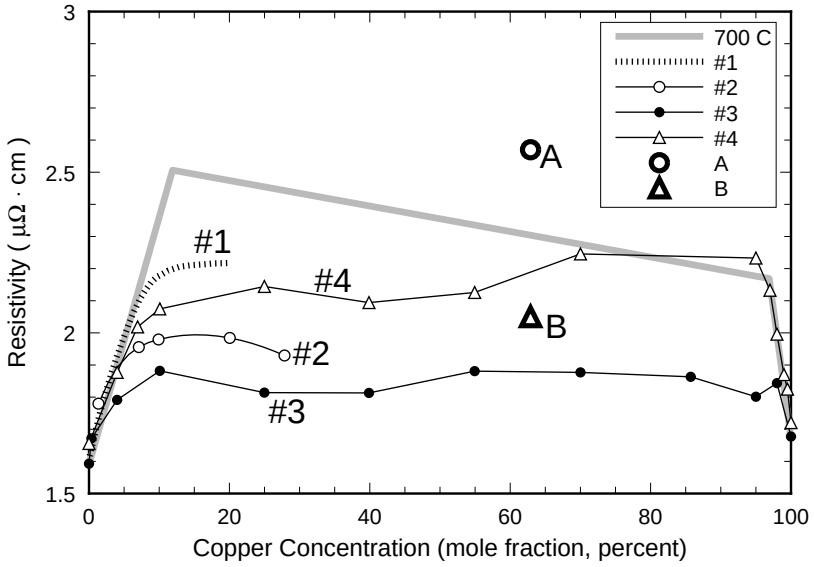

Figure C.7: Electrical resistivity of the Cu-Ag system. Curves #1 through # 4 are from Figure 3 of the chapter "Properties of Silver & Silver Alloys" in the *Metals Handbook*, Volume 2, Ninth Edition (1979); the abscissa has been transformed from weight fraction to mole fraction. Curve #1 is "commercial wire, annealed"; #2 is "quenched from 725 °C"; #3 is "quenched and then annealed for 2.5 hours at 280 °C"; #4 is "quenched and then annealed for 17 hours at 280 °C." The model curve for 700 °C is computed as per the discussion in the text. Point A is from the specification used by Littelfuse. Point B is measured from a fuse rated at 3 A that had been operated at its rated current for an hour.

the copper-rich grains contain about 1% silver, appropriate to an equilibrium temperature of about 550 °C.

The specification that Littelfuse uses as part of their procurement of Cu-Ag wire specifies a resistivity of 2.57 $\mu\Omega$·cm (Point A in Figure C.7); apparently, this wire is not fully annealed, and still contains an appreciable degree of work-hardening which contributes to an increase in resistivity. After use as a fuse element, its resistivity (Point B in Figure C.7) decreases into the range of the values for annealed Cu-Ag wire.

C.4 The Lorenz number and thermal conductivity

So long as electronic conduction dominates lattice conduction, then theory assures that introducing electronic scattering centers will affect both electrical and thermal conductivities equally, and hence the Lorenz number $\mathcal{L} = k_T\rho/T$ will be unchanged. Experiment confirms this. Since the Lorenz numbers of both copper and silver are nearly the same from about 200 K to 1200 K, then the Lorenz number of the alloy is estimated with good accuracy as the mole fraction weighted average: $\mathcal{L}(T,x) = x\cdot\mathcal{L}_{Cu} + (1-x)\cdot\mathcal{L}_{Ag} = (2.40\pm0.05)\times10^{-8}$ V^2/K^2 where x is the mole fraction of copper.

This allows computation of the thermal conductivity of the alloy once the electrical resistivity ρ is known: $k_T(T, x) = T\mathcal{L}(T, x)/\rho(T, x)$.

C.5 Heat capacity

The molar heat capacity of the alloy is estimated with good accuracy as the mole-fraction weighted average of the molar heat capacity of the elements:

$$C_p(T, x) = x \cdot C_{p,Cu}(T) + (1 - x) \cdot C_{p,Ag}(T)\,, \tag{C.6}$$

where x is the mole fraction of copper.

Table C.1: Solid Solubilities of Copper in Silver and of Silver in Copper

T (°C)	Cu in Ag (atomic %)	Ag in Cu (atomic %)
779	14.1	4.9
750	11.9	—
700	9.5	3.1
600	5.5	1.55
500	3.0	0.8
400	1.2	0.3
300	0.7	0.12
200	0.35	<0.06

Appendix D

Hysteresis

Suppose that we apply a "ramp up/ramp down" current to a fuse:

$$I(t) = \left\{ \begin{array}{ll} 0 & \text{if } t < 0 \text{ or if } t > 2\mathcal{T} \\ I_{max} \cdot (t/\mathcal{T}) & \text{if } 0 \le t \le \mathcal{T} \\ I_{max} \cdot (2\mathcal{T} - t)/\mathcal{T} & \text{if } \mathcal{T} \le t \le 2\mathcal{T} \end{array} \right\} \tag{D.1}$$

where $\mathcal{T}$ is the time for the current to increase from zero to its full value, I_{max}. An example is shown in Figure D.1. Then we observe the resistance of the fuse to also ramp up and then ramp down: see Figure D.2. The current will take a particular value at two times, t_1 and t_2: t_1 is earlier than $\mathcal{T}$ by a duration t_3, and t_2 is later than $\mathcal{T}$ by the same duration t_3; that is, $t_1 = \mathcal{T} - t_3$ and $t_2 = \mathcal{T} + t_3$: these times are shown on Figure D.2.

In practice, we observe that the resistance of the fuse at the time t_1 is slightly less than at the time t_2, even though the currents are identical: this called *hysteresis*.[1] This hysteresis is present in the data[2] shown in Figure D.3. However, it is hardly visible in this plot, since the long test cycle ($\mathcal{T} = 1000$ seconds) was deliberately chosen to make this effect small. The hysteresis is more visible in Figure D.3 which plots the same resistances versus current.

The hysteresis is convincingly visible in Figure D.4, which plots the difference between the two resistances versus current: $\Delta R(I) = R_{down}(I) - R_{up}(I)$ vs. I. The results for three fuses are shown; the similarities and differences are discussed in the following part of this appendix.

This hysteresis has its origin in the dynamics of the heating of the fuse and of its immediate environment. Initially, the fuse and its immediate environment and its external environment are at room temperature (about 22 °C). During current ramp up, the fuse increases its tem-

[1] The word is from the Greek *hysterē sis*: shortcoming, from *hysterein*: to be late, to fall short. It's present scientific use is to refer to a delay in the effect of a change in forces.

[2] The data shown in this appendix are for fuses made by Littelfuse. All were rated at 3 A. Some of these were flown in the Hubble Space Telescope, and recovered from it in December 1993: they were in Fuse Plug Serial Number 1012, and are identified by the pins numbers. Others were individual flight-grade fuses, identified by a serial number.

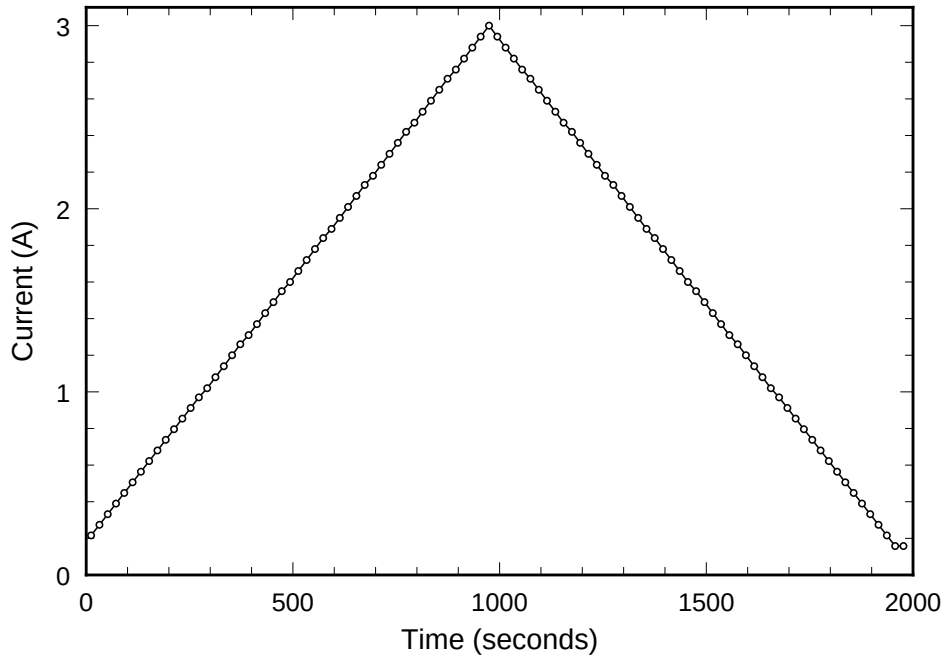

Figure D.1: The "ramp up/ramp down" current-history used for this appendix. This is a plot of the actual currents produced by our test apparatus.

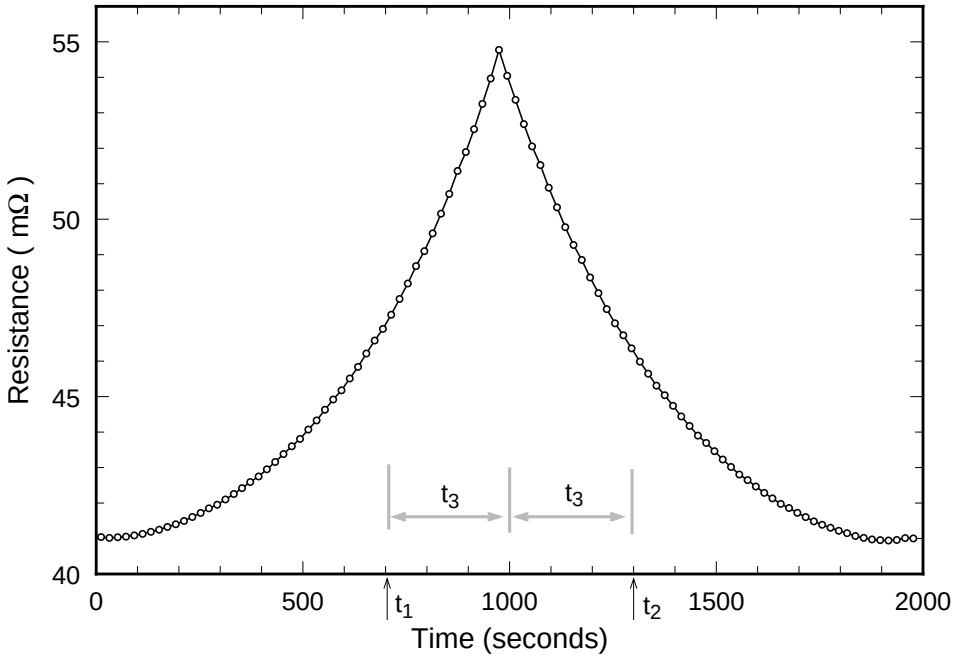

Figure D.2: The measured resistance for fuse SN1012 pins 57&58 for the "ramp up/ramp down" current-history used for this appendix. Typical instants t_1 and t_2 are marked, along with the corresponding duration $t_3 = \mathcal{T} - t_1 = t_2 - \mathcal{T}$, where $\mathcal{T} = 1000$ sec in this example.

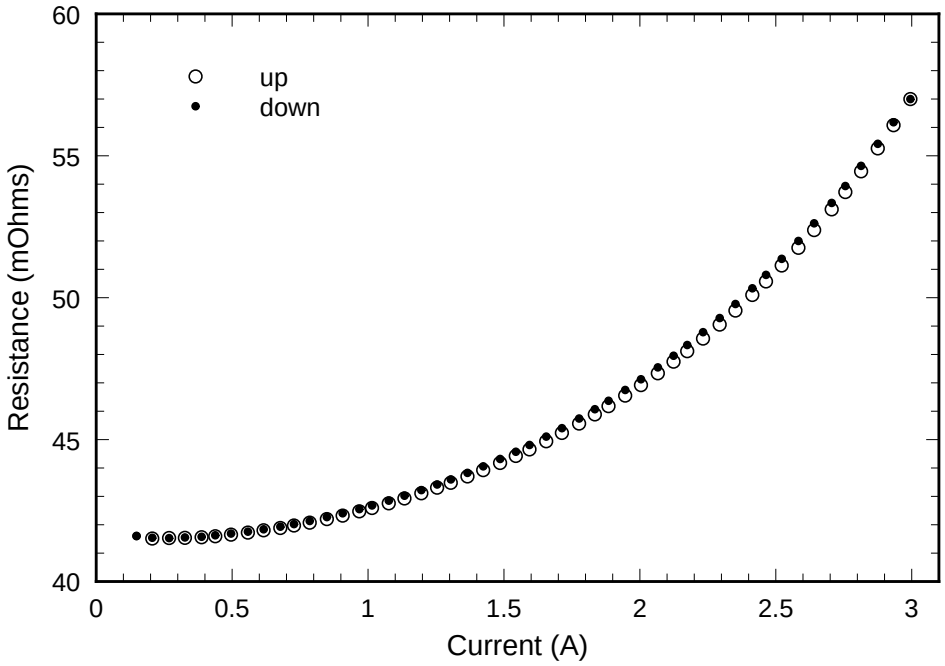

Figure D.3: The resistance versus current for a fuse rated at 3 A, for a "ramp up/ramp down" current-history. Hysteresis is visible to the discerning eye for currents in the range 1.5 A to 2.7 A.

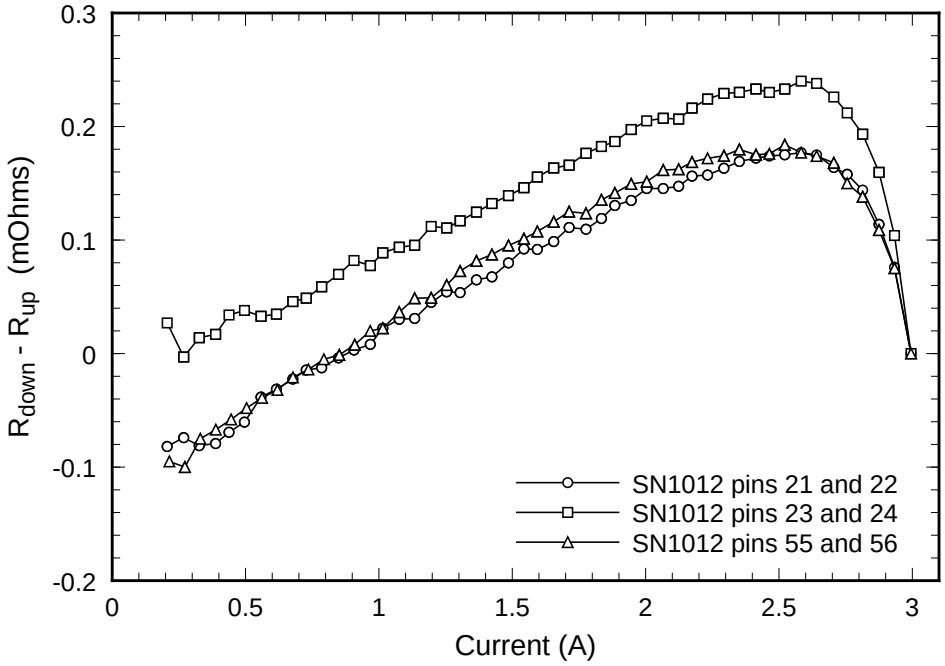

Figure D.4: The resistance-hysteresis of three fuses versus current. Fuses between pins 21 and 22, and between pins 55 and 56, have similar thermal environments, while the fuse between pins 23 and 24 has a different thermal environment.

perature, and then after some delay, increases the temperature of its immediate environment; we suppose that the temperature of the external environment is constant throughout this process. During current ramp down, this timing is reversed. Hence, the fuse is at a higher temperature during the descending part of the current sawtooth than during the ascending part, and this causes its resistance to be higher. Therefore, this increase in resistance is a measure of how the intermediate environment thermally couples the fuse to its external environment.

The purpose of this appendix is to develop a model that will allow the measured hysteresis to be quantitatively related to the heat sinking of the fuse. We find that we can measure the thermal resistance of the immediate environment of the fuse, and the relaxation time for thermal equilibration.

D.1 Dynamic model for the heat sinking of a fuse.

We are interested in making things "as simple as possible, but no simpler." So we must distinguish between the fuse and its environment, and model each, and we will chose the simplest model for each that captures the effect we are after.

D.1.1 Fuse model

We have modeled the fuse elsewhere, and learned that it reaches steady-state behavior in roughly 3 to 10 seconds when the temperature of its immediate environment, and the current passing through it, are held constant or change only very slowly on a time-scale of seconds. Hence we will simplify by supposing that neither the current nor the case/cap temperature change rapidly on this time-scale. For example, this is the case for the ramp up/ramp down current-history for $\mathcal{T} = 1000$ seconds (except within a few seconds of the turn-a-round at $t = \mathcal{T}$).

In steady-state, the temperature of the case and the caps are isothermal at a temperature T_{cap}. (We will not need to consider the temperature of the filament in this appendix; it can be much higher than T_{cap}, of course.) The resistance of the fuse depends both on the current I and the temperature T_{cap}. We have learned that this dependence is, to good approximation,

$$R(I, T_{cap}) = \left[\frac{T_{cap}}{T_0}\right] \cdot R(I, T_0) \tag{D.2}$$

where T_0 is a reference temperature chosen to be 300 K = 27 °C in this Report, and T is measured on an absolute scale. Hence, we can relate the resistance-hysteresis to the temperature hysteresis:

$$\Delta R(I) = R_{down}(I) - R_{up}(I) = \frac{R(I, T_0)}{T_0} \cdot [T_{cap,down}(I) - T_{cap,up}(I)] \tag{D.3}$$

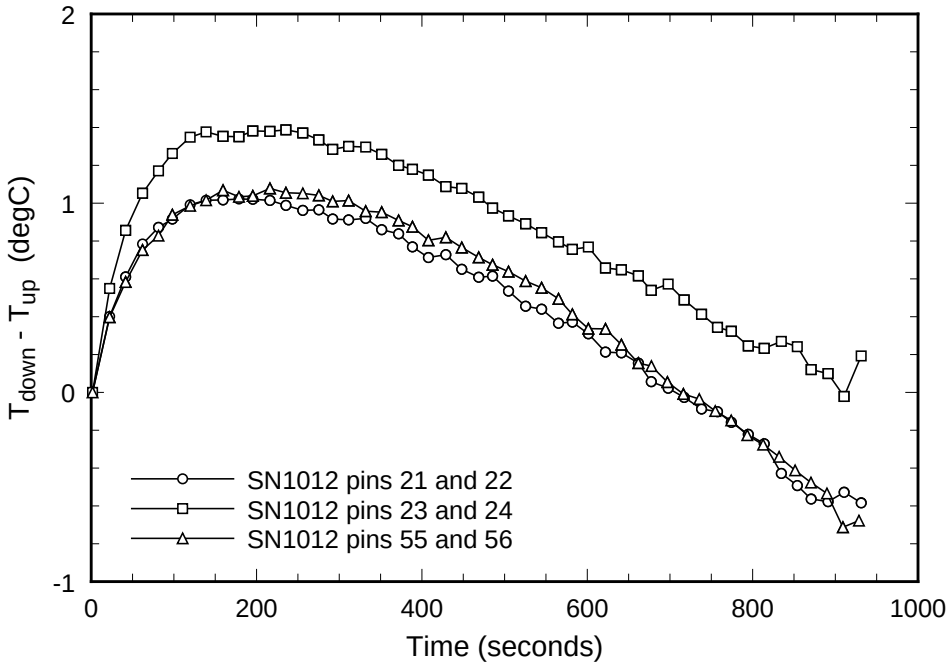

Figure D.5: The data of the previous figure plotted as a temperature hysteresis versus time.

or

$$\frac{\Delta R(I)}{R(I,T_0)} = \frac{\Delta T(I)}{T_0}. \tag{D.4}$$

where $\Delta T(I) = T_{cap,down}(I) - T_{cap,up}(I)$ is the temperature hysteresis. That is, the hysteresis in resistance is essentially the hysteresis in the fuse's temperature. This relation will be used to process the resistance-hysteresis data into temperature hysteresis data. For example, the data shown in Figure D.4 are replotted in this way as Figure D.5. Additionally, the abscissa-scale is changed from the current I to half the time-delay between the "up" and "down" measurements, to better indicate that the magnitude of this effect is a dynamic one and will change as the time delay between I_{up} and I_{dowm} changes. The ideas are these: (a) since the cause of the resistance-hysteresis is the temperature hysteresis, then we should exhibit ΔT rather than ΔR; and (b) since the time-scale is important in controlling the size of the hysteresis, then we should exhibit the time t_3 rather than the current I.

Sometimes we need the function $R(I,T_0)$ itself. Elsewhere, we have developed analytic forms for $R(I,T_0)$ accurate for fuses; for the purposes of this appendix, the form

$$R(I,T_0) = R_0 \frac{\tan(I/I_r)}{(I/I_r)} \tag{D.5}$$

a useful approximation. When there is no air inside the fuse barrel, then $I_r = 2\sqrt{\mathcal{L}}\,T_0/R_0$, where $\mathcal{L}$ is the Lorenz number ($\approx 2.45 \times 10^{-8}$ (V/K)^2), and R_0 is the cold resistance of the fuse at T_0. When there is air, then I_r is about 8% larger for a fuse rated at 3 A.

We now focus on computing the time-dependence of the temperature of the case of the fuse,

T_{cap}. The power dissipated within the fuse causes it to heat at a rate

$$\mathcal{C}\left(\frac{dT_{cap}}{dt}\right) = \left[\frac{T_{cap}}{T_0}\right] \cdot I^2 \cdot R(I, T_0) - \text{heat leak} \tag{D.6}$$

where $\mathcal{C}$ is the heat capacity of the fuse, and the "heat leak" measures how rapidly heat is conducted away from the fuse by its immediate environment. We must now address the modeling of the environment in order to specify this "heat leak."

D.1.2 Environment model

There is no such thing as a "standard environment." Rather, there are a variety, each behaving differently enough to require distinct treatments.

We will suppose that we can divide the whole environment into two parts: the immediate and the remote. And we will simplify by supposing that the remote environment has a constant temperature throughout the tests. (This means that we do not have to consider the dynamics of this part of the world, which is an important simplification.) Since this part of the world surrounds both the fuse and the immediate environment of the fuse, we could also call it the ambient environment,[3] and its constant temperature is the ambient temperature: T_{amb}.

We know of two sorts of immediate environments that each need distinct treatment:

- Suppose that the fuse is inserted into a PC board and soldered into place, with a gap between the fuse and the board. Or each lead of the fuse is attached to a terminal, which itself is connected to some other conductor. The common feature is that, when there is no air surrounding the fuse case, the only conduit for heat is through the fuse leads and then into the electrical conductors connected to these.

  Unfortunately, these arrangements differ greatly in the details of their thermal properties: we have met thermal resistances for PC board mounting and for post mounting that vary from a few tens to many hundreds of degrees celsius per watt as one moves from one fuse to the next — clearly, these arrangements have been made by people who have not attended to thermal issues!

  But the preferred practice for spacecraft-rated PC boards used for power-dissipating parts is that there be one or (preferably) more thick copper plates within the board which act as heat-sinks. Hence, in the spirit of simplicity, and as a description of such spacecraft-rated practices, we will suppose that each fuse lead is connected to a perfect heat sink which is always at a fixed temperature; that is, the fuse leads are the immediate environment and the perfect heat sink is the remote environment at T_{amb}. We will also suppose that the thermal mass of the leads is small compared with that of the fuse, so that the leads can be characterized entirely by their thermal resistance

[3] Webster's defines *ambient*: surrounding on all sides: encompassing.

$\mathcal{R}$: we do not need to consider the dynamics of heat flow along these leads (which would require attention to the thermal diffusion equation). We can closely approach this situation in the laboratory.

Hence, the "heat leak" is $\mathcal{R} \cdot (T_{cap} - T_{amb})$, and the dynamics of T_{cap} are controlled by

$$\mathcal{C} \left(\frac{dT_{cap}}{dt} \right) = \left[\frac{T_{cap}}{T_0} \right] \cdot I^2 \cdot R(I, T_0) - \mathcal{R} \cdot (T_{cap} - T_{amb}). \tag{D.7}$$

- Suppose the fuse is electrically connected as just described, and then is totally encapsulated in a potting material. Reasons for doing so include: increased thermal conductivity, increased resistance to shock and vibration, increased hermeticity, and increased resistance to environmental corrosion. For example, the Hubble Space Telescope fuses are assembled within tubes that are then filled with RTV-566 potting material.

  This presents a complex thermal environment: the leads have a much larger thermal conductivity than the potting material, and so they transport heat rapidly away from the fuse. But as the distance this heat is transported increases, then so too does the the surface of contact between the leads and the potting material, so that the leads then leak this heat into the potting material. And the potting material also transports heat away from the fuse: its relatively smaller thermal conductivity is compensated by its relatively larger area of contact. The bookkeeping requires attention to the full dynamics of the potting material and of the leads: that is, one must solve the full coupled thermal diffusion equations.

  There is a crude simplification: we can suppose that the leads thermally entrain a certain volume of potting material, and that this whole mass — fuse, leads, and entrained potting material — is roughly isothermal (i. e., heat transport throughout it is rapid), and is characterized by a (rather larger) heat capacity $\mathcal{C}'$. This mass is then connected to the remote environment through the remaining wires and potting material, which present only a thermal resistance $\mathcal{R}'$ between the mass and the remote environment. The form of the equation controlling the dynamics of T_{cap} is then identical in form with the first case.

  This crude simplification will be made in this appendix. We shall see some of its strengths and weaknesses when we consider its agreement with the data on the HST fuses in the later part of this appendix. Perhaps a less crude model can be developed for this important case, at some other time.

D.1.3 Solution of the dynamical equation

Our simplifications give the equation for the dynamics of the temperature of the fuse:

$$\frac{dT_{cap}}{dt} = -\frac{T_{cap}}{\tau} + \frac{T_{amb}}{\tau} + \left[\frac{T_{cap}}{T_0} \right] \frac{\mathcal{R} I^2 R(I, T_0)}{\tau} \tag{D.8}$$

where $\tau = \mathcal{R}\mathcal{C}$ is a time constant.

Digression on the solution of the first-order linear ordinary differential equation: Suppose we have the equation

$$\frac{dy}{dt} = -\phi(t) \cdot y + \psi(t) \tag{D.9}$$

and we have the initial condition $y(0)$, and $\phi(t)$ and $\psi(t)$ are known functions of t only. Then

$$y(t) = \exp(-\int_0^t \phi(t')\,dt') \cdot \left[y(0) + \int_0^t \exp(\int_0^{t'} \phi(t'')\,dt'') \cdot \psi(t')\,dt' \right] \tag{D.10}$$

End of digression.

We can use this solution by introducing iteration: we define $T_{cap}^{(0)} = T_{amb}$ and use this in the right-most term of Equation D.8, converting it into an equation of the same form as Equation D.9, so that the solution Equation D.10 applies: call the result $T_{cap}^{(1)}$. Increasingly better results can be obtained by repeating this process.

We note that fuses rated at 7 A and below are supposed to be fixtured such that their temperature rise is no more than 70 °C even when driven at full rated current. Hence $T_{cap}/T_0 < 70\ ^\circ\text{C}/300\ ^\circ\text{C} = 0.23$, and so even the relatively crude substitution of T_{amb} for T_{cap} should introduce no more than a 23% error into just the one term in the equation, and so we can expect that even $T^{(1)}(t)$ should have useful accuracy. In practice, we usually find much smaller temperature rises, and correspondingly more accurate $T^{(1)}(t)$.

We find for the first step:

$$\phi(t) = 1/\tau \tag{D.11}$$

$$\psi^{(1)}(t) = \frac{T_{amb}}{\tau} + \left[\frac{T_{amb}}{T_0}\right] \frac{\mathcal{R} I^2 R(I, T_0)}{\tau} \tag{D.12}$$

$$T_{cap}^{(1)}(t) = T_{amb} + \left[\frac{T_{amb}}{T_0}\right] \frac{\mathcal{R}}{\tau} \exp(-t/\tau) \int_0^t \exp(t'/\tau)[I(t')]^2 R(I(t'), T_0)\,dt' \tag{D.13}$$

Using the ramp up/ramp down current-history $I(t)$ given in the Introduction and a fairly accurate form for $R(I, T_0)$, the integration can be carried out analytically in closed form; however, the result is several pages long. While too long to usefully display, it is straightforward to use with computer programs such as *Mathematica* and `Maple`, and this has allowed the plots shown in this appendix to be produced.

The essential character of the answer is already contained when $R(I, T_0) = R_0$ is used. This simplified result is short enough to be worth displaying:

$$\begin{aligned} \Delta T^{(1)}(t_3) &= T^{(1)}(t_2) - T^{(1)}(t_1) \\ &= \mathcal{R} R_0 I_{max}^2 \frac{T_{amb}}{T_0} \frac{\tau}{\mathcal{T}} \left\{ 4 \left[1 - \frac{t_3}{\mathcal{T}} - e^{-t_3/\tau} \right] + 2 \frac{\tau}{\mathcal{T}} e^{-(\mathcal{T}-t_3)/\tau} \left[e^{(2t_3/\tau)} - 1 \right] \right\} \end{aligned} \tag{D.14}$$

where t_1 is the time while the current is increasing and t_2 is the time when the current is decreasing such that $I_{up} = I(t_1) = I(t_2) = I_{down}$, and $t_3 = \mathcal{T} - t_1 = \mathcal{T} + t_2$ is the time between the maximum current and the times t_1 and t_2. That is, $t_1 = \mathcal{T} - t_3$ and $t_2 = \mathcal{T} + t_3$.

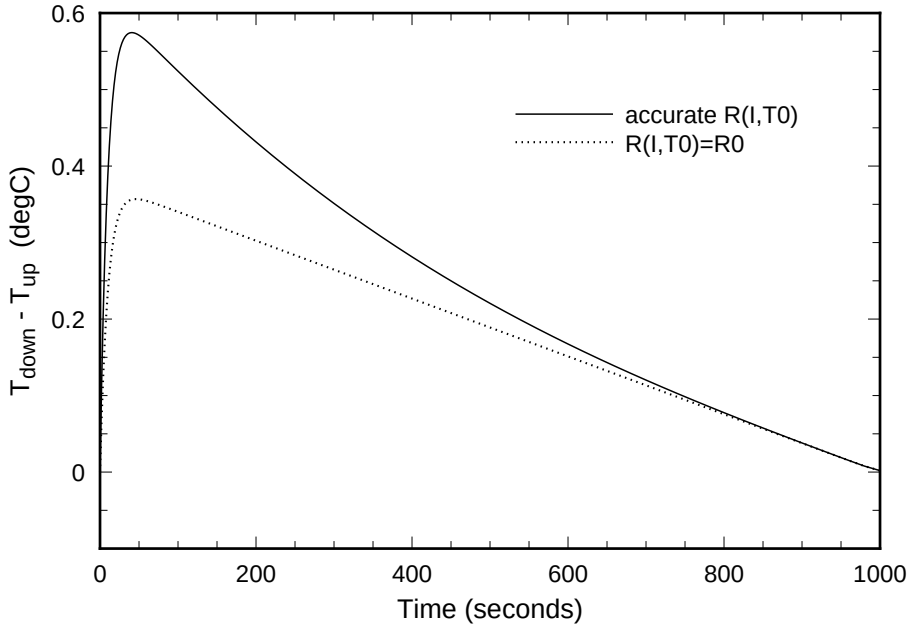

Figure D.6: The first-order approximation to the temperature hysteresis, computed from the model developed in this appendix. The heating of the fuse is ignored in the curve labeled "$R(I, T_0) = R_0$," and described to good accuracy in the curve labeled "accurate $R(I, T_0)$." The thermal relaxation time is $\tau = 10$ seconds and the thermal resistance is $\mathcal{R} = 30$ °C/watt.

These first-order approximations to the temperature hysteresis, both with $R(I, T_0) = R_0$ and with $R(I, T_0)$ as per Equation D.5, are shown in Figure D.6.

Inspection of Figure D.6 shows that using $R(I, T_0) = R_0$, which ignores the heating of the fuse in the source-term of the differential equation, still captures the character of the hysteresis; the main error is that the heating is too small. The effect of using the more accurate $R(I, T_0)$ gives greater hysteresis at the shorter times, which is easy to understand: most of the heating is produced by the I^2-term working on the "cold resistance" R_0. The correct resistance $R(I)$ is greater throughout most of the current-history, but not much greater. **Temperature hysteresis essentially results from the joule power I^2R heating a thermal mass (characterized by $\mathcal{C}$) while a thermal resistance $\mathcal{R}$ drains the heat**.

We can use this observation to estimate that the second iteration, giving $T^{(2)}(t)$, would also show the same character, and would be, in fact, only a little greater than the first iteration, $T^{(1)}(t)$. We will not carry out the second iteration at this time.

The result for the first iteration can be fit to data obtained on potted HST fuses: see Figure D.7. One $(\tau, \mathcal{R})$-pair fits the data better for short times ($t < 100$ sec) and the other pair fits the data better for longer times ($t > 300$ sec). Since this data set is not quite described by a single choice of $(\tau, \mathcal{R})$, then this model is not quite apt for this fuse; rather, this potted fuse requires a more complicated model with (at least) two relaxation times. However, the difference between the $(\tau, \mathcal{R})$-pairs is not enormous, and so the model allows a

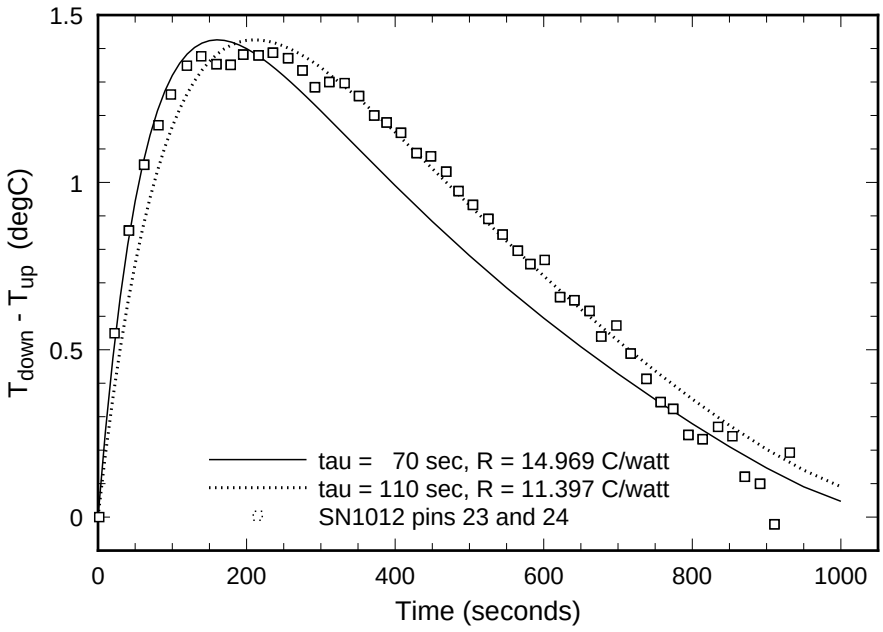

Figure D.7: The first-order approximation to the temperature hysteresis, computed from the model developed in this appendix, for two choices of τ and $\mathcal{R}$, and an observed temperature hysteresis curve. Notice that the temperature difference has not vanished even at 1000 seconds.

useful beginning to the understanding of the immediate thermal environment of this potted fuse: its thermal resistance to thermal ground $\mathcal{R}$ is about 11 to 15 °C/watt and it's thermal relaxation time τ is in the range from 70 to 110 seconds. We can use this to estimate the actual rise in the temperature of the fuse when the full 3 A was applied: temperature rise $= \mathcal{R}\, I^2 R_{hot} \approx 13$ °C/watt $\cdot\, 9\text{A}^2 \cdot 0.055\text{m}\Omega = 6$ °C. Hence, the error of the first iteration, replacing T_{cap} with T_{amb}, is about 6 °C/300 °C = 2% in one term of the full equation, and further iterations are not necessary for this case.

We can analyze these values to learn a little more about the role played by the potting. These pairs imply that the heat capacity $\mathcal{C} = \tau/\mathcal{R}$ is in the range 5 to 10 joules/°C. However, the heat capacity of the fuse is roughly 0.05 joules/°C, about 100 to 200 times smaller — clearly, considerable additional mass is thermally engaged. This is too much extra mass for leads alone: most of the extra mass must be the potting material. The specific heat of the potting material (RTV–566) is 1.46 joules/(gm°C), and so roughly 3.4 to 6.6 grams of potting material are involved. Since the density of the potting material is 1.51 gm/cc, then the involved mass occupies a volume of between 2.3 and 4.4 cc,. A sphere[4] of this volume has a radius of 0.8 to 1.0 cm, which is about twice the length of the fuse. Since the thermal diffusivity of the potting material is 0.0014 cm^2/sec, then the time for a thermal pulse to traverse this distance is roughly radius^2/diffusivity $\approx$ 450 to 700 seconds — this is much

[4]The shape of the thermal pulse launched by the fuse tends to become spherical with time, and so a sphere is appropriate for this semi-quantitative discussion. Also, substantial changes in the shape of a boundary, at constant enclosed mass, make distinctly small changes in thermal times: the argument in the text is not sensitive to the assumed spherical shape.

longer than the relaxation times and so there must be some other transport mechanism. The copper leads have a thermal diffusivity of about 1 cm^2/sec, and hence a thermal pulse can travel along them a distance on the order of 8 to 10 cm during the τ-times used for the fit; hence, it is probably the fuse leads that thermally entrain enough potting material to give the observed heat capacity. Hence, analysis shows that the two-component model (using just $\mathcal{C}$ and $\mathcal{R}$) is indeed simplistic for the potted fuses: we should treat the leads and the potting material as coupled thermal transmission lines rather than ignore their dynamics and pretend to characterize them with only a thermal resistance $\mathcal{R}$ (which is fundamentally a steady-state concept).

The other two HST fuses

We notice several things when we examining the ΔT curves of the other three fuses shown in Figure D.5.

- While the temperature hysteresis vanishes for times approaching 1000 seconds for the fuse between pins 23 and 24, it does not vanish for the other two fuses; rather, it tends to about -0.8 °C. I suspect that this is caused by a drift in the ambient temperature, T_{amb}, by these amounts over the 2000 second duration of the current-history (1000 seconds for the ramp up, and another 1000 seconds for the ramp down). If so, the drift could be removed by subtracting a term of the form αt_3 from the curves, with α adjusted so that ΔT is about 0.1 °C at $t_3 = 1000$ seconds.
- The observed ΔT for small values of t_3 for the HST fuses are not affected by changes in ambient temperature, since the low thermal diffusivity of the potting material insulates the fuses from such changes for hundreds of seconds. Hence, the observed differences in the maximum values of ΔT, and the time at which this maximum occurs, are probably real, and can be interpreted as actual differences in the thermal environment of these individual fuses.

Other data

We have collected these kind of data on a set of 3 A fuses of flight quality that were mounted by clamping each lead to a massive brass block: each lead length was about 1.0 cm, and only air (no potting material) surrounded each fuse. A thermocouple (3 mil wires) was attached with a small blob of thermal epoxy to the middle of the fuse case. Direct measurement of the thermal resistance gave 90 °C/watt; calculation gave the same value, both with uncertainties of about 15%. The temperature hysteresis is shown in Figure D.8. The agreement is satisfactory for τ in the range of 20 to 25 seconds, and for $\mathcal{R} = 90$ °C/watt. Hence, the heat capacity is 0.22 to 0.28 joules/(gm·°C), which is about 5 times the value for the fuse without its leads. Adding the mass of the leads and of the epoxy bead gives about the observed value.

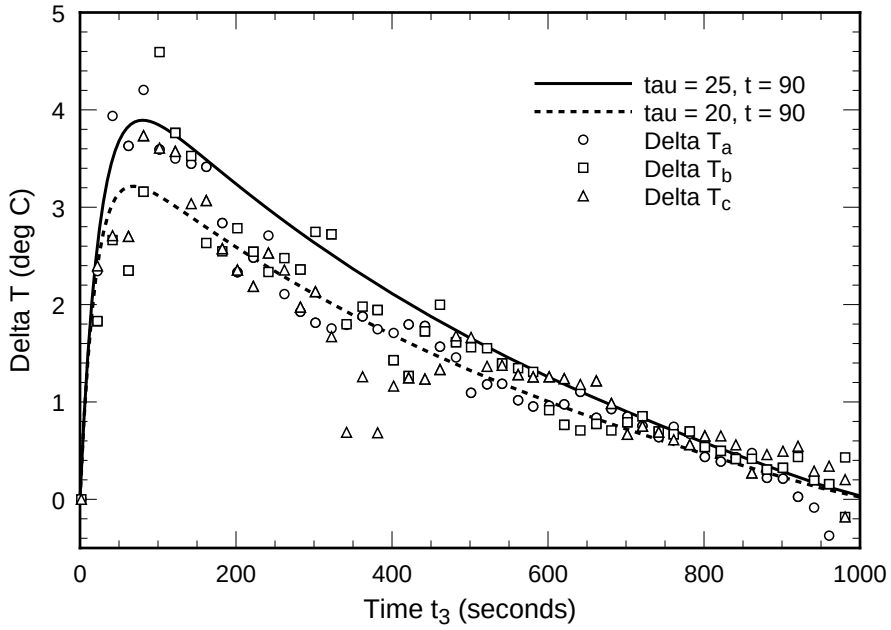

Figure D.8: The observed temperature hysteresis curves for three fuses, each mounted using 1.0-cm leads clamped directly to massive heat sinks. Also shown is the first-order approximation to the temperature hysteresis, computed from the model developed in this appendix, for two choices of τ and $\mathcal{R} = 90\ ^\circ\mathrm{C}/\mathrm{watt}$.

Appendix E

Oxidation of the filament

Oxidation transforms electrically conducting metal into electrically nonconducting metal oxide: this increases the current density through the remaining conducting metal and leads to increased heating, which accelerates the rate of oxidation (other things being equal): this can lead to a runaway acceleration that results in interruption. Thus, a current that initially produces a mid-filament temperature that is safely below melting, but high enough for an appreciable oxidation rate, can degrade a fuse. This is an important process for filaments made of copper and of copper-silver alloy, and a possible process for nickel filaments. The purpose of this Appendix is to sketch a model for this process, to compare this model with experiments, and to estimate when this process is important.

I will begin by supposing the filament is pure copper. Then oxidation of the copper-silver alloy will be described. Finally, a sketch is given of the effect of oxidation on the resistance of a fuse.

E.1 Oxidation of copper

We must consider both the equilibrium situation characterized by an equilibrium constant, and the dynamic situation characterized by an oxidation rate.

E.1.1 Equilibrium situation

Copper has many oxides; only two are important for present purposes: "black" or cupric oxide (CuO), and "red" or cuprous oxide (Cu_2O). Selected properties are listed in Table E.1.

The free energy of formation of each oxide from its elements is reported by the CRC Handbook (38th edition; pp 1716 and following, [14]) in the form

$$\Delta F^0 = \Delta H^0 + A \cdot T \cdot \log_{10}(T) + (B \times 10^{-3}) \cdot T^2 + (C \times 10^5)/T + D \cdot T\,, \qquad \text{(E.1)}$$

where T is measured in degrees Kelvin, and ΔF^0 is in calories per mole; the constants given in [14] are listed in Table E.2 and some values are given in Table E.3. The numerical values are for the formula given in the listing.

Application of standard thermodynamics shows that the pressure of oxygen gas (O_2) in an enclosed vessel containing metallic copper and one of the oxides in equilibrium at a temperature T is

$$p_{O_2}(T) = \exp(\frac{2\Delta F^0}{\mathbf{R}T}) \text{ atmospheres}, \tag{E.2}$$

where ΔF^0 is the free energy of formation of the oxide, and the reaction formula is that given in Table E.2. This is used to compute the oxygen pressures shown in Table E.3. Inspection of this Table shows that gaseous oxygen in the fuse cavity will combine with copper in the fuse filament until the pressure of the gaseous oxygen drops to a small fraction of an atmosphere, and that the formation of cuprous oxide (red Cu_2O) is favored over cupric oxide (black CuO) in equilibrium. If the temperature is fixed at a value T' and the the pressure of oxygen gas is forced to be lower than $p_{O_2}(T')$ for one of the oxides, then that oxide will dissociate: hence p_{O_2} is also called the dissociation pressure.

The free energy of formation for cuprous oxide, and the pressure of oxygen gas over copper and cuprous oxide, are plotted from 0 °C to 1000 °C in Figure 14-4 on page 349 of *Physical Chemistry of Metals* by L. Darken and R. Gurry ([16]). They write the reaction for formation of cuprous oxide as "4 Cu + O_2 = 2 Cu_2O," and so their values for the free energy of formation, $\Delta F^{0\prime}$, are double those of the CRC Handbook ([14]) since they apply to twice as many molecules; hence, the recipe for the pressure of oxygen gas is $p_{O_2} = \exp[\Delta F^{0\prime}/(\mathbf{R}T)]$. Indeed, their values for $\Delta F^{0\prime}$ are twice those in Table E.3, and are identical for the pressure of oxygen gas.

Tables of the dissociation pressure of CuO and of Cu_2O are also given on page 622 of *The Corrosion Handbook* edited by H. Uhlig ([17]). There is modest agreement between the dissociation pressure of Cu_2O given by Uhlig and that listed in Table E.3, but there is a difference of about three orders of magnitude for CuO. (This thousand-fold difference can be sharply reduced if we assume that one of the Tables has confused "atmosphere" and "torr"; then, there is the same modest agreement as for Cu_2O.) Uhlig reports (page 622) that "Above 1025 °C in the atmosphere, CuO does not appear in the oxide scale on copper." Since the partial pressure of oxygen gas in a normal atmosphere is 20% of 760 torr, or 152 torr, this is the statement that the dissociation pressure of CuO is 152 torr at 1025 °C, and this agrees precisely with the table given by Uhlig for CuO. The situation is confusing: additional information will be necessary to resolve this conflict.

The number of moles of available oxygen, and film thickness limits

The fuse cavity has a volume $V_{fuse} = \pi b^2 \ell = 1.74 \times 10^{-3}$ cc, where $b = 0.034$ cm is the inside radius of the barrel and $\ell = 0.48$ cm is its length. (The volume occupied by the filament is never more than a few percent of this, and so I will ignore the volume displaced by it.)

The end caps are sealed at a temperature of roughly 200 °C, and an ambient pressure of 1 atmosphere: I will suppose that this seal is effective enough to trap the air. A mole of gas occupies 22,400 cc at a pressure of 1 atmosphere and a temperature of 0 °C. And oxygen constitutes about 20% of normal air. Hence, the number of moles of oxygen (O_2) sealed within the fuse when it is capped off is:

$$\mathcal{N} = 0.20 \cdot 1.74 \times 10^{-3} \text{ cc} \cdot \frac{273 \text{ K}}{(273+200) \text{ K}} \cdot \frac{\text{mole}}{22400 \text{ cc}} = 9.0 \times 10^{-9} \text{ moles} .$$

Twice this many moles of red oxide (Cu_2O) will form, and will have a volume of

$$\mathcal{V}_{Cu_2O} = 2\mathcal{N} \cdot \frac{\text{molecular weight}}{\text{density}} = 2 \cdot 9.0 \times 10^{-9} \text{ moles} \cdot \frac{143.08 \text{ gm/mole}}{6.0 \text{ gm/cc}} = 4.3 \times 10^{-7} \text{ cc} .$$

As we shall see later in this Appendix, the oxide does not form with uniform thickness along the filament; rather, it forms fastest where the filament is hottest. For our present purposes, we will suppose that only the central millimeter (ℓ') of the 4.8 mm long filament captures essentially all the film. Then the limiting thickness of the oxide film on a filament of radius $a = 35 \times 10^{-4}$ cm (3 A rated fuse) is

$$h_{limit} = \frac{\mathcal{V}}{2\pi a \ell'} = \frac{4.3 \times 10^{-7} \text{ cc}}{2\pi \cdot 35 \times 10^{-4} \text{ cm} \cdot 0.1 \text{ cm}} = 2.0 \times 10^{-4} \text{ cm} = 2.0 \ \mu\text{m}.$$

We shall see later in this Appendix that such thicknesses are in fact observed. And this computation shows that there is not sufficient oxygen present to allow the formation of substantially thicker films on the filament of an FM08 style fuse rated at 3 A.

Also of interest is the ratio of this limiting thickness to the total radius of the filament, since that measures the effect of the oxide film on the performance of the filament:

$$\frac{h_{limit}}{a} = \frac{\mathcal{V}}{2\pi a^2 \ell'} = 0.057 \cdot \left(\frac{1 \text{ mm}}{\ell'}\right) \cdot \left(\frac{35\mu\text{m}}{a}\right)^2 .$$

Hence this ratio increases from 5.7% for a fuse rated at 3 A ($a = 35$ μm) to 36% for a fuse rated at 3/4 A ($a = 14$ μm). That is, the increase is substantial for fuses of lower ratings.

If the filament is strongly heated, then the effective length ℓ' of the oxide-forming part of the filament is relatively shorter than when it is weakly heated: stronger heating allows a thicker oxide to form over a shorter length, before the oxygen is exhausted. This effect is included in the previous estimate, and may be important in practice.

Can a fuse's filament act as its own getter?

Suppose a fuse is operated at a current low enough so that oxide forms over a large part of the fuse's filament, but large enough so that all the oxygen reacts in a practical time. Then, after all the oxygen has reacted into oxide, the fuse may be immune to further oxidation when driven at higher currents. If this can happen, then probably it does happen in practice, leading to the occasional encounter of a fuse with substantially greater staying power.

Choice of fuse element material

Fuses rated at 5 A and above use copper filaments; fuses rated between 3/4 A to 4 A use copper-silver alloy filaments; and fuses rated at 1/2 A and below use nickel filaments. Presumably, the manufactures found that the oxidation of a filament of pure copper becomes too damaging in practice when the filament's radius decreases to values appropriate for 4 A and below, and hence switched from pure copper to copper-silver alloy (which does not oxidize as much). And even copper-silver alloy oxidizes too much when the filament radius drops to values appropriate for 1/2 A and below, and so nickel (which is particularly resistant to oxidation) is used.

This begs the question as to why nickel is not used for all ratings, or why copper-silver is not used for fuses rated at 5 A (and above) as well as for ratings between 3/4 A and 4 A.

Leaky fuses

If the fuse's seal is not perfect, then air will be expelled when the fuse filament heats, and fresh air (i. e., air containing 20% oxygen) will be captured when the filament cools. Hence, the growth of this oxide layer can continue indefinitely in operations that involve repeated heating and cooling.

But if the fuse is always maintained at precisely the same hot temperature, then the only way for oxygen to enter is by diffusion through the (presumably small) hole and this is (presumably) a slow process — the oxide layer will grow slowly.

Hence, a set of leaky fuses would be expected to show a considerable spread in behaviors after being used in these different ways.

If the fuse is used in a vacuum and leaks its air away, then in principle, the oxide film will decompose into metallic copper and gaseous oxygen when the pressure of the oxygen gas drops below the value shown in Table E.3. However, in practice, the pressure of oxygen in close Earth-orbit is above the dissociation pressure for a filament operated at the de-rated currents used (the filament temperature is below 150 °C), so the oxide film would remain; however, it's thickness would not increase. (This conclusion supposes that the values for p_{O_2} for $T < 200$ °C are not too low by more than roughly half a dozen orders of magnitude.)

E.1.2 Relative amounts of red and black oxide

We have considered the relative thermodynamic phase stability of CuO and Cu_2O when a specimen of copper is in thermal equilibrium with oxygen gas and with the oxides: for practical temperatures and pressures, there is no black CuO; rather, all the oxide is red Cu_2O. However, black CuO is sometimes seen in dynamic situations: this is a rate effect, and will now be discussed.

Consider a specimen of pure copper exposed to air when both are in thermal equilibrium at a temperature T: the copper grows a film of copper oxides. Growth is by dissociation of copper into ions at the metal-oxides interface, and diffusion of these ions through the film of oxides, followed by reaction with oxygen gas at the oxides-air interface. Oxygen ions also diffuse into the oxides layer, but this process is slower and does not contribute in an important way.

As the oxides layer thickens with time by new copper ions arriving at the oxides-gas interface, these newly arrived copper ions first form CuO. As this CuO is buried beneath the outwardly growing oxide film, the buried CuO converts into Cu_2O. Thus, the oxides film is Cu_2O from the metal substrate out to almost its outer surface, and there is a superficial coating of CuO. The relative thickness of the CuO coating is thicker at high rates of formation. Thus, low temperatures and low oxygen pressure favor a relatively thin skin of black CuO on top of the layer of red Cu_2O: this black oxide layer may be so thin as to be invisible to ordinary inspection. But high temperatures (below 1025 °C) and high oxygen pressure favor a relatively thick skin of black CuO on top of a layer of red Cu_2: this black layer is often visible as a soot deposit. Heating above 1025 °C forms only red Cu_2O.

A Cu-Ag filament forms copper oxides predominantly as the silver does not play a noticeable role. Visual inspection of filaments that have carried sufficient current to be heated but not interrupted, show a sooty-black superficial layer at their mid-region, a redish transparent layer (with optical interference fringes) from the sooty-black region to near the caps, and a "polished copper" appearance near the caps. Auger scans (see page 163 for example) show that the redish transparent layer is indeed red Cu_2O.

A Cu-Ag filament that was run at rated current in open air, however, became covered with material with a sooty appearance almost to the caps. This illustrates that filaments operated within the fuse's barrel are noticeably starved for oxygen relative to a filament operated in open air.

Since most of the oxide that forms in fuses with Cu-Ag filaments is the red Cu_2O, only this oxide will be considered further.

It has been claimed that Cu_2O is actually not an equilibrium structure at temperatures below 375 °C and therefore decomposes very slowly at room temperatures into metallic copper and cupric oxide.[1] This is not consistent with the values shown in Table E.3 or in Uhlig's table, but perhaps these values are wrong at low temperatures.

E.1.3 Dynamic situation

When copper is exposed to oxygen gas or air under conditions appropriate for understanding fuse filaments, a film of Cu_2O forms. After the thickness becomes greater than a few molecu-

[1] See page 875 of the chapter "Copper Oxides" in *Handbook of Optical Constants of Solids, II* edited by E. Palik. Academic Press. 1991.

lar layers, the thickness then increases parabolically with the time t at constant temperature T:

$$h(t,T) = \sqrt{g(T)\,t}, \tag{E.3}$$

where $g = g(T)$ is the growth constant. One way of following this growth is to periodically weigh an oxidizing specimen: if the weight increase caused by the oxygen alone is $w(t)$, then we have

$$\begin{aligned} w &= (hA)\cdot\left[\frac{\text{No. moles of } Cu_2O}{\text{cc}}\cdot\frac{\text{Atomic Mass of Oxygen}}{\text{mole of } Cu_2O}\right] && \text{(E.4)}\\ &= (hA)\cdot[(0.0419 \text{ moles/cc})(16.0 \text{ gms/mole of } Cu_2O)] && \text{(E.5)}\\ &= (hA)\cdot(0.671 \text{ gms/cc})\,, && \text{(E.6)} \end{aligned}$$

and this means that the relation of the thickness of the film to the weight increase per area is:

$$h = (1.490 \text{ cc/gm})\cdot w/A\,, \tag{E.7}$$

which can be used to convert the growth constant reported in units of "$\text{gm}^2\cdot\text{cm}^{-4}\cdot\text{hr}^{-1}$" to its value in units of "$\text{cm}^2\cdot\text{hr}^{-1}$." This conversion factor is much less than the density of the oxide, 6.0 gm/cc, since the latter includes the mass of the copper ions too.

Figure E.1 (based on a figure on page 383 of [18]) displays the weight gain versus time for pure copper. It illustrates the rule that $w/A = \sqrt{g\,t}$ over an interval of five hours, and that $g = 30$ $(\text{mg}\cdot\text{cm}^{-2})^2\cdot\text{hour}^{-1}$ for a temperature of 800 °C. It also exhibits a table illustrating the effect of adding certain other elements to the copper: in particular, the effect of adding even 2% beryllium is dramatic — the oxidation rate is reduced by a factor of 100.

Table E.4 (based on Table A.25 of [19], page 196) lists the rate of oxidation of copper in oxygen at various temperatures. The value of g from Figure E.1 implies that the oxidation after one hour at 800 °C will amount to $\sqrt{30}$ $\text{mg}\cdot\text{cm}^{-2} = 5.48$ $\text{mg}\cdot\text{cm}^{-2}$, while the corresponding value in Table E.4 gives $\sqrt{3.14\times10^{-5}}$ $\text{gm}\cdot\text{cm}^{-2} = 5.60$ $\text{mg}\cdot\text{cm}^{-2}$, which is 2% higher: clearly, these are in good agreement.

Uhlig states that there "are significant differences among the oxidation rates found by various investigators, but the values reported by N. B. Pilling and R. E. Bedworth[2] appear to be most widely accepted." Uhlig also mentions that the rate is variable below 800 °C caused by spalling of the oxide.

Figure E.2 is a plot of the data in Table E.4; also included are the data of Pilling and Bedworth as referenced by Uhlig: there is satisfactory agreement. The value of $g(700\ ^\circ\text{C})$ given in Table A.25 is shown as a square; my value is shown as a circle: clearly, the value in Table A.25 is a misprint.

The growth constant is roughly Arrhenius: $g(T) = g_0\exp[-E^\star/(\mathbf{R}T)] = g_0\exp(-T_g/T)$ where T is the temperature measured on an absolute scale and $\mathbf{R}$ is the gas constant, and where g_0 and $T_g = E^\star/\mathbf{R}$ are characteristic of the reaction; $E^\star$ is called the activation energy,

[2]Uhlig gives the reference as *Trans. Am. Inst. Mining Met. Engrs.*, **143**, 246–267 (1941).

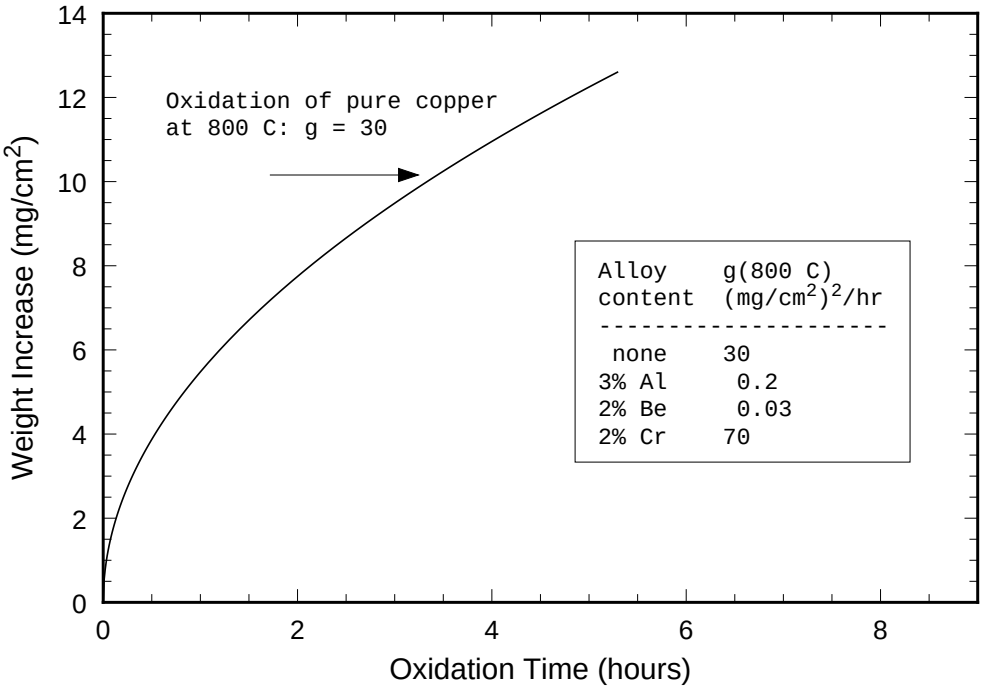

Figure E.1: Experimental data on the oxidation rate of copper. The data are from [16].

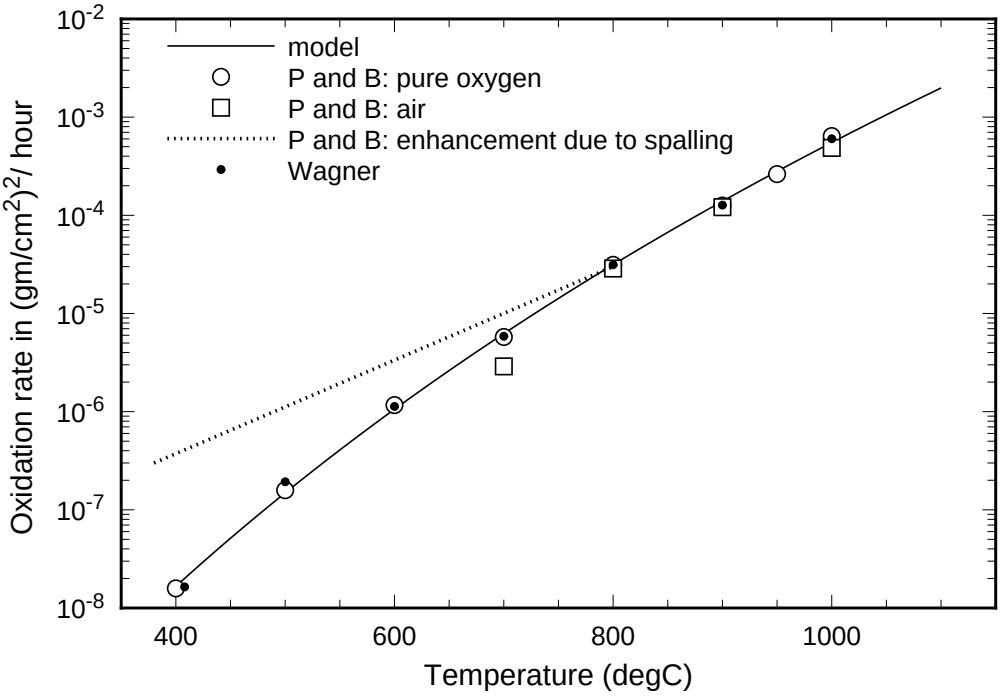

Figure E.2: Selected measured oxidation rates versus temperature. The references for the data labeled "P and B" (Pilling and Bedworth) and for "Wagner" are given in the text. The curve labeled "model" is for the empirical function discussed in the text.

and T_g is the activation temperature. However, careful examination of the data shows that the activation energy $E^\star$ has a definite temperature dependence and that this dependence increases with temperature. Using the definition $T_g(T) = E^\star/\mathbf{R} = d\ln(g)/d(1/T)$, I compute the results shown in Table E.4.

Figure E.2 shows the empirical curve $g = \exp(-13.30 + 1765\ \mathrm{K}/T - 18.268\ln(1000\ \mathrm{K}/T))$, with T in degrees Kelvin; this is as good a fit to the data as is appropriate, given the scatter among the several data sets. This empirical curve has been chosen so that the activation energy is linear with T: $T^\star = (18.268/\mathrm{K}) \cdot T - 1765\ \mathrm{K}$; this is the simplest function that allows a fit to the data, and it is also adequate.

It has been suggested that Cu_2O is not an equilibrium structure below 375 °C: perhaps the properties of a film of Cu_2O change near this temperature. In this connection, it seems curious that the lowest temperature in Table E.4 is 408 °C, and not for example 400 °C.

The underlying reaction is as follows. Ions of copper detach at the metal-oxide interface and diffuse through the film to the oxide-oxygen interface where they combine with oxygen, while oxygen atoms and electrons diffuse through the oxide film to the metal-oxide interface. The growth rate of the oxide film is dominated by the diffusion rate of copper ions through the copper oxide film, and it is also limited by the increasing thickness of the film; hence,

$$\frac{dh}{dt} = \frac{1}{2}\frac{g(T)}{h}. \tag{E.8}$$

This has the solution, when T is a function of time,

$$h(t) = \sqrt{\int_0^t g(T(t'))\,dt'}\,. \tag{E.9}$$

When the temperature is constant, the the earlier result is obtained: $h(t) = \sqrt{g(T)\,t}$.

Effect of gas pressure: Uhlig quotes the results of Pilling and Bedworth: there is little difference between the oxidation rates of copper in air and in pure oxygen, at normal pressures; and the oxidation rate at 800 °C suddenly begins to decrease rapidly with oxygen pressure for pressures below 0.3 torr.

The dissociation pressure of CuO at 800 °C that is extrapolated from Uhlig's table of values is between 2 and 3 torr; on this basis, CuO would not form when the oxygen pressure falls below 2 to 3 torr, and this might affect the rate of formation of Cu_2O.

E.1.4 Spalling of the oxide layer

The ratio of the volume of a metal oxide (Me_aO_b) to the volume of the metal (Me) that formed that oxide is called the *Pilling-Bedworth* ratio:

$$\mathcal{R}_{PB} = \frac{\text{volume of oxide}}{\text{volume of metal}} = \frac{M\,d}{a\,m\,D}\,, \tag{E.10}$$

where M is the molecular weight of the oxide and D is its density, and m is the atomic weight of the metal and d is its density, and a and b are the stoichiometric coefficients of the oxide Me_aO_b. We have for Cu_2O: $M = 143.08$ gms/mole; $D = 6.0$ gms/cc; $m = 63.55$ gms/mole; $d = 8.92$ gms/cc; $a = 2$; and $b = 1$; hence, $\mathcal{R}_{PB} = 1.67$. This corresponds to observation: the oxide is dense and nonporous, and "protective." In particular, this corresponds to a parabolic growth law.

However, this ratio is large enough so that there are considerable compressive stresses in the film. As the film thickness increases, the stress accumulates until a part of the film heaves and cracks off, a process called "spalling," and this exposes fresh metal, which then oxides relatively rapidly. As mentioned previously, Uhlig states that the variability of the observed oxidation rate of copper is variable below 800 °C caused by spalling. We have directly observed spalling along copper-silver alloy filaments: see for example Figure E.10. Models for spalling have been under under active development for the last decade, and there is hope that these may provide a quantitative understanding of why the variability in the growth rate caused by spalling is relatively large at low temperature and decreases to vanishingly small values as the temperature is increased to 800 °C.

E.1.5 Thin film interference fringes

A film of red cuprous oxide is transparent enough to show thin film interference effects so long as the thickness is less than roughly 500 nm when visible light is used (or several thousand nanometers when near IR light is used) and these can be used to infer the film's thickness. I have computed the reflectivity versus wavelength from the optical constants of copper and of cuprous oxide using the data in [29] and then computed the fringe visibility and fringe color using the standard methods developed by the Commission Internationale de l'Eclairage (CIE) for daylight illumination and for incandescent light illumination: see Section 9, "Colorimetry" in [30] for example. Figure E.3 shows the computed visibility under incandescent illumination of the fringes as a function of the thickness of the oxide, and Figure E.4 shows the relation of the thicknesses for minimum and maximum visibility as a function of this thickness. I obtained these data by inspecting the computed visibility curve: the locations of the minimum and maximum features are increasing uncertain as the amplitude of the oscillations decreases, and becomes useless for the interpretation of experimental data beyond about 500 nm of thickness. Further, the steady decease in the baseline visibility introduces a small systematic error in the locations of the minima and maxima beyond about 250 nm: the minima begin to arrive early and the maxima late, as is apparent in Figure E.4. This effect is large enough to notice in this plot but is too small to have significance in the interpretation of experimental data.

The absorption of the oxide and the width of the spectral range used for visual inspection produces a steady decrease in the visibility of the interference fringes until they become useless for the measurement of film thickness: the limit is about 500 nm for visual examination under incandescent illumination. Note also that one cannot fit the locations of the observed min/max features using only the slope [48.1 nm/(feature index)] and correctly extrapolate

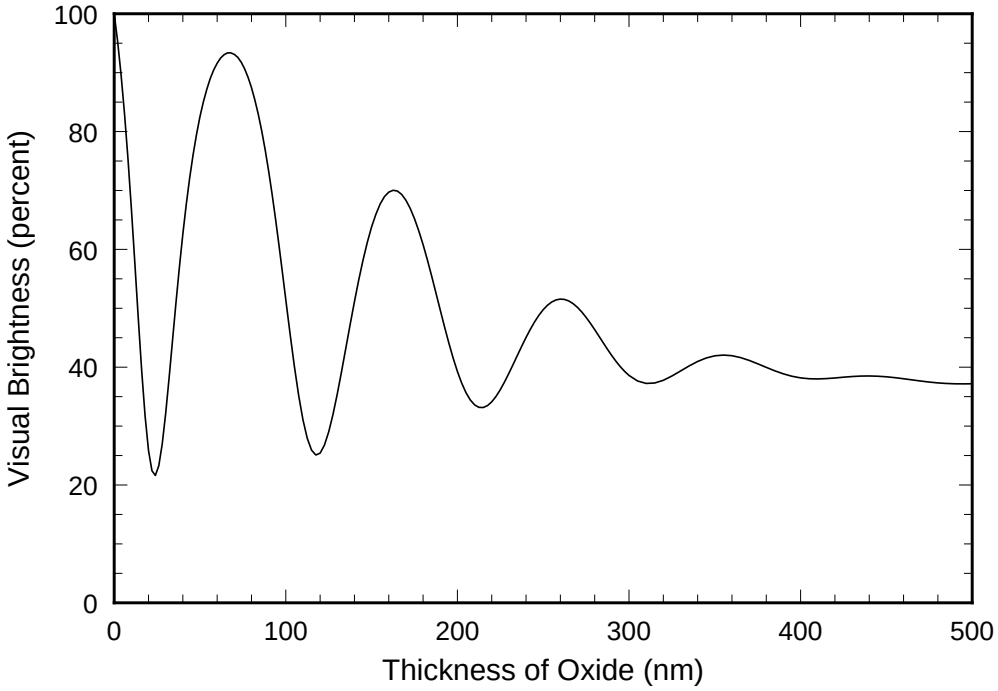

Figure E.3: The change in the visual reflectivity of copper versus the thickness of a film of Cu_2O when the system is illuminated by incandescent light.

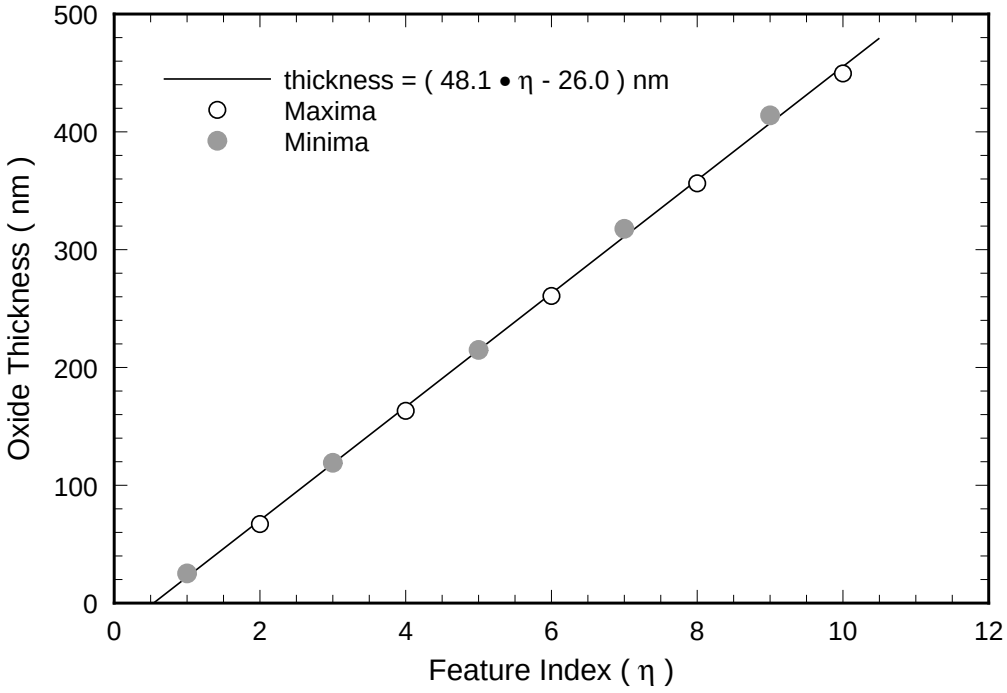

Figure E.4: The thickness of a film of Cu_2O on copper for which the visual reflectivity displays a particular feature: a minimum or a maximum, as labeled.

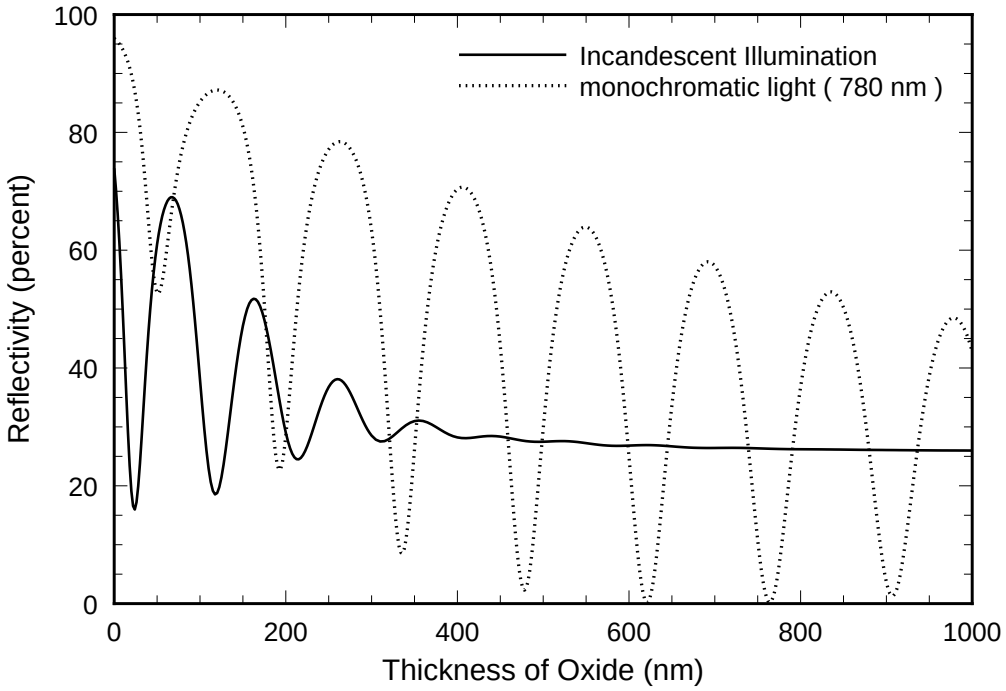

Figure E.5: The thickness of a film of Cu_2O on copper inspected using monochromatic light of wavelength 780 nm and using visual examination under incandescent illumination.

to the location of the zero-thickness region as is commonplace for films on nonabsorbing substrates; rather, one must use the relation with nonzero intercept given in Figure E.4.

These results depend on the illuminant and the detector since these affect the dominant wavelength of the light that is effective in producing the interference fringes. Visual examination under daylight (which contains more blue and less red light than incandescent light) shifts the locations of the minima and maxima to smaller thicknesses by about 5%, and noticeably affects both the hue and the saturation of the sequence of colors. For example the relation between fringe color and film thickness recommended in [20] and copied here as Table E.5 is for illumination under daylight, and not incandescent light.

Inspection using a CCD camera and monochromatic red light allows fringes to be observed in micron-thick films: see Figure E.5. The locations of the minima and maxima are shifted to greater thicknesses. Use thickness $= (71.4 \cdot \eta - 22.6)$ nm, where η is the index of the feature: $\eta = 1, 3, 5, \ldots$ for the minima and $\eta = 2, 4, 6, \ldots$ for the maxima.

Figure E.6 displays for a particular fuse three data sets of oxide thickness that I acquired using visible and near IR inspection, and analyzed using the relations between fringe order (η) and thickness previously given. Also shown is the thickness computed by assuming that the temperature of the fuse's filament is given by the models discussed earlier, and that the growth rate is Arrhenius with an activation temperature of 9 000 K, and that the current was applied for 7 hours with a strength such that $\kappa\ell = 2.3$. The actual strength and times were not accurately recorded for this fuse, but are on this order. The agreement is satisfactory

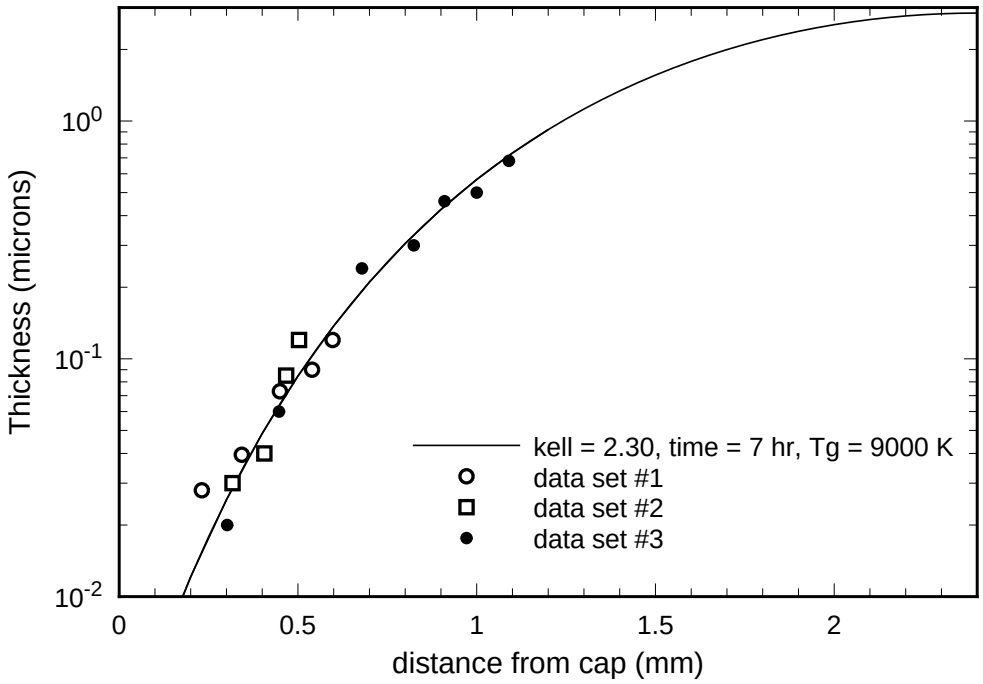

Figure E.6: The thickness of the copper oxide film, inferred from color bands, for three cases. Also shown is a model fit. The log scale is used to accommodate the wide dynamic range.

from 20 nm to 700 nm: the larger thickness is 35 times the lower one; that is, the model fits these data over a range of one and one half magnitudes. The model implies an oxide film thickness of about 3 000 nm (= 3 μm) near its center, which is about 4.3 times larger than the largest thickness measured for this fuse. This fuse was not examined using other methods; however, mid-filament oxide film thicknesses on the order of one to several μm have been observed by SEM and ESCA for some other fuses, as illustrated in Figures E.9 and E.10 and this tends to support the prediction of this model.

Suppose we know that a fuse has endured a constant current I for an extended time t, but that we do not know the amount of the current or the time. Suppose we observe an oxide film of a particular thickness h_a at a location z_a: we then know the product $g(T_a) \cdot t$ since this equals h_a^2, but we do not know enough to factor this product into separate $g(T_a)$ and t — we can imagine that the temperature T_a is low and that the time t is long, or we can imagine the opposite. But if we now observe the oxide thickness at a number of locations, $h(z)$, we can form the ratios:

$$\left[\frac{h(z)}{h_a}\right]^2 = \frac{g(T(z)) \cdot t}{g(T_a) \cdot t} = \frac{g(T(z))}{g(T_a)}\,, \tag{E.11}$$

and this set of ratios can be fit only by one particular temperature distribution (i. e., value of electrical current I). And when this current is computed, then we can compute the time t it took for the observed oxide film to form.

For example, Figure E.8 shows some preliminary explorations of the same data. I began

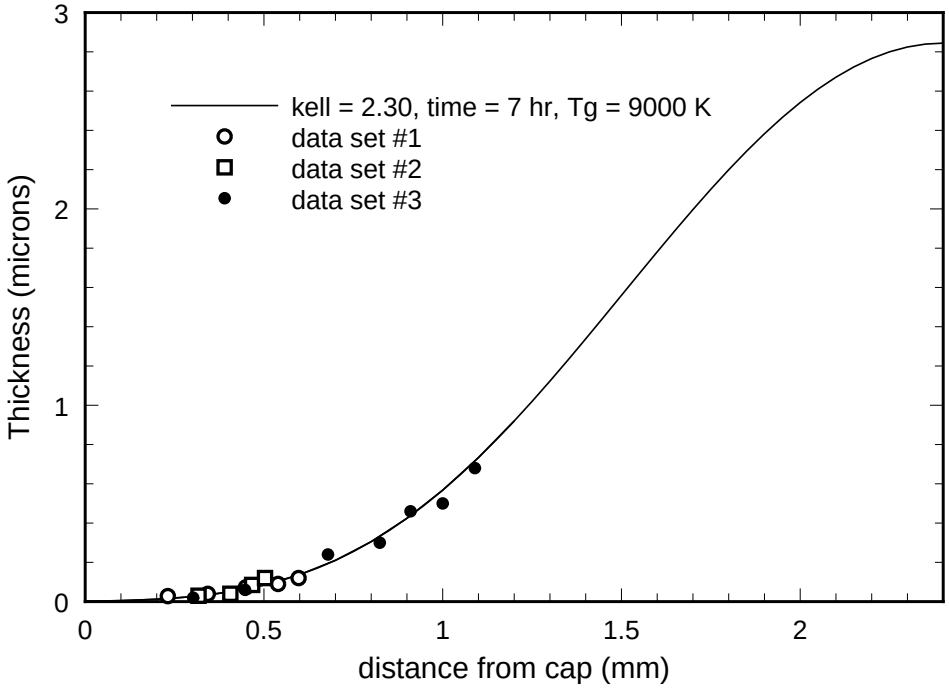

Figure E.7: This plots the same data as the previous figure; the linear scale is used here to provide an alternative display of the concentration of thickness around the center of the filament.

by focusing attention on the oxide thickness at $z = 0.4$ mm: $h \approx 600$ Å. This thickness is produced in 1 hour at a current of $\kappa\ell = 2.45$, or in 100 hours at the lower current $\kappa\ell = 1.95$. (Recall that $\kappa\ell = (IR_0)/(\sqrt{\mathcal{L}}\,T_0)$, so $I = (0.0939\ \Omega) \cdot (\kappa\ell)/R_0$, or $I = 2.68\ \text{A} \cdot (\kappa\ell)$ for a 3 A fuse, for which $R_0 = 35\ \text{m}\Omega$.) But these different choices give different slopes at this location, and apparently a time of about 10 000 hours would be required to fit the data. This illustrates the way in which a current-history can be extracted from an observed $h(z)$-profile.

But I knew that this fuse had been powered for between 10 and 50 hours, and so the result of the fit, 10 000 hours, is absurd. This led me to reexamine the value for the activation energy and to find that it depended on temperature, and that a value of about 9 000 K was more appropriate than the value of 12 000 K used for the curves of Figure E.8. Indeed, about 9 000 K is more in line with the fact that the actual filament temperatures are closer to the range 400 K to 500 K, than to 500 K to 600 K. Thus, the behavior illustrated in Figure E.8 remains unchanged.

Thin film interference fringes — conclusions: Many workers have seen color bands along the filaments of fuses that have carried enough current to heat them. However, no one has previously supplied a quantitative description of these color bands as caused by optical interference fringes in the layer of copper oxide that forms on a heated copper wire. The analysis of this section is meant to demonstrate that this is in fact the explanation of these colored bands. It is also meant to show that an analysis of these bands can, in some cases at

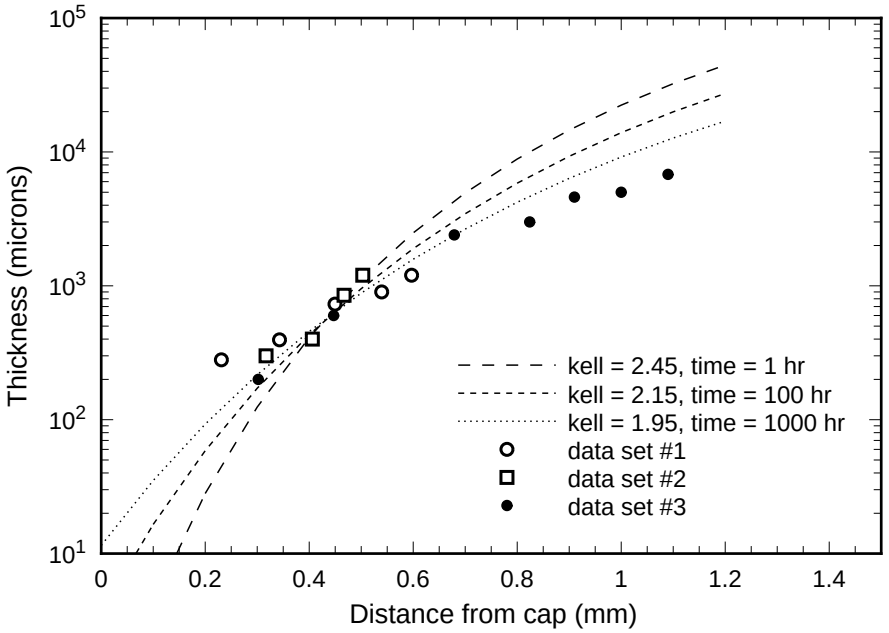

Figure E.8: This plots the same data as the previous figures. The model-curves (all for $T_g = 12\,000$ K), show that the oxide film thickness can be fit at one location by any value of time (with the current adjusted accordingly), but that the shape of the $h(z)$ vs. z curve can be fit only by one particular pair of values of time and current.

least, be used to measure both the current that the fuse has carried and the length of time that the fuse has carried this current.

Literature values were used for the growth rate of Cu_2O on copper and for the optical constants of Cu and of Cu_2O, and these are good enough to establish this analyses. But these may not be the best possible values for conditions within a fuse, particularly when the filament is Cu-Ag alloy, or copper with a silver coating, or nickel. Further work is now timely, such as a series of controlled experiments, growing films when a known constant current is applied for a known time, and then making measurements of the thickness of the films using thin film interference effects and also direct SEM and ESCA.

E.2 Oxidation of copper-silver alloy

Silver oxidizes when exposed to air at room temperature. But above 144 °C, silver no longer oxidizes; indeed, any previously formed silver oxide dissociates. Copper oxidizes when exposed to air at temperatures even higher than copper's melting temperature. The oxidation-behavior of an alloy of two metals cannot be reliably predicted from that of its separate constituents, but [17] reports that copper-silver alloys form copper oxides in the same way that pure copper does, including the development of a thin CuO layer in the presence of a surplus of oxygen. However, oxidation of copper-silver alloy has different

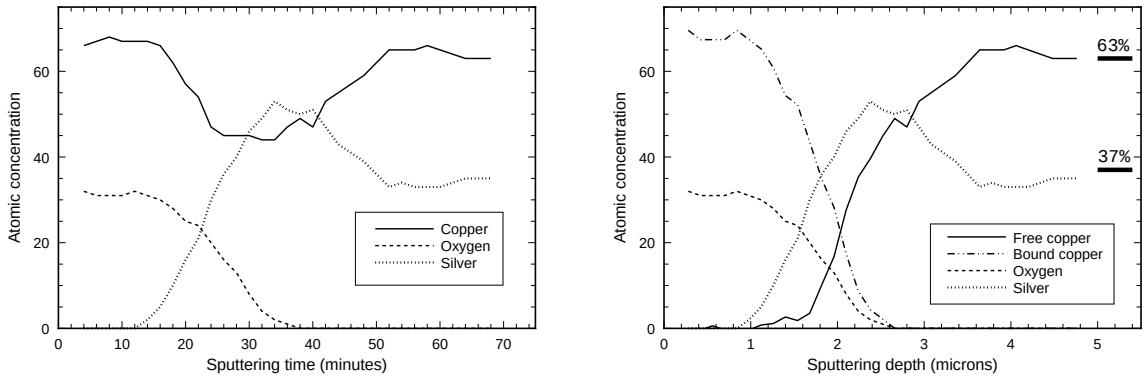

Figure E.9: The left panel is produced directly by an Auger analyzer during a depth profiling run (an ion beam removed surface material at a rate of 700 Å per minute): this data was supplied by Lockheed Missiles & Space Company as part of a failure analysis of some fuses used in the Extreme Ultraviolet Explorer Project. The right panel has been processed: I have converted the ion beam duration into a depth, and resolved the observed concentration of copper into free copper and bound copper (i. e., oxidized copper).

dynamics than pure copper.

Just as for the pure copper case, the underlying reaction is that ions of copper detach at the oxide-metal interface and diffuse through the oxide film to the oxide-oxygen interface where they combine with oxygen. However there is now this difference: the silver ions remain, and so the metal-side of the oxide-metal interface becomes copper-poor and silver-rich as oxidation progresses.

Figure E.9 displays an Auger-based analysis of the concentration of copper, oxygen, and silver at various depths of the filament of a fuse rated at 1.5 A that had been operated for some time; an ion beam was used to sputter-remove material after each Auger inspection to obtain the concentrations versus depth. The left-hand panel shows the unprocessed Auger results, while the right-hand panel shows processed results: the sputtering time has been converted into a depth (using the reported sputtering rate of 700 Å per minute) and the copper concentration has been analyzed into the part that is chemically bound as Cu_2O and the unbound (i. e., free) remainder.

Down to a depth of about 0.9 μm, the ratio of copper to oxygen is 2:1 to within observational accuracy: that is, this is a film of Cu_2O. Also, the atomic concentration of copper is about 67% and of oxygen is about 33% of the total materials present: this film is essentially pure Cu_2O; there are no other elements present in amounts larger than a few percent. Only copper and silver are visible deeper than about 3.6 μm, and the observed concentrations are close to the values of 63% copper and 37% silver, corresponding to 50%-50% by weight, as expected.

The concentrations of oxygen and oxidized copper decrease steadily beginning at about 0.9 μm, and vanish at about 2.4 μm: I estimate the thickness of the copper oxide film

as $(2.4 - 0.9)$ μm$=$ 1.5 μm. This would consume all the copper in a layer of thickness 1.5 μm/1.67 $\approx$ 0.90 μm (where $\mathcal{R}_{PB} = 1.67$ is the Pilling-Bedworth ratio), or some of the copper throughout a thicker layer. Indeed, the concentration of free copper is markedly reduced (relative to silver) down to a depth of about 3.6 μm: the concentration is essentially zero at a depth of 1.6 μm and rises steadily to 63% at a depth of about 3.6 μm, following the standard concentration profile of a one-dimensional diffusion-dominated concentration gradient shown in many texts. The copper lost from this extended region is

$$\int [(0.63 - x_{Cu})/0.63]\, dx \approx (3.6\ \mu\text{m} - 1.6\ \mu\text{m})/2.2 = 0.9\ \mu\text{m},$$

which agrees with the prediction made from the $\mathcal{R}_{PB}$-ratio corrected oxide thickness.

As the thickness of the copper-depleted layer increases, copper ions have further to travel to get to the oxide film: hence, this copper-depleted layer acts as a diffusion barrier and decreases the growth parameter $g(T)$. The Cu-Ag alloy contains eutectic structure of α phase and β phase, and also primary β phase grains: the β phase material is discontinuously distributed in a continuous matrix of α phase material. As the copper diffuses to the outer shell of copper oxide, cavities are left at the locations of the β phase. We can expect an easily noticeable decrease in the rate of formation of copper oxide after the last of the originally superficial primary β phase grains has emptied, since there is then a substantial increase in the distance additional copper has to travel to reach the surface, and since this time scales as the square of this distance. This is one of the reasons for the use of a copper-silver alloy, rather than pure copper, for filaments that have small diameters: they are less subject to oxidation-degradation.

Figure E.10 is a SEM image of the filament of a fuse rated at 3 A that was removed from test equipment after satisfactory operation for a long time: the oxide film shows cracking and an area of it has spalled away to reveal the silver-rich layer underneath, which is observed to contain numerous cavities: these mark the former locations of β phase material.

The silver that is left in the copper-depleted layer is electrically conductive: even if *all* the copper were oxidized, all the silver would remain to carry current. Hence, oxidation is intrinsically a less damaging process for a copper-silver alloy than for pure silver and this is a second reason for the use of copper-silver alloy for fuse filaments.

The impact of the formation of a film of copper oxide of thickness h on a filament of initial radius a can be estimated as follows. Suppose as a rough model that all the copper is removed between the radii a and $a - h'$ where $h' = h/\mathcal{R}_{PB}$, and that the alloy's resistivity is ρ_{alloy} and the cavity-loaded silver's resistivity is $\rho_{Ag,cav} = \rho_{alloy} + \delta\rho$. Then the relative change in the cross-section averaged resistivity is $(2h'/a)(\delta\rho/\rho_{alloy})$. The resistivity of the cavity-loaded silver in this layer is roughly that of pure silver (1.6×10^{-6} Ω·cm), scaled by the volume of the silver to the total volume (we will estimate this to be the volume fraction of the silver in this alloy, 0.46): 3.5×10^{-6} Ω·cm. This replaces the resistivity of the alloy, $\rho_{alloy} = 2.2 \times 10^{-6}$ Ω·cm, so $\delta\rho/\rho_{alloy} = 0.59$. Hence the relative change in the cross-section averaged resistivity upon formation of an oxide of thickness h for a filament of initial radius a is roughly $0.71 \times h/a$. For example, the oxide thickness of the fuse shown in Figure E.9

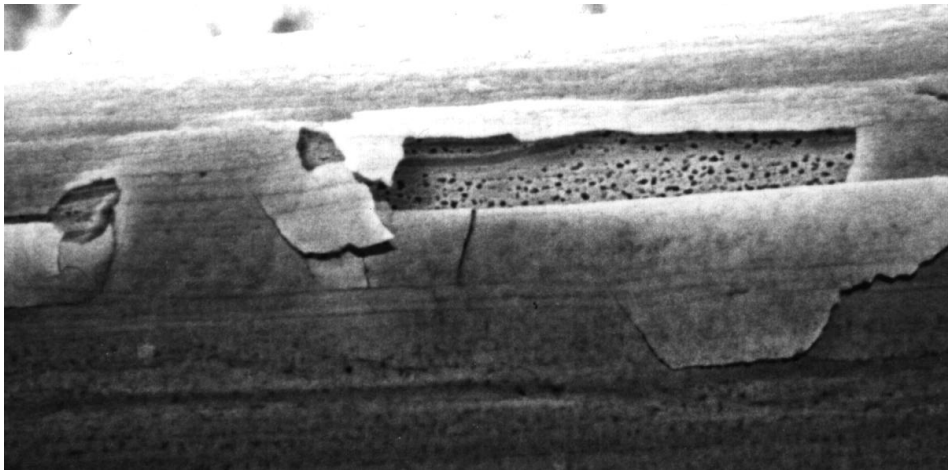

Figure E.10: SEM image of a region of a filament showing spalling of a flake of copper oxide that exposes the silver-rich layer underneath. Also visible are the cavities in the now silver-rich layer. Ms. Kolos (Code 313) provided this SEM.

is estimated at 1.5 μm and the initial radius is $a = 22.2$ μm, so the cross-section averaged resistivity would increase by about 5%. This increase applies to the middle of the filament; elsewhere, the oxide thickness is less, and so the increase in the resistivity is less. The total current-carrying capacity of this particular fuse is reduced by less than 2% by this oxide film. While the oxide film may appear to be substantial, and the spalling may give the appearance of profound damage, the net impact on the *use* of the fuse is small.

Many failure analyses have described this oxide film as a degradation, and sometimes reported this as the cause of interruption. However, it is rare for an oxide film to produce interruption of the fuse: it is simply a natural by-product of operation in an air-filled cavity, and is merely a cosmetic defect, until very thick. Only under prolonged operation can the film grow thick enough to initiate the thermal runaway that leads to interruption — examples of this runaway, and the times required for it, are given in the last section of this Appendix.

E.3 Model for the effect of oxidation

We turn now to the construction of a model for the effect of an oxide film on the behavior of a fuse filament.

We start by estimating the extent that a jacket of oxide will thermally insulate the filament. The thermal conductivity of Cu_2O is reported from 102 K to 362 K in Volume 2 of [21]: it has a maximum of about 70 mwatt/(cm$\cdot$K) at 200 K, and decreases to about 55 mwatt/(cm$\cdot$K) at 300 K, and then to about 50 mwatt/(cm$\cdot$K) at 360 K. On the other hand, the thermal conductivity of air steadily increases with temperature: it is 0.26 mwatt/(cm$\cdot$K) at

300 K, 0.30 mwatt/(cm·K) at 360 K, and 0.57 mwatt/(cm·K) at 800 K. That is, the ratio $k_T^{Cu_2O}/k_T^{air}$ is 212 at 300 K, and 167 at 360 K. The oxide of thickness h reduces the heat flux density J_r by roughly the ratio $1-(h/b)\cdot(k_T^{air}/k_T^{Cu_2O}) \approx 10^{-4}$: this is negligible, and so we will ignore this insulation. The oxide darkens the filament, however, and so increases the heat lost through gray body radiation as the effective emissivity changes from roughly 0.1 for bare copper to roughly 0.9 for sooty-appearing copper. Since the entire gray body radiation loss impacts the filament's temperature by at most a few percent, then changes in it are not very important and will also be ignored; however, in a careful experiment, one could probably observe the formation of a dark oxide as a slight drop in the resistance resulting from the drop in temperature.

When an oxide film grows to a thickness h, the filament radius decreases by $h' = h/\mathcal{R}_{PB}$ where $\mathcal{R}_{PB}$ is the Pilling-Bedworth ratio, and so the cross-sectional area of the fuse changes from $A = \pi a_0^2$ to $A' = \pi(a_0 - h')^2 = A\cdot[1 - h/(\mathcal{R}_{PB}\cdot a_0)]^2$, where a_0 is the initial radius of the filament. Hence the Joule heating term in the equation for the temperature distribution $T(z)$ changes from $\rho\cdot(I/A)^2$ to $\rho\cdot(I/A')^2 = [\rho(I/A)^2]\cdot[1-h/(\mathcal{R}_{PB}\cdot a_0)]^{-4}$. And we must solve the modified temperature distribution equation simultaneously with the one controlling the growth of the oxide, Equation E.9, paying proper attention to the dependence of the growth rate on the temperature. There is no useful way to do this using simple analytic methods. Numerical methods should work, but usually provide limited insight into the relative importance of different parts of the processes.

Oxidation dynamics for a particular case — simultaneous equations

We now study a particular case that captures the most important dynamics of oxidation. We ignore the effect of the air on the temperature distribution along the filament: this approximation overestimates the mid-filament temperature and hence overestimates oxidation rates. Also, we assume a strictly Arrhenius form for the oxidation rate. This leads us to the set of coupled equations to be solved simultaneously:

$$T''(z,t) = -(\kappa^2)\cdot[1-h/(\mathcal{R}_{PB}\cdot a_0)]^{-4}\cdot T(z,t) \tag{E.12}$$

$$h(z,t)^2 = g_0\int_0^t \exp(-T_g/T(z,t'))\,dt', \tag{E.13}$$

and where $\kappa = (IR_0)/(\sqrt{\mathcal{L}}\,T_0\ell)$, where I is the current, R_0 is the cold resistance of the fuse at the temperature T_0, $\mathcal{L}$ is the Lorenz number, and ℓ is the length of the fuse filament.

We focus on those cases in which the filament is initially bare: $h(z,0) = 0$, so that the initial temperature distribution is $T = T^{(0)}(z,t) = T_0\cos(\kappa z)/\cos(\kappa\ell/2)$. We now write the temperature distribution at any later time as a perturbation on this: $T = T^{(0)} + \delta T$. The perturbation δT is the solution of

$$\delta T'' = -(\kappa^2)\cdot\delta T - (\kappa^2)\cdot\left[\frac{1}{[1-h/(\mathcal{R}_{PB}\cdot a_0)]^4} - 1\right]\cdot T^{(0)}\,, \tag{E.14}$$

subject to $\delta T(\pm\ell/2,t)=0$. The solution, which is exact for any value of δT, is

$$\delta T(z,t)=\kappa^2\,T_0\int_{-\ell/2}^{+\ell/2}G(z|z')\left[\frac{\cos(\kappa z')}{\cos(\kappa\ell/2)}\right]\left[\frac{1}{[1-h(z',t)/(\mathcal{R}_{PB}\cdot a_0)]^4}-1\right]dz'\,, \tag{E.15}$$

where $G(z|z')$ is Green's function, defined as the solution of the equation

$$\partial_z^2 G(z|z')=-(\kappa^2)\cdot G(z|z')-\delta(z-z') \tag{E.16}$$

subject to $G(z=\pm\ell/2|z')=0$, and where $\delta(z)$ is the dirac function. We find that

$$\begin{aligned}G(z|z') &= \frac{\sin(\kappa\ell/2)\cos(\kappa\ell/2)}{\kappa}\left[+\frac{\sin(\kappa z)}{\sin(\kappa\ell/2)}+\frac{\cos(\kappa z)}{\cos(\kappa\ell/2)}\right]\left[-\frac{\sin(\kappa z')}{\sin(\kappa\ell/2)}+\frac{\cos(\kappa z')}{\cos(\kappa\ell/2)}\right]\\ &= \frac{\sin(\kappa\ell/2)\cos(\kappa\ell/2)}{k}\left[-\frac{\sin(\kappa z)}{\sin(\kappa\ell/2)}+\frac{\cos(\kappa z)}{\cos(\kappa\ell/2)}\right]\left[+\frac{\sin(\kappa z')}{\sin(\kappa\ell/2)}+\frac{\cos(\kappa z')}{\cos(\kappa\ell/2)}\right],\end{aligned} \tag{E.17}$$

where the top line applies for $z<z'$ and the bottom line for $z>z'$. We observe the usual features: $G(\pm\ell/2|z')=0$, $G(z'_+|z')=G(z'_-|z')$, $G'(z'_+|z')=G'(z'_-|z')-1$, $G''(z|z')=-\delta(z-z')$, and $G(z|z')=G(z'|z)$.

Equations E.15 and E.13 are now solved simultaneously for the oxide thickness $h(z,t)$ and the excess temperature $\delta T(z,t)$: the excess temperature δT at the position z and instant t depends on the oxide thickness h at all positions along the filament at the instant t; and the oxide thickness h at the position z and instant t depends on the excess temperature δT (and the reference temperature $T^{(0)}$) at the position z and on all previous instants.

The resistance of the filament can be directly expressed in terms of the part related to $T^{(0)}(z)$, the part related to $\delta T(z,t)$, and the part related to $h(z,t)$:

$$\begin{aligned}R(t) &= \int_{-\ell/2}^{+\ell/2}\frac{\rho(T)}{A}\,dz \qquad\qquad (\text{E.18})\\ &= \int\frac{\rho_0 T}{A_0T_0}\frac{1}{[1-h/(\mathcal{R}_{PB}\cdot a_0)]^2}\,dz\\ &= \frac{\rho_0}{A_0T_0}\int(T^{(0)}+\delta T)\left[1+\left(\frac{1}{[1-h/(\mathcal{R}_{PB}\cdot a_0)]^2}-1\right)\right]dz\\ &= \frac{\rho_0}{A_0T_0}\int\left[T^{(0)}+\delta T+T^{(0)}\cdot\left(\frac{1}{[1-h/(\mathcal{R}_{PB}\cdot a_0)]^2}-1\right)\right]dz\\ &= \frac{\rho_0}{A_0T_0}\int_{-\ell/2}^{+\ell/2}T^{(0)}\,dz+\frac{\rho_0}{A_0T_0}\int\left[\delta T+T^{(0)}\cdot\left(\frac{1}{[1-h/(\mathcal{R}_{PB}\cdot a_0)]^2}-1\right)\right]dz\\ &= R^{(0)}+\delta R(t)\,,\end{aligned}$$

where

$$R^{(0)} = R_0\,\mathrm{tanc}(\kappa\ell/2), \tag{E.19}$$

$$\delta R(t) = \frac{R_0}{\ell}\int\left[\frac{\delta T(z,t)}{T_0}+\frac{T^{(0)}(z)}{T_0}\cdot\left(\frac{1}{[1-h/(\mathcal{R}_{PB}\cdot a_0)]^2}-1\right)\right]dz. \tag{E.20}$$

Inspection of this result shows that an oxide film increases the resistance in two distinct ways: directly (the second term in the integral for δR) and indirectly by producing a temperature excess, δT.

The oxide thickness can by observed by destructive measurements such as those already discussed. And the excess resistance $\delta R(t)$ can be nondestructively observed at any time.

Oxidation dynamics for a particular case — approximate solutions

The coupled Equations E.15 and E.13 cannot be solved in analytic form. They can be solved numerically.

We introduce a particular set of instants $\{t_j | j = 0, \cdots, N\}$, and use these to partition the total time interval from the initial instant $t = 0$ to the present t into a set of subintervals $(0, t) = (t_0 = 0, t_1) \cup (t_1, t_2) \cup (t_2, t_3) \cup \cdots \cup (t_{N-1}, t_N = t)$, where the duration of the j^{th} subinterval is $\Delta t_j = t_{j+1} - t_j$. Then the thickness (squared) of the oxide film is

$$[h(z,t)]^2 = \int_0^t g(T(z,t'))\, dt' \approx \sum_{j=0}^{N-1} g(T(z,t_j))\, \Delta t_j \,. \tag{E.21}$$

We need a criterion for choosing the value of Δt_j. The simplest choice is a constant time interval, $\Delta t_j = \Delta t$; however, the choice of a large value for Δt would give inaccurate results when the oxidation rate grows large, while the choice of a small value would result in many early steps in which very little growth would occur. It is more efficient to use a time interval that is large when the oxidation rate is small, and decreases when the oxidation rate is large. One possibility is

$$\Delta t_j = (\epsilon a_0)^2 / g(T(0, t_j)), \tag{E.22}$$

where ϵ is a small number such as 0.01, so that the increment in the square of the mid-filament oxide thickness over each interval Δt_j is the same: $(\epsilon a_0)^2$. We now assume that some choice has been made.

At the j^{th}-step, we know t_j and $h(z, t_j)$. We use these to compute $\delta T(z, t_j)$ and from it, $\delta R(t_j)$ and $g(z, t_j)$. We then use these to compute the next time interval $t_{j+1} = t_j + \Delta t_j$ and $h(z, t_{j+1}) = \sqrt{h(z, t_j)^2 + g(z, t_j) \cdot \Delta t_j}$, which allows us to repeat this series of computations.

And we start this procedure with the choices $t_0 = 0$ and $h(z, t_0) = 0$, obtaining $\delta T(z, t_0) = 0$, $\delta R(t_0) = 0$, and $g(z, t_0) = g_0 \exp(-T_g / T^{(0)}(z))$.

At each step, the total oxygen bound into oxide can be computed, and used to adjust the oxidation rates: the oxidation rate is almost independent of oxygen pressure until the pressure drops below a threshold value[3] Also, the temperature can be tested, to see if the

[3]While this effect is known to exist, it does not seem to have been characterized over the range of temperatures and pressures required for this model. We have already mentioned in the paragraph "Effect of gas pressure" that Pilling and Bedworth found that this threshold value is "2 to 3 torr at 800 °C, and then rapidly vanishes as the oxygen pressure drops further." Additional information is needed.

filament has reached its melting temperature; of course, the current is interrupted within a few tenths of a millisecond of the time this happens.

Digression on the pressure of the oxygen gas: The pressure of the oxygen gas is $p = n\mathbf{R}T/V$ where n is the number of moles of the oxygen gas, $\mathbf{R}$ is the gas constant, T is the absolute temperature, and V is the volume; all apply to the inside of the fuse case. The number of moles of oxygen gas after some oxidation has occurred is $n = n_{init} - n_{\mathrm{Cu_2O}}$, where n_{init} is the initial number of moles of oxygen gas present, and $n_{\mathrm{Cu_2O}}$ is the number of moles of oxide that has formed. And $n_{\mathrm{Cu_2O}} = V_{oxide}(t)/\nu_{\mathcal{M}}$ where $V_{oxide}(t) = \int_{\ell/2}^{+\ell/2} 2\pi a_0 h(z,t)\,dz$ is the volume of the oxide at the time t, and $\nu_{\mathcal{M}}$ is the molar volume of the oxide. Hence, the pressure of the oxygen gas can be computed at each time-step.
End of digression.

We now introduce two further approximations:

$$[1/(1-\mathcal{R}_{PB}h/a_0)^n - 1] \approx n\mathcal{R}_{PB}h/a_0 \tag{E.23}$$

$$\exp(-T_g/T) = \exp(-T_g/(T^{(0)}+\delta T)) \approx \exp(-T_g/T^{(0)})\exp(T_g\delta T/{T^{(0)}}^2)\,. \tag{E.24}$$

The coupled equations are now expressed in terms of $T^{(0)}(z)$, $\delta T(z,t)$, and $h(z,t)$:

$$\delta T(z,t) = \frac{4(\kappa\ell)^2\mathcal{R}_{PB}T_0}{a_0\ell^2}\int_{-\ell/2}^{+\ell/2} G(z|z')\cos(\kappa z')h(z',t)\,dz' \tag{E.25}$$

$$h(z,t) = [g(T^{(0)}(z))\int_0^t \exp(T_g\,\delta T(z,t')/T^{(0)}(z)^2)\,dt']^{1/2}\,. \tag{E.26}$$

That is, the excess temperature δT at the position z and instant t depends on the oxide thickness h at all positions along the filament at the instant t. And the oxide thickness h at the position z and instant t depends on the excess temperature δT (and the reference temperature $T^{(0)}$) at the position z and on all previous instants. The thickness of the oxide layer can be eliminated, to give a single equation for the evolution of the temperature increase δT caused by oxidation.

Neither the pair of integrals for δT and h, nor the single integral for δT, can be evaluated using elementary forms, but an iterative approach gives some insights. Consider the case in which the filament is initially bare of oxide, and define $h^{(0)}(z,0) = 0$. Then Equation E.25 gives $\delta T = 0$ at all positions along the filament: define this as $\delta T^{(0)}$. Define $h^{(1)}(z,t)$ as the solution of Equation E.26 using $\delta T^{(0)}$:

$$h^{(1)}(z,t) = [g(T^{(0)}(z))\,t]^{1/2}; \tag{E.27}$$

that is, in this first approximation, the oxide thickness at a particular position grows in proportion to $\sqrt{t}$, at a particular rate given by the reference temperature at that position. Define $\delta T^{(1)}(z,t)$ as the solution of Equation E.25 using $h^{(1)}$; inspection shows that it, and the resistance, grow in proportion to $\sqrt{t}$. Figure E.11 shows a δT-distribution computed this way, after one hour at $\kappa\ell = 2.0$ and $a_0 = 35\mu$m. While the shapes are probably about right, the numerical values could be wrong by orders of magnitude: more experiments must

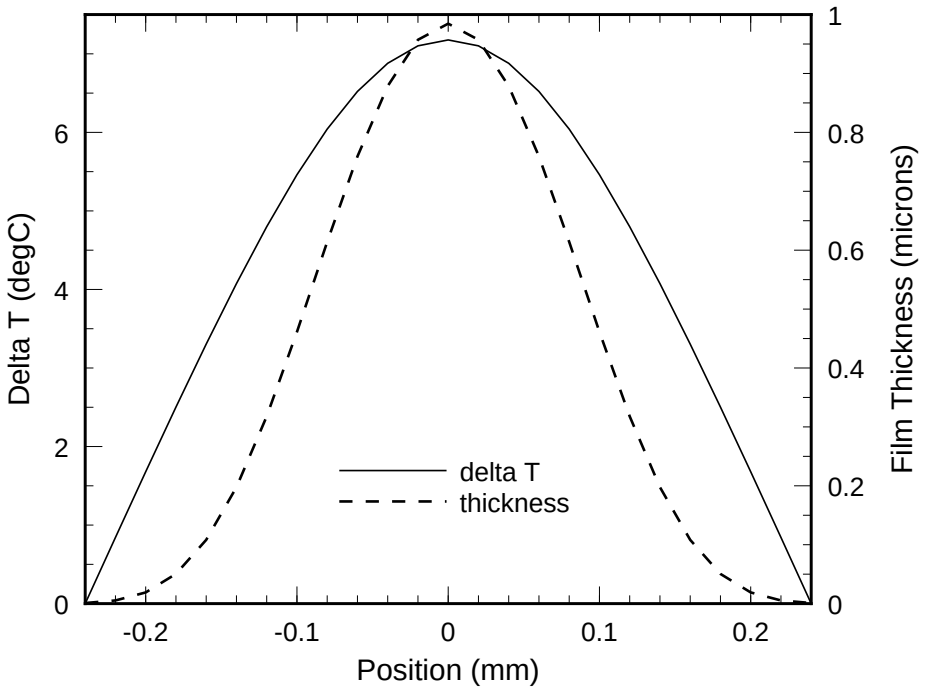

Figure E.11: The computed thickness of the oxide film formed on the filament of a fuse rated at 3 A after an hour at a current of 2.7 A. Also shown is the computed excess temperature it causes.

be done before the numerical values could be regarded as trustworthy. Note that the oxide film's thickness h is more concentrated near the center of the filament, since its growth rate increases exponentially rapidly with temperature; and the excess temperature δT is less concentrated, since thermal conductivity spreads this excess temperature to other locations. So long as $h \ll a_0$, the shape of these distributions remain unchanged: only the sizes change, growing as $\sqrt{t}$.

As the film thickness increases, then the increasing temperature δT will get large enough to effect its own increase in the growth rate: $g(T) \approx g(T^{(0)}) \exp[(T_g \delta T)/(T^{(0)})^2] \approx g(T^{(0)}) \cdot [1 + (T_g \delta T)/(T^{(0)})^2]$. Hence, this first iteration begins to break down when the excess temperature δT increases beyond roughly $(T^{(0)})^2/T_g \approx 10$ K. When this happens, then additional iterations are necessary in order to accurately follow the increase in the excess temperature: the result is that h, δT, and δR begin to increase faster than $\sqrt{t}$; indeed, *these increases eventually become exponential with time, and the fuse filament then soon melts.*

Lambert's W-function

The solution of the equation

$$w \exp(w) = x \tag{E.28}$$

is defined to be *Lambert's W-function*. Lambert set the first problem which required $W(x)$ for its solution, and Euler attributed to Lambert the series that Euler used to solve that problem.

The equation for the distribution of δT that results from combining Equations E.25 and E.26 has the form

$$\theta = \sqrt{\tau}\exp(\theta) \tag{E.29}$$

if we ignore the presence of the integral, and scale the temperature and time appropriately: $\theta = \delta T/T_{scale}$ and $\tau = t/t_{scale}$. This has the solution

$$\theta = -W(-\sqrt{\tau}) \tag{E.30}$$

and this is plotted in Figure E.12.

Figure E.13 shows the resistance of each of a pair of fuses rated at 3 A versus time. Each fuse was presented with a current of 3.35 A for 20 seconds, and then with vanishing current for 40 seconds, so that each cycle endured for one minute; the resistance was measured in the middle of the high-current part of each cycle.[4] Since these fuses had already been operated for some time, each already had some oxide along their filament; hence, the initially parabolic growth in resistance had already happened. The resistance of each fuse begins to diverge to large values, beginning at roughly 1 500 to 1 800 cycles. Fuse LMSC 207 always shows the higher resistance; interruption is at cycle 1875. Fuse LMSC 206 always shows the lower resistance; interruption is at cycle 2350.

Fuse LMSC 206 shows an abrupt increase in resistance starting at cycle 1600: this is induced by a sizable flake of copper oxide spalling off the fuse, leading to a sizable area of fresh metal newly exposed to oxidation, and subsequent formation of an oxide film whose thickness would increase in proportion to $\sqrt{cycle - 1600}$. Guided by this obvious feature at cycle 1600, we can then understand some of the other events in a similar way: for example, fuse LMSC 207 shows such features (but much weaker in strength) near cycle 1400 and near 1550.

The resemblance between Lambert's W-function and the observed resistances of oxidizing fuses is stimulating. It suggests that the essentials of the impact of oxidation on resistance might be captured by the much simpler Lambert's equation. In any case, we can study ways of solving Lambert's equation to learn ways of solving the more complicated coupled pair that describe oxidation. In particular, since $\tau = 0$ implies $\theta = 0$, then we might hope to achieve a useful solution by iteration: We define the zeroth approximation to be $\theta^{(0)} = 0$, and the n^{th} approximation as $\theta^{(n+1)} = \tau^{1/2}\exp(\theta^{(n)})$. Hence, $\theta^{(1)} = \tau^{1/2}$. And the second approximation is $\theta^{(2)} = \tau^{1/2}\exp(\tau^{1/2})$. The third iteration is $\theta^{(3)} = \tau^{1/2}\exp(\tau^{1/2}\exp(\tau^{1/2}))$. These approximations are also shown in Figure E.12: they are successful when τ is small, but

[4] Using the model developed in Chapter 6, I calculate that the temperature of the middle of the filament rises to roughly 600 °C in about five seconds and remains there for the remainder of the 20 seconds of this part of the cycle, and then cools to near 25 °C in about five seconds and remains there for the remainder of the 40 seconds of this part of the cycle. This applies for the first few hundred cycles, before the oxide layer develops to a significant extent. Later, the mid-filament temperature begins to rise above the (roughly) 600 °C value caused by the formation of the oxide layer: see Figure E.13.

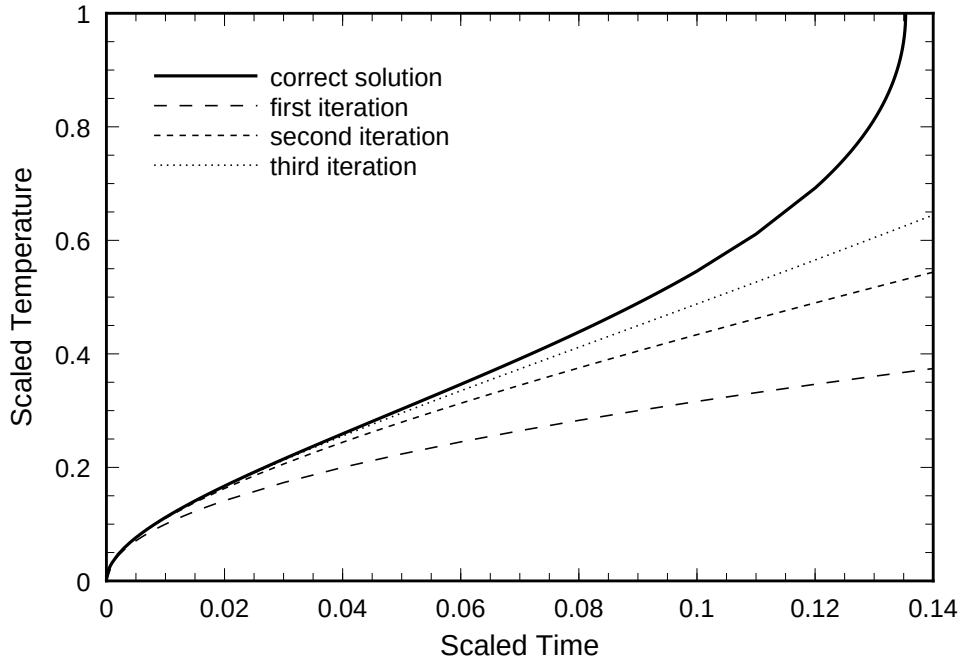

Figure E.12: Lambert's W-function, which resembles the resistance of an oxidizing fuse.

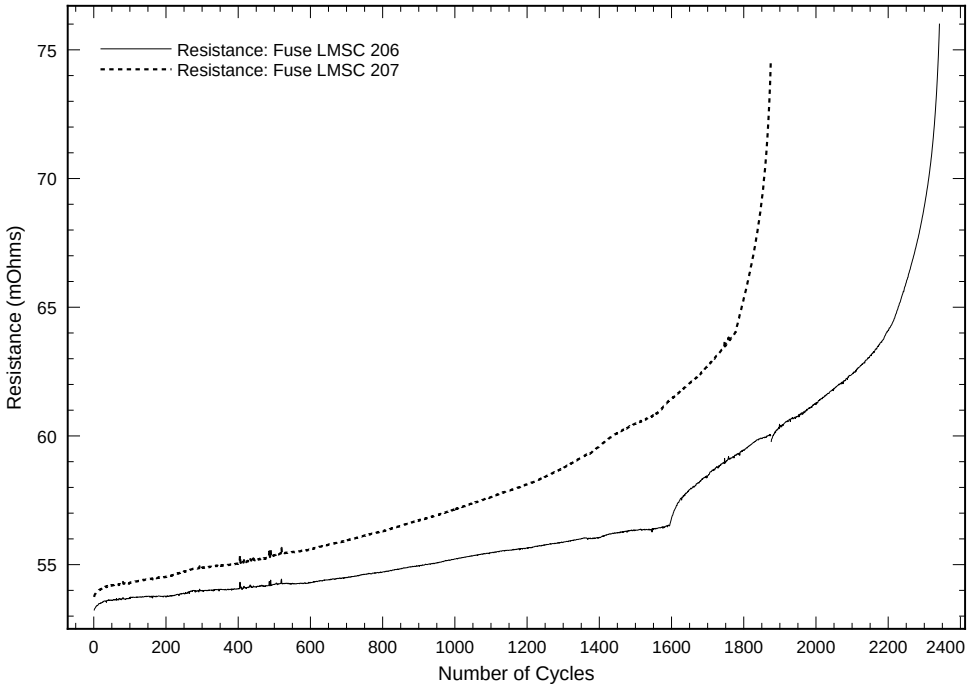

Figure E.13: Resistance of a pair of fuses, each rated at 3 A, driven at 3.35 A for 20 seconds and at 0.3 A for 40 seconds, versus the number of cycles. Fuse LMSC 206 experienced a spalling near cycle 1600 which exposed fresh metal, and produced a parabolic increase in resistance.

they completely fail at capturing the divergence that starts at $\tau \approx 0.1$: it turns out that the rapid increase for $x > 0.10$ requires at least seven to nine iterations to begin to capture. (We do even worse if we linearize the equation by using a series expansion for $\exp(\tau)$; this failure however is not shown in the Figure.) Hence, we predict that it will be necessary to carry out iteration on the coupled pair of equations at least to the seventh order to capture the divergence of the resistance: this is interesting behavior but elusive to conventional analysis. Numerical methods seem called for.

Table E.1: Selected Properties of Copper Oxides

Oxide name	chemical formula	temperature limits (°C)	density (gm/cc)	molecular weight (gm/mole)
cupric	CuO	1026 (decomposes)	6.45	79.54
cuprous	Cu_2O	1235 (melts)	6.0	143.08

Table E.2: Constants for the Free Energy of Formation of Copper Oxides

Oxide name	chemical reaction	ΔH^0	A	B	C	D
cupric	$Cu+\frac{1}{2}O_2 = CuO$	$-37,740$	-0.64	-1.40	-0.10	24.87
cuprous	$2\ Cu+\frac{1}{2}O_2 = Cu_2O$	$-40,550$	-1.15	-1.10	-0.10	21.92

Table E.3: The Free Energy of Formation, and the Pressure of O_2, for Copper Oxides

T	cupric oxide		cuprous oxide	
(°C)	ΔF^0	p_{O_2}	ΔF^0	p_{O_2}
0	$-31,517$	2.3×10^{-51}	$-35,449$	1.1×10^{-57}
200	$-27,121$	7.0×10^{-26}	$-31,904$	2.6×10^{-30}
400	$-22,870$	1.2×10^{-15}	$-28,500$	2.6×10^{-19}
600	$-18,750$	3.8×10^{-10}	$-25,216$	2.1×10^{-13}
800	$-14,757$	9.3×10^{-7}	$-22,045$	9.7×10^{-10}
1000	$-10,887$	1.8×10^{-4}	$-18,982$	2.9×10^{-7}

The free energy is in kcal/mole, and the pressure of O_2 is in atmospheres.

Table E.4: Rate of Formation of Copper Oxide on Copper, and the Apparent Activation Temperature

Temperature (°C)	Oxidation Constant ($gm^2 \cdot cm^{-4} \cdot hour^{-1}$)	T_g (k K)
408	1.64×10^{-8}	10.7
500	1.93×10^{-7}	12.4
600	1.13×10^{-6}	14.2
700	5.86×10^{-6}	16.0
800	3.14×10^{-5}	17.8
900	1.27×10^{-4}	19.7
1000	6.02×10^{-4}	21.5

Table E.5: Daylight Color of Cuprous Oxide Film Versus Film Thickness

Thickness (nm)	Color
18	darkened
27	light rose
30	deep rose
39	light blue
40	light blue
73	yellow II
99	orange II

Appendix F

Creep of the filament

The steady state midfilament temperature of a fuse carrying its rated current is hundreds of degrees less than the melting temperature for all ratings, so long as the thermal resistance is within the limits implied by MIL–F–23419/8F and so long as oxidation or any other process does not degrade the filament to the point of inducing the thermal runaway discussed in the previous Appendix. Under these circumstances (rated current, nonexcessive thermal resistance, and nondegraded fuse), there is no possibility that the filament can melt.

On the other hand, the steady state midfilament temperature can exceed half the melting temperature of the material when the fuse's electrical resistance and thermal resistance are towards the upper ends of the ranges allowed by MIL–F–23419/8F. Further, inspection of a number of fuses demonstrates that some of them have significant assembly stresses within their filaments. The combination of stress and temperature produces creep which can lead to rupture. Indeed, inspection of fuses shows that some have filaments whose shapes suggest that substantial creep has certainly happened, and that the interruption might be caused by creep.

The purpose of this Appendix is to consider creep as a mechanism that can lead to degradation and even interruption of a fuse carrying a current too low to melt the filament. The first section computes the steady state midfilament temperature of the fuses specified by MIL–F–23419/8F. The next section considers a frequently observed filament shape which resembles a tilde $\sim$ and relates this shape to assembly stresses. Then the creep of metals is discussed, and some results are used to estimate the impact of creep on the shape of a filament originally having an $\sim$-shape. These computed results are compared with observation.

Oxidation converts electrically conducting metal into electrically nonconducting oxide, and concentrates the current into a smaller radius. Hence, the midfilament temperature increases as oxidation advances. This temperature increase leads to an increase in the rate of creep. Hence, oxidation exacerbates creep rather than being an independent mechanism of interruption.

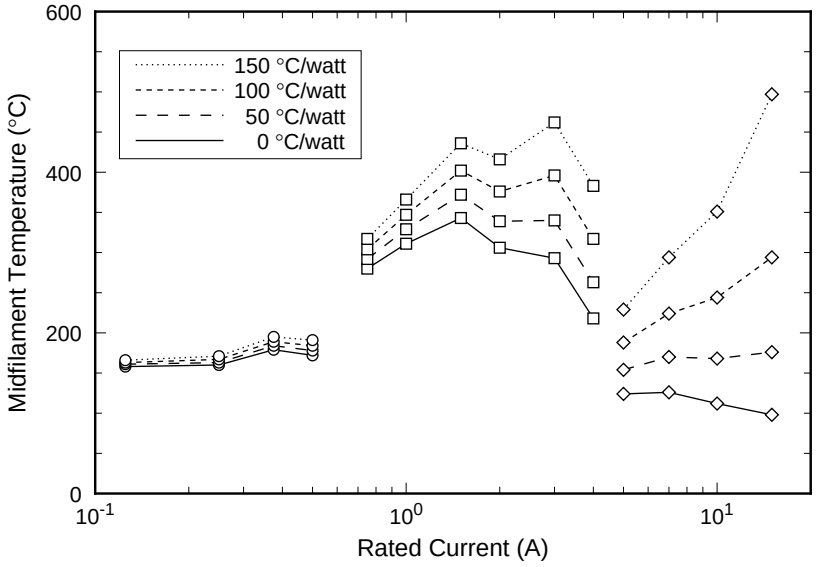

Figure F.1: Midfilament temperatures at the rated current computed according to the model presented in Chapter 6. The fuse barrel contains air, and the fuse's caps are clamped to 300 K = 27 °C through each of four values of thermal resistance: $\mathcal{R} = 0, 50, 100$, and 150 °C/watt.

F.1 Steady state midfilament temperature

Suppose a steady current is applied to a fuse for at least a few seconds, and that the fuse is thermally clamped to a thermal ground so that the temperature of the case and leads reaches steady state within these few seconds: then the middle of the filament achieves thermal steady state within these few seconds also.

Under these steady state conditions, we find good agreement between the observed and computed resistance for currents up to and even beyond the rated current for fuses with copper-silver and with copper filaments; we have not made measurements on fuses with nickel filaments. Hence we can have confidence in the computed temperature of the middle of the filament for this range of currents, at least for the fuses using copper-silver and copper filaments. Figure F.1 shows that the midfilament temperature increases as the thermal resistance increases and the more so as the rating increases, but that this temperature is hundreds of degrees below the melting point. Indeed, $T_{mid}/T_{melt} < 0.7$ at the rated current so long as the cold resistance has the value specified by MIL–F–23419/8F and the thermal resistance is within the bounds implied by MIL–F–23419/8F.[1] This is consistent with observation: melting the filament within some ten seconds requires a current that is distinctly larger (120% to 200%) than the rated current.

[1]The effect of increasing the thermal resistance $\mathcal{R}$ is even larger for the 10 A and 15 A ratings than shown here since the model ignores (a) the increase in the thermal resistance with increase in temperature and (b) the joule heat generated within the leads of the fuse. These two effects generate additional increases of 20% to 50% for the largest ratings.

Not shown in Figure F.1 is the effect of the variability of R_0. MIL–F–23419/8F allows a $\pm 10\%$ variation in R_0, and this affects T_{mid} in a nonlinear way. When the fuse is carrying its rated current, an increase of 10% in R_0 produces increases ranging from 20% to nearly 40% in T_{mid} depending on the rating of the fuse and the value of the thermal resistance. Calculation shows that T_{mid}/T_{melt} can reach 0.9 for fuses with copper-silver filaments carrying their rated current and operating within the specifications of MIL–F–23419/8F.

Observation shows that this style of fuse will not survive at the rated current for very much longer than the four hours guaranteed by the manufacturers: laboratory tests demonstrate interruption in times ranging from six hours to a few days. This cannot be caused by melting: the filament cannot melt when its midfilament temperature is hundreds of degrees less than T_{melt}. Rather, interruption at the rated current must be caused by some process that proceeds while the filament is solid (not liquid). One possible mechanism is oxidation of the filament: Appendix E discussed oxidation and presented a model that quantitatively described the build-up of oxide along the length of a hot filament, and another model that semi-quantitatively described a thermal runaway that ends in melting. Another mechanism is creep-to-rupture under stresses built into the filament during the assembly of the fuse: this Appendix is concerned with creep.

Creep becomes important when there is enough applied stress, and the temperature is high enough, and the time is long enough: we will quantify these terms later in this Appendix. There are two mechanisms producing stress in a fuse filament: (a) the stresses built into the filament during the assembly of the fuse, when each end of the filament is bent around the fuse barrel (this produces a shearing stress along the filament) together with possible stretching of the filament wire and (b) the stresses produced by thermal expansion as the filament heats: this produces a compressive stress along the filament and the shape of some filaments turns some of this into a shearing stress.

F.1.1 Assembly stress

We know that the filament wire is bent in a hairpin curve around each end of the ceramic barrel just before each cap is slid onto the barrel: these bends produce a shear stress along the length of the filament. We also know that soldering temperatures are low enough, and the soldering times are short enough, that these assembly stresses are not annealed away during soldering. Further, each end of the filament is kept cold enough by the end caps that these assembly stresses are not annealed away during operation of the fuse.

We must now estimate the size of this built in shear stress. We have two ways of doing this: one based on inspection of the shape of the filament before interruption, and one based on inspection of the shape after interruption.

F.1.2 Estimate from preinterruption filament shape

Inspection of noninterrupted fuses shows that the filament usually has a compound curve that somewhat resembles a tilde $\sim$: see Figure F.2.

The filament can be modeled as an elastic beam subject to forces and moments acting along its length and at its ends. Draw a straight line between the soldered-in ends of the filament and use this line as the x-axis for the beam model. Define $\eta(x)$ as the height of the midsection of the beam above this axis. Suppose the tensile force (called tension when it is positive and compression when it is negative) acting along the filament is $F_\parallel$, and the force density normal to the filament is $f_\perp(x)$, i. e., the normal force $dF_\perp$ acting on the beam between x and dx is $dF_\perp = f_\perp(x)\,dx$. Then the shearing force $S(x)$ acting on the beam is

$$\frac{S}{YI} = \eta''' - \mathcal{K}^2\eta' \,, \tag{F.1}$$

where Y is Young's modulus and I is the geometrical moment of inertia,[2] and where

$$\mathcal{K}^2 = \frac{F_\parallel}{YI} \tag{F.2}$$

is a measure of the importance of the tensile force to the bending modulus; it has the dimensions of inverse squared length; it is often convenient to use the dimensionless tensile force $(\mathcal{K}\ell)^2 = (F_\parallel\,\ell^2)/(YI)$. The shape is determined from

$$\frac{d^2}{dx^2}\left(YI\left(\frac{d^2\eta}{dx^2}\right)\right) - F_\parallel\left(\frac{d^2\eta}{dx^2}\right) - f_\perp = 0 \tag{F.3}$$

and the boundary conditions.

Introduce $\hat{\mathbf{x}}$ as a unit vector pointing along the x-axis. If the fuse is placed in a magnetic field $\mathbf{B}$ that is perpendicular to $\hat{\mathbf{x}}$, and a sinusoidally varying current $i(t) = i_0 + i_1\sin(2\pi f t)$ is passed through the fuse, then a transverse force density $\mathbf{f}_\perp \propto i(t)\,\hat{\mathbf{x}} \times \mathbf{B}$ is exerted on the filament: this will cause the filament to oscillate at the frequency f, and the amplitude of this oscillation can be inferred from the back electromotive force, or the change in the electrical impedance. By varying the frequency f, the bias current i_0, and the direction of $\mathbf{B}$, one can nondestructively infer some filament parameters and their change with temperature, including $F_\parallel$. Presentation of the details is left for another time. For the present, we restrict to the case $f_\perp = 0$.

If we suppose that Y and I are constant along the beam, then the differential equation for the shape of the beam is

$$\left(\frac{d^4\eta}{dx^4}\right) = \mathcal{K}^2 \cdot \left(\frac{d^2\eta}{dx^2}\right) \,. \tag{F.4}$$

[2]For a circular cross section of radius a, $I = \pi a^4/4$ and $A = \pi a^2$. For a rectangular cross section of width w and height h, $I = wh^3/12$ and $A = wh$.

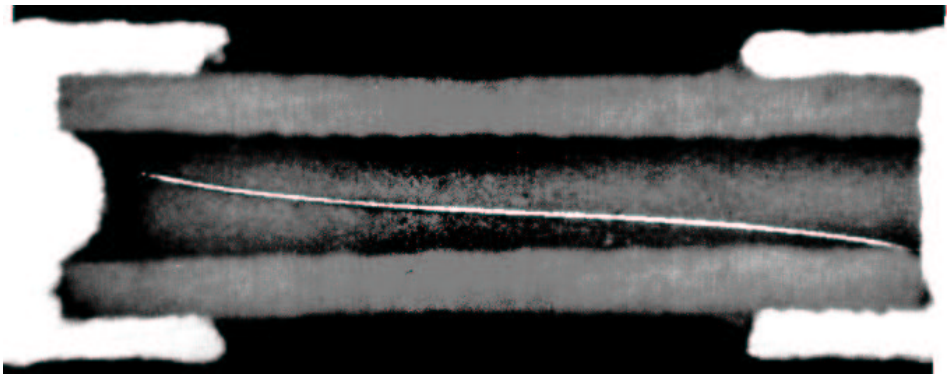

Figure F.2: This unused fuse was cross-sectioned by Ms. Kolos (Code 313) without damage to the filament. She also made this optical photograph, shown here at $24\times$. The curvature of the filament changes sign when crossing from the left to the right of the barrel. The length of this barrel is $\ell = 4.80$ mm, and it's inner radius is $b = 0.34$ mm.

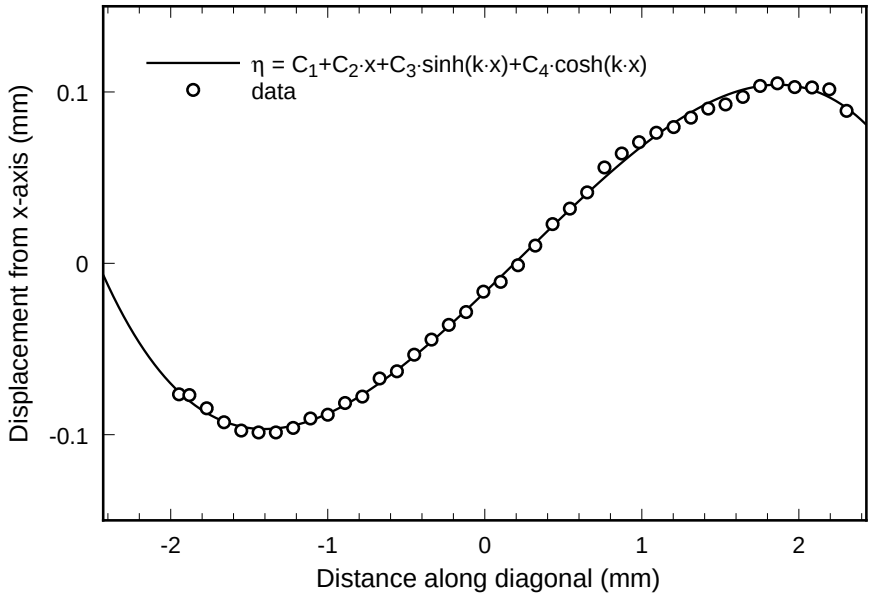

Figure F.3: The data are the measured deviations of the filament in Figure F.2 from the diagonal line joining the soldered-in ends of the filament, while the line is a solution of the beam equation. The least square fit values of the coefficients are $C_1 = (-0.119\,0 \pm 0.001\,1)$ mm, $C_2 = (0.187\,0 \pm 0.002\,3)$, $C_3 = (-0.127\,0 \pm 0.002\,2)$ mm, $C_4 = (0.022\,571 \pm 0.000\,66)$ mm and $\mathtt{k} = \mathcal{K}^{1/2} = (0.778 \pm 0.030)$/mm.

When the cross sectional area A is also constant, then the solutions have the form:

$$\eta(x) = \begin{cases} C_1 + C_2 x + C_3 \sinh(\sqrt{\mathcal{K}^2}\, x) + C_4 \cosh(\sqrt{\mathcal{K}^2}\, x) & \text{for } \mathcal{K}^2 > 0 \text{ (tension)} \\ C_5 + C_6 x + C_7 x^2 + C_8 x^3 & \text{for } \mathcal{K}^2 = 0 \\ C_9 + C_{10} x + C_{11} \sin(\sqrt{-\mathcal{K}^2}\, x) + C_{12} \cos(\sqrt{-\mathcal{K}^2}\, x) & \text{for } \mathcal{K}^2 < 0 \text{ (compression).} \end{cases} \tag{F.5}$$

where the C_1 through C_{12} are constants of integration.[3] I used a nonlinear least square fit program to adjust the four integration constants C_i and the tension $\mathcal{K}^2$ to obtain a best fit with the filament shape shown in Figure F.2. The result is shown in Figure F.3. The residuals are random, and have an average rms value of 2.6 μm: this is about 5% of the diameter of this filament and is caused by the errors made while measuring the location of the filament. That is, the beam model gives a satisfactory description of the shape of this filament.

The shearing force can now be computed from the shape: $S/(YI) = -0.113/\text{mm}^2 \pm 1\%$ between the two ends; there is no x-dependence.

If a satisfactory fit to a particular filament's shape cannot be obtained, then we would reject this model of an originally straight beam subject to elastic deformation under end moments and tension only, for that particular filament; rather, we would conclude that that filament had experienced plastic deformation: see for example Figure 5.7.

Figure F.4 shows the beam model shape appropriate to the real filament shown in Figure F.2, along with the straight line that osculates the filament at each of its ends. If the filament were severed at or near its middle, then each filament stub would straighten out into these dotted lines: this sort of straightening is observed in practice, and shows that the stress that is stored at the roots of the filament's stubs still remained up to the moment of interruption: this stress does not relax during operation of the fuse. In this example, the straight lines miss each other at the middle of the barrel by $0.221 - (-0.583) = 0.804$ mm. If this filament were severed at its middle and if there is no plastic deformation of the roots of the stubs, then the bottom stub would move downward until its tip collided with the barrel at -0.34 mm and the top stub would move upwards with its tip coming to rest at $+0.221$ mm.

We have just shown that this particular filament can be fit with high accuracy. Sometimes the full accuracy of the least square fitting procedure is not necessary and a simpler but more approximate method is satisfactory. The tensile force in this particular filament is low and its behavior can be approximated by a tensionless filament running along the diagonal of the barrel in a symmetric manner with a left (right) intercept of -0.40 mm ($+0.40$ mm). Call this common value $\eta_0 = 0.40$ mm: it can be estimated directly from an image of the filament by using a ruler. Then the shape can be approximated by the simple $\sim$-shape:

$$\eta_{simple}(x) = \{(\eta_0/2)[1 - (2x/\ell)^2] - b\}(2x/\ell) \ . \tag{F.6}$$

The shearing force for the simple tensionless shape is $S/(YI) = -24\eta_0/\ell^3$. This evaluates

[3]The top and bottom forms are the same when interpreted on the complex plane and so only one version is needed. The middle form is the limit of either of the other two, for vanishing tensile force, and so it too can be obtained (when needed) from either of the others.

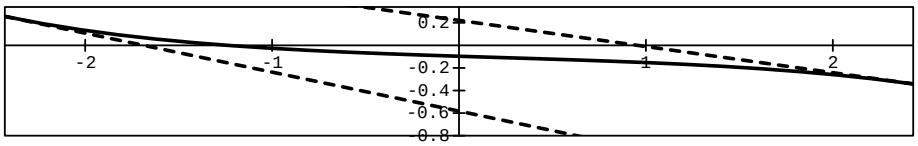

Figure F.4: This shows the shape of the beam adjusted to fit the data of the previous two figures. Also shown as dotted lines are the positions that the filament stubs will assume when the filament is severed in the middle if there is no plastic deformation at the roots of the stubs. The left dotted line intercepts the midpoint at -0.583 mm, and the right dotted line intercepts at $+0.221$ mm.

to $-0.086/\mathrm{mm}^2$ for $\eta_0 = 0.40$ mm. This is in good agreement with the value $-0.113/\mathrm{mm}^2$, considering the simplicity of the approximation.

We need to relate the shearing force to the shear stress. When the beam has a rectangular cross section and is under no tension, then the shear stress is

$$\sigma_{shear}(\delta y) = \frac{3}{2}\frac{S}{bh}\left[1 - \left(\frac{\delta y}{h/2}\right)^2\right] , \tag{F.7}$$

where δy is the distance within the filament from its midline; i. e., δy ranges from $-h$ to $+h$ where h is the height of the beam. Thus, the shear stress vanishes at the top and bottom surfaces of the filament, and is largest in the middle of the filament. The average shear stress is

$$\langle \sigma_{shear} \rangle = \frac{b \int_{-h/2}^{+h/2} \sigma_{shear}(\delta y)\, dy}{A} = \frac{S}{A} , \tag{F.8}$$

which is the needed relation, at least for a tensionless beam.

When the beam has a circular cross section, then again the average shear stress is again S/A for the tensionless case; the details are found in standard texts such as *Strength of Materials* by J. P. Den Hartog (Dover, 1962), pages 44 to 46.

Thus, for both cross sections, the simple tensionless shape gives

$$\frac{\langle \sigma_{shear} \rangle}{Y} = \frac{S}{AY} = \frac{24 I \eta_0}{A\ell^3} . \tag{F.9}$$

F.1.3 Estimate from postinterruption filament shape

Fuses that are interrupted at low values of overcurrent have filaments that are separated at their midpoints with melting that is strongly localized to the very tips of the filament-stubs; there is little or no missing length of filament. Further, the free tips of each filament stub are displaced somewhat from their premelted position, and no longer line up; rather, the tips of the stubs are displaced from each other. In many cases, each free tip is either near the side of the barrel, or is tightly pressed into the side of the barrel, on opposite sides of the barrel.

Each stub is usually straight near its root, indicating that the wire was originally straight and that no observable plastic deformation has happened near either cap.

This tip-disalignment and the straightness of the stubs near their roots is evidence that the stresses built into the filament during the assembly of the fuse were still present up to the moment of interruption. These stresses can be estimated using standard beam theory. Each filament stub is a cantilever beam, free of tension, and the force to displace the free tip of a cantilever beam sideways by the distance η_0 is

$$W = \left(\frac{3YI}{L^3}\right) \cdot \eta_0 \,, \tag{F.10}$$

where Y is Young's modulus, I is the geometrical moment of inertia of the beam, and L is the length of the beam. My inspection of interrupted fuses finds that most values of η_0 are in the range of $b/2$ to $2b$, which agrees with observations of the shapes of preinterrupted filaments. We estimate the ratio of the shear stress at the middle of the filament to the Young's modulus, before interruption, as

$$\frac{\sigma_{shear}^{post-int}}{Y} = \frac{1}{Y}\frac{W}{A} = \frac{24I\eta_0}{A\ell^3} \,, \tag{F.11}$$

where A is the cross section area of the filament, and the length of the stub is $L = \ell/2$. This gives the same result as Equation F.9.

For ratings from 1/8 amp to 3 amp, the filament's cross section is circular and the radius is a. For ratings from 4 amp to 15 amp, the filament's cross section is rectangular, with height roughly constant at $h_0 \sim 80$ μm and width $w = \pi(a^{eff})^2/h_0$: the radius and the effective radius are given in Table 3.3. Thus,

$$\frac{\sigma_{shear}^{post-int}}{Y} = \left(\frac{6a^2}{\ell^3}\right) \cdot \eta_0 \,, \qquad \text{rating} \leq 3 \text{ amp}, \tag{F.12}$$

$$= \left(\frac{2h_0^2}{\ell^3}\right) \cdot \eta_0, \qquad \text{rating} \geq 4 \text{ amp} \,. \tag{F.13}$$

F.1.4 Numerical evaluation

Modeling preinterrupted and postinterrupted fuses gives the same result:

$$\frac{\sigma_{shear}}{Y} = \frac{24I\eta_0}{A\ell^3} \,. \tag{F.14}$$

Further, inspection of the shapes of a number of preinterrupted fuses and of a number of postinterrupted fuses both finds the same range for η_0: the majority of values are between $b/2$ and $2 \cdot b$. The observation that the same range of η_0 is found for both preinterruption and for postinterruption shapes is evidence that the stress that is assembled into the roots of the filaments during their assembly remains there until interruption: it does not relax away.

In the following, we shall use $\eta_0 = b$; results will have a range of roughly a factor of two around values computed on this basis.

We can now use this result to compute the shear stress for a filament of rectangular cross section for which $\ell = 4.8$ mm, $b = 0.34$ mm, and $h \sim h_0 = 80$ μm for all ratings of 4 amps and over. We suppose $\eta_0 \sim b$. Then, to within about a factor of two,

$$\frac{\sigma_{shear}}{Y} \sim 4.0 \times 10^{-5} \cdot \text{rating}/(4\text{ A}) \text{ for ratings of less than 4 A} \quad \text{(F.15)}$$

$$\sim 4.0 \times 10^{-5} \text{ for ratings of 4 A and greater ;} \quad \text{(F.16)}$$

values are steadily smaller as the rating is reduced below 4 amps since the radius is smaller.

Table 2 of the *Handbook of Physics* published by the American Institute of Physics (second edition, 1963) gives the ratio of the shear strength to Young's modulus for copper and for nickel:

$$\left(\frac{\text{shear strength}}{Y}\right)_{copper} = 0.0020 \quad \text{(F.17)}$$

$$\left(\frac{\text{shear strength}}{Y}\right)_{nickel} = 0.0017 \text{ ;} \quad \text{(F.18)}$$

Hence, when $\eta_0 \sim b$, then the filaments are stressed by about a factor of 40 to 50 less than what would be needed to shear them.

Beam models are conventionally described using Young's modulus. However, it is more natural to compare shear quantities to the shear modulus G. When the material is isotropic, then $G = Y/[2(1+\nu)]$ where ν is Poisson's ratio. For copper and nickel, $\nu \sim 0.31$ and so $G = 0.38 \cdot Y$; hence, to within about a factor of two,

$$\frac{\sigma_{shear}}{G} \sim 1.0 \times 10^{-4} \cdot \text{rating}/(4\text{ A}) \text{ for ratings of less than 4 A} \quad \text{(F.19)}$$

$$\sim 1.0 \times 10^{-4} \text{ for ratings of 4 A and greater .} \quad \text{(F.20)}$$

F.1.5 Thermal expansion stresses

The estimates in the previous section of the shear stress apply to a nearly tensionless beam. Thermal expansion, however, creates tensile force in the beam and changes its shape: this can significantly increase the shear stress. The purpose of this section is to estimate this increase.

We first average the thermal expansion $\alpha(T)$ over the steady state temperature distribution $T(x)$ along the filament:

$$\bar{\alpha} \cdot (T_{mid} - T_0) = \int_{-\ell/2}^{+\ell/2} \alpha(T(x;\, i)) \cdot [T(x;\, i) - T_0]\, dx \quad \text{(F.21)}$$

using the expressions for $\alpha(T)$ given in Appendix B, to obtain

$$\hat{\alpha}_{Cu} = [10.1 + 0.0048 \cdot (T_{mid} - T_0)/^\circ\mathrm{C}] \times 10^{-6}/^\circ\mathrm{C} \quad \text{(F.22)}$$

$$\hat{\alpha}_{Ni} = [\ 9.6 + 0.0018 \cdot (T_{mid} - T_0)/^\circ\mathrm{C}] \times 10^{-6}/^\circ\mathrm{C}\ . \quad \text{(F.23)}$$

The thermal expansion of filaments made of copper-silver alloy is close to that of copper. Inspection of Figure F.1 shows that the midfilament temperatures at the rated current are in the range of 150 °C to 500 °C, and so the unconstrained thermal expansion is in the range of 0.1% to 0.6%.

If the filament had free ends, then its arc length $\mathcal{L}$ would be related to the temperature through unconstrained thermal expansion

$$\mathcal{L}_{free} = \bar{\alpha} \cdot (T_{mid} - T_0)\ . \quad \text{(F.24)}$$

But the filament has both ends soldered into the caps and so these ends can neither move nor bend: they are built in, and so the actual arc length $\mathcal{L}_{built\text{-}in}$ will be less than $\mathcal{L}_{free}$. The entire shape of the filament changes during this constrained thermal expansion. We must compute this shape over the temperature range of interest so that we can obtain the correct shearing force.

We model the filament as a beam with build in ends: both the position η and the slope η' have fixed values at each end. We find the position $\eta(x)$ of the beam as a function of its tensile force, $(\mathcal{K}\ell)^2 = (F_\parallel\, \ell^2)/(YI)$, and then compute its arc length

$$\mathcal{L}_{built\text{-}in} = \mathcal{L}[\eta(x)] = \int_{\ell/2}^{\ell/2} [1 + (\eta')^2]^{1/2}\, dx \quad \text{(F.25)}$$

as a function of this force $(\mathcal{K}\ell)^2$. In the linear model, the arc length is also given by

$$\mathcal{L}_{built\text{-}in} = \mathcal{L}_0 \cdot \left[1 + \bar{\alpha} \cdot (T_{mid} - T_0) + \left(\frac{I}{A\ell^2}\right) \cdot (\mathcal{K}\ell)^2\right]\ , \quad \text{(F.26)}$$

where $\mathcal{L}_0$ is the arc length of the filament at the reference temperature T_0 and at zero tensile force. The simultaneous solution of these two equations gives the tensile force as a function of the temperature, and from this we find the shape and then the shearing force as functions of temperature.

We consider the behavior of the filament when its initial shape at the reference temperature T_0 and vanishing tensile force is the simple $\sim$-shape. The arc length $\mathcal{L}_0$ of the simple $\sim$-shape depends only on the parameters ℓ, b and η_0. There is no analytic expression for this arc length; however, the truncated Taylor's series is adequate:

$$\mathcal{L}_{built\text{-}in}((\mathcal{K}\ell)^2 = 0) = \mathcal{L}_0 = \ell \cdot \left[1 + 2\left(\frac{b}{\ell}\right)^2 + \frac{2}{5}\left(\frac{\eta_0}{\ell}\right)^2 + (\text{higher order terms})\right]\ . \quad \text{(F.27)}$$

Solving the beam equation for $(\mathcal{K}\ell)^2 \neq 0$ and the same end conditions as for the simple $\sim$-shape, we find that this series becomes

$$\mathcal{L}_{built\text{-}in}((\mathcal{K}\ell)^2) = \mathcal{L}_0 \cdot \left[1 - \left(\frac{\eta_0}{\ell}\right)^2 \cdot \left(\frac{(\mathcal{K}\ell)^2}{175}\right) + \mathcal{O}((\mathcal{K}\ell)^4)\right]\ . \quad \text{(F.28)}$$

Hence the tensile force caused by this constrained thermal expansion is

$$(\mathcal{K}\ell)^2 = -\frac{\bar{\alpha}\cdot(T_{mid}-T_0)}{\frac{1}{175}\left(\frac{\eta_0}{\ell}\right)^2+\frac{I}{A\ell^2}}\ ; \tag{F.29}$$

thus, increasing the temperature from T_0 compresses the filament and decreasing the temperature places it into tension, as is intuitively clear. The strain caused by this constrained thermal expansion is

$$\begin{aligned}\epsilon_{built\text{-}in} &= \frac{\mathcal{L}_{built\text{-}in}((\mathcal{K}\ell)^2)-\mathcal{L}_0}{\mathcal{L}_0} &\text{(F.30)}\\ &= \frac{\bar{\alpha}\cdot(T_{mid}-T_0)}{1+175\left(\frac{I}{A\eta_0^2}\right)} &\text{(F.31)}\\ &= \bar{\alpha}_{built\text{-}in}\cdot(T_{mid}-T_0)\ , &\text{(F.32)}\end{aligned}$$

where the coefficient of free thermal expansion $\bar{\alpha}$ is replaced by the coefficient of constrained thermal expansion:

$$\bar{\alpha}_{built\text{-}in} = \frac{\bar{\alpha}}{1+175\left(\frac{I}{A\eta_0^2}\right)}\ ; \tag{F.33}$$

since I, A, and η_0 are all always positive, then $\bar{\alpha}_{built\text{-}in} < \bar{\alpha}$ is always true. For a beam with a circular cross section of radius a, $I/(A\eta_0^2) = [a/(2\eta_0)]^2$. For a beam of rectangular cross section of thickness h, $I/(A\eta_0^2) = [h/(2\eta_0)]^2/3$. Thus, the effect of the constraint on $\bar{\alpha}_{built\text{-}in}$increases as the square of the radius (thickness) of the beam and decreases as the square of the initial offset η_0. A typical offset is $\eta_0 = 0.5$ mm, and the radius of the filament of a fuse rated at 3 A is $a = 32.3$ μm; thus, $\bar{\alpha}_{built\text{-}in} \sim 0.85\cdot\bar{\alpha}$.

This analysis is only accurate as long as the higher order terms of $(\mathcal{K}\ell)^2$ are negligible in Equation F.28. For the 3 A fuse, Equation F.29 is $(\mathcal{K}\ell)^2 = -(T_{mid}-T_0)/(5\ ^\circ\text{C})$ and so the higher order terms become important when T_{mid} differs from T_0 by more than roughly 5 °C. The root of this is that the result given in Equation F.29 supposes that the shape $\eta(x)$ is essentially the simple $\sim$-shape, while in fact this ceases to be true for these fuses for temperature excursions of more than roughly five degrees: the actual shape $\eta(x)$ is important. Extending the Taylor's series of Equation F.28 to include higher order terms is not a good strategy since the complexity of these terms increases explosively and the singularity at the critical value $(\mathcal{K}\ell)^2_{crit} = -80.7629\ldots$ means that many terms are required as soon as one moves away from $(\mathcal{K}\ell)^2 = 0$. However, numerical analysis is effective: we repeat each of the steps numerically.

The ratio of the constrained thermal expansion to the free thermal expansion is shown in Figure F.5 over a range of temperatures: this ratio is always less than unity, and the more so as the off set η_0 is smaller since the lever arm used by the tensile force to change the shape is getting smaller. For the same reason, the constrained thermal expansion decreases as the temperature decreases and the filament is pulled more nearly into a straight line along the diagonal of the barrel.

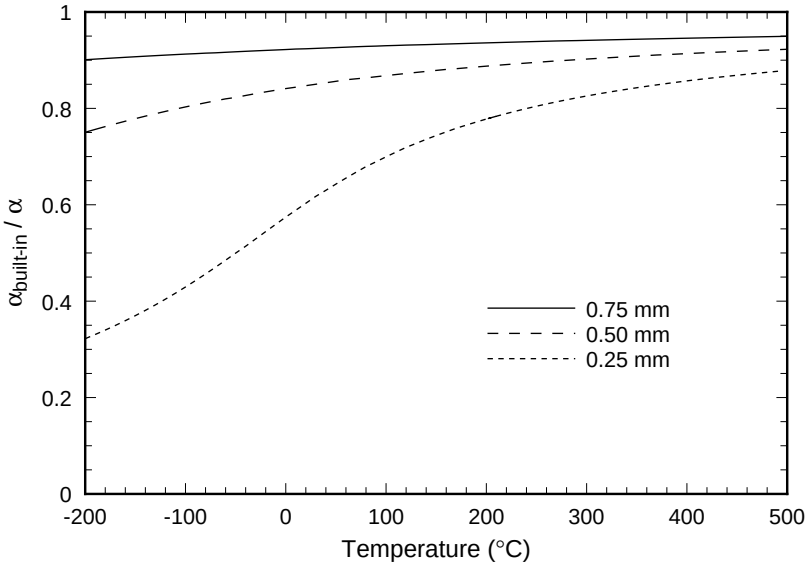

Figure F.5: The ratio of the constrained thermal expansion $\alpha_{built\text{-}in}$ to the free thermal expansion α for three values of the offset η_0. The parameters are for a fuse rated at 3 A.

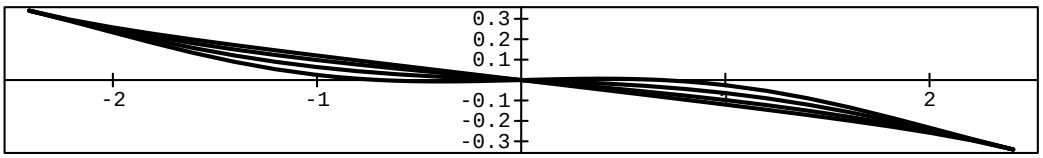

Figure F.6: The computed thermal expansion induced deformation of a filament of a fuse that starts as a simple ∼-shape at $T_0 = 27$ °C with an offset of $\eta_0 = 0.25$ mm. The temperatures are -200 °C (nearly straight line), $+27$ °C, $+200$ °C, and $+500$ °C (the most curved line). Note that the ends are built-in: the location and the slope of all curves are the same at both ends. The parameters are for a fuse rated at 3 A. The x-axis goes from $-\ell/2 = -2.41$ mm to $+\ell/2 = +2.41$ mm, while the y-axis goes from $-b = -0.34$ mm to $+b = +0.34$ mm.

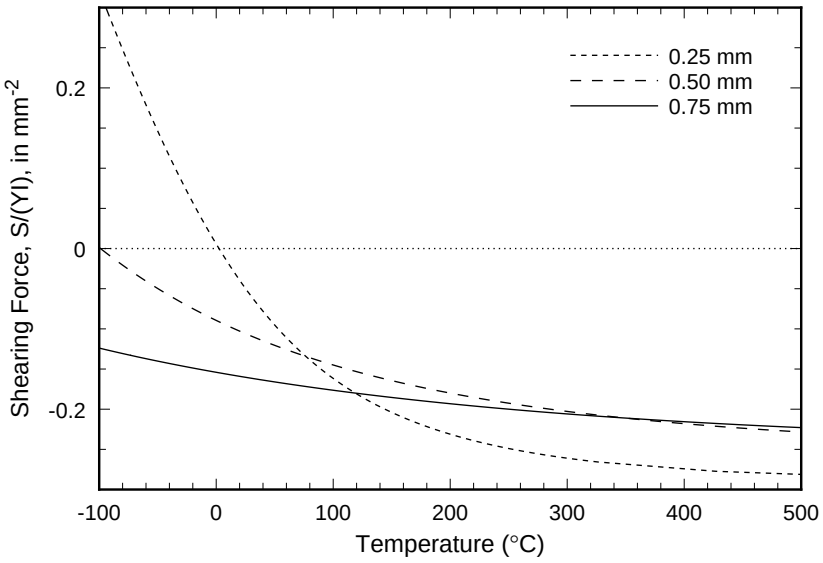

Figure F.7: The computed shearing force $S/(YI)$ (in units of mm^{-2}) caused by the thermal expansion induced deformation of a filament of a fuse that starts as a simple $\sim$-shape at $T_0 = 27$ °C with an offset of $\eta_0 = 0.25$ mm. Also shown are the shapes when the offset is 0.50 mm, and 0.75 mm. The zero-shear axis and the $T_0 = 27$ °C axes are also shown.

Figure F.6 shows how the beam deforms from the simple $\sim$-shape as thermal expansion and the built-in end conditions creates a nonvanishing tensile force. The shape is pulled into a straight line along the diagonal as the filament is placed under increasing tension: the arc length approaches $[\ell^2 + (2b)^2]^{1/2} \approx 4.868$ mm as the tensile force becomes increasingly positive, where $\ell = 4.82$ mm is the length of the barrel and $b = 0.34$ mm is the inside radius of the barrel. On the other hand, the initial bending is exaggerated when the filament is compressed, and so the arc length increases: in the linear elastic approximation of beams that is used here, the arc length diverges towards infinity as the compression approaches the critical value $(\mathcal{K}\ell)^2_{crit} = -80.7629\ldots$ but a real filament will collide with the barrel first.

Figure F.7 displays the shearing force over a range of temperatures for three different offsets. The values at T_0 are the same as those computed from Equation F.1; however, this plot shows that constrained thermal expansion can produce large increases in the magnitude of this T_0-result. For example, if the off set is $\eta_0 = 0.25$ mm, then the shearing force increases in magnitude from $S/(YI) = -0.054/\text{mm}^2$ at 27 °C to $-0.28/\text{mm}^2$ at 500 °C: this is an increase of about 5 times. The temperature changes become more extreme as the offset decreases: the shape is important.

This is the result we were seeking: the magnitude of the shear stress can change substantially with temperature, and the amount depends strongly on the shape of the filament when it is cold.

F.2 The rate of creep

Metals creep at rates that are of practical importance when the temperature exceeds about half their melting temperature. Upon application of a constant stress σ, there is typically a prompt strain ϵ_0 in accordance with the conventional value of the modulus, followed by a steady increase in strain. This increase shows three distinct stages as discussed in standard texts. We are concerned with the secondary stage of creep, in which the creep rate $\dot{\epsilon}$ is a constant versus time. We suppose that a filament will rupture when its middle strains by $\epsilon \sim 0.3$, with an uncertainty of a factor of two or three. If this happens in 24 hours (the minimum guaranteed lifetime of a fuse carrying its rated current is 4 hours) then the strain rate is $\dot{\epsilon} \sim 0.3/(24 \cdot 3600 \text{ sec}) = 3.5 \times 10^{-6}/\text{sec}$.

Experiment shows that the creep rate increases strongly with increasing temperature. For copper and for nickel, as for many other metals, the temperature dependence is closely similar with that of diffusion. The dependence on applied tensile stress is typically that of a power law

$$\dot{\epsilon} \propto \left(\frac{\sigma}{G}\right)^n \exp(\frac{-T^\star}{T}) \,, \tag{F.34}$$

where the activation temperature $T^\star$ is the same as for diffusion and n depends on both the stress level and the temperature. Standard texts[4] give $n_{Cu} \sim 5.1$ for σ/G varying from 10^{-4} to 10^{-3} and also gives $\dot{\epsilon} k_B T/(DGb) = 5.0 \times 10^{-14}$ for $\sigma/G = 10^{-4}$ where D is the diffusion parameter at T and b is the Burgers vector. Since $D_{Cu} = (11 \text{ cm}^2/\text{sec}) \exp(-28\,889 \text{ K}/T)$ and the Burgers vector is roughly 10Å then we obtain the creep rate of $3.5 \times 10^{-6}/\text{sec}$ at 910 °C when $\sigma/G = 10^{-4}$; the required temperature decreases to 514 °C when $\sigma/G = 10^{-3}$. These lower temperatures and higher stresses are obtained in the operation of some fuses: creep is therefore a possibility for some fuses.

F.3 The effect of creep on the shape

When the deformations are elastic, the stress and strain are related as $\sigma/\epsilon = Y$. When secondary creep is advanced, then the strain is $\epsilon = \epsilon_0 + \dot{\epsilon} t$, and this prompts the introduction of the creep modulus, $Y_{creep} = \sigma/(\epsilon_0 + \dot{\epsilon} \cdot t)$. We return to the beam equation, and use the creep modulus to compute the shape of the beam at the time t. We find, qualitatively, that the modulus becomes small near the middle of the beam, where it is hot and creep advances relatively quickly. Hence the beam bends near its middle, deforming from the shape of Figure F.3 into a shape like that of Figure F.8.

[4]See for example Figure 5.11 of *Deformation and Fracture Mechanics of Engineering Materials* by R. Hertzberg. John Wiley. Second Edition, 1983.

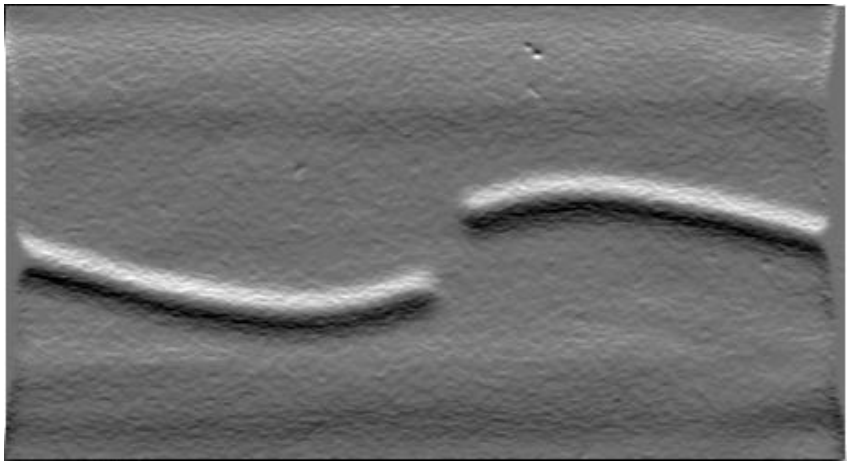

Figure F.8: This is an enhancement of an x-ray image of a fuse that was interrupted at the rated current; x-ray by Mr. O'Shea. The x-ray exposure was adjusted to penetrate the caps and, hence, the filament and barrel were overexposed to the point of being nearly invisible on the x-ray negative. A median filter followed by a gradient filter allows the filament and the barrel to be seen. The roots of the filament are straight; hence, their behavior is elastic in this region. However, the filament has taken on a pronounced set near its middle: this is evidence of creep.

Appendix G

Collection of Symbols, Terms, and Definitions

The following is a classified collection of the terms used in this report.

Symbols The following is the list of symbols and their definitions. The values for the fundamental physical constants are copied from Table 1.01 of Reference [5].

$\mathcal{A}_{\mathcal{M}}$ is the molar weight of a material.

A is the area of the cross section of the filament.

A_{XinM} measures the rate at which a small amount of the element X dissolved in the metal M changes the electrical resistivity of M. See page 127.

a is the radius of the filament when it is circular in cross section. An effective radius is used for other cross sections: $a_{\mathit{eff}} = (A/\pi)^{1/2}$.

α is the linear thermal expansion: $\alpha = (d\ell/dT)/\ell = d(\ln \ell)/dT$, where ℓ is the length.

b is the inside radius of the barrel of the fuse. For FM08 fuses, $b = 0.034$ cm $\pm$ 5%.

C_p is the heat capacity at constant pressure of an object, also called the isobaric heat capacity. C_v is the heat capacity at constant volume, also called the isochoric heat capacity. The specific heat c results from dividing C by a measure of the amount of material in the object (e.g., the number of moles, or the volume, or the mass). In particular, $c_{\mathcal{M}}$ is the molar specific heat.

$\chi = [\frac{T_0}{T_{cap}} \frac{\langle k_T^{air} \rangle}{k_T} \frac{2\ell^2}{a^2 \ln(b/a)}]^{1/2}/\ell$ is a parameter with dimensions of inverse length that measures the importance of the heat extracted from a filament of radius a by conduction through the air into a barrel of radius b, relative to the heat conducted along the filament

into the caps. The thermal conductivity of of the filament is k_T, and of the air is $k_T^{air}(T) = k_T^{air,0}(T/T_0)^\delta$: its average value, $\langle k_T^{air} \rangle$, is given by Equation 6.17. When the dimensionless parameter $\chi\ell$ is large, then conduction through the air is more important than conduction through the filament, and vice versa.

D is the diffusion parameter for one type of material diffusing into another.

$\mathcal{D}$ is the thermal diffusivity of a material, which is a measure of the rate at which a temperature pulse will diffuse. It is related to the thermal conductivity k_T and the isobaric specific heat per volume c_p: $k_T = c_p\mathcal{D}$.

$\mathcal{D}(x)$ is the Debye function, which gives the heat capacity of the Debye model of a crystal lattice at a temperature $T = \Theta_D/x$.

$\Delta\rho_{M,X}$ is the influence coefficient in Matthiessen's rule: see page 127.

ΔF^0 is the free energy of formation in a specified chemical reaction.

ΔH^0 is the enthalpy of formation in a specified chemical reaction.

δ is the exponent in an approximate expression for the thermal conductivity of air: $k_T^{air} = k_T^{air,0}(T/T_0)^\delta$.

$E^\star$ is the activation energy for a process.

e is the elementary unit of charge $e = 1.602\,177\,33 \times 10^{-19}$ coulomb, with an uncertainty of 0.30 parts per million.

ϵ is the thermal emissivity of a surface.

$G(x|x')$ is Green's function for a specified differential equation with specified boundary conditions (where x is the independent variable).

$\mathcal{G}(x)$ is the Grüneisen function, which gives a good approximation to the electrical resistivity of an independent electron model embedded within a Debye model of a crystal lattice at a temperature $T = \Theta_D/x$.

g is the growth constant for the thickening of an oxide film on copper; $g(T)$ expresses this as a function of temperature.

γ_G is the Grüneisen constant for a solid.

$\mathcal{F}$ **function** is a measure of the rate at which a liquid column will deform into a string of beads.

$\mathcal{H}$ **ratio** is defined as $\rho/(k_T T)$. It is nearly constant at the value 2.40 for copper, and for copper-silver alloy, and this permits a simple model for the heating caused by an electrical current.

h is the thickness of an oxide film on a filament.

h is Planck's constant: $h = 6.626\,075\,5 \times 10^{-34}$ joules·sec^{-1}, with an uncertainty of 0.60 parts per million.

I is the electrical current.

I_{melt} is the electrical current that just melts the filament, in steady state. I_{melt}^{air} applies when the filament is surrounded by air, and I_{melt}^{vac} applies when the filament is in a vacuum.

$I_\nu(x)$ is the Bessel function of index ν and imaginary argument: $I_\nu(x) = J_\nu(ix)$ where $i = \sqrt{-1}$.

I_{rating} is the rated current of the fuse. This is a number permanently marked on the case of the fuse; it is related in a complicated way to the current that interrupts the fuse.

$\mathcal{I}$ is the radiant intensity.

$\mathbf{J}_E$ is the electrical current density. It is the rate at which electrical charge flows through an area.

$\mathbf{J}_h$ is the heat current density. It is the rate at which heat flows through an area.

J_r is the radial component of the vector $\mathbf{J}$.

$J_\nu(z)$ is Bessel's function of the first kind, of order ν and argument z; both order and argument can be complex numbers.

k is the fourier variable complimentary to position.

k_B is Boltzmann's constant: $k_B = 1.380\,658 \times 10^{-23}$ joules$\cdot\,\mathrm{K}^{-1}$, with an uncertainty of 8.5 parts per million.

k_T is the thermal conductivity of a material.

$\kappa = (IR_0)/(\sqrt{\mathcal{L}}\,T_0\ell)$ is a parameter with dimensions of inverse length that measures the importance of joule heating of a filament of resistance R_0 and length ℓ, relative to thermal conduction. A small value of the dimensionless ratio $\kappa\ell$ means that the filament experiences a small temperature rise (thermal conduction dominates) and a large value of $\kappa\ell$ means a large temperature rise (joule heating dominates). The parameter κ, or its dimensionless associate $\kappa\ell$, can be interpreted as the scaled electrical current: $\kappa\ell = I/I_{scale}$ where $I_{scale} = \sqrt{\mathcal{L}}\,T_0/R_0$.

$\mathcal{L}$ is the Lorenz number: $\mathcal{L} = k_T\rho/T$. The classical theory of electronic conductivity (Drude, Lorenz, Lorentz) gives $\mathcal{L}_c = 3(k_B/e)^2 = 2.227\,8 \times 10^{-8}$ (V/ K)^2, and the quantal theory of electronic conductivity (Sommerfeld) gives $\mathcal{L}_q = (\pi^2/3)(k_B/e)^2 = 2.443\,02 \times 10^{-8}$ (V/ K)^2; the uncertainties are 8.5 parts per million.

ℓ is the length of the filement. For FM08 fuses, $\ell = (0.480 \pm 0.003)$ cm.

ℓ_{lead} is the length of a lead attached to the cap of the fuse.

N_i is the number of moles of the ith element in a mixture.

$\hat{\mathbf{n}}$ is a vector of unit length.

$\nu_{\mathcal{M}}$ is the molar volume of a material.

$\nu(f)$ is the number density of all vibrational modes in a solid, that have the frequency f.

$\mathcal{P}_h$ is the heat power density.

$\mathcal{P}_J$ is the Joule power density.

$\psi = (2\epsilon\sigma_{SB}\ell T_0^3)/(ak_T)$ is a parameter with dimensions of inverse length that measures the importance of the heat extracted from a filament of radius a by radiation into a barrel of inside radius b, relative to the heat conducted along the filament into the caps. When the dimensionless parameter $\psi\ell$ is large, then radiation into the barrel is more important than conduction through the filament, and vice versa.

Q is the heat flowing in the parts of the fuse and its environment.

$\mathbf{R}$ is the gas constant: $\mathbf{R} = 8.314\,510$ joules $\cdot$ gm$\cdot$mole$^{-1}\cdot$ K, with an uncertainty of 8.5 parts per million.

R is the electrical resistance of the fuse. Since this resistance is low for most ratings of interest, it is necessary to measure it using a Kelvin arrangement, also called a "four wire" arrangement: an ammeter measures the current through the fuse, I, while a high resistance voltmeter measures the voltage drop across the fuse, ΔV: negligible current flows through the voltmeter since it presents a high resistance and the fuse presents a low resistance to the flow of current. Hence, the resistance of the fuse can be accurately computed, $R = \Delta V/I$, with no interference from the ammeter leads.

However, the length of the fuse's leads between the voltmeter's connections and the fuse caps are included in this measurement of R. MIL–F–23419/8F states that the voltmeter's leads are to be attached "as closely as possible"; however, this is not precise enough to specify the resistance of a fuse rated at 15 A to with 10%. It would be more desirable to specify the actual length of lead to be included, as the LM&SC document does: "$1/4 \pm 1/32$ inch on each side of the fuse caps."

R_{cold} is the "cold resistance" of the fuse filament, defined as its electrical resistance measured at 10% or less of the rated current, at a temperature between 20 °C and 25 °C. This limited current will limit the increase in resistance caused by joule heating to 0.4% or less.

R_{hot} is the "hot resistance" of the fuse filament, defined as its electrical resistance measured at 100% of the rated current, at a temperature between 20 and 25 °C.

$\mathcal{R}$ is the thermal resistance between the fuse and a heat sink at ambient temperature.

$\mathcal{R}_{max}$ is the maximum value of the thermal resistance, $\mathcal{R}$.

$\mathbf{r}$ is a position vector.

ρ is the electrical resistivity of a material.

ρ_m is the mass density of a material.

σ is the electrical conductivity of a material.

σ_P is Poisson's ratio for a material.

σ_{SB} is the Stefan-Boltzmann constant: $\sigma_{SB} = 5.670\,51 \times 10^{-8}$ W·m^{-1}·K^{-1}, with an uncertainty of 34 parts per million.

T is the temperature. Temperature is always regarded as measured on a kelvin scale in this report, with values on a celsius scale usually given parenthetically.

$T(z)$ is the temperature of the filament at the location z, and T_{mid} is the temperature at the middle of the filament.

T_0 is a reference temperature, always chosen as 300 K (27 °C) in this report.

T_{amb} is the ambient temperature.

T_{cap} is the temperature of the end cap of the fuse.

T_{barrel} is the temperature of the barrel of the fuse.

T_g is the activation temperature for growth of an oxide film on a filament with growth constant g.

T_C is the magnetic Curie temperature of a ferromagnetic material. Below this temperature, the material is magnetized even in the absence of an applied magnetic field (spontaneous magnetization); above it, there is no spontaneous magnetization.

Θ_D is the Debye temperature of a material. It is a measure of the temperature necessary to thermally excite most of the phonon modes of the material.

t is the time.

τ is a time constant.

$\mathcal{T}$ measures the duration of an interval.

tanc() = tan()/() and tanhc() = tanh()/() are functions of a real number ().

u is the volume density of energy in a material: $u = U/V$, where U is the energy and V is the volume.

V is the electrical potential at a particular location in an electrical circuit.

V_i is the volume of the ith element in a mixture.

v_i is the relative volume of the ith element in a mixture whose total volume is V.

$W(x)$ is Lambert's W function, which is the solution of the equation $w \cdot \exp(w) = x$.

W_i is the weight (or mass) of the ith element in a mixture.

w_i is the relative weight (or relative mass) of the ith element in a mixture whose total weight (or mass) is W.

x is the mole fraction of an element, and x_i is the mole fraction of the ith element in a series.

Y is the Young's modulus of a material.

z is the position along the filament of length ℓ; the left end is at $z = -\ell/2$ and the right end is at $z = +\ell/2$.

Words and terms The following is the list of words and terms, and their definitions.

to blow a fuse : When a great overcurrent is applied to a fuse, the temperature of the filament rises so rapidly that much of its length may vaporize before interruption happens. Indeed, the hot vapor may (if ionized by a voltage spike) continue to conduct even after there is a substantial gap in the middle of the filament. Hence, enough energy can be deposited in the fuse to raise the pressure within the cavity high enough to violently burst the case, or blow off the caps; thus, a fuse can literally "blow."

However, the usual interruption situation is that the current is only large enough to melt the middle of the filament and then the remaining parts of the filament move apart, interrupting the current flow. Or the current may be too low to melt the middle of the fuse, but large enough to permit sufficient creep that the filament ruptures and interrupts the current. These processes should not be confused with "blowing a fuse."

current rating is the number indelibly written on the case of the fuse. It is related in a complicated way to the interruption current.

to fuse means "to melt," and indicates the origin of the name of this device. The word **fuse** is also used for "detonating device," but this use comes from the spindle shape (in Italian, *fuso*) of the squibs used to ignite early cannons, and is unrelated.

to operate is a term of art in England, with the same meaning as "to interrupt."

indefinitely : Webster's *New Collegiate Dictionary* (9^{th} Edition) defines "indefinite" as: *not definite*, as

a: typically designating an unidentified or not immediately identifiable person or thing;

b: not precise: *VAGUE*;

c: having no exact limits.

Thus, *an indefinite time* does not mean "an unlimited (or infinite) time"; rather, it means "a vague (or inexactly limited) time." Hence, the word *indefinite* is not apt in a specifications document.

interrupt current is that value of electrical current that leads to a break in the filament of the fuse, thus *interrupting* the flow of current through the fuse.

Normally, this is the current that melts the filament, and maintains it molten long enough for it to separate into distinct parts. But sometimes the mechanism is "fatigue fracture" produced by repeated application of current pulses, no one of which is ever large enought to effect melting. Also, it is known that a single intense pulse of current can, by mechanical shock, effect interruption with no sign of melting. Further, a current that heats the filament to near melting, but does not melt it, will oxidize it (when there is oxygen present): if this oxidation converts enough conducting metal into nonconducting oxide, then the resulting rise in temperature can lead to melting: the midregion of the filament then appears "burned" since the oxide is dark, and one could say that the fuse has "burned out." Finally, the current may be too small to melt any part of the filament, and oxidation may not advance to the point of inducing separation, but the current is still high enough to elevate the temperature and the creep rate such that stresses lead to rupture.

The terms "burn out current," "blow current," and "melting current" describe particular processes that lead to interruption; while the term "interruption" describes the result only, without committing to its cause.

ambient temperature is the temperature of the part of the world that is in contact with the fuse, and surrounding it. Further, this temperature is supposed to remain unchanged by events within the fuse.

However, these criteria cannot all be meet for fuses rated at several amperes and above: these heat the part of the world that they are in direct contact with. Hence, we suppose that there is a "fuse holder" in contact with the fuse on one side, and in contact with a heat sink on the other: the heat sink is always at the ambient temperature despite events within the fuse, while the heat sink will have a distribution of temperatures between that of the fuse and that of the heat sink.

"Room temperature ambient" is a temperature in the range 293 K to 298 K (20 °C to 25 °C).

Units and abbreviations The following is the list of units, and their abbreviations and definitions.

A = ampere, the MKSI unit of electrical current.

°C = degrees celsius, a scale of temperature.

K = (degrees) kelvin, the MKSI scale of temperature.

Ω = ohms, the MKSI unit of electrical resistance.

V = volt, the MKSI unit of electrical emf.

Bibliography

[1] Hermann W. Reichenstein. *Applying low voltage fuses: classes and characteristics.* Electrical Construction and Maintenance, a McGraw-Hill Publication. 1979.

This is the best introduction to the subject of power line fuses. Mr. Reichenstein focuses on the general behavior of a fuse under AC current load in a reactive circuit, and then presents and discusses the applicable specifications of the U.S.A. regulating organizations. He gives detailed instructions on how to read the manufactures' literature, and on how to select a fuse that is appropriate for each of a variety of applications. However, he has no explicit treatment of fuses similar with the FM04/FM08 style, operated on DC current. This book is unfortunately out of print at this time.

[2] H. Läpple. *Electric fuses; a critical review of published information.* Butterworths Scientific Publications, London. 1952.

Herr Läpple's book of 173 pages discusses the history of the development of fuses, the behavior of fuses, and testing standards that have been found to be necessary. He then lists 267 papers and books topical to fuses, and gives a detailed abstract for each.

[3] Roy Griffith. *The fuse: its story from the sources of its invention through its progress to maturity.* Published by the Chase-Shawmut Company, Newburyport, Massachusets. 1943.

Chase-Shawmut commissioned this 48 page history of the development of the fuse for its fiftieth anniversary in 1943.

[4] Arthur Wright, P. Gordon Newbery. *Electric fuses: Second Edition.* Institution of Electrical Engineers, London), 1995.

[5] Herbert L. Anderson, Editor in Chief. *A Physicist's Desk Reference.* Published by AIP, New York, NY. Second edition, 1989.

This is a dependable source for physical constants, material constants, conversions among units, definitions and standards, and general laws of physics.

[6] William H. McAdams. *Heat Transmission.* McGraw-Hill Book Company, ©1954.

This is a standard reference for the principles of heat transmission through solids; radiative transfer is also treated.

[7] *Conference on the Exploding Wire Phenomenon.* Plenum Press. Volume One published in 1959; Volume Two published in 1961; Volume Three published in 1964; and Volume Four published in 1967.

[8] *SSD Preferred Parts Handbook: Volume 1. Electronics for Flight Vehicle; Part 1. Passive & Electromechanical Devices; Section 5. Fuses.* Lockheed Missiles & Space Company

This is a manual of standard practices in use at the Lockheed Missiles & Space Company. It started on 23 January 1968, and has sixteen revisions since, the most recent (labeled Revision AL) being 1 August 1991.

[9] Samuel J. Keene, Jr. GSFC, Published in 6^{th} *International Reliability Physics Symposium, 1967*

[10] MIL-F-23419/8F: "Fuse, Cartridge, Instrument Type, Style FM08 (Subminiature — High Performance)", 17 August 1989.

MIL-F-23419D, and MIL-F-23419D: Supplement 1.

[11] Esther H. Williams and Steven J. Battel, *Incremental Failure Mechanism in Subminiature Hermetically Sealed Fuses*, ISTFA 1981 symposium paper, pp. 26–38.

[12] Esther H. Williams and Steven J. Battel, *Study To Establish Limits For Reliable Fuse Application In Transient Environment*, ISTFA 1982 symposium paper, pp. 1–11.

[13] William H. Press, Saul A. Teukolsky, William T. Vettering, and Brian P. Flannery. *Numerical Recipes in C.* Cambridge University Press, 1988; second edition 1992.

This is the finest treatment of numerical methods effective for the sorts of problems discussed in this Report.

[14] C. D. Hodgman, Editor in chief. *Handbook of Chemistry and Physics*: 38th Edition. Chemical Rubber Publishing Co. 1956.

[15] Robert C. Weast, Editor. *Handbook of Chemistry and Physics*: 56th Edition. Chemical Rubber Publishing Co. 1975.

[16] L. Darken and R. Gurry. *Physical Chemistry of Metals.* McGraw-Hill, 1953.

[17] H. Uhlig, Editor. *The Corrosion Handbook.* John Wiley.

[18] A. G. Guy. *Elements of Physical Metallurgy.* Addison-Wesley, 1959.

[19] J. Brophy, R. Rose, and J. Wulff. *the Structure and Properties of Materials*, Volume II. John Wiley & Sons, 1964.

[20] B. Chalmers and A. G. Quarrell. *The Physical Examination of Metals.* Arnold Limited, Second Edition 1960.

[21] Y. S. Touloukian, R. W. Powell, C. Y. Ho, and P. G. Klemens. *Thermophysical Properties Of Matter.* Volumes 1 to 13. Plenum, 1970.

[22] Charles Kittel. *Introduction to Solid State Physics.*, Third edition. John Wiley, 1968.

[23] W. Jost. *Diffusion in Solids, Liquids, and Gases.* Academic Press, 1952.

[24] Paul L. Rossiter. *The electrical resistivity of metals and alloys.* Cambridge, 1987.

[25] C. V. Drysdale. *International Critical Tables*, Volume I.

[26] Max Drysdale and Kurt Anderko. *Constitution of Binary Alloys.* McGraw-Hill. 1958.

[27] Robert E. Reed-Hill. *Physical Metallurgy Principles.* Second Edition, D. Van Nostrand Company. 1973.

[28] *Metals Handbook.* Ninth Edition. 1979.

[29] *Handbook of Optical Constants.* Edited by Edward Palik. Academic Press. Volume I, 1985; Volume 2, 1991.

[30] *Handbook of Optics.* Edited by Walter Driscoll and William Vaughan. McGraw-Hill. 1978.